

SUPERCONDUCTIVITY DEVICES: COMMERCIAL USE OF SPACE

Annual Report

**ORIGINAL CONTAINS
COLOR ILLUSTRATIONS**

to

National Aeronautics and Space Administration
Langley Research Center
Hampton, VA 23665-5225

Period: July 2, 1993 - January 31, 1995

Principal Investigator:

Gene Haertling

Co-Investigator:

Eugene Furman

Supporting Investigator:

Guang Li

Contract No. NAG-1-1301

March 17, 1995



The Gilbert C. Robinson
Department of Ceramic Engineering

College of Engineering

Table of Contents

Introduction

Part I. PSZT Antiferroelectric Rainbow Actuators
Part II. Stress-Enhanced Displacements in PLZT Rainbows
Part III. Strain-Electric Field Hysteresis of PLZT, PBZT and PMN
Part IV. Displacement Properties of Rainbows
Part V. General Studies of Rainbow Processing and Properties
Part VI Publications

I. Introduction

This report details work that was performed in the Ceramic Engineering Department of Clemson University over the period from July 2, 1993 to January 31, 1995 under NASA contract No. NAG-1-1301. The work described in this report covers various aspects of the Rainbow solid-state actuator technology. It is presented in six parts dealing with materials, processing, fabrication, properties and associated phenomena.

The Rainbow actuator technology is a relatively new materials development which had its inception in 1992. It consists of a new processing technology for preparing piezoelectric and electrostrictive ceramic materials. It involves a high temperature chemical reduction process which leads to an internal pre-stressing of the oxide wafer, thus the name Rainbow, an acronym for Reduced And Internally Biased Oxide Wafer. Ceramics fabricated by this method produce bending-mode actuator devices which possess several times more displacement and load bearing capacity than present-day benders (unimorphs, bimorphs).

It is anticipated that these solid-state, electromechanical actuators which can be used in a number of applications in space such as cryopump motors, anti-vibration active structures, autoleveling platforms, telescope mirror correctors and autofocusing devices. When considering any of these applications, the key to the development of a successful device is the successful development of a ceramic material which can produce maximum displacement per volt input; hence, this initiative involving a solid-state means for achieving unusually high electromechanical displacement can be significant and far reaching. An additional benefit obtained from employing the piezoelectric effect in these actuator devices is the ability to also utilize them as sensors; and, indeed, they can be used as both motor (actuator) and generator (sensor) in multifunction devices.

Part I.

Fabrication and Properties of PSZT Antiferroelectric Rainbow Actuators

Fabrication and Properties of PSZT Antiferroelectric Rainbow Actuators

Abstract: The fabrication and properties of PSZT antiferroelectric Rainbow actuators with compositions near the antiferroelectric-ferroelectric (AFE-FE) phase boundary were investigated. The kinetics of the reduction reaction was found to be considerably more rapid in PSZT ceramics than in PLZT ceramics. The optimal processing conditions for the fabrication of PSZT Rainbows were 850 °C for 2 - 3 hours. Large axial displacements ranging from 102 to 273 μm were obtained from the PSZT Rainbow samples by application of electric fields greater than the AFE to FE phase switching levels. The field-induced displacements of the Rainbow samples were found to be dependent on the manner of applying load on the samples. At room temperature, the antiferroelectric PSZT Rainbows exhibited negative curvature (with the oxide layer concave) which was attributed to the cubic to antiferroelectric phase transition in the oxide layer. The AFE-FE phase transitions occurred at lower field levels in the Rainbows as compared to the corresponding normal ceramics.

1. Introduction

Rainbow ceramics (Reduced And INternally Biased Oxide Wafer), which are characterized by very high field-induced displacements and good load-bearing capability, show potential application in a variety of technologically important areas.¹ A Rainbow is obtained via chemical reduction of one major surface of a high lead-containing ferroelectric ceramic wafer, such as PLZT, by placing the wafer on a flat carbon block and heat treating it at an elevated temperature. As the partially reduced ceramic wafer is cooled to room temperature, a dome-shaped, internally stressed ceramic-reduced layer structure is formed. Very high axial displacement is obtainable from an electroded Rainbow sample by application of an electric field

across the ceramic oxide layer. More detailed descriptions of Rainbow ceramics can be found in a number of publications.¹⁻³

The $\text{Pb}(\text{Sn,Zr,Ti})\text{O}_3$ (PSZT) ceramics with compositions in the vicinity of the FE-AFE phase boundary were first investigated by Berlincourt et. al. over three decades ago.⁴ Recently, very high field-induced strains resulting from the transition from the AFE to the FE state were reported on these ceramics.⁵⁻⁶ A strain of 1.1% (the highest reported in the literature for ferroelectric ceramics) was claimed in the PSZT system in a study by Shebanov et. al.⁶ Furthermore, the strain characteristics of these ceramics can be modified through selection of appropriate compositions.⁷ For example, a PSZT ceramic may have a shape-memory effect or digital-like strain characteristics depending on the location of its composition in the phase diagram. Ceramics with specific compositions in the AFE phase region near the AFE-FE phase boundary (note that the phase boundary is not a stable boundary and its location is affected strongly by external mechanical stresses and electric fields)⁸ are easily switched to the ferroelectric state by application of an electric field and remain ferroelectric upon removal of the field. As a result, a shape-memory effect is achieved. The AFE compositions away from the phase boundary exhibit well-defined AFE characteristics with the digital-like strain characteristics under applied electric fields. A number of potential applications have been proposed to utilize the strain properties of the PSZT ceramics.^{7,9}

The objective of this work was to combine the high induced strains of PSZT ceramics with the Rainbow technology to produce high-displacement actuators. In this paper, the fabrication and properties of PSZT antiferroelectric Rainbow actuators with compositions in the vicinity of the FE-AFE phase boundary are presented.

2. Sample Preparation

Bulk PSZT ceramics used for the fabrication of the Rainbow samples were prepared according to the formula $\text{Pb}_{0.97}\text{La}_{0.02}(\text{Zr}_x\text{Sn}_y\text{Ti}_z)\text{O}_3$. The samples studied are designated as

PSZT X/Y/Z or Rainbow X/Y/Z in the following discussion, where the X, Y and Z are the molar percentages of Zr, Sn and Ti ions in the B site of the perovskite structure, respectively. For example, Rainbow 64/26/10S represents a Rainbow made from a sintered PSZT 64/26/10 (Zr/Sn/Ti) wafer. The letter S at the end of the designation indicates that the ceramic wafer is prepared by sintering. Similarly, HP is used to indicate hot-pressed wafers. The locations of the samples in the PSZT phase diagram are shown by the double-cross hatched area in Figure 1. Reagent grade PbO, ZrO₂, TiO₂, SnO₂ and La₂O₃ were used as the starting materials. Weighed components were mixed in distilled water for 30 minutes and dried at 105 °C. The dried powders were calcined at 925 °C for 2 hours, and then milled for 8 hours in trichloroethylene using a polyethylene jar and ZrO₂ balls. Bulk ceramics were obtained either by sintering sample pellets at 1280 °C for 4 hours or by hot pressing the pellets at 1200 °C for 6 hours at 14 MPa in an oxygen atmosphere. The sintered ceramic blocks were cut and lapped into wafers of various diameters and thicknesses. In the fabrication of Rainbow samples, a PSZT wafer was chemically reduced on one major surface by placing the wafer on a graphite block and introducing the assembly into a preheated furnace. After the reduction, the wafer together with the graphite block was removed from the furnace and cooled down in air to room temperature. Epoxy silver electrodes cured at 200 °C were used for determination of the Rainbow's electrical properties. The dimensions of the Rainbow samples are shown in Table 1. Samples with two different diameters of 2.16 and 2.72 cm were studied. The oxide/reduced layer thickness ratio was varied by means of the different processing conditions.

3. Measurements

The phases of the reduced PSZT samples were examined with an X-ray diffractometer (Scintag XDS 2000TM) using Ni-filtered Cu K α radiation at a scan rate of 2 degrees per minute. The thicknesses of the reduced layer of the Rainbows were measured from the sample cross-sections by means of an optical microscope. Room temperature dielectric properties of the

samples were determined at 1 kHz using an LCR meter (LEADER, 7450-01). Conventional dc hysteresis loop equipment was employed to measure the relationship between polarization and electric field. Electric fields greater than the AFE to FE phase transition levels were applied gradually to the samples.

A measuring set-up with an LVDT (Linear Variable Differential Transformer, 050 DC-E Lucas Schaeritz Co.), as seen in Figure 2, was used to determine the change of the field-induced displacement with electric field and the change of bending deflection with temperature. A Rainbow sample with electrodes on its major surfaces was placed on a metal ring in a small container. The ring supported only the edge of the sample so that the center part of the Rainbow could move up and down without touching the bottom of the container. The container was filled with silicon oil for insulating and temperature control purposes. The movable core of the LVDT was adjusted to contact the center of the Rainbow sample.

Mechanical loading on the Rainbow samples was accomplished by placing weights on top of the LVDT movable core. The variations of polarization and axial displacement with electric field were measured simultaneously when the samples were loaded.

4. Results and Discussion

4.1 Chemical Reduction of PSZT Ceramics

Temperature is an important factor in controlling the reduction process during fabrication of Rainbow samples. For PLZT ferroelectric ceramics (the most frequently used Rainbow materials), the optimal reduction temperature was around 975 °C. It was found that the reduction reaction is considerably more rapid in PSZT than in PLZT ceramics. A significantly thicker reduced layer in a PSZT than in a PLZT ceramic is produced when they are reduced at the same temperature for a given time. Figure 3(a) shows the reduced layer thickness of a PSZT Rainbow as a function of reduction temperature for a time of 1 hour. The thickness of the reduced layer began to increase rapidly at about 875 °C, but became saturated at higher temperatures. An

approximately 650 μm thick reduced layer was produced in the PSZT sample at 975 $^{\circ}\text{C}$, as compared to the 150 μm thick reduced layer in a typical PLZT Rainbow obtained under identical conditions. Further manifestation of the rapid reaction in PSZT ceramics is the enhanced reoxidation of the reduced layers observed at elevated temperatures. For example, a reduced layer 200 μm thick was completely reoxidized almost instantaneously when exposed to air at a temperature used for the reduction.

Reduction time is another important factor that affects the reduction process. Figure 3(b) shows the change of the reduced layer thickness with time at a constant temperature of 850 $^{\circ}\text{C}$ for PSZT 64/26/10HP. A nearly linear relationship with a slight tendency for saturation at longer times was seen. At higher temperatures, significant saturation of the reduced layer thickness was observed.

Although the reduction reaction is very rapid in PSZT ceramics, the reduction of the PSZT phase, unlike that of PLZT, is incomplete. Figure 4(a) shows the X-ray diffraction pattern from a PSZT sample reduced at 975 $^{\circ}\text{C}$. Even at this high temperature a significant amount of the original PSZT phase remains in addition to the oxide phases such as PbO (massicot), ZrO_2 , ZrTiO_4 , and SnO_2 which result from the reduction process. At 975 $^{\circ}\text{C}$, the rapid reaction led to precipitation of a large amount of lead phase on the sample surface. With the additional loss of lead phase due to reoxidation during cooling, metallic lead was nearly absent from the reduced region. The diffraction pattern in Figure 4(a) was obtained after removal of the lead particles from the surface, and hence the diffraction peaks for the lead phase were not observed. Figure 4(b) shows the X-ray diffraction pattern from a sample reduced at 850 $^{\circ}\text{C}$. In this case, only metallic lead and the original PSZT phases are evident, and the lead phase was uniformly distributed within the reduced layer.

As mentioned above, at a high temperature such as 975 $^{\circ}\text{C}$, the rapid reaction in PSZT ceramics results in the loss of a large amount of lead phase from the reduced region. As a result, the reduced region has poor conductivity or even becomes an insulator. This is detrimental to the

performance of Rainbow actuators since the reduced layer must be electrically conductive in order for a Rainbow to operate properly. To avoid the loss of the lead phase, lower reduction temperatures must be used. However, a very low temperature requires impractically long reduction times. It was noted that the useful temperature range for the production of PSZT Rainbows is very narrow, approximately 850 ± 30 °C. The optimal conditions for producing Rainbow samples from PSZT ceramics were found to be 850 °C for 2-3 hours.

4.2. Properties of PSZT Antiferroelectric Rainbows

Figure 5 shows the polarization (P) - electric field (E) hysteresis loop of Rainbow 64/26/10HP. The hysteresis loop of a normal (non-Rainbow) sample is also given for comparison. Significant differences between the two hysteresis loops are seen. First, a finite net polarization Δp , indicating partial poling of the sample, was found to exist in the virgin state of the Rainbow sample. This phenomenon, which was also observed in ferroelectric PLZT Rainbows,¹⁰ is believed to be associated with the internal stress in Rainbows. Second, the AFE to FE phase switching in the Rainbow occurred at a much lower field level and was less abrupt compared to the normal sample. Since the composition of PSZT 64/26/10 is located near the AFE-FE phase boundary, an intermediate P-E hysteresis loop characteristic of the two phases, namely a double hysteresis loop with a marked remanent polarization, was observed.

The hysteresis loops of Rainbow 66/24/10S and the corresponding normal sample are shown in Figure 6. Because the composition is well inside the AFE phase region, a typical double hysteresis loop with no remanent polarization is seen for the normal sample. The marginal remanent polarization observed in the Rainbow was probably caused by the internal stress, which will be discussed later.

Figure 7 shows the variation of axial displacement with electric field for Rainbows 64/26/10HP and 66/24/10S-1. A displacement as large as 273 μm was obtained from Rainbow 64/26/10HP as a result of the AFE-FE phase switching. The remanent displacement is attributable to the remanent polarization as shown in Figure 5(a). Rainbow 66/24/10S-1 also exhibited a large

axial displacement due to the phase switching but little remanent displacement was found to exist. The step-like displacement-field relationship of Rainbow 66/24/10S-1 was similar to that of the normal sample as shown in Figure 8.

The polarization-electric field and axial displacement-electric field relationships of Rainbow 66/23/11HP are shown in Figure 9. Of the samples studied, this sample is nearest the FE phase region. As can be seen in the figure, Rainbow 66/23/11HP is antiferroelectric in the virgin state, but stabilized in the ferroelectric state after being switched by the applied electric field. A large displacement, approximately 145 μm , was produced during the initial AFE to FE phase switching. The reorientation of ferroelectric domains after the initial switching led to a butterfly-like loop of typical ferroelectrics, and moderate changes in the displacement.

Tables 2 and 3 summarize the results obtained from the PSZT Rainbows and the normal samples, respectively. The Rainbow samples in general possessed a lower dielectric constant and a higher loss factor than the normal samples. The phase switching fields, E_{AF} and E_{FA} , of the Rainbow samples were lower than those of the normal ceramics, varying with composition. The saturated polarization, however, was similar in the Rainbows and the normal samples. The total field-induced axial displacement of the Rainbows due to the phase transitions varied from sample to sample and was in the range of 102 to 273 μm , depending on the geometry as well as the material properties of both the oxide and reduced layers. The largest displacement was found in Rainbow 64/26/10HP, which is equivalent to a 63% displacement relative to the total thickness of the sample.

The displacements obtained from the PSZT Rainbows were not as large as anticipated. In Rainbow ceramics the displacements are controlled by the transverse field-induced strains of the Rainbow oxide layer. Although the longitudinal strain in PSZT ceramics is particularly high, their transverse strains are only approximately 1/4-1/5 the longitudinal strain, which are close to those of the ferroelectric ceramics such as PLZT. The composition of PSZT 66/23/11, in which the highest strains known were reported in the literature, exhibited different characteristics from those

reported; i.e., the unusually high induced strains, as reported,⁵⁻⁶ were not reproduced in this study. Moreover, this composition, after subjected to a cyclic applied field, was stable in the ferroelectric state instead of the antiferroelectric state as described in the literature.

The effects of axial mechanical loading on the field-induced displacement and P-E hysteresis loops of Rainbow 66/24/10S-1 are shown in Figures 10-11 for loads applied to the surfaces of the oxide and reduced layers, respectively. The maximum displacement from each displacement-field loop was evaluated, and plotted against loading weight in Figure 12. Clearly, the displacements of the Rainbow depend on the manner in which load is applied. There is only a slight change in the maximum displacement up to 530 grams when load was placed on the oxide layer. The displacement with load on the reduced layer, however, decreased continuously with increasing load. In both cases, loading has no significant influence on the polarization-electric field hysteresis loop. In addition, both the AFE to FE and the FE to AFE phase transitions became more abrupt as the loading force was increased.

The different characteristics under the two loading conditions discussed above can be accounted for by the behavior of antiferroelastic domains under stress. Antiferroelastic domains tend to align with the directions in which stress is effectively relieved. When load is applied to the oxide layer of a Rainbow, antiferroelastic domains are aligned parallel to the Rainbow surfaces due to the compressive stresses in the planar directions. This is because that the lattice constant of the c-axis (domain direction) is smaller than that of the a-axis for the PSZT antiferroelectric phase.⁶ In contrast, when load is placed on the reduced layer, antiferroelastic domains are oriented vertical to the surfaces as a result of the tensile stresses. Figure 13 shows schematically the transverse dimensional change (which determines the field-induced displacement in Rainbows) of the oxide layer upon application of an electric field under different loading conditions. The loading conditions affect the displacement by altering the initial state of the oxide layer through stress-induced preferred domain alignment. It should be pointed out that the geometry stiffness and initial curvature of the Rainbow also influence the displacement during loading. The

combined effects of the geometry stiffness, curvature, and domain alignment lead to the behavior of the displacements shown in Figure 12. Because antiferroelastic domains are not polar, the domain alignment under stress will not affect the P-E hysteresis loop, which is in good agreement with the experimental results.

4.3 Curvature and Internal Stress of PSZT Rainbows

At room temperature, a Rainbow has a dome-shaped configuration due to the dimensional mismatch between the oxide and reduced layers. Accordingly, internal stress exists in the Rainbow. The contributions to the dimensional mismatch include: (1) the difference in thermal expansion coefficient between the oxide and reduced layers, (2) the dimensional change of the reduced layer due to oxygen (and possibly lead) loss, and (3) the dimensional change of the oxide layer resulting from phase transitions. Generally, Rainbows made of ferroelectric ceramics have positive curvature (reduced layer concave). It was found that all the PSZT Rainbows prepared in this study exhibited negative curvature (oxide layer concave). Negative curvature implies that the oxide layer is predominantly in tension. If the composition of a PSZT Rainbow is close to the AFE-FE phase boundary, the tensile stress is sufficient to induce the antiferroelectric to ferroelectric phase change. The net polarization observed in virgin Rainbow 64/26/10HP and the reduction of the AFE-FE switching fields in the PSZT Rainbows are probably consequences of the tensile stress.

The data shown in Figures 14(a)-(b) indicate that the negative curvature in the PSZT Rainbows is attributable to the cubic-to-AFE phase transition at which the unit cell volume of the PSZT ceramics is reduced. The bending deflection, h , is defined as the axial deflection of a Rainbow with respect to the unreduced wafer, see the graph inserted in Figure 14(b). A positive bending deflection corresponds to positive curvature. As is shown in Figure 14(a), the curvature of Rainbow 66/23/11HP was changed from negative to positive after the Rainbow was subjected to an applied electric field, which indicates that the FE and AFE states are responsible for the positive and negative curvatures respectively. As the temperature was increased, the positive

curvature of the Rainbow changed back to a negative value at the FE-AFE phase transition, $T_{\text{FE-AFE}}$. The curvature remained negative within the AFE phase range and became positive again near the Curie point. The reduction of temperature brought the sample back to the original antiferroelectric state (negative curvature). Figure 14(b) shows the same relationship for Rainbow 62/28/10S. A change from negative to positive curvature was found near the temperature of the AFE-to-cubic phase transition. Figure 15 indicates that the phase transitions shown in Figure 14 are identical to those obtained from the temperature dependence of dielectric constant.

4. Conclusion

The fabrication and properties of PSZT antiferroelectric Rainbow actuators have been investigated. The reduction reaction in PSZT ceramics proceeds much more rapidly than in PLZT ceramics. The optimal reduction conditions for the fabrication of PSZT Rainbows are 850 °C for 2 - 3 hours. The antiferroelectric-ferroelectric phase transitions occur at a lower field strength in Rainbows as compared to normal samples. Large axial displacements in a range of 102 to 273 μm were obtained from the Rainbow samples by application of electric fields exceeding the phase switching levels. The field-induced displacements of the PSZT Rainbows are dependent on the manner of applying load to the samples. When load is placed on the oxide layer, there is only a slight change in the displacements for loads up to 530 grams. The displacement with load on the reduced layer, however, decreases continuously with increasing load. Antiferroelectric PSZT Rainbows generally have negative curvature at room temperature due mainly to the paraelectric to antiferroelectric phase transition in the oxide layer during cooling. The changes of material properties of PSZT Rainbows with respect to normal ceramics are associated with the internal stress resulting from the processing.

5. References

1. G. H. Haertling, *Am. Ceram. Soc. Bull.*, **73**(1), 93 (1994).
2. G. H. Haertling, *Ferroelectrics*, **154**, 101 (1994).
3. E. Furman, G. Li and G. H. Haertling, *Ferroelectrics*, **160**, 357 (1994).
4. D. Berlincourt and H. H. Krueger, *Research on Piezoelectric Materials and Phenomena*, an Annual Progress Report from Clevite Corporation, Cleveland, Ohio (1964).
5. W. Pan, C. Q. Dam, Q. M. Zhang and L. E. Cross, *J. Appl. Phys.*, **66**(12), 6014 (1989).
6. L. Shebanov, M Kusnetsov and A. Sterberg, *J. Appl. Phys.*, **76**(7), 4301 (1994).
7. A. Furuta, K. Oh and K. Uchino, *Sensors and Materials*, **3-4**, 205 (1992).
8. D. Berlincourt, H. H. Krueger and B. Jaffe, *J. Phys. Chem. Solids*, **25**, 659 (1964).
9. K. Uchino, *Am. Ceram. Soc. Bull.*, **65**(4), 647 (1986).
10. G. H. Haertling, *Proceedings of the Ninth International Symposium on Applications of Ferroelectrics-ISAFE'94*, (1994), to be published.

Table 1. Identification of PSZT Rainbow samples.

Rainbow Sample	Diameter (cm)	Oxide/Reduced (μm)
66/23/11 _{HP}	2.72	302/135
64/26/10 _{HP}	2.72	294/135
64/26/10 _S	2.16	378/140
66/23/11 _S	2.16	271/190
66/24/10 _S -1	2.72	334/165
66/24/10 _S -2	2.16	400/115
62/28/10 _S	2.16	195/165

HP=Hot Pressed

S=Sintered

Table 2. Properties of PSZT Rainbow samples.

Rainbow Sample	Dielectric Constant	$\tan\delta$ (%)	E_{AF}/E_{FA} (kV/cm)	P_S or P_R ($\mu\text{C}/\text{cm}^2$)	D_M (μm)	S_M (%)
66/23/11 _{HP}	796	2.2	7.5 (E_C)	35	195*	45
64/26/10 _{HP}	730	3.4	19.5/-4.0	33	273	63
64/26/10 _S	821	3.9	16.5/-3.0	30	187	37
66/23/11 _S	734	3.1	7.0 (E_C)	31	102*	22
66/24/10 _S -1	626	5.4	28.5/10.0	31	208	42
66/24/10 _S -2	735	5.1	26.5/4.5	32	150	29
62/28/10 _S	826	2.3	27.5/6.5	31	110	31

Table 3. Properties of PSZT normal (non-Rainbow) ceramics.

Normal PSZT	Dielectric Constant	$\tan\delta$ (%)	Density (g/cm^3)	E_{AF}/E_{FA} (kV/cm)	P_S or P_R ($\mu\text{C}/\text{cm}^2$)	$S_{2,S}$ ($\times 10^4$)	$S_{1,S}$ ($\times 10^4$)
66/23/11 _{HP}	810	2.3	8.11	7.0 (E_C)	35	5.5	45.2*
64/26/10 _{HP}	876	1.6	8.22	23/-2.0	36	6.8	29.5
64/26/10 _S	913	1.9	8.05	28/1.0	31	7.9	28.0
66/24/10 _S	990	1.2	7.93	30/11.5	31	8.2	45.3
62/28/10 _S	882	1.9	7.97	30/9.5	32	8.5	45.7

E_{AF} = Antiferroelectric to ferroelectric switching field.

E_{FA} = Ferroelectric to antiferroelectric switching field.

P_S = Saturated polarization.

P_R = Remanent polarization.

E_C = Coercive field of ferroelectric phase.

D_M = Maximum axial displacement with an applied electric field of $1.2 \times E_{AF}$.

S_M = Maximum axial displacement (D_M) divided by Rainbow thickness.

$S_{2,S}$ = Transverse field-induced strain.

$S_{1,S}$ = Longitudinal field-induced strain.

* obtained from initial phase switching.

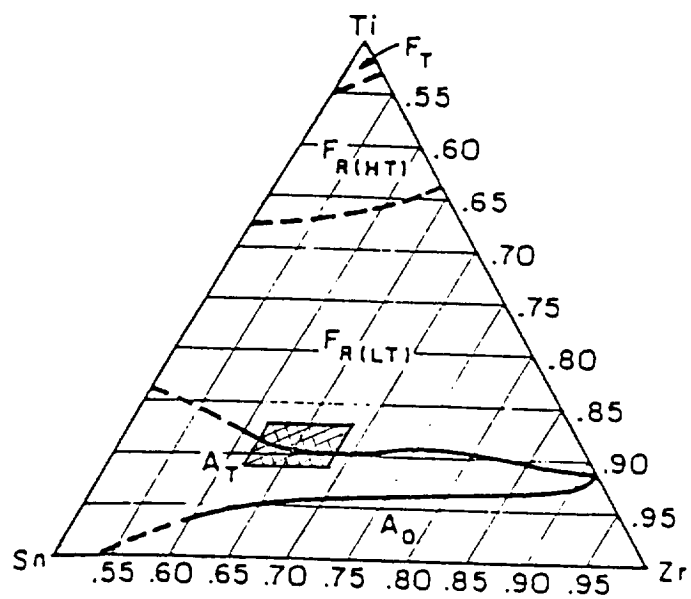


Figure 1. Phase diagram of PSZT ceramic system.⁵

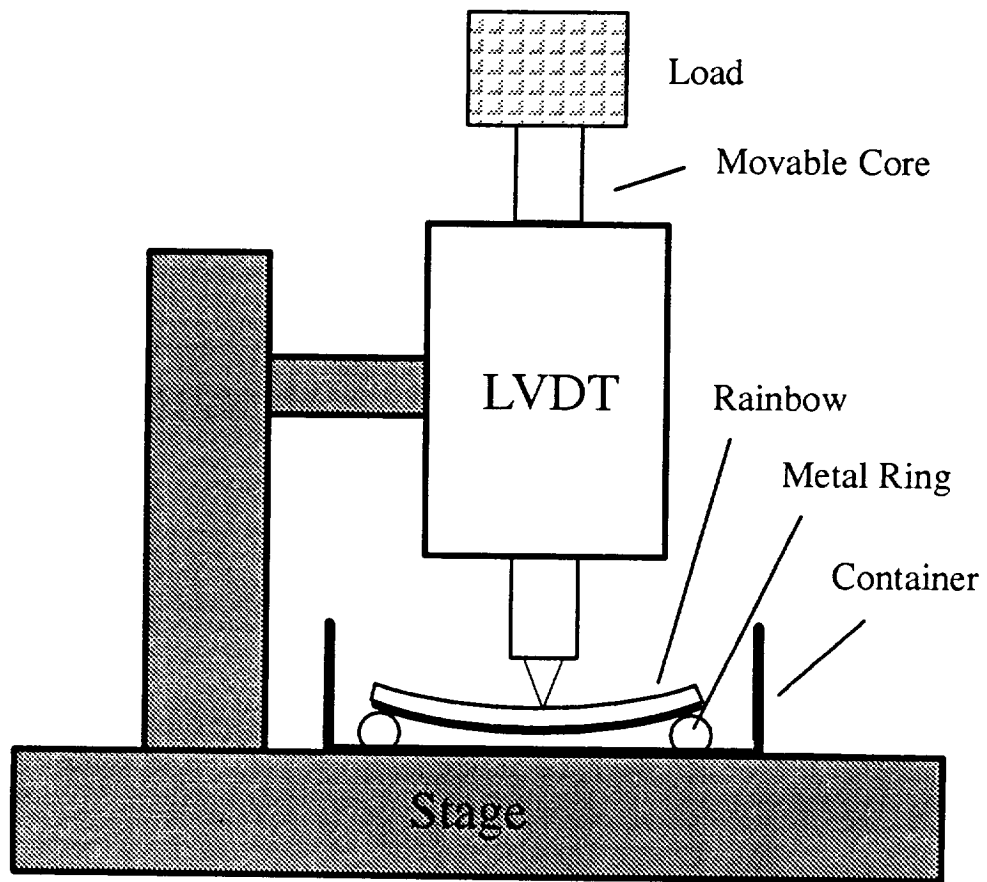


Figure 2. Schematic of apparatus for displacement measurement.

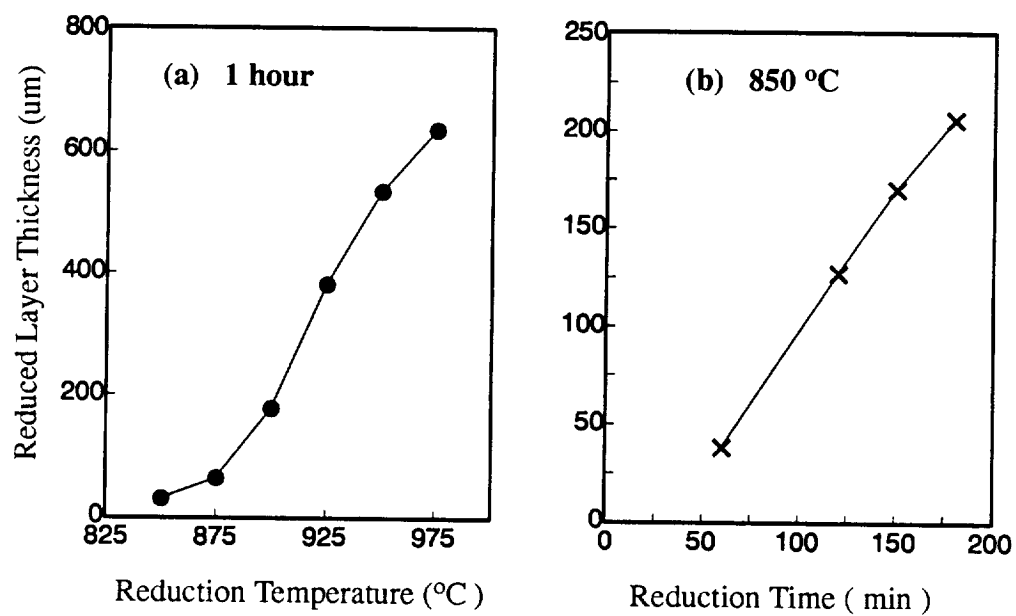


Figure 3. Variation of reduced layer thickness with (a) temperature and (b) time for Rainbow 64/26/10HP.

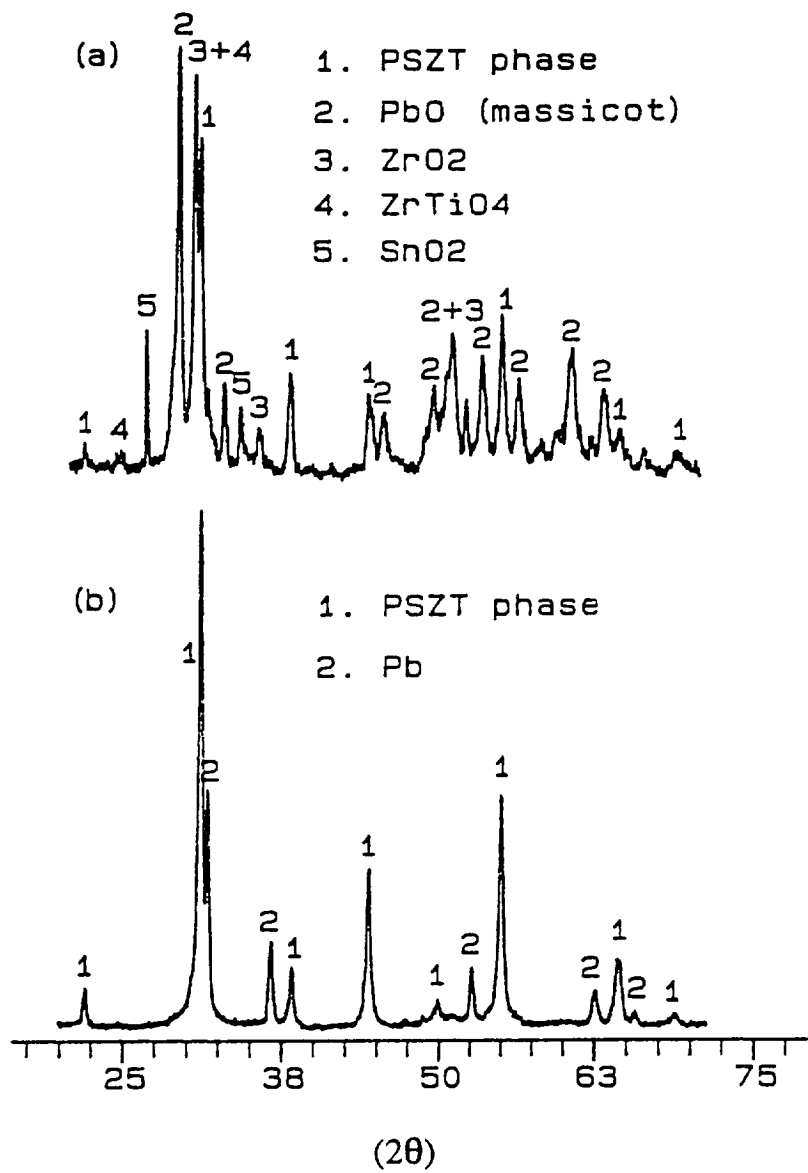


Figure 4. X-ray diffraction patterns of PSZT 64/26/10 ceramics reduced at (a) 975 °C and (b) 850 °C.

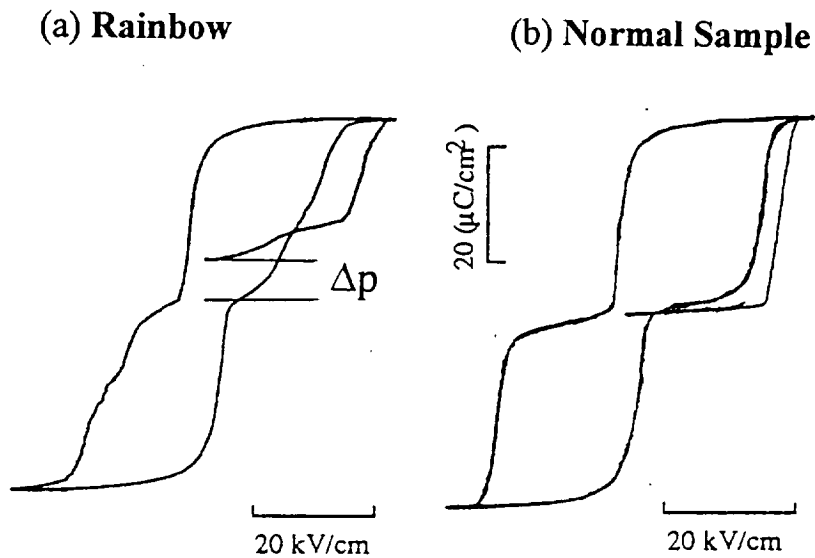


Figure 5. Polarization-electric field hysteresis loops of (a) Rainbow 64/26/10HP and (b) normal PSZT 64/26/10HP.

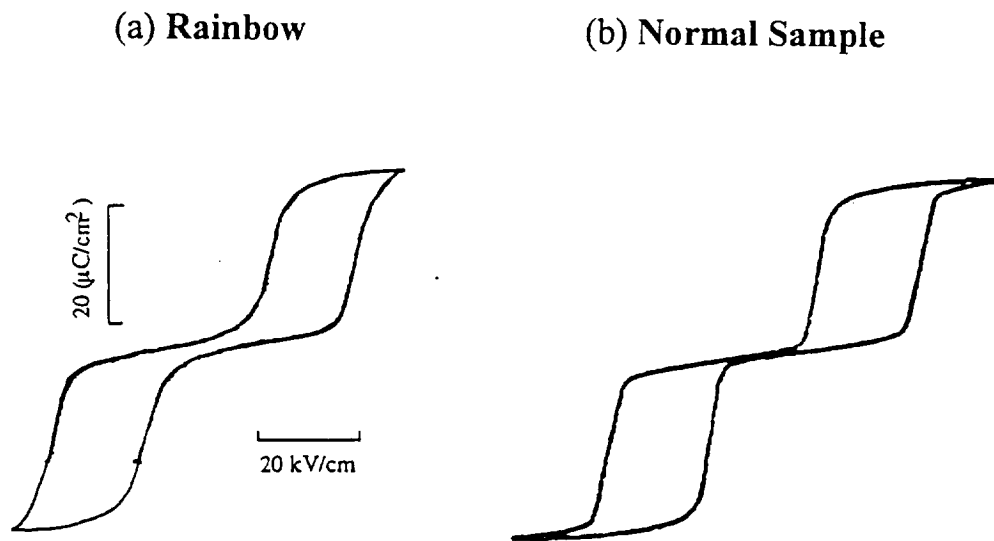


Figure 6. Polarization-electric field hysteresis loops of (a) Rainbow 66/24/10S-1 and (b) normal PSZT 66/24/10S.

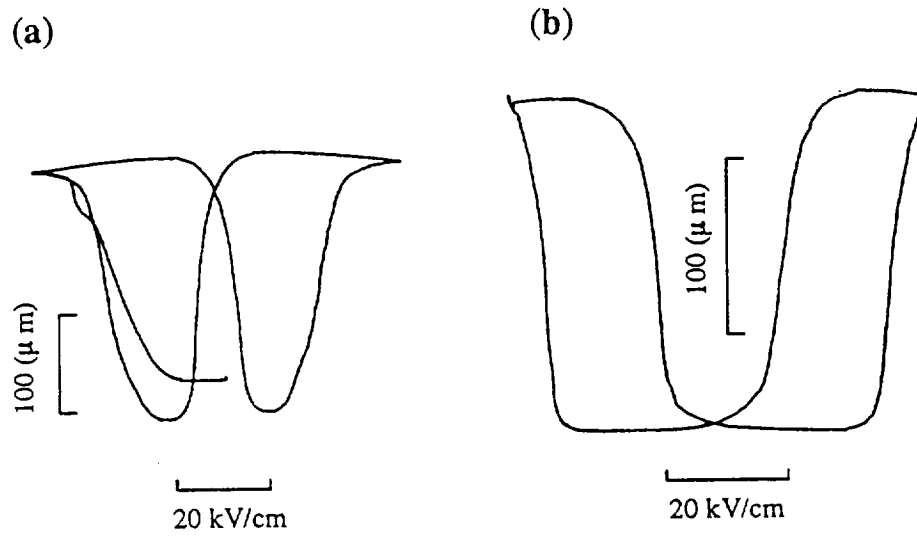


Figure 7. Change of axial displacement with electric field for (a) Rainbow 64/26/10HP and (b) Rainbow 66/24/10S-1.

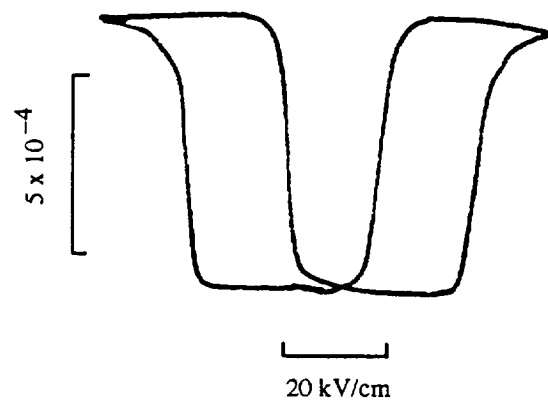


Figure 8. Change of lateral dimension of PSZT 66/24/10S ceramic with electric field.

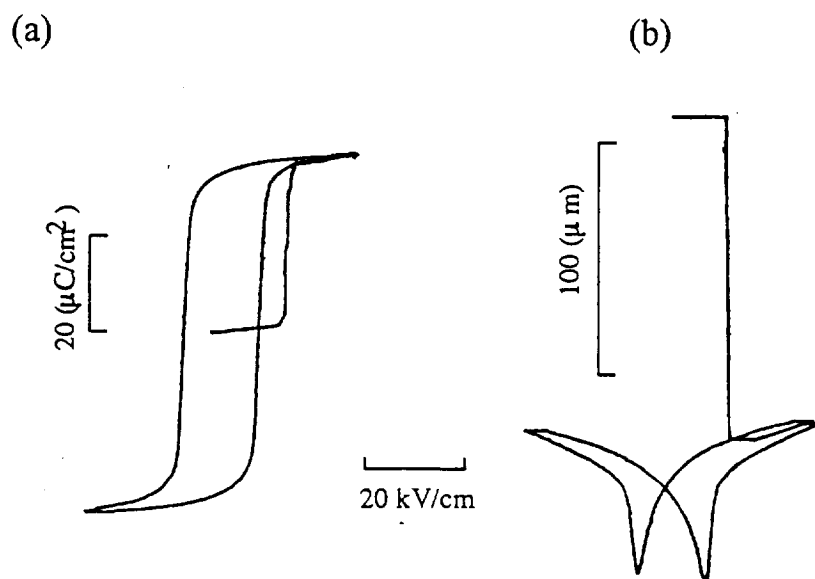


Figure 9. Variations of (a) axial displacement and (b) polarization with electric field for Rainbow 66/23/11HP.

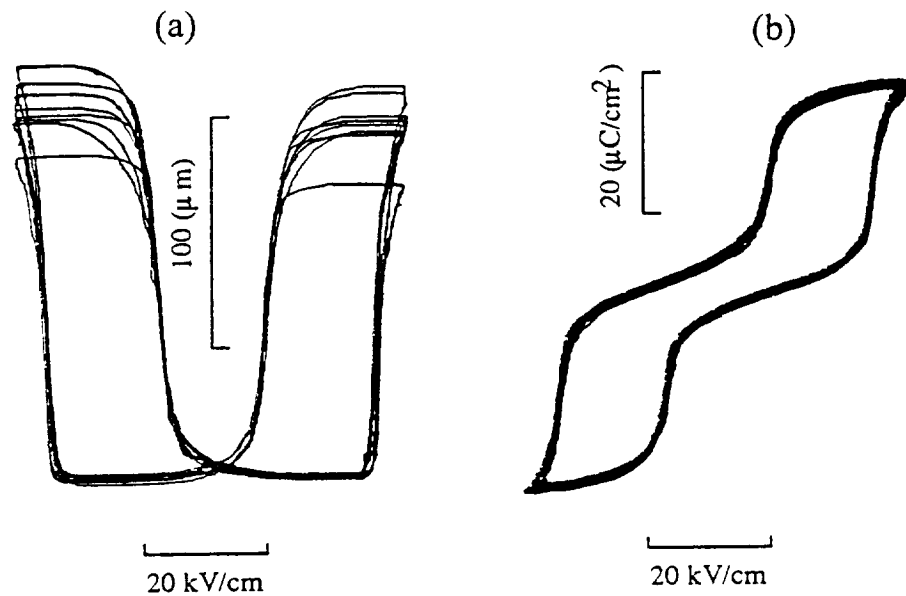


Figure 10. Influence of axial mechanical loading on (a) field-induced axial displacement and (b) hysteresis loop of Rainbow 66/24/10S-1 for loads on the oxide layer.

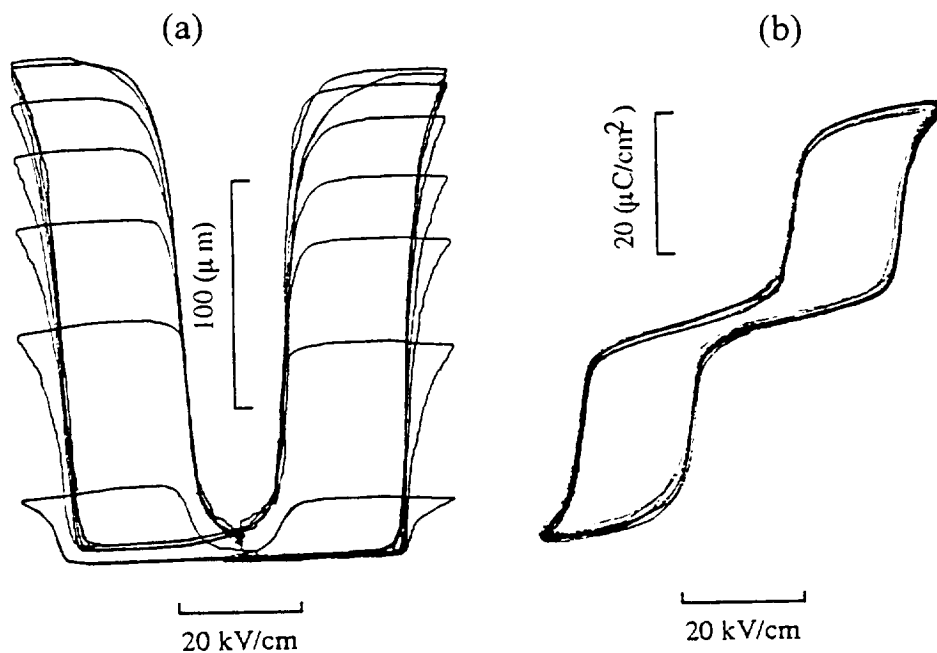


Figure 11. Influence of axial mechanical loading on (a) field-induced axial displacement and (b) hysteresis loop of Rainbow 66/24/10S-1 for loads on the reduced layer.

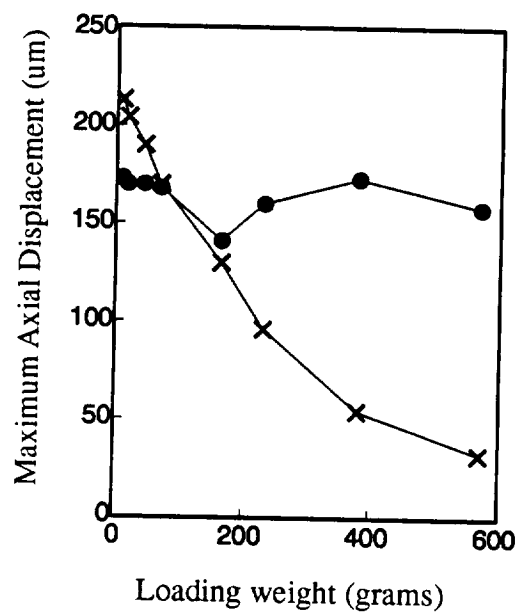


Figure 12. Variation of maximum axial displacement with loading weight for Rainbow 66/24/10s-1. ● for load on the oxide layer, ✕ load on the reduced layer.

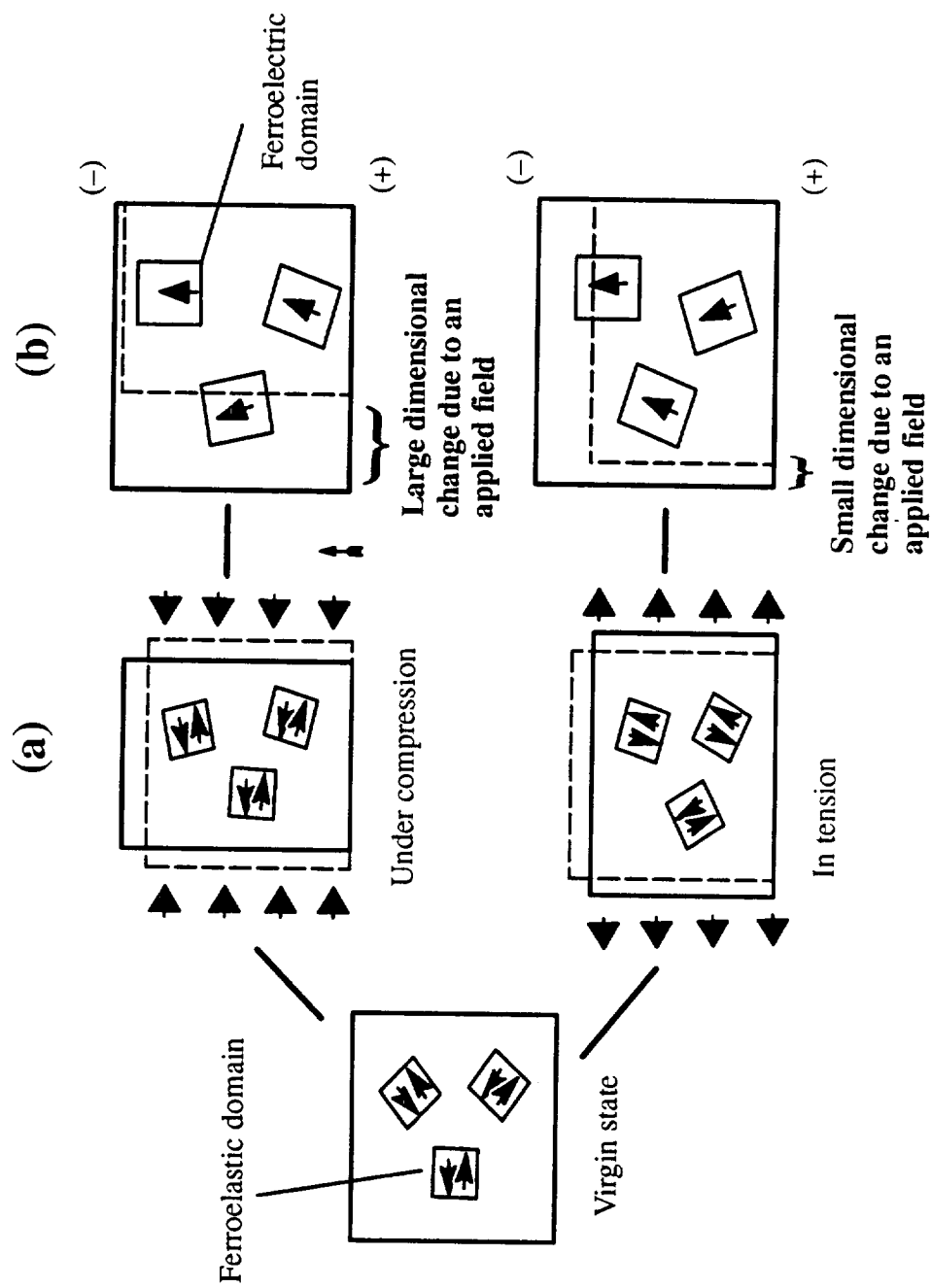


Figure 13. Schematic diagram of the dimensional changes of the oxide layer due to stress and electric field. Dashed lines represent unit cell in (a) and (b) prior to the application of mechanical loading and electric field, respectively.

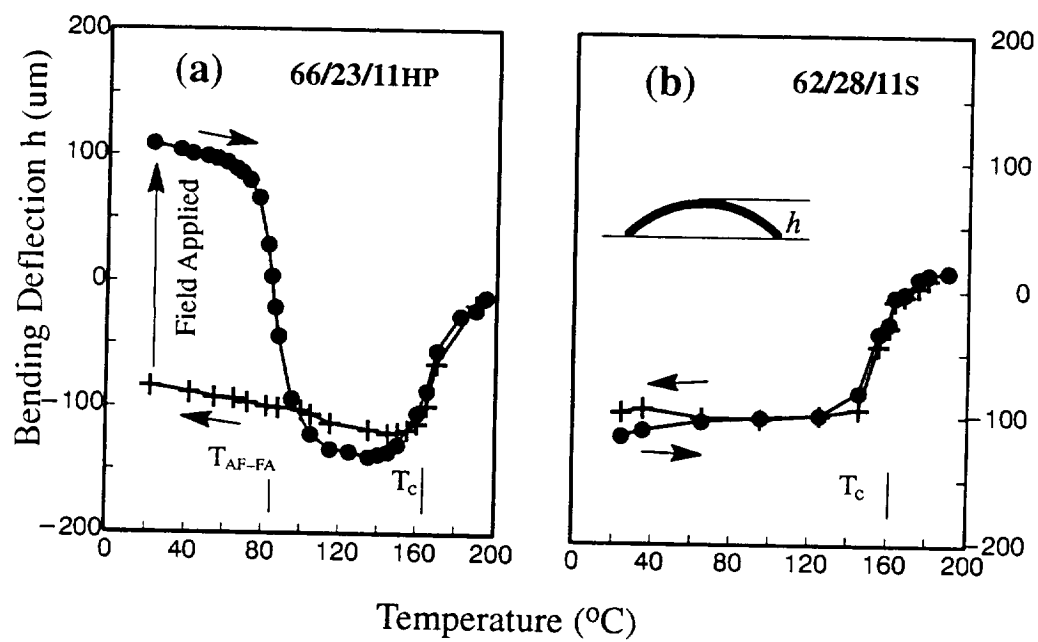


Figure 14. Changes of bending deflection, h , with temperature for (a) Rainbow 66/23/11HP and (b) Rainbow 62/28/10s.

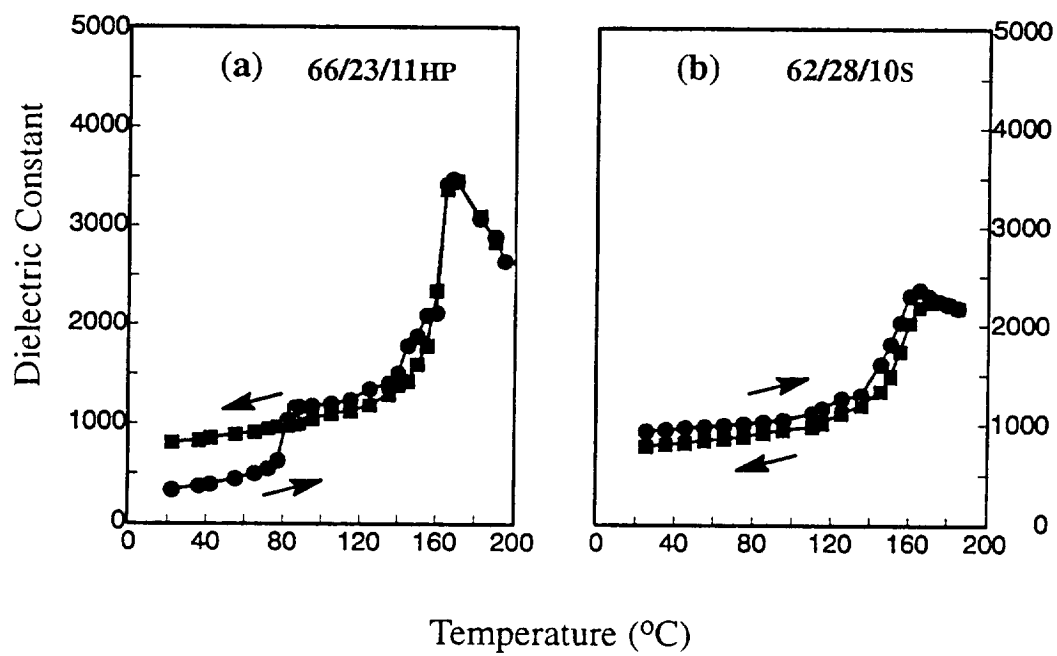


Figure 15. Temperature dependence of dielectric constant for the PSZT ceramics identified.

Part II.

Stress-Enhanced Displacements in PLZT Rainbow Actuators

Stress-Enhanced Displacements in PLZT Rainbow Actuators

Abstract: The effects of stress-enhanced domain reorientation on the displacements from PLZT Rainbow actuators were studied. Finite element modeling was used to analyze the bending and internal stress of the Rainbows. The measured bending deflections were consistent with the modeling data. The stress distribution revealed by the X-ray diffraction studies agreed well with the modeling. Enhanced domain reorientation by the internal stress was observed from the behavior of the XRD peaks under the influence of electric field. The maximum stress-enhanced domain reorientation was found at the reduced/total thickness ratios where field-induced displacements were maximized. The result indicates that the stress-enhanced domain reorientation is an important contribution to the field-induced displacements in Rainbow actuators

1. Introduction

A new type of ceramic actuator - RAINBOW (Reduced And INternally Biased Oxide Wafer), has recently been developed, which shows promising characteristics in a variety of potential applications.¹ A Rainbow is produced by chemically reducing one major surface of a high-lead containing ferroelectric which is placed on a graphite block and heat treated at an elevated temperature. When the Rainbow is cooled to room temperature, a dome-like pre-stressed oxide/reduced layer configuration is created. One useful feature of Rainbow actuators is their strain amplifying effect which leads to very high electric field-induced displacements from piezoelectric and electrostrictive materials. Although a Rainbow is similar in operation to the conventional unimorph type benders in which displacements are controlled by transverse piezoelectric or electrostrictive coefficients, it is considered that other mechanisms such as enhanced domain reorientation and enhanced phase transition may contribute to the strain amplifying effect owing to the unique structure of the Rainbow.²

A Rainbow develops significant curvature and bending deflection due to the dimensional mismatch between the oxide and reduced layers at room temperature. Accordingly, there exists a

nonuniform high-stress field within the Rainbow. One of the fundamental differences between a Rainbow actuator and a unimorph bender is the internal stress in the Rainbow. Results of this work indicate that the electric field-induced displacements from Rainbow actuators are enhanced by interaction of ferroelectric domains with the internal stress.

Because the bending deflection in a Rainbow is generally so large that it is beyond the limit of linear (small deflection) theory of thin plates, finite element modeling (FEM) was used for analysis of the internal stress distribution. The nature of the stress at the oxide layer surface of a Rainbow was studied with an X-ray diffraction technique. The contribution of stress-enhanced domain reorientation to the field-induced displacements was determined from the changes of X-ray diffraction peaks during application of electric field. The influence of the internal stress on the properties of Rainbow ceramics, such as dielectric constant and piezoelectric coefficient d_{33} , was observed.

2. Finite Element Modeling

The dimensional mismatch between the oxide and reduced layers results in the bending and nonuniform internal stress of a Rainbow. In this paper, the axial deflection of a Rainbow relative to its edge due to the bending during cool down is called bending deflection while the axial deflection induced by electric field is referred to as field-induced displacement or simply displacement. If the bending deflection is larger than one-half of the thickness of the Rainbow, linear bending theory of thin plates will cause considerable errors.³ In reality, Rainbow ceramics generally exhibit bending deflections considerably larger than their thicknesses; therefore, nonlinear (large deflection) bending theory must be used. Unfortunately, the exact solutions of the equations from the nonlinear theory are generally unknown. Approximate solutions are available only for simple situations.

In this study finite element modeling based on a commercial package ABAQUS (Hibitt, Karlsson & Sorenson, Inc., version 5.3) was used to analyze the bending and internal stress as well as field-induced displacement. Table 1 lists the sample dimensions and material parameters

which were used in the modeling. Effective thermal expansion coefficients were used to account for all the mechanisms that cause the dimensional mismatch between the oxide and reduced layers. The detailed procedures of the finite element modeling will be given elsewhere.

Figure 1 shows the dome-mode configuration of a Rainbow obtained from 3-dimensional modeling. Since the dome mode has axial symmetry, the bending can also be modeled with the 2-dimensional, axisymmetric elements. Figure 2 illustrates the cross-sections of one-half of an unreduced wafer and the corresponding Rainbow derived from the 2-dimensional modeling. The important stress component for a Rainbow is the planar stress S_{rr} in the radial direction, for example, 1-direction in Figure 1. The following results were based on the 2-dimensional modeling.

Figure 3 shows the bending deflection as a function of the ratio of the reduced layer thickness to the total thickness (hereafter referred to as the thickness ratio). The values of 0 and 1 for the thickness ratio correspond to unreduced and fully reduced wafers, respectively. The designations, RB1053 and RB5553, were used to represent Rainbows made from PLZT 1.0/53/47 and PLZT 5.5/53/47 ceramics, respectively. As can be seen in Figure 3, the bending deflection changes drastically when the thickness ratio is either small or close to 1, and there is a broad maximum at the thickness ratio of approximately 0.5. The field-induced displacement exhibits a similar dependence on the thickness ratio as shown in Figure 4; however, the broad maximum is shifted to the thickness ratio of 0.6.

The distribution of the planar stress S_{rr} through thickness at the different locations is shown in Figure 5 for an RB1053 of the thickness ratio equal to 1/3. While the whole reduced layer is in tension, the upper portion of the oxide layer is in tension and the lower portion is under compression.

The change of the planar stress S_{rr} with the thickness ratio at the different locations on the oxide layer surface of an RB1053 is shown in Figure 6. The results indicate that the entire oxide layer is under compressive stress when the thickness ratio is greater than 0.7. Relationships similar to Figure 6 occur in RB5553.

The distribution of the stress S_{II} across the oxide layer surface is shown in Figure 7 for RB1053 with different thickness ratios. As can be seen, the entire surface is in tension when the thickness ratio is equal to 0.3, which is typical of a Rainbow with a thick oxide layer. In contrast, when the thickness ratio is equal to 0.8, which corresponds to a Rainbow with a thin oxide layer, the whole surface is under compression. When the thickness ratio is equal to 0.6, the oxide layer surface is partially in tension and partially under compression. The abrupt change of the stress near the Rainbow edge is caused by the mechanical boundary conditions at the edge.

3. Sample Preparation

The PLZT ceramics used for the production of the Rainbow samples were prepared via the mixed oxide process. Compositions 1.0/53/47 and 5.5/53/47 (La/Zr/Ti) were batched and then mixed in water for 30 min. Calcining was performed at 925 °C for 2 hours, and milling was carried out in an alumina ball mill with trichloroethylene. Sample pellets were sintered at 1250 °C for 4 hours or hot pressed at 1200 °C for 6 hours at 14 MPa in an oxygen atmosphere. The densities of the sintered ceramics were in the range from 7.65 to 7.80 g/cm³ and those of the hot-pressed ceramics were approximately 7.95 g/cm³.

The Rainbow samples were produced from lapped wafers by placing the wafers on a graphite block and chemically reducing them at 925-975 °C for 10-240 min. The different reduction conditions were used to achieve a series of samples with different thickness ratios. After cooling down to room temperature, the samples were sanded lightly on the reduced side to remove any metallic lead and to expose the reduced layer. The samples were also sanded along their edge to remove any reoxidized portions in the reduced layers which occurred during the cool down. The dimensions of the Rainbows made from the sintered ceramics were 2.24 cm in diameter and 0.0432 cm in thickness whereas those of the hot-pressed Rainbows were 2.92 cm in diameter and 0.0508 cm in thickness. Epoxy silver electrodes cured at 200 °C were used for test and evaluation of the samples.

4. Measurements

Domain orientation on the oxide layer surface of a Rainbow was examined with an X-ray diffractometer (Scintag XDS 2000TM) using Ni-filtered Cu $K\alpha$ radiation at a scan rate of 2 degrees per minute. The intensities of the diffraction peaks were determined using the Gaussian profile fitting. In examination of domain reorientation under the influence of applied electric fields, thin aluminum electrodes, which can be penetrated by X-ray beams, were deposited on the Rainbows in a vacuum chamber. Room temperature dielectric properties of the samples were determined at 1 kHz using an LCR meter (LEADER, 7450-01). Piezoelectric coefficient d_{33} was measured with a piezo d_{33} tester (Pennbaker Model 8000). Conventional dc hysteresis loop equipment was employed to determine the relationship between polarization and electric field. An apparatus containing an LVDT (Linear Variable Differential Transformer, 050 DC-E Lucas Schaeritz Co.) was used to measure the bending deflection and field-induced displacements. The thickness ratios were determined from the cross-sections of the Rainbows under an optical microscope, or from the coercive fields of the Rainbows with assumption that Rainbows and normal (non-Rainbow) materials have an identical coercive field. Good agreement between the two types of measurements was obtained.

5. Experimental Results

A comparison of the measured bending deflections with the FEM results for RB1053 and RB5553 with different thickness ratios are given in Figures 8 and 9, respectively. The experimental data for RB1053 are generally in agreement with the modeling. The deviation from the modeling for larger thickness ratios may result from stress-induced preferred domain orientation which leads to reduced bending curvature. Agreement between the experiment and modeling for RB5553 seems excellent in the entire range of the thickness ratio. This is surprising because, similar to RB1053, a difference between the experiment and modeling was expected due to the preferred domain orientation. It should be pointed out, however, that since the effective

thermal expansion coefficients used in the modeling are not precisely known, the values of the bending deflection from the modeling for RB5553 may have considerable errors.

Both the PLZT 1.0/53/47 and PLZT 5.5/53/47 ceramics exhibited a tetragonal structure, though mixed structures (tetragonal and rhombohedral) were observed in the hot-pressed PLZT 1.0/53/47. The nature of the planar stress in the proximity of the Rainbow surface was studied by examining the intensity ratio of the (200) and (002) X-ray diffraction peaks. Figure 10 shows the intensity ratio of the (200)/(002) diffractions, which were obtained from the center portion of a sample, as a function of the thickness ratio for Rainbows and normal (thickness ratio=0) samples. The diffraction profiles for selected samples of different thickness ratios are displayed in Figure 11. Theoretically, the intensity ratio is equal to 2 for a virgin, stress-free, normal sample. A value slightly greater than 2 was observed for the normal samples of both PLZT 1.0/53/47 and PLZT 5.5/53/47. The intensity ratio will be greater or smaller than 2 when a sample is subjected to a tensile or compressive stress in the planar directions. The data shown in Figure 10 are in good agreement with the stress distribution derived from the FEM (Figure 6). That is, the tensile and compressive stresses correspond, respectively, to the intensity ratios greater and smaller than 2.

The initial, switching, and unipolar field-induced displacements, which are defined from the displacement-electric field relationship in Figure 12, are plotted in Figure 13 against the thickness ratio. The three types of displacements reach a maximum in the vicinity of the thickness ratio of 0.3 for both RB1053 and RB5553. The thickness ratios corresponding to the maximum unipolar displacements are apparently different than that predicted by the modeling (Figure 4). It is, however, noted that the displacement maxima are consistent with the maximum of the tensile stress on the Rainbow surface (Figure 6). This suggests that the displacement maxima are very likely associated with stress-enhanced domain reorientation.

Figure 14 shows the variation of the intensity ratio of the (200)/(002) peaks with unipolar applied field for a normal PLZT 1.0/53/47 sample and Rainbows with different thickness ratios. The change in the intensity ratio is associated with the amount of 90° domain reorientation. From the average slope of each loop in Figure 14, it is evident that more 90° domain reorientation was

involved for those Rainbows possessing higher displacements. Similar effects were also observed in RB5553 (Figure 15) and hot-pressed RB1053 (Figure 16). Some of the loops shown in Figures 15-17 have been deliberately shifted along the vertical axes for a clear comparison. It is not yet known if the absolute values of the intensity ratio are significant for Rainbows of different thickness ratios.

The variations of dielectric constant and piezoelectric constant d_{33} with the thickness ratio are shown in Figures 17-18, respectively. There is a marked reduction, particularly for RB1053, in both dielectric constant and piezoelectric constant at the thickness ratios where the surface stress is changed from tension to compression. It should be noted that, due to clamping effects by the reduced layer, the dielectric and piezoelectric constants of a Rainbow are distinguishable from those of the normal (thickness ratio=0) sample even if no internal stress exists.

6. Discussion

For the ordinary ferroelectric ceramics with tetragonal or rhombohedral structure, the major contributions to field-induced strains include the piezoelectric effect and domain reorientation which are usually referred to as the intrinsic and extrinsic piezoelectric effects in the literature, respectively. The extrinsic effect may contribute more than half of the total piezoelectric effect depending on the lattice structure and composition of a ceramic, as well as temperature.⁵⁻⁸ Extrinsic contributions, enhanced by prestressing a ceramic, were considered in the past as a means of obtaining a larger piezoelectric effect.⁹⁻¹⁰ For those Rainbows having a tensile stress in their oxide layer, domains in the tensile stress region tend to align parallel to the surface. When an electric field is applied across the oxide layer, these domains will be switched normal to the surface. As the applied field is reduced to zero, the domains will be switched back to the parallel direction under the influence of the tensile stress. These processes introduce additional contribution to the field-induced displacements in the Rainbow actuators. A Rainbow actuator provides an example of a stress-enhanced piezoelectric effect.

To obtain a significant result from the extrinsic contribution, (1) domain structures must be easily controlled by stress, and (2) the reorientation of domains must lead to significant strains. Compositions on the morphotropic phase boundary usually meet these requirements. This is probably one of the reasons why Rainbow actuators with compositions on the phase boundary produce considerably higher displacements than those of other compositions.² The displacements from the phase boundary compositions are also significantly higher than those predicted by modeling without considering the stress-enhanced effect as given in Figure 4 and Reference 11.

The contribution of field-enforced phase transitions to displacement for compositions in or near the morphotropic phase boundary was also studied by X-ray diffraction. A study on composition 1.0/53/47 showed no significant contribution from the field-enforced phase transition. It is possible to quantitatively estimate the contribution of the domain reorientation to field-induced displacements in Rainbow actuators by evaluating the degree of the domain reorientation in terms of the intensity ratio of XRD peaks. This work will be given in a future report.

7. Conclusion

Effects of stress-enhanced domain reorientation on the displacements from the Rainbow actuators made of PLZT 1.0/53/47 and PLZT 5.5/53/47 ceramics have been studied. Finite element modeling was used to analyze the internal stress distribution and field-induced displacements. The results of the finite element modeling indicate that the stress component in the radial direction of a Rainbow changes along the radius as well as through the thickness, which is typical of large-deflection bending. From the modeling, both the bending deflection and the displacement induced by a unipolar electric field are a maximum at the ratios of the reduced layer thickness to the total thickness equal to 0.5~0.6.

Stress in the Rainbows was revealed from the preferred domain orientation through examination of the intensity ratio of the (200)/(002) X-ray diffraction peaks. The stress

distributions deduced from the XRD studies agreed well with the modeling. The bending deflections from the experiment were basically consistent with the modeling data. Enhanced domain reorientation, which was related to the internal stress, was observed from the behavior of the XRD peaks under the influence of electric field. The maximum stress-enhanced domain reorientation was found at the thickness ratios where field-induced displacements were maximized. This result, combined with a significant difference in the displacement between the experiment and modeling, indicates that the stress-enhanced domain reorientation is an important contribution to the field-induced displacements in Rainbow actuators

8. References

1. G. H. Haertling, *Am. Ceram. Soc. Bull.*, **73**(1), 93 (1994).
2. G. H. Haertling, *Proceedings of the Ninth International Symposium on Applications of Ferroelectrics-ISAF'94*, (1994), to be published.
3. S. Timoshenko and S. Woinowsky-Krieger, *Theory of Plates and Shells*, Second Edition, McGraw-Hill Book Company, Inc., New York (1959).
4. D. Berlincourt, D. R. Curren and H. Jaffe, *Physical Acoustics*, vol.1, Part A, Academic Press, New York (1964).
5. Q. M. Zhang, H. Wang, N. Kim and L. E. Cross, *J. Appl. Phys.* **75**(1), 454 (1994).
6. S. Li, W. Cao, R. E. Newnham and L. E. Cross, *Ferroelectrics*, **139**, 25 (1993).
7. G. Arlt and N. A. Pertsev, *J. Appl. Phys.* **70**(4), 2283 (1991).
8. A. G. Luchaninov, L.Z. Potikha, and V. A. Rogozin, *Sov. Phys. Tech. Phys.*, **25**(3), 368 (1980).
9. H. H. A. Krueger and Don Berlincourt, *J. Acoust. Soc. Am.* **27**, 73 (1955).
10. H. H. A. Krueger, *J. Acoust. Soc. Am.* **42**(3), 636 (1967).
11. E. Furman, G. Li and G. H. Haertling, *Ferroelectrics*, **160**, 357 (1994).

Table 1. Material Parameters for Bending and Displacement Modeling.

Parameters for Modeling of Bending	
Diameter = 22.4 mm, Total Thickness = 0.432 mm	
Young's Modulus (RB1053) = 7.42×10^{10} N/m ² (oxide), 6.26×10^{10} N/m ² (reduced)	
Young's Modulus (RB5553) = 7.79×10^{10} N/m ² (oxide), 6.68×10^{10} N/m ² (reduced)	
Poisson's Ratio (RB1053) = 0.374 (oxide), 0.342 (reduced)	
Poisson's Ratio (RB5553) = 0.300 (oxide), 0.380 (reduced)	
Effective Thermal Expansion Coefficients = 0.5×10^{-5} (oxide) and 1.0×10^{-5} (reduced)	
Parameters for Modeling of Field-Induced Displacement*	
$c_{11}^E = 12.1 \times 10^{10}$ N/m ² , $c_{12}^E = 7.54 \times 10^{10}$ N/m ² , $c_{13}^E = 7.52 \times 10^{10}$ N/m ²	
$c_{33}^E = 11.1 \times 10^{10}$ N/m ² , $c_{44}^E = 2.11 \times 10^{10}$ N/m ²	
$d_{33} = 374 \times 10^{-12}$ C/N, $d_{31} = -271 \times 10^{-12}$ C/N, $d_{15} = 584 \times 10^{-12}$ C/N	
$\epsilon_{33}^T / \epsilon_0 = 1730$, $\epsilon_{11}^T / \epsilon_0 = 1700$	

Unless specified, the same parameters were used for modeling of RB1053 and RB5553. The parameters for the reduced layer are identical in the analyses of bending and displacement.

* All the parameters except for d_{31} are those from PZT-5.⁴

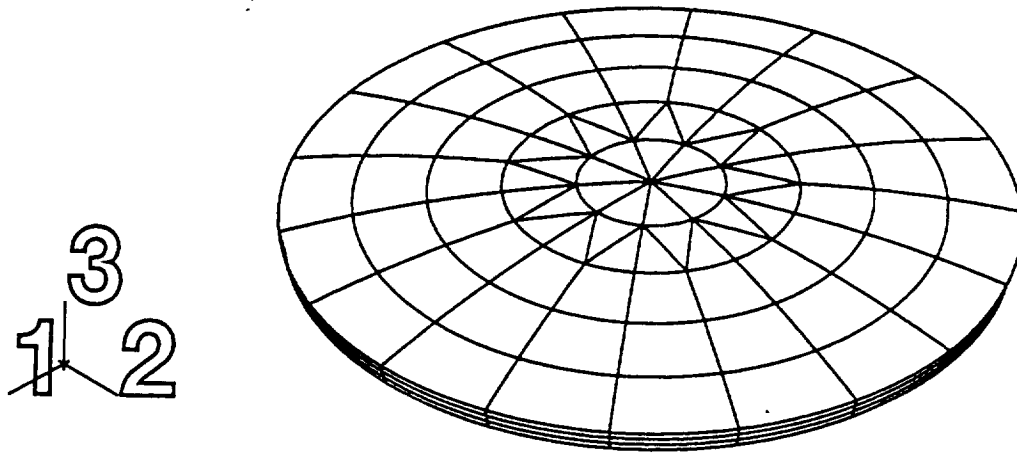


Figure 1. Dome-mode configuration of a Rainbow obtained from 3-dimension finite element modeling.

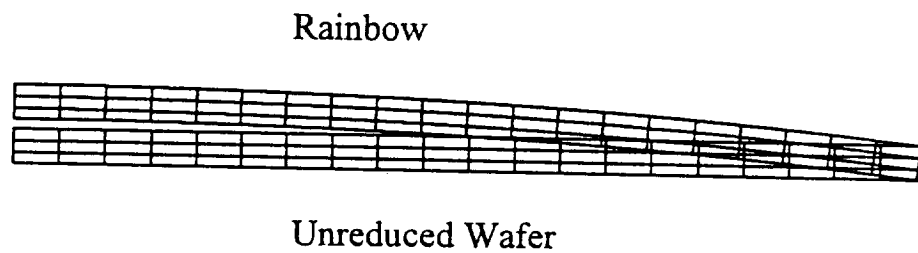


Figure 2. Cross section of one-half of an unreduced wafer and the corresponding Rainbow derived from axial symmetry modeling.

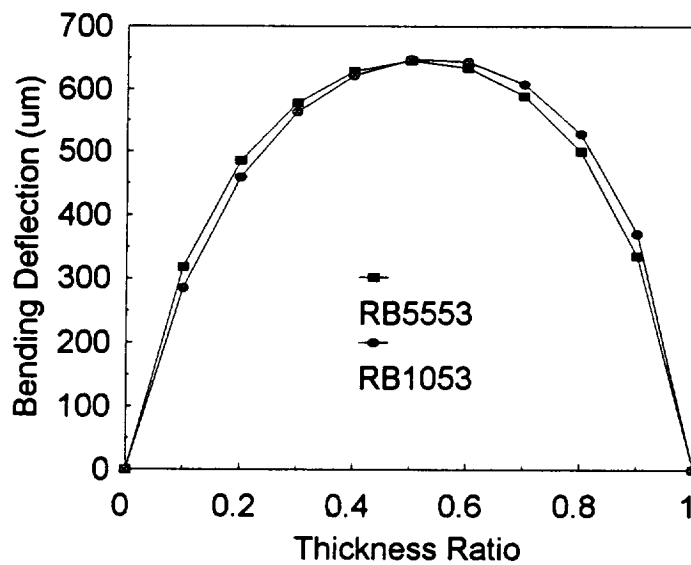


Figure 3. Dependence of bending deflection on thickness ratio derived from finite element modeling.

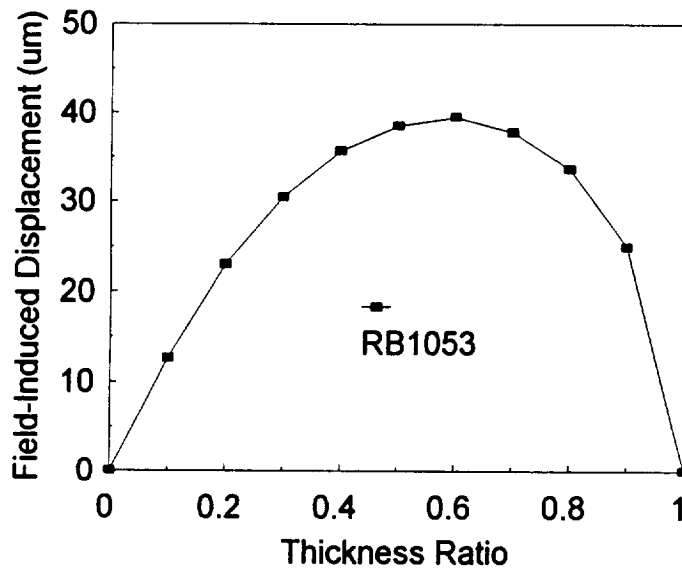


Figure 4. Field-induced displacement as a function of thickness ratio determined from FEM with an applied field of 16 kV/cm.

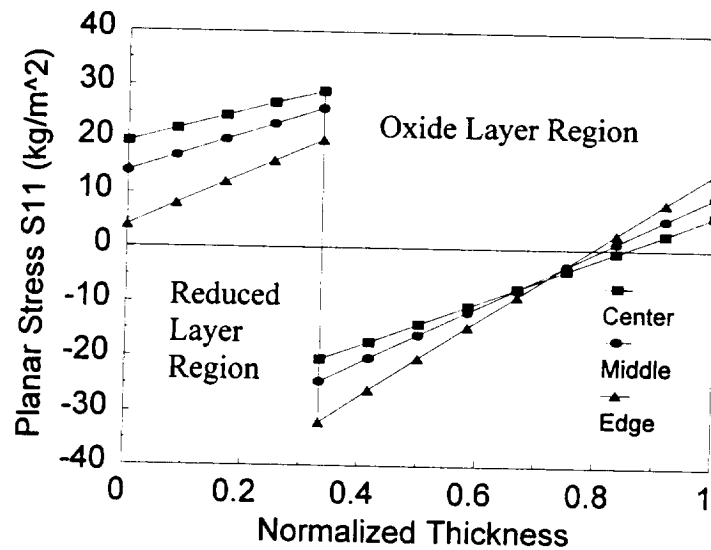


Figure 5. Distribution of planar stress S_{11} through thickness for RB1053 (the vertical axis is to be multiplied by 10^7). Center=the center of a Rainbow, Edge=the edge of a Rainbow, and Middle=halfway between the center and the edge. Negative values in the vertical axis represent compressive stress.

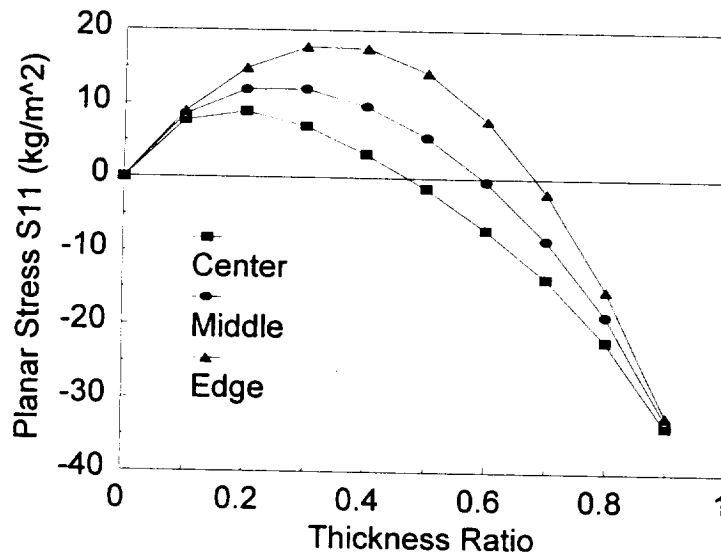


Figure 6. Change of planar stress S_{11} with thickness ratio for RB1053 (the vertical axis is to be multiplied by 10^7).

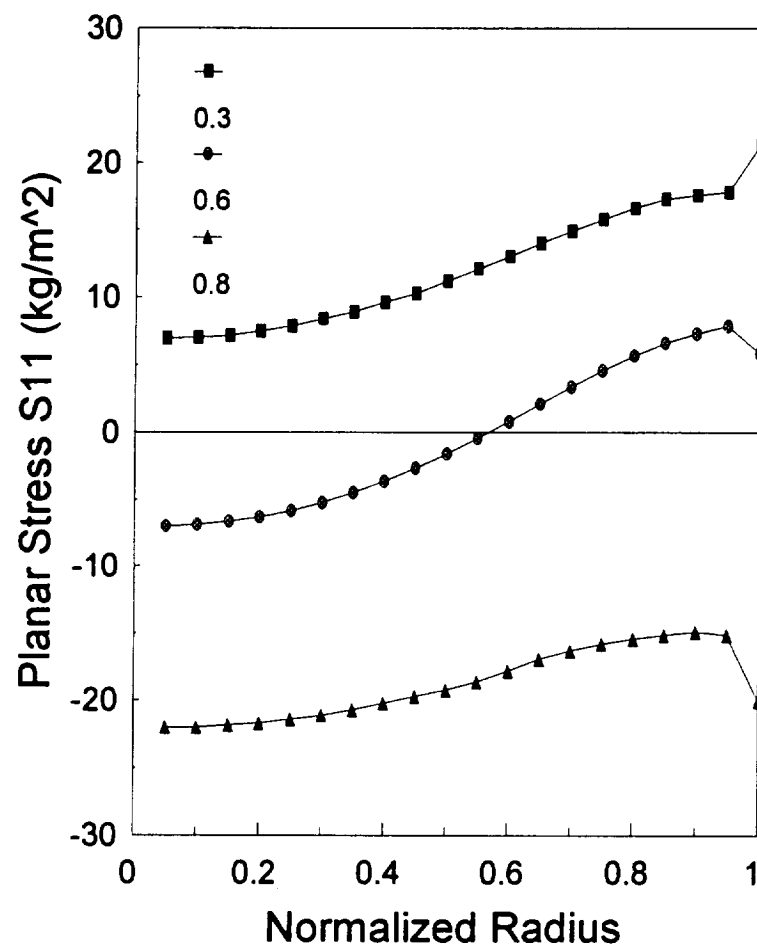


Figure 7. Variation of planar stress S11 with normalized radius for RB1053 at three different thickness ratios. The vertical axis is to be multiplied by 10^7 .

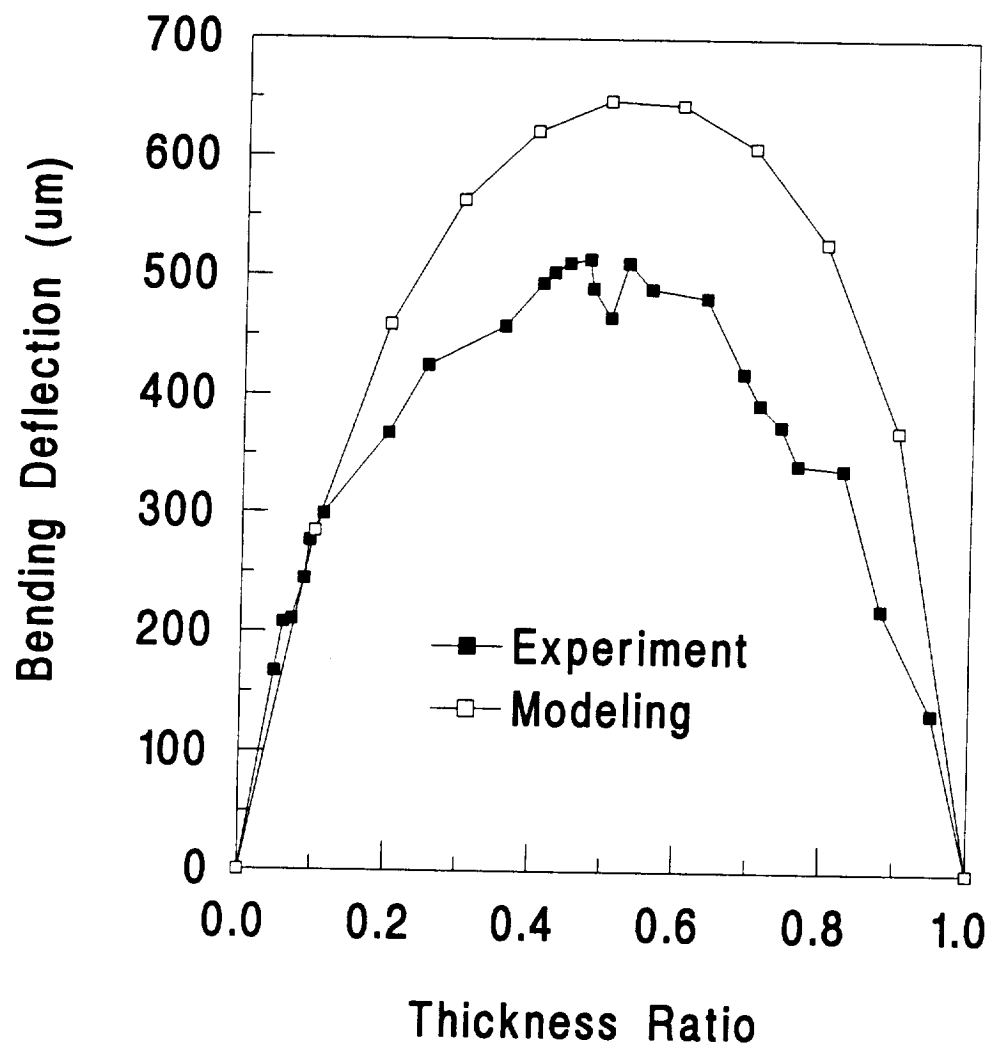


Figure 8. Variation of bending deflection with thickness ratio for RB1053.

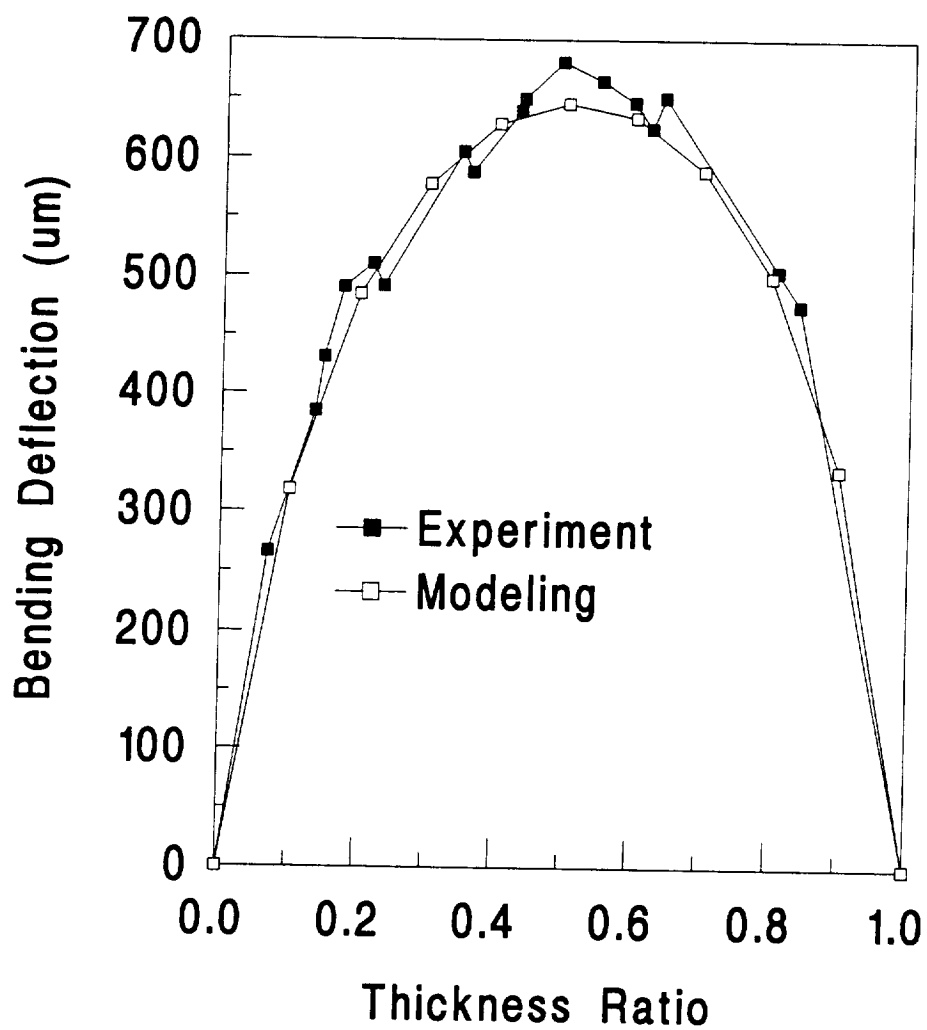


Figure 9. Variation of bending deflection with thickness ratio for RB5553.

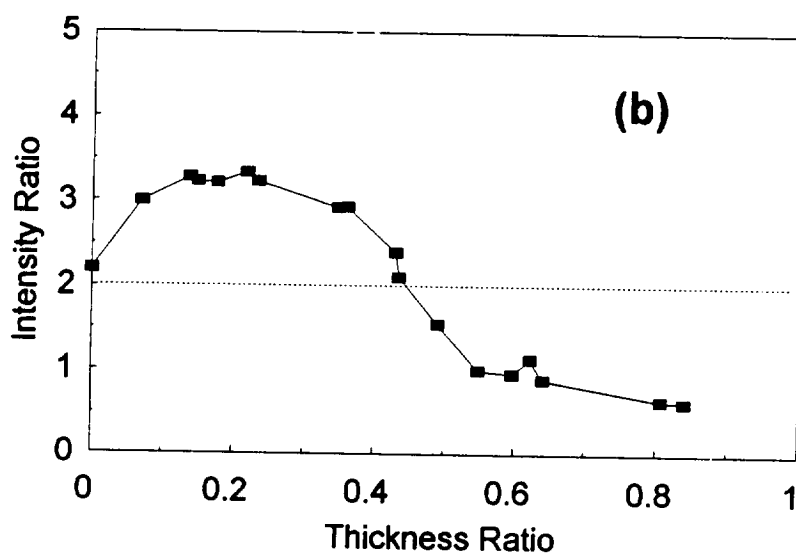
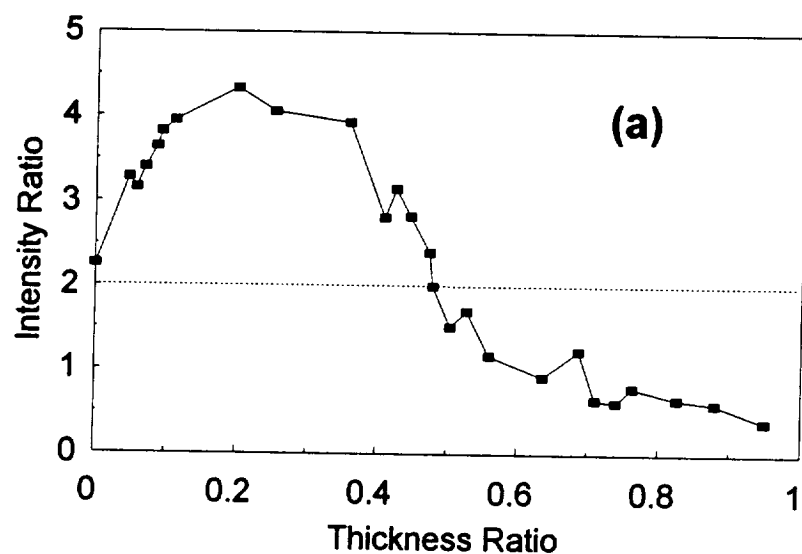


Figure 10. The intensity ratio of the (200)/(002) XRD peaks as a function of thickness ratio for (a) normal 1053 and RB1053, (b) normal 5553 and RB5553.

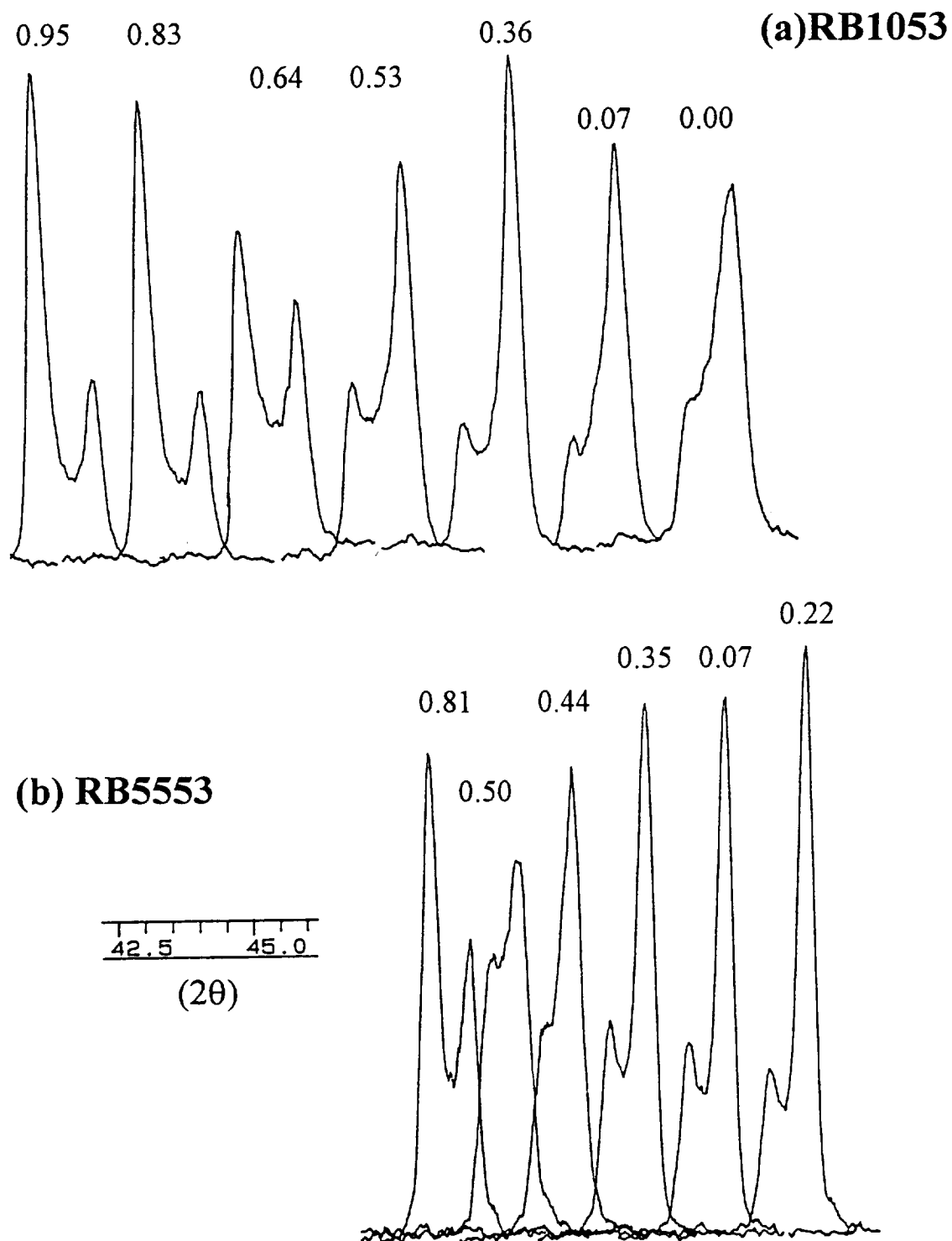


Figure 11. The profiles of the (200) and (002) diffraction peaks for (a) RB1053 and (b) RB5553 of different thickness ratios. The numbers on top of the peaks represent the thickness ratio

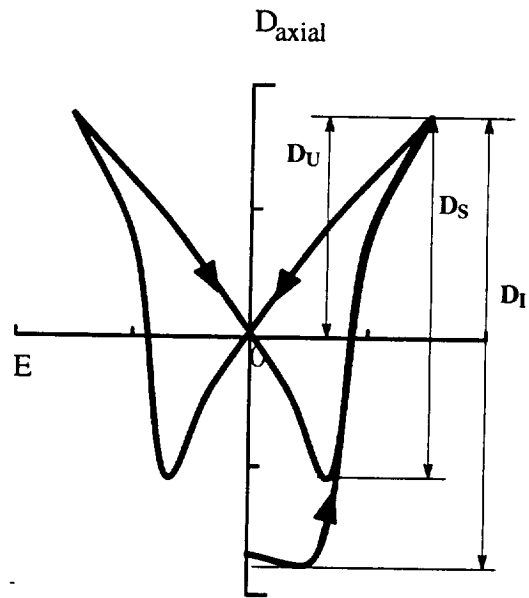


Figure 12. Typical displacement–electric field loop for RB1053 or RB5553, showing the unipolar (D_U), switching (D_S), and initial (D_I) displacements.

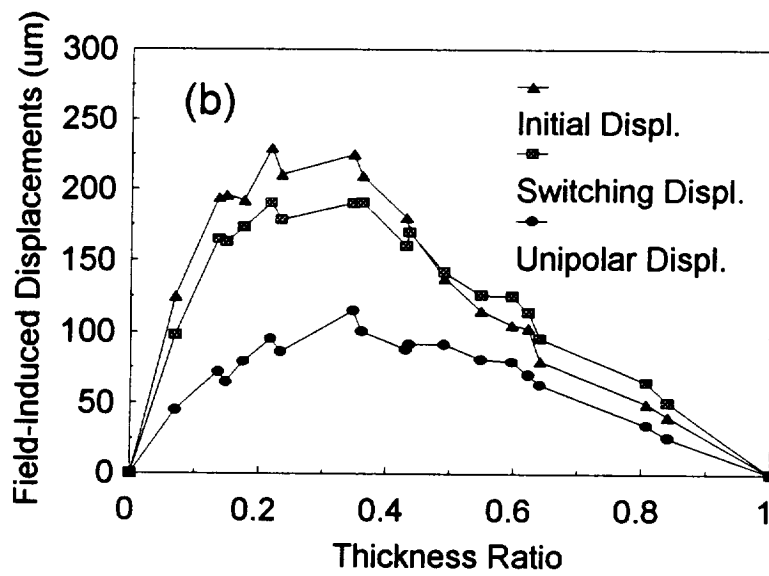
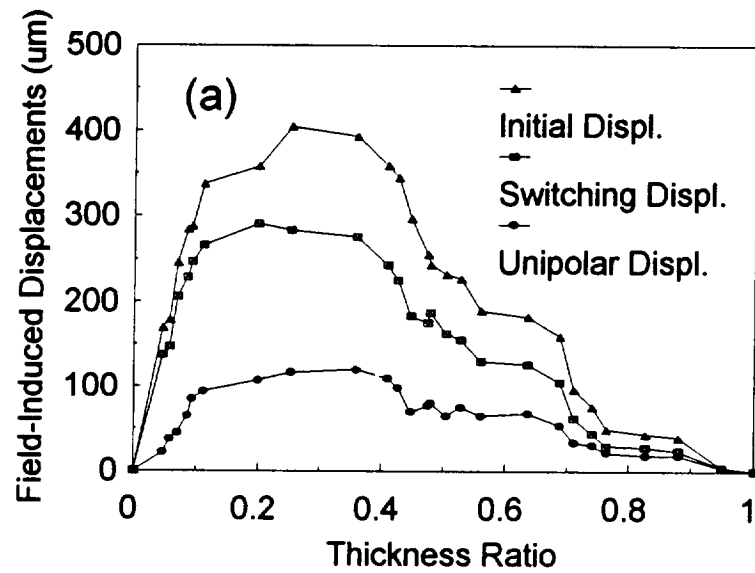


Figure 13. Variation of field-induced displacements with thickness ratio for (a) RB1053 and (b) RB5553. The displacements were determined under applied electric fields of 16 kV/cm for RB1053 and 18kV/cm for RB5553.

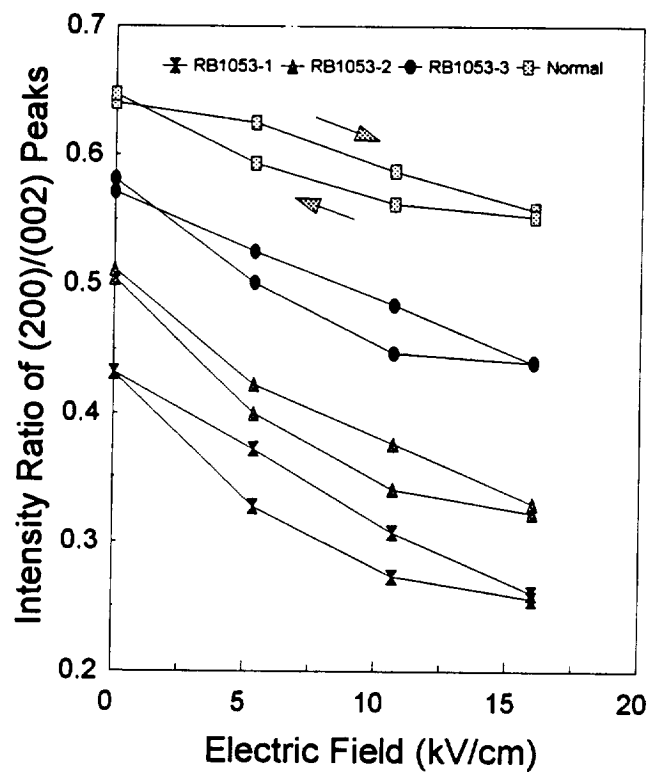


Figure 14. Effect of applied electric field on the XRD peaks of a normal sample and RB1053 with different thickness ratios. The thickness ratios of RB1053-1, RB1053-2 and RB1053-3 are 0.25, 0.20 and 0.47, respectively.

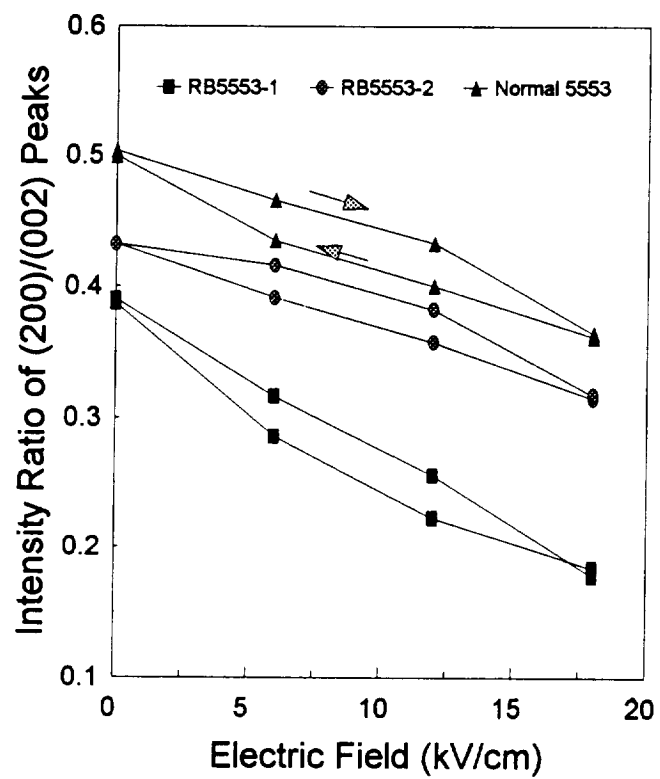


Figure 15. Effect of applied electric field on the XRD peaks of a normal sample and RB5553 with different thickness ratios. The thickness ratios of RB5553-1 and RB5553-2 are 0.22 and 0.43, respectively.

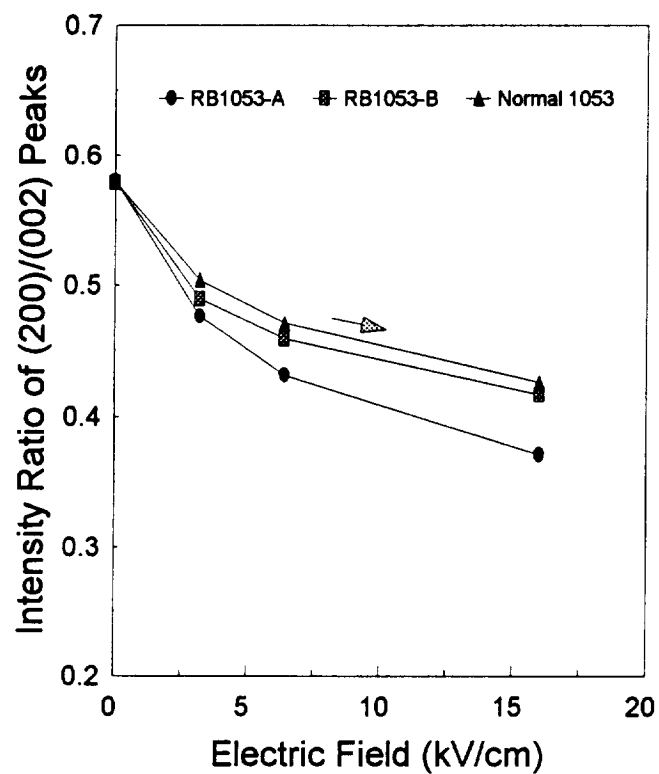


Figure 16. Effect of applied electric field on the XRD peaks of (hot-pressed) normal and RB1053 samples. The thickness ratios of RB1053-A and RB1053-B are 0.32 and 0.45, respectively.

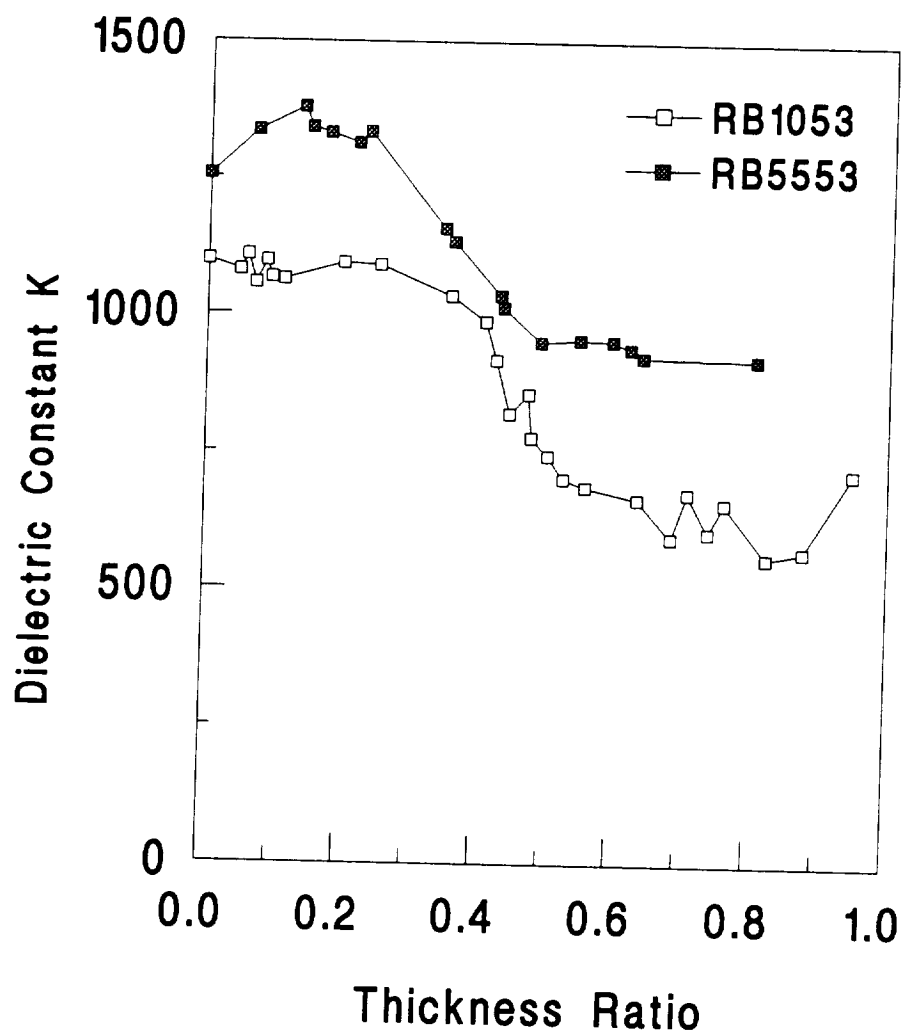


Figure 17. Variation of dielectric constant K with thickness ratio.

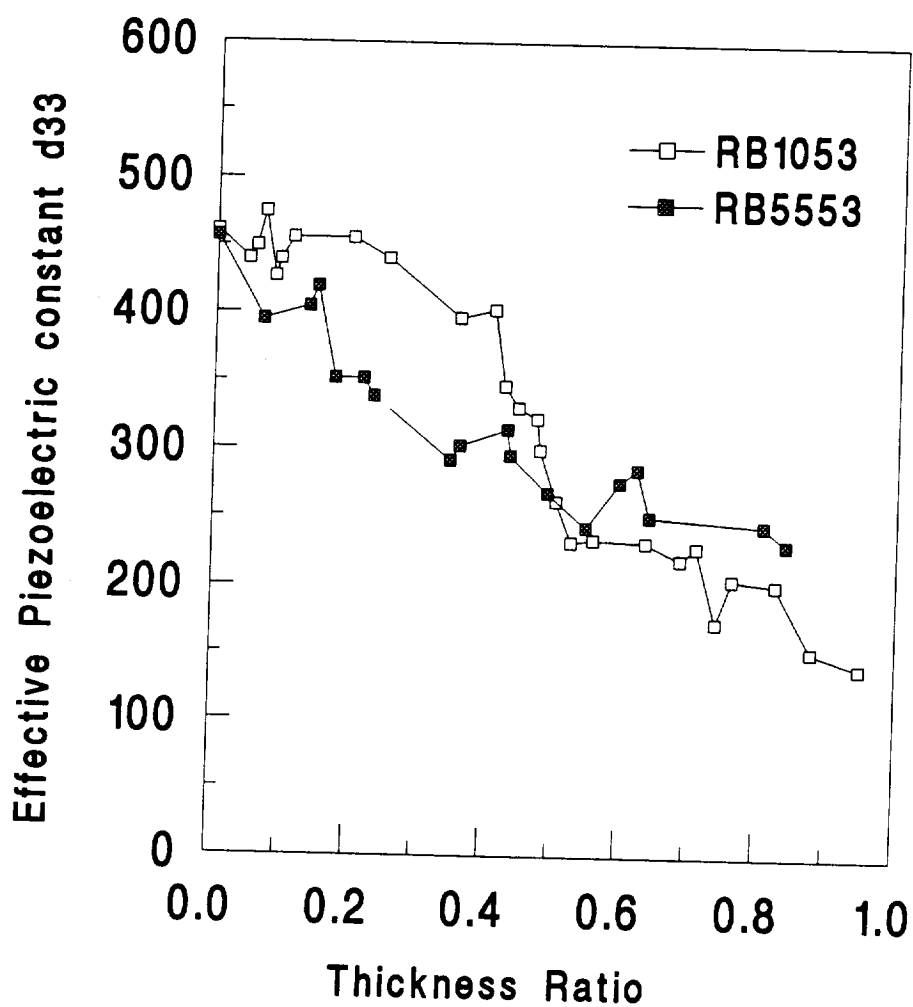


Figure 18. Variation of effective piezoelectric coefficient d_{33} with thickness ratio.

Part III.

**Strain-Electric Field Hysteresis of Some PLZT, PBZT and PMN-Based
Ferroelectric Ceramics**

Strain-Electric Field Hysteresis of Some PLZT, PBZT, and PMN-Based Ferroelectric Ceramics

Abstract: The characteristics of strain-field hysteresis for some $(\text{Pb,Lu})(\text{Zr,Ti})\text{O}_3$ (PLZT), $(\text{Pb,Ba})(\text{Zr,Ti})\text{O}_3$ (PBZT), and $\text{Pb}(\text{Mg,Nb})\text{O}_3$ (PMN)-based ceramics were investigated in terms of the quantities of maximum absolute hysteresis and percentage hysteresis. Under a unipolar applied field of 20 kV/cm, the maximum absolute hysteresis exhibited a broad maximum near the tetragonal-rhombohedral morphotropic phase boundary for the PLZT 5.5/100-y/y series of ceramics while the percentage hysteresis changed only slightly with composition. When the applied field ranged from $-0.5E_c$ to +30kV/cm, a sharp peak in both the maximum absolute hysteresis and percentage hysteresis was observed near the phase boundary due mainly to enhanced domain relaxations. For the PLZT x/65/35 series, the maximum absolute hysteresis and the percentage hysteresis displayed a maximum at ~8 atom% Lu. The PMN, PLZT and PBZT samples with relaxor characteristics possessed considerably less hysteresis compared to other ferroelectric samples studied. The best of the PMN samples had a percentage hysteresis less than one. It was found that the ferroelectric ceramics with larger field-induced strains usually possessed more hysteresis.

1. Introduction

The hysteresis accompanying electric field-induced strain in ferroelectric ceramics has been a major concern in the application of these materials to actuators.¹⁻³ Among other relevant properties, desired materials for actuators should exhibit large electric field-induced strains and little strain-field hysteresis. Ordinary ferroelectric ceramics are known for their special characteristics including significant nonlinearities and marked hysteresis. When an electric field is applied to a ferroelectric ceramic, the dimensions of the ceramic will change due to the piezoelectric effect, electrostrictive effect, and reorientation of ferroelectric domains. Hysteresis

is manifested as the difference between the strain curves of increasing and decreasing electric fields.

The phenomena of hysteresis (dielectric and elastic) in ferroelectrics have been the subject of many investigations.⁴⁻⁹ It is generally considered that the hysteresis is mainly attributed to the field-induced relaxations of ferroelectric domains. Specifically, the hysteresis in ferroelectric materials is determined by the relaxations associated with the nucleation and growth of new ferroelectric domains antiparallel to the applied electric field and the reorientation of existing domains by domain wall motion. Although a good deal of work has been carried out in order to understand polarization reversal and domain dynamics,¹⁰⁻¹⁸ the mechanisms for the hysteresis are not yet fully understood. Along with the complexity of domain configurations, the hysteresis effect can also be greatly influenced by the nature of the electrodes on the samples, the nature of sample surfaces, electrical conductivity, the presence of defects and imperfections, and by the microstructures (particularly the grain sizes).¹⁹⁻²¹

The purpose of this investigation was to characterize and analyze the strain-field hysteresis of some PLZT, PBZT, and PMN-based ferroelectric ceramics which may be used for RAINBOW (Reduced And Internally Biased Oxide Wafer) actuators. The experimental results will be discussed in terms of current theories on the hysteresis phenomena.

2. Sample Preparation and Measurements

Conventional mixed-oxide processing techniques for ferroelectric ceramics were used to prepare a majority of the samples. Some of the PLZT samples were made by a hot-pressing method. Details of the preparation procedures can be found elsewhere.²² The sintered and hot-pressed ceramics were lapped to dimensions of 1.0x1.0x0.76 cm. The two major surfaces of the samples were electroded with electroless nickel plating for measurements.

An apparatus containing an LVDT (Lucas Schaertz Co. 050 DC-E), as shown in Figure 1, was used to determine the change of sample dimensions with electric field. The measurement

sensitivity was estimated to be approximately $0.05 \mu\text{m}$. Transverse strain of the samples was measured with a low-frequency applied field. The strain hysteresis discussed in this paper was the hysteresis of transverse strain. It is worth mentioning that the strain hysteresis was sensitive to experimental conditions. The main sources of errors for the measurements were the small loading and electronic noise from the LVDT. The loading exaggerated hysteresis due to mechanical inertia while the electronic noise degraded measurement reproducibility. The overall error of the measured strain was approximately 5%.

3. Experimental Results

In most of the literature, the strain hysteresis was discussed only qualitatively. No consistent quantitative definition has been found. This is probably due to the fact that, in addition to the material properties, the hysteresis effect strongly depends on measurement conditions such as the magnitude and frequency of the applied field and the level of the loading on the sample. In this study, the quantities of maximum absolute hysteresis and percentage hysteresis were used for characterization of the hysteresis. The maximum absolute hysteresis is defined as the maximum strain difference between the curves of increasing and decreasing electric fields, and the percentage hysteresis is defined as the maximum absolute hysteresis as a percentage of the total strain within the range of the applied field, as is illustrated in Figure 2.

The percentage hysteresis has been previously used in the literature; and in most cases, this parameter can adequately represent the extent of hysteresis. The maximum absolute hysteresis indicates the actual hysteresis a sample may produce under certain conditions. Both of these parameters vanish for materials with zero hysteresis. If the applied field is cycled between negative and positive field strengths greater than the coercive field of the sample, a butterfly-like strain-field hysteresis loop is produced. In this case, a quantitative description of the strain hysteresis is more difficult and not under consideration here.

The strain-electric field relationships with a unipolar applied field of 20 kV/cm are given in Figures 3 through 5 for PLZT, PBZT and PMN ceramics, respectively. Hysteresis data were

determined from the figures and are listed in Table 1. The variations of maximum absolute hysteresis and percentage hysteresis with Zr content were plotted in Figures 6(a)-(b) for the PLZT 5.5/100-y/y series ceramics which is located across the ferroelectric morphotropic tetragonal (F_T) - rhombohedral (F_R) phase boundary. As can be seen, the maximum absolute hysteresis, ΔS_{\max} , exhibits a broad maximum in the vicinity of the phase boundary. The percentage hysteresis, however, increases gradually with Zr concentration due to the reduction of the total strain at higher Zr concentration.

For the other PLZT compositions in Table 1, PLZT 8.5/65/35 has a large percentage hysteresis because of the large ΔS_{\max} resulting from high strain nonlinearity. The relaxor PLZT 9.5/65/35 shows a percentage hysteresis considerably smaller than that of other PLZT compositions. The hysteresis data for PBZT ceramics in Table 1 are similar to those of the PLZT 5.5/100-y/y series. The PMN ceramics, in general, have hysteresis considerably less than the PLZT and PBZT ceramics, with the percentage hysteresis being only a few percent or less.

The hysteresis data obtained in an applied field range from $-0.5E_C$ up to $+30$ kV/cm are given in Table 2. In this case, the contribution of enhanced domain switching to the strain is included. The strain-field relationships for selected compositions are shown in Figures 7-8. Table 2 also lists S_0 , S_{10} and S_{20} which are the absolute hysteresis measured at 0, 10 and 20 kV/cm, respectively. The S_0 , S_{10} and S_{20} combined can be used to indicate strain nonlinearity. Because of the enhanced domain switching, the total strain, S_{total} , shown in Table 2 are much larger than those in Table 1 for the compositions with a definite coercive field. The maximum absolute hysteresis, which is usually found near zero electric field, is also greatly enhanced by the domain switching. As a result, the values of the percentage hysteresis in Table 2 are considerably larger than those in Table 1.

Figures 9(a)-(b) show the changes of the hysteresis with Zr content for the data in Table 2 for PLZT 5.5/100-y/y samples. It can be seen that both the maximum absolute hysteresis and the percentage hysteresis are a sharp maximum at the F_T - F_R phase boundary. The PLZT x/65/35 series samples display a maximum in the hysteresis at ~ 8 atom% La, as shown in Figures 10(a)-

(b). In addition, it was found that the hot-pressed ceramics exhibited less hysteresis than the sintered ceramics.

4. Discussion

A number of mechanisms, depending on composition and crystal structure, may contribute to the electric field-induced strain in ferroelectric ceramics. These mechanisms include the electrostrictive effect, piezoelectric effect, domain reorientation, and field-enforced phase transitions. The major contribution to the strain hysteresis is considered to be associated with ferroelectric domain switching and reorientation. When a ferroelectric ceramic is cooled down through its Curie point, special domain configurations are formed so as to relieve the internal stresses resulting from spontaneous strain and to minimize depolarization energy. Both 180° and 90° domain walls exist in the domain configurations of tetragonal ceramics, but only 90° domain switching contributes to field-induced strains. The relaxations associated with domain nucleation and domain wall motion give rise to significant strain-field hysteresis.

It has been found that defects and imperfections markedly affect domain behavior.⁵ The sharp peaks at the F_T - F_R phase boundary in Figures 9(a)-(b) are probably ascribed to the complex microstructures at the boundary which enhance relaxations associated with domain switching. The influence of the phase boundary on domain reorientation, however, is less pronounced under a unipolar applied field, since in that case a broad peak was seen (Figure 6(b)).

The grain size of ferroelectric ceramics has a significant effect on the strain hysteresis. As the grain size is decreased, the amount of 90° domain wall is reduced considerably; therefore the strain hysteresis is diminished.²⁵ In addition, a high internal stress field is built up as grain size decreases further. This stress field tends to suppress the lower symmetry ferroelectric phase, forcing it into a pseudo-cubic structure.^{8, 26-28} It follows that both the strain magnitude and strain hysteresis are reduced drastically. The smaller values of the hysteresis for the hot-pressed samples, as compared to the sintered samples, are likely due to the smaller grain sizes of the former. Reducing grain sizes through processing has been found to be a very effective way to

minimize the strain hysteresis but usually at the expense of decreasing strain magnitude considerably.

The much less hysteresis which was observed in the relaxor ferroelectrics of PMN and some PLZT and PBZT compositions involved a different mechanism. In relaxor materials, domain walls are non-existent, but there are the so-called microdomain regions resulting from compositional fluctuations.²⁹⁻³² Apparently, very little hysteresis will occur in the relaxor materials. Relaxor ferroelectrics are very promising for actuator applications due to their little hysteresis; however, strains generated by these materials are usually smaller than those of ordinary ferroelectrics.

The electrodes on a sample can influence the nucleation rate of new domains because the new domains are often initiated at the interface between the electrode and the ferroelectric.²²⁻²⁴ It was found that more hysteresis occurred for certain compositions when silver electrodes were used instead of nickel electrodes.

The experimental results in this study indicate that the ferroelectric ceramics with larger strains usually possess more hysteresis due to the inherent nature of these materials. This can be seen by plotting the maximum absolute hysteresis against the total strain for all the samples (Figure 11). A similar phenomenon is also seen in a plot of the percentage hysteresis vs. the total strain. It appears that a method capable of decreasing the hysteresis will also reduce the strain magnitude. It should be noted that the hysteresis is not a material property since the former depends on measurement conditions. For this reason, caution must be exercised when hysteresis data are compared in the literature.

4. Conclusions

The characteristics of low-frequency strain-electric field hysteresis for some PLZT, PBZT, and PMN-based ceramics have been investigated. The quantities of maximum absolute hysteresis and percentage hysteresis were used to characterize and analyze the hysteresis effect.

Under a unipolar applied field of 20 kV/cm, the maximum absolute hysteresis exhibits a broad maximum near the tetragonal-rhombohedral morphotropic phase boundary for the PLZT 5.5/100-y/y series samples while the percentage hysteresis changes only slightly with composition. When the applied field range is $-0.5E_C$ to +30kV/cm, a sharp peak in both the maximum absolute hysteresis and percentage hysteresis is observed near the phase boundary due to enhanced domain relaxations. For the PLZT x/65/35 series ceramics, the maximum absolute hysteresis and the percentage hysteresis display a maximum at ~8 atom% La. The hot-pressed PLZT ceramics have less hysteresis than the sintered ceramics, probably because of different grain sizes.

The PMN, PLZT and PBZT samples with relaxor characteristics possess considerably less hysteresis compared to other samples studied. The best of the PMN samples has a percentage hysteresis less than one. It was found that ferroelectric ceramics with larger field-induced strains usually exhibit more hysteresis.

6. References

1. K. Uchino, *Ceramic Bulletin*, **65**, 647 (1986).
2. E. H. Anderson, D. M. Moore, J. L. Fanson and M. A. Ealey, *Optical Engineering*, **29**, 1333 (1990).
3. M. Kondo, K. Ohya and S. Shimizu, *IEEE-ISAF*, 530 (1990).
4. P. J. Chen and S. T. Montgomery, *Ferroelectrics*, **23**, 199 (1980).
5. M. E. Lines and A. M. Glass, *Principles and Applications of Ferroelectrics and Related Materials*, pp102-112, Clarendon Press, Oxford (1977).
6. D. Berlincourt, D. Curran and H. Jaffe, *Physical Acoustics*, Academic Press, New York and London, **1(a)**, 169 (1964).
7. B. Jaffe, W. Cook and H. Jaffe, *Piezoelectric Ceramics*, Academic Press, London (1971).
8. K. Uchino, *IEEE-ISAF*, 153 (1990).
9. J. Fousek, *IEEE-ISAF*, 171 (1992).

10. W. Pan, C. Yue and S. Sun, *Ferroelectris*, **133**, 97 (1992).
11. S. Sherrut, D. Van Nice, J. Graham, B. Mukherjee and H. Wiederick, *IEEE-ISAF*, 167 (1992).
12. G. Arlt and N. Pertsev *J. Appl. Phys.*, **70**(4), 2283 (1991)
13. Y. Ishibashi, *Ferroelectrics*, **104**, 299 (1990).
14. P. Lambeck and G. Jonker, *J. Phys. Chem. Solids.*, **47**(5), 453 (1986).
15. G. Arlt and P. Sasko, *J. Appl. Phys.*, **51**(9), 4956 (1980).
16. P. Gerthsen and G. Kruger, *Ferroelectrics*, **11**, 489 (1976).
17. G. Kruger, *Ferroelectrics*, **11**, 417 (1976).
18. S. Ikegami and I. Ueda, *J. Phys. Soc. Jpn.*, **22**(3), 725 (1967).
19. N. Okada, K. Ishkawa and T. Nomura, *J. J. Appl. Phys.*, **30**(9B), 2276 (1991).
20. K. Uchino, M. Tatsumi, I. Hyyashi and T Hayashi, *J. J. Appl. Phys.*, **24**, suppl 24-2, 733 (1985).
21. G. Arlt, D. Hennings and G. de With, *J. Appl. Phys.*, **58**(4), 1619 (1985).
22. G. Li and G. Haertling, *Commercial Use of Space*, a semiannual research report in the department of Ceramic Engineering, Clemson University (1993).
23. E. Fatuzzo and W. Merz, *Ferroelectricity*. North-Holland, Amsterdam (1967).
24. I. Camlibel, *J. Appl. Phys.*, **40**, 1690 (1969).
25. A. Yamaji, Y. Enomoto, K. Kinoshita and T. Murakami, *J. Am. Ceram. Soc.*, **60**(1), 97 (1977).
26. W. Buessem, L. Cross and A. Goswami, *J. Am. Ceram. Soc.*, **49**(1), 33 (1966).
27. K. Gachigi, U. Kumar and J. Dougherty, *IEEE-ISAF*, 492 (1992).
28. S. Wang, U. Kumar, W. Huebner and P. March, *IEEE-ISAF*, 148 (1992).
29. L. E. Cross, *Ferroelectrics*, **76**, 241 (1987).
30. Yao Xi, Chen Zhili and L. E. Cross, *J. Appl. Phys.*, **54**(6), (1983).
31. M. Yokosuka and M. Marutake, *J. J. Appl. Phys.*, **25**(7), 981 (1986).
32. G. Schmidt and H. Arndt, *Phys. Stat. Sol. (a)*, **63**, 501 (1981).

Table 1. Strain-field hysteresis of PLZT, PBZT, and PMN-based ceramics.

Sample	ΔS_{\max} $\times 10^4$	ΔS_{10} $\times 10^4$	S_{per} (%)	S_{total} $\times 10^4$
PLZT 5.5/53/47 (La/Zr/Ti)	0.78	0.72	15.7	5.1
PLZT 5.5/55/45	0.80	0.72	15.1	5.3
PLZT 5.5/56/44	0.89	0.79	17.3	5.2
PLZT 5.5/57/43	0.86	0.70	17.0	5.3
PLZT 5.5/58/42	0.92	0.66	16.4	5.5
PLZT 5.5/59/41	0.92	0.70	17.0	5.4
PLZT 5.5/60/40	1.00	0.72	17.5	5.7
PLZT 5.5/61/39	0.92	0.72	20.0	4.5
PLZT 5.5/62/38	0.79	0.66	19.0	4.2
PLZT 5.5/64/36	0.76	0.72	21.1	3.8
PLZT 7.0/65/35	0.66	0.52	14.3	4.2
PLZT 8.5/65/35	1.00	0.74	17.5	5.7
PLZT 9.5/65/35	0.65	0.55	7.9	7.8
PBZT 27/70/30 (Ba/Zr/Ti)	0.81	0.79	14.0	5.7
PBZT 27/57/43	2.30	0.80	26.4	8.7
PMN:PT:BT 83.75/13.75/2.5	0.05	0.05	2.6	1.9
PMN:PT:BT 89.86/8.89/1.25	<0.05	<0.05	<1	2.3

see Figure 2 for the definition of the relevant parameters.

Table 2. Strain-field hysteresis of PLZT, PBZT, and PMN-based ceramics.

Sample	S_0 $\times 10^4$	S_{10} $\times 10^4$	S_{20} $\times 10^4$	ΔS_{\max} $\times 10^4$	S_{per} (%)	S_{total} $\times 10^4$
PLZT 5.5/51/49		1.5		2.0	30.3	6.6
PLZT 5.5/53/47		2.0		2.5	28.0	8.9
PLZT 5.5/55/45	2.5	2.7	1.0	2.9	25.7	11.3
PLZT 5.5/56/44	2.6	2.5	1.2	3.2	26.7	12.0
PLZT 5.5/57/43		2.2		4.7	34.5	13.6
PLZT 5.5/58/42	6.5	2.0	1.1	6.5	39.5	16.5
PLZT 5.5/59/41	5.3	2.0	0.7	5.3	40.2	13.2
PLZT 5.5/60/40		1.3		4.4	37.3	11.8
PLZT 5.5/61/39		1.2		3.0	33.3	9.1
PLZT 5.5/62/38		1.1		2.6	30.6	8.5
PLZT 5.5/64/36		1.0		1.8	24.7	7.3
PLZT 7.0/65/35	1.9	1.1	0.5	2.0	21.1	9.5
PLZT 7.5/65/35	2.7	0.9	0.4	2.8	34.1	8.2
PLZT 8.0/65/35	3.2	0.7	0.5	3.4	27.2	12.5
PLZT 8.5/65/35	1.5	0.7	0.4	2.2	21.8	10.1
PLZT* 9.0/65/35	0.0	0.8	0.4	1.6	20.3	7.9
PLZT* 9.5/65/35	0.0	0.6	0.2	0.7	10.4	6.7
PLZT 6.0/65/35		2.1		3.0	24.0	12.5
PLZT 8.0/65/35		0.7		2.3	19.0	12.1
PLZT* 9.0/65/35		0.8		1.4	14.6	9.6
PLZT* 9.5/65/35		0.4		0.5	5.6	8.9
PBZT* 27/70/30	0.0	0.5	0.2	0.5	7.0	7.13
PBZT 27/57/43	0.5	0.5	0.4	2.0	19.2	10.2
PBZT 27/50/50	1.4	1.6	1.1	1.7	19.1	8.9
PMN:PT:BT* 83.75/13.75/2.5	0.0	0.2	0.1	0.3	8.1	3.7
PMN:PT:BT* 89.86/8.89/1.25	0.0	0.3	0.2	0.4	8.9	4.5

see Figure 2 for the definition of the relevant parameters.

* composition with relaxor characteristics

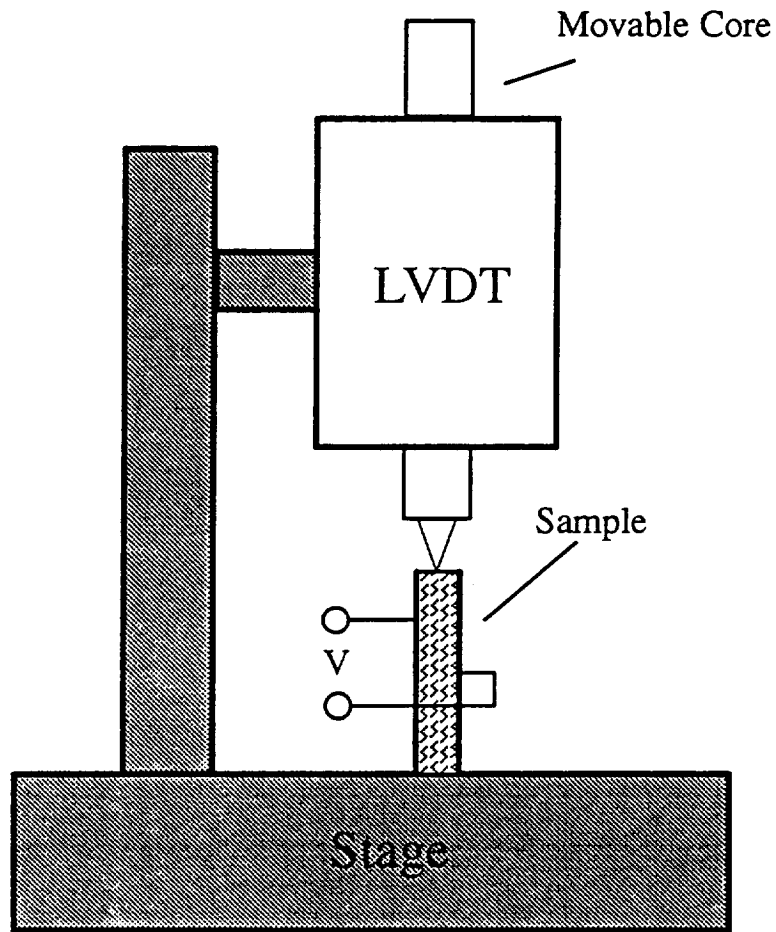


Figure 1. Schematic of apparatus for displacement measurement.

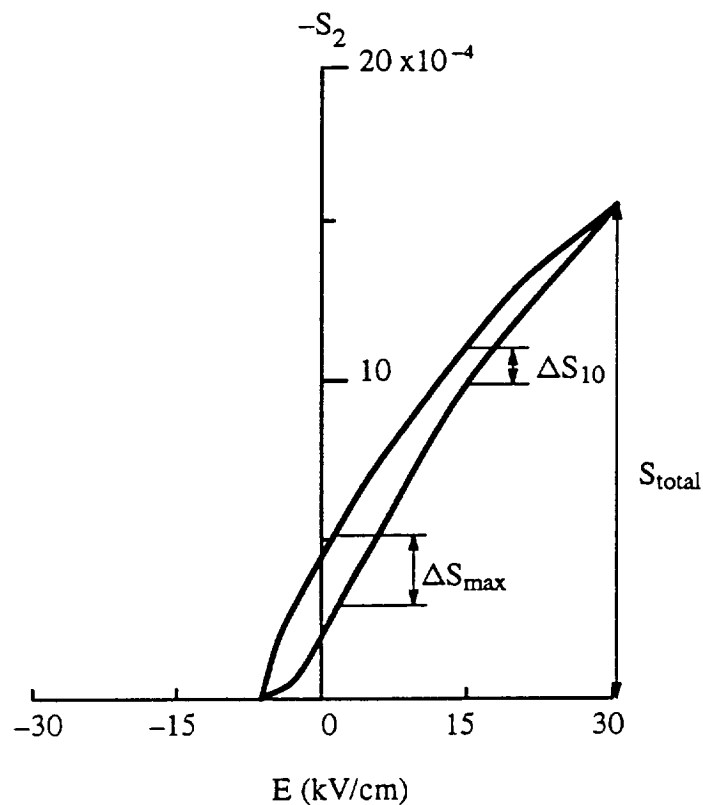


Figure 2. A typical transverse strain–electric field loop with an applied field range from $-0.5E_C$ to $+30$ kV/cm, showing the definitions of parameters for the strain hysteresis.

ΔS_{max} : Maximum absolute hysteresis

ΔS_{10} : Absolute hysteresis at 10 kV/cm

$S_{per} = \Delta S_{max}/S_{total}$: Percentage hysteresis

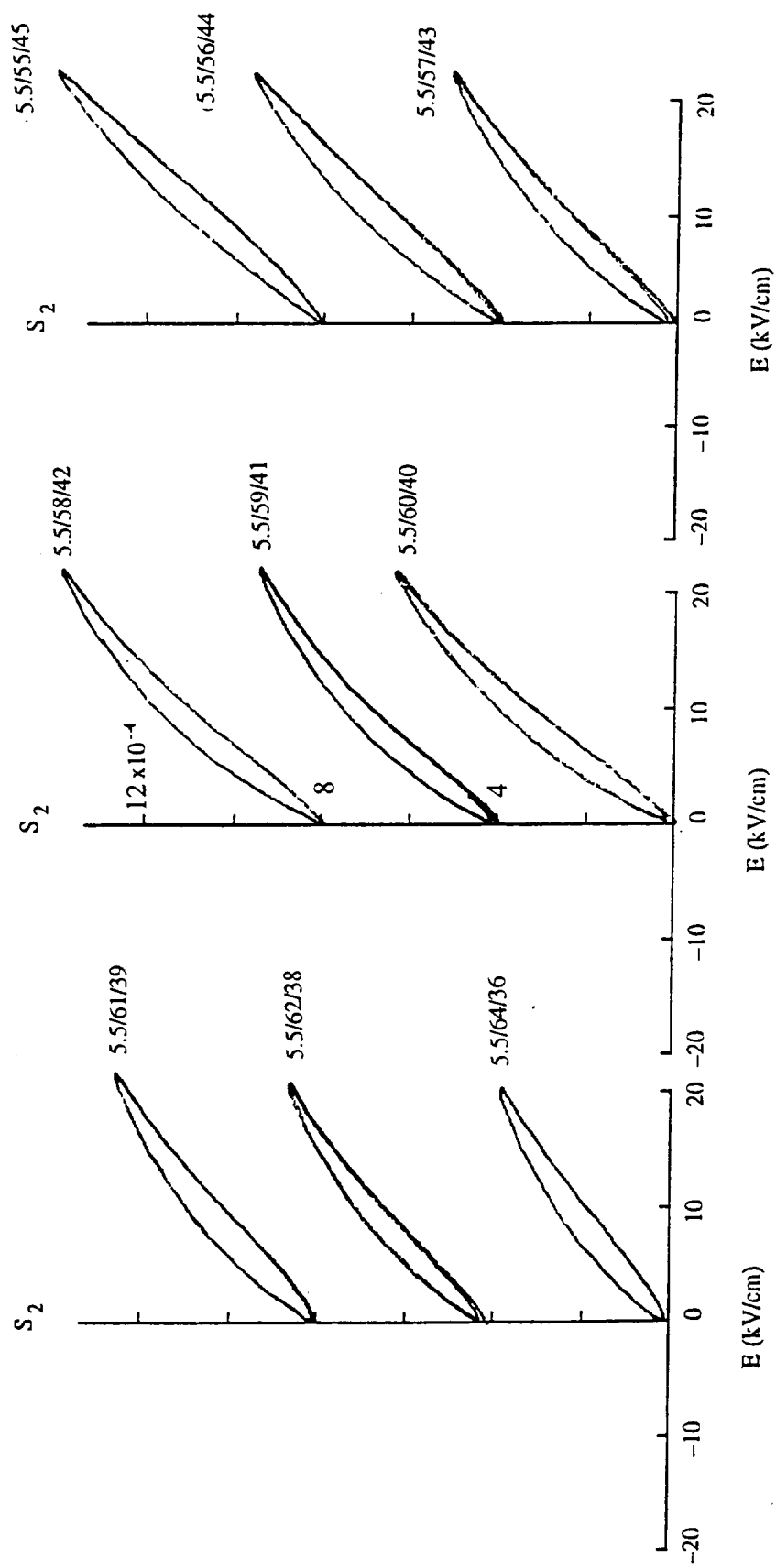


Figure 3. Strain-field curves of PLZT ceramics under unipolar electric fields.

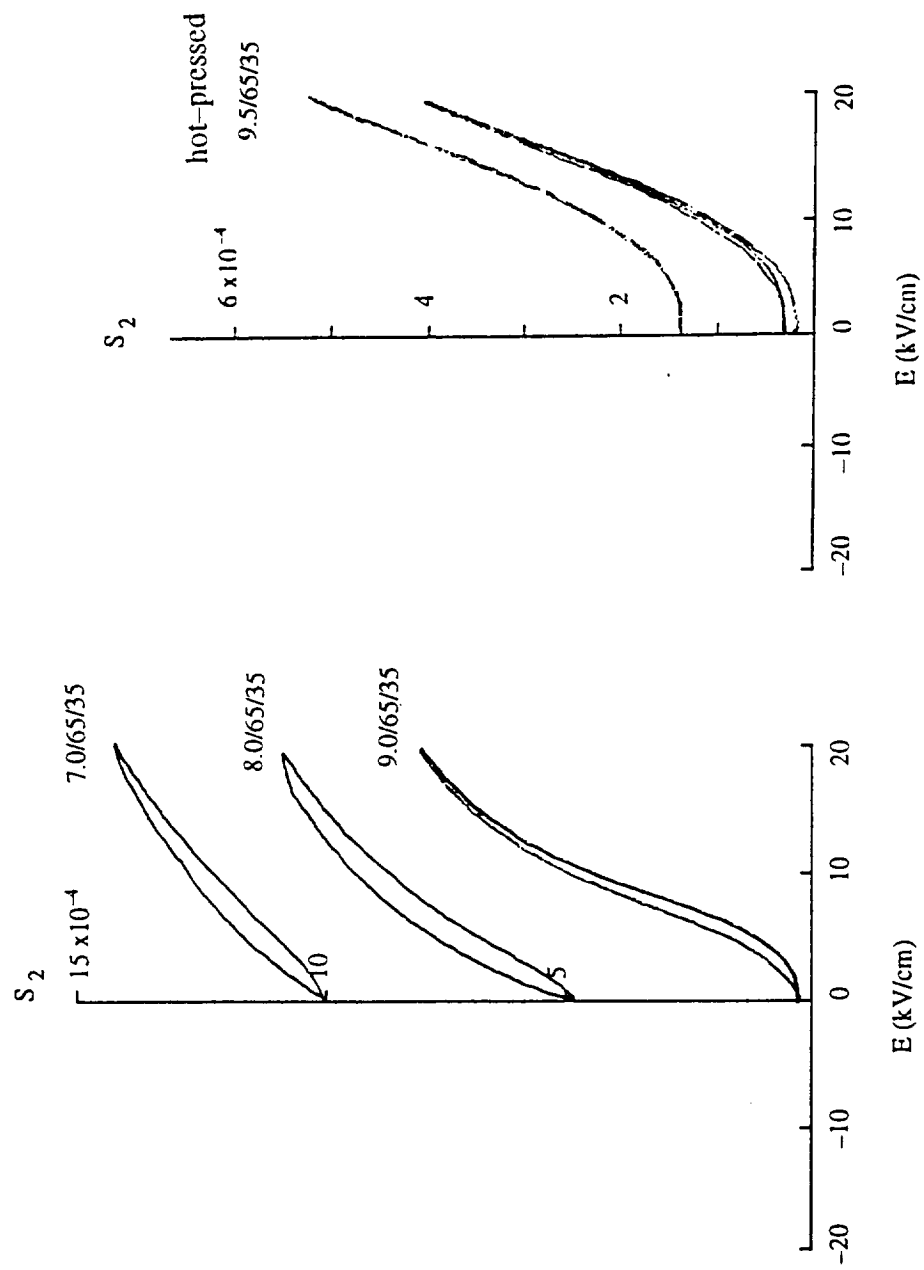


Figure 3. (continued)

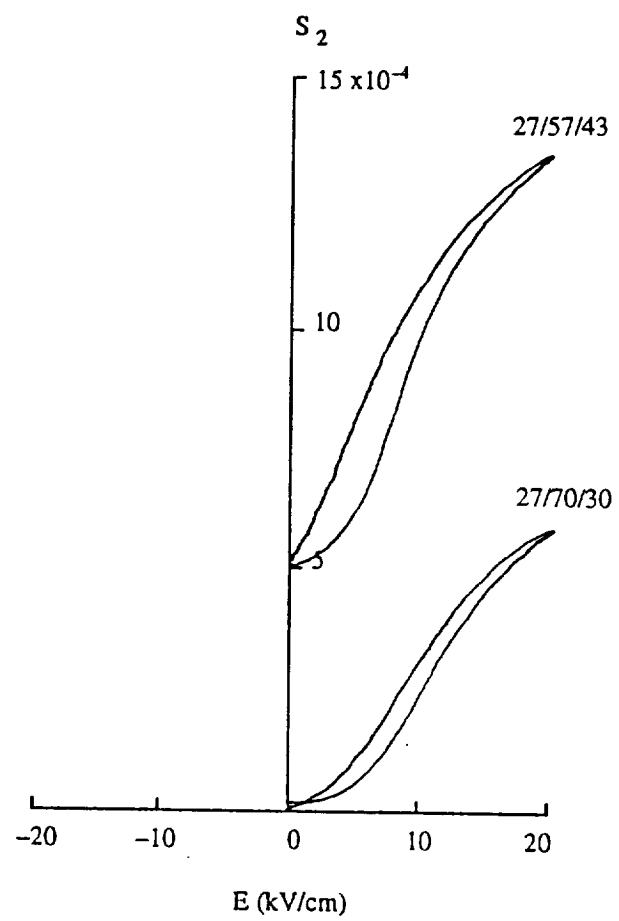


Figure 4. Strain-field curves of PBZT ceramics under unipolar electric fields.

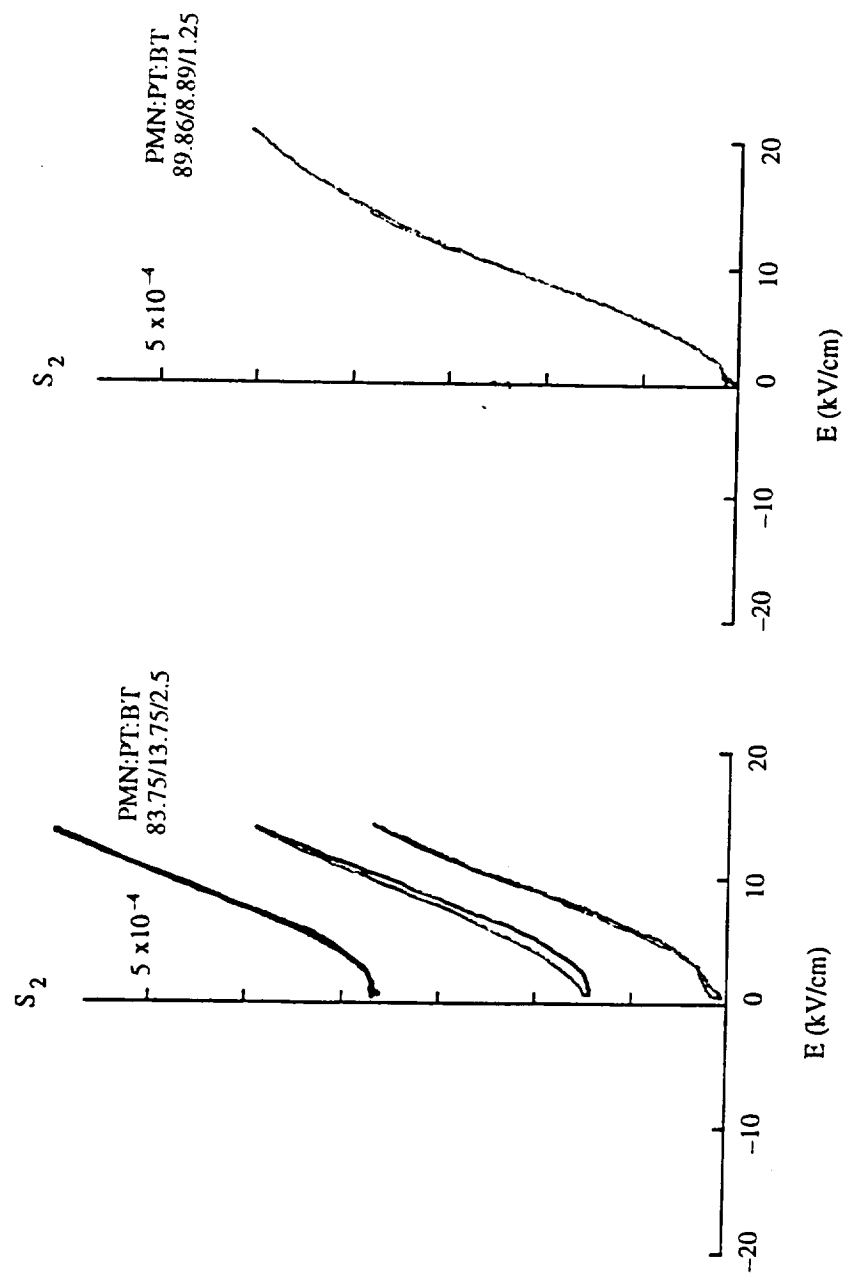


Figure 5. Strain-field curves of PMN ceramics under unipolar electric fields.

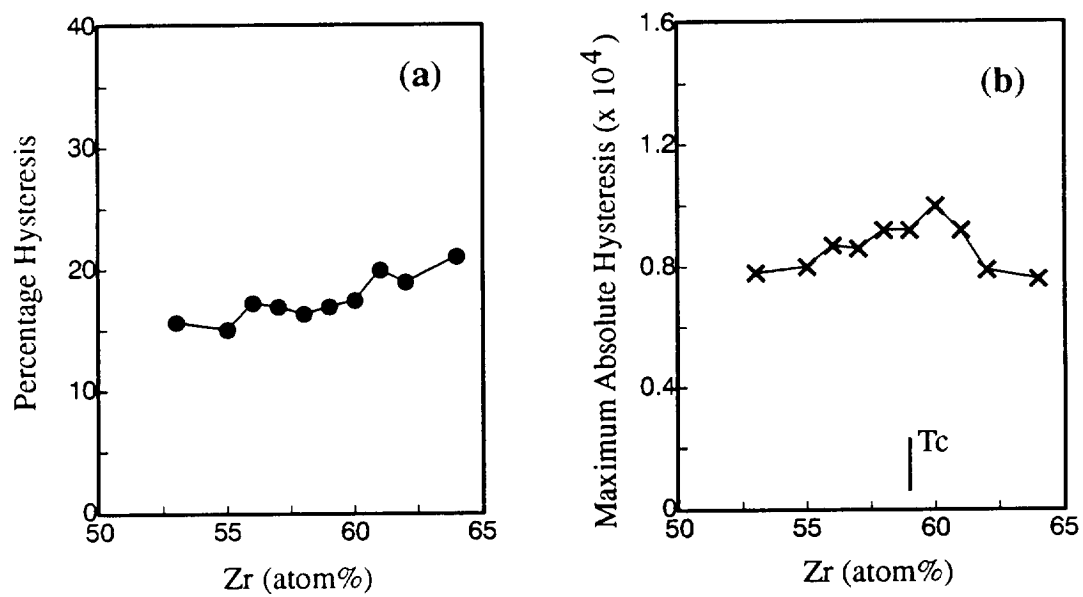


Figure 6. Variation of the strain hysteresis with Zr content for PLZT 5.5/100-y/y ceramics with a unipolar applied field of 20 kV/cm.

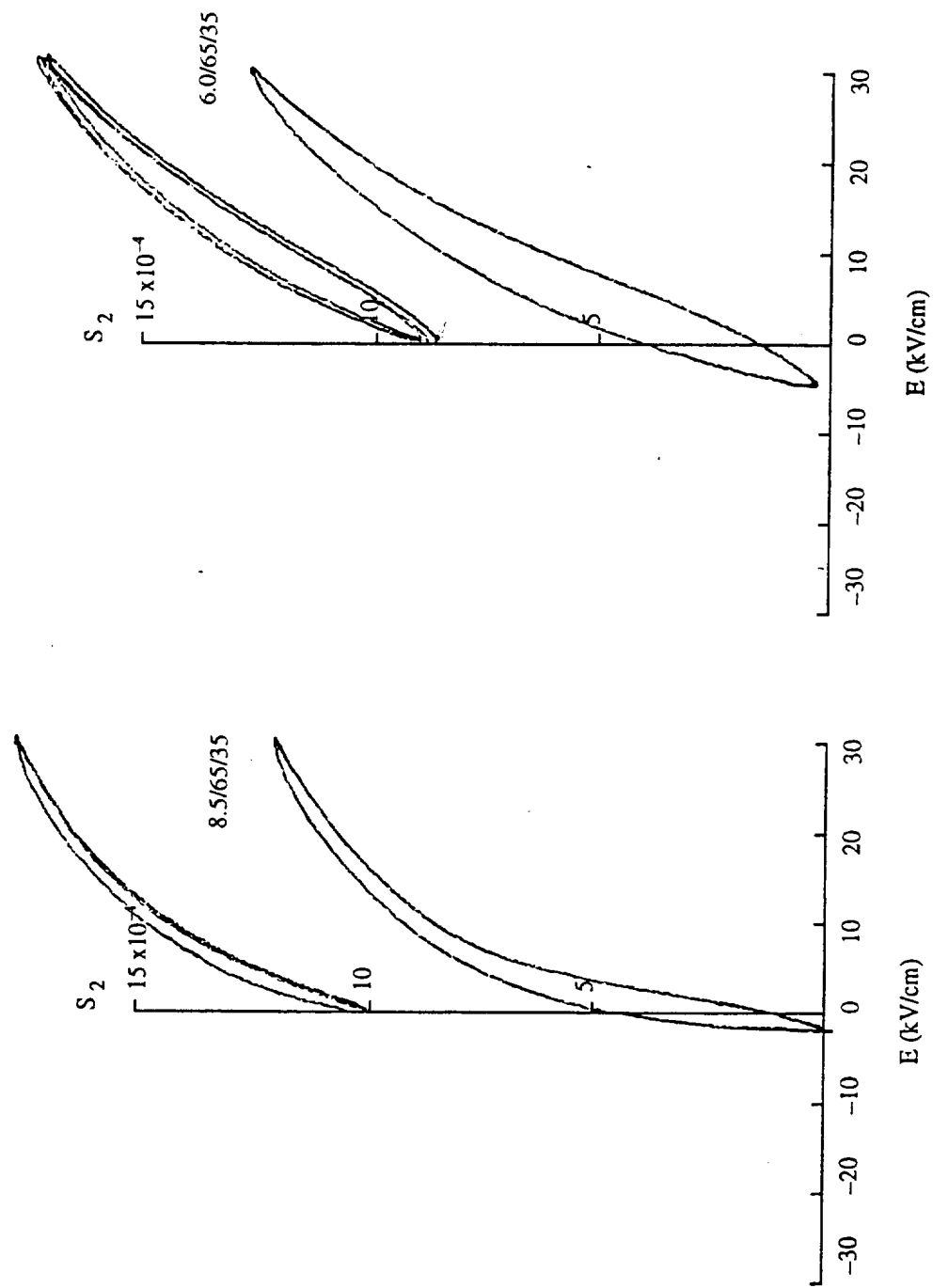


Figure 7. Strain-field relationship of hot-pressed PLZT ceramics.

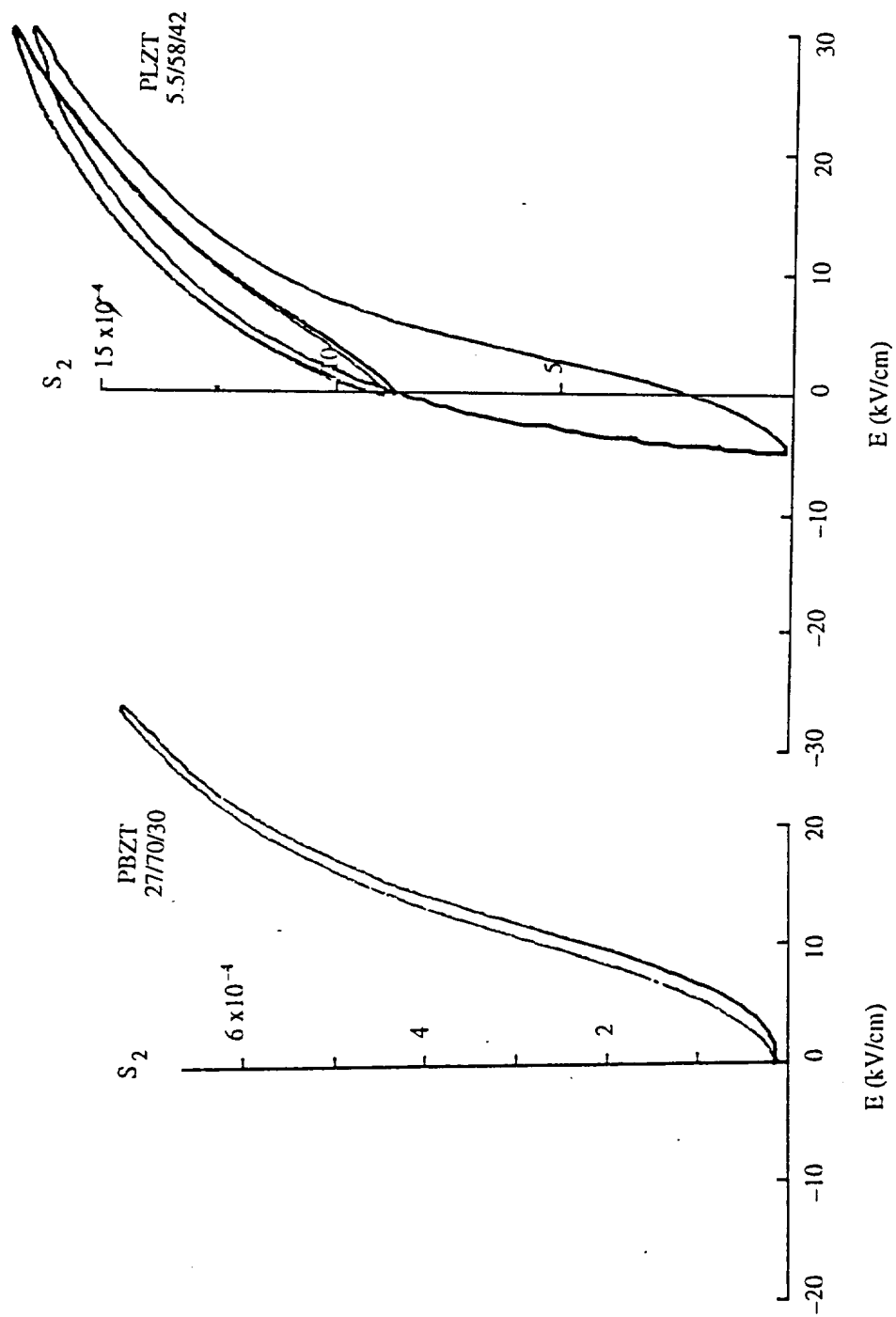


Figure 8. Strain-field relationship of sintered PLZT and PBZT ceramics.

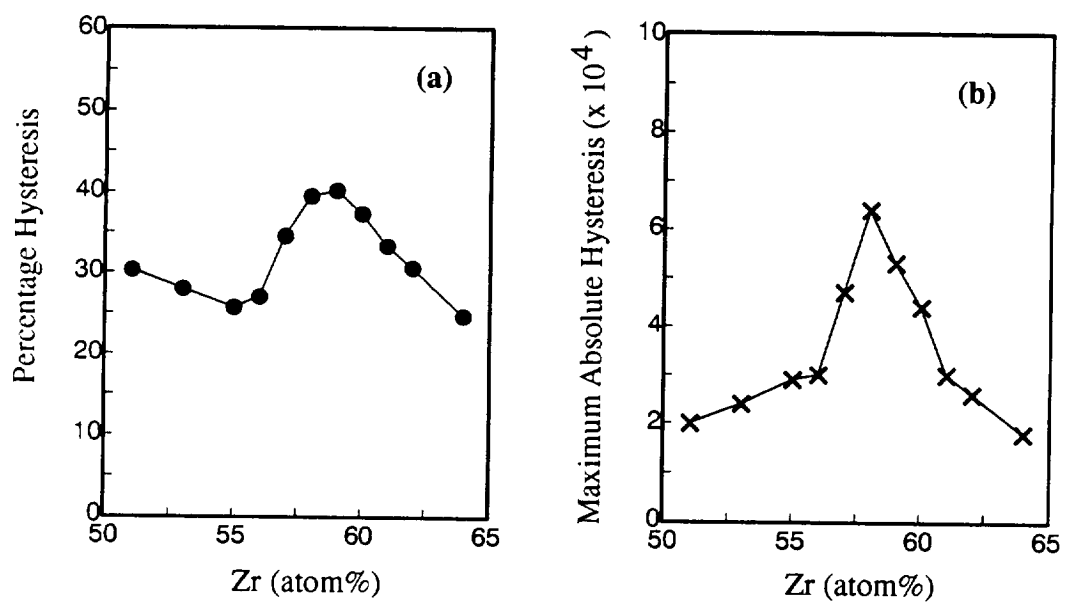


Figure 9. Change of the strain hysteresis with Zr content for PLZT 5.5/100-y/y ceramics with an applied field range from $-0.5E_c$ to $+30$ kV/cm.

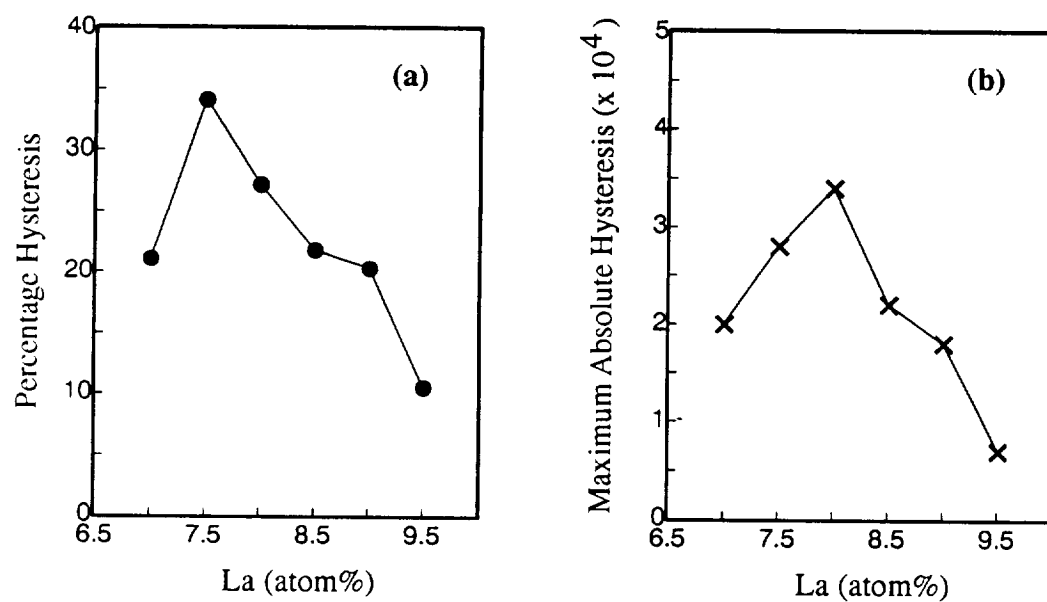


Figure 10. Variation of the strain hysteresis with La content for PLZT x/65/35 ceramics with an applied field range from $-0.5E_c$ to $+30$ kV/cm.

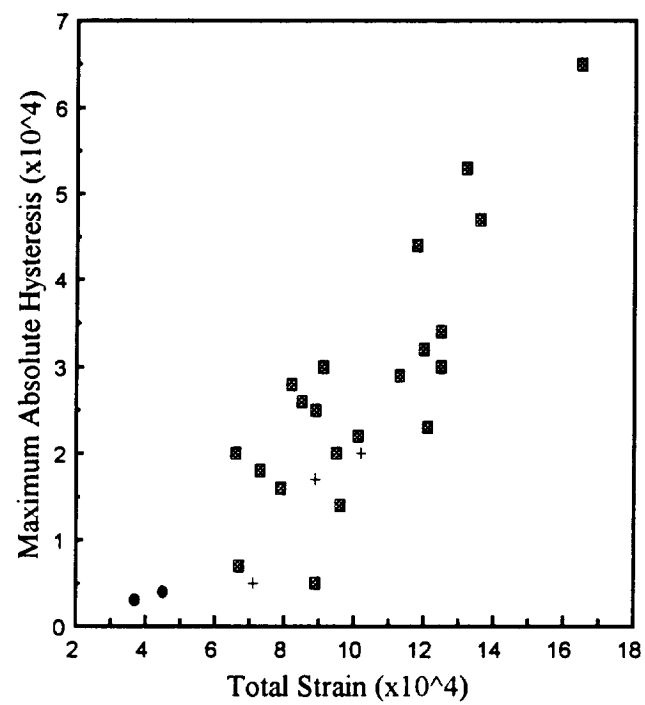


Figure 11. Variation of maximum absolute hysteresis with total strain for the data from Table 2. ■ for PLZT, + for PBZT, and ● for PMN.

Part IV.

Displacement Properties of Rainbow Devices

DISPLACEMENT PROPERTIES OF RAINBOW DEVICES

E. Furman, G. Li and G. H. Haertling

Gilbert C. Robinson Department of Ceramic Engineering
Clemson University
Clemson, South Carolina 29634-0907 USA

ABSTRACT

Rainbow devices are benders with promising displacement and load bearing capabilities. Benders are often used in the audio range with large driving electric fields. In this report properties of piezoelectric Rainbow devices based on PLZT compositions near the morphotropic phase boundary are reported for a wide range of frequencies. The fundamental bending mode is shifted to lower frequencies with increasing AC field. With DC bias the fundamental bending mode can be shifted in either direction. All of the observed shifts in resonant frequencies are consistent with the changes in the geometry of a Rainbow with the applied field. Rainbow devices displayed a reduction in switchable polarization and field-induced displacement in the low frequency range for high driving field conditions. Reduction of the displacement was also observed at moderate field levels in the frequency range well below the fundamental bending mode. Possible mechanisms to account for the observed behavior of Rainbow devices are presented.

INTRODUCTION

There are a number of devices, including pumps, speakers, laser deflectors, optical scanners, and relays, which use piezoelectric benders to obtain desired displacement levels.^{1,2} A novel bender called a Rainbow (**R**educed **A**nd **I**nternally **B**iased **O**xide **W**afer) with promising characteristics was recently developed at Clemson University. Rainbow actuators consist of an electromechanically active layer (piezoelectric, antiferroelectric, or electrostrictive) constrained by an electrically conducting, chemically reduced layer. Unlike the traditional unimorphs, the Rainbow is a monolithic device. The conducting layer is formed by exposing one side of a lead-containing ceramic to a reducing atmosphere produced by placing the ceramic in contact with a carbon block at high temperature. The reduced layer is not piezoelectric, and it acts both as the electrode and the constraining part of the bender. Rainbow devices with up to 1 mm displacement and 10 kg load-bearing capability were built.³ Not surprisingly, load-bearing capability and displacements have an inverse relationship to each other. In previous publications large field electromechanical properties of Rainbow devices were characterized at low frequencies.⁴ In addition, impedance measurements identified a number of low frequency

bending modes.⁵ Experimentally determined locations of resonance modes were in reasonable agreement with the results of Finite Element Modeling (FEM). However, the FEM results significantly underestimated the observed high field displacements. Nonlinear contributions to ferroelectric properties are known to be especially important at high fields, so the discrepancy between the FEM and experimental results in part may be accounted for by ferroelectric nonlinearities, since the FEM utilizes primarily low field linear properties. Rainbow devices have considerable internal stress which develops during the cool down stage following the reduction step. The internal stress originates from three sources: 1) the difference in thermal expansion between the reduced and oxide layers, 2) the volume change of the reduced layer occurring during the high temperature reduction step, and 3) the volume change of the oxide layer due to the ferroelectric phase transition. Internal stress influences all of the important properties of ferroelectric ceramics.⁶

In this report, the electromechanical characterization of Rainbow devices is extended to high frequency, high drive conditions. This information is important in assessing Rainbow applicability for the previously mentioned devices. A considerable amount of work has been done to characterize the nonlinear response of ferroelectric ceramics to high drive conditions. The field-induced enhancement of the piezoelectric properties was measured using an interferometer at frequencies well below that of the fundamental piezoelectric resonance and has been attributed to the nonlinear domain wall contribution.^{7,8} The occurrence of low frequency bending modes in Rainbow devices permits the direct observation of nonlinearities in the vicinity of the fundamental resonance.

Rainbow samples were prepared from PLZT 1.0/53/47 (La/Zr/Ti) and PLZT 6.0/56/44 ceramics. These materials were chosen because of their proximity to the morphotropic phase boundary where ceramics with excellent piezoelectric properties are known to exist.⁹

EXPERIMENTAL PROCEDURE

PLZT 1.0/53/47 and PLZT 6.0/56/44 ceramics were prepared using a conventional mixed oxide process. Following calcination at 925 °C for 2 hours, the milled and dried PLZT 6.0/56/44 powders were cold pressed as preform slugs and then hot pressed at 1200 °C for 6 hours at 14 MPa in an oxygen atmosphere. The PLZT 1.0/53/47 samples were sintered at 1250 °C for 4 hours. The PLZT wafers were then placed on graphite blocks and reduced in a preheated furnace at 925-975 °C from 10 to 240 minutes to obtain Rainbows with a wide range of oxide/reduced layer thickness ratios. Epoxy silver paint, cured at 200 °C, was applied as an electrode. To avoid reoxidation, the samples were poled at room temperature. The poling fields were typically twice the strength of the coercive field. The Rainbow geometry and poling direction are shown in Figure 1.

The location of the resonances of the Rainbow devices were determined with an HP 4194 impedance analyzer as previously described.⁵ A ZMI-1000 (Zygo Corp.) interferometer was used for the direct observation of the field-induced displacements. The experimental arrangement is shown in Figure 2. The laser head consists of a stabilized laser, an acousto-optic modulator, and a 20 MHz oscillator. The laser head provides a

beam with two orthogonal polarizations having different frequencies, f_1 and f_2 , which are separated by 20 MHz. The interferometer consists of a polarizing beamsplitter and two reflectors; one is fixed and the other is the Rainbow sample. The polarizing beamsplitter divides the laser beam into two frequency components. It directs the f_2 component to a stationary reflector and the f_1 component to the Rainbow sample. The optical path change modulates the frequency difference f_1-f_2 . The recombined signal is transmitted to the measurement board by a fiber optic cable. The measurement board compares the modulated signal F_m to the unmodulated signal F_r . The accumulated phase information is converted to the absolute displacement. The interferometer has 24 Å resolution and a maximum sampling rate of 133 KHz. Reflective tape (3M) was attached to the top of the Rainbow sample to obtain the necessary reflectivity for the sample to serve as the nonstationary reflector. A BK precision 3011B waveform generator supplies an AC voltage, which is amplified by a Kepko BOP 500M precision amplifier. At low frequency and large drive conditions, the field-induced displacement and polarization hysteresis loop were measured simultaneously. The reported displacement data are the averages of two or more measurements. For the hysteresis loop measurements a 15 μF capacitor C_{ref} was inserted in series with the sample. An HP 54504A digitizing oscilloscope was used to store the hysteresis loops. The oscilloscope was interfaced with a personal computer which was used for data analysis.

RESULTS AND DISCUSSION

The mechanical boundary conditions imposed on a Rainbow sample strongly influence its electrical field-induced characteristics. Modeling clay was applied along the periphery of the samples to keep them in intimate contact with the conducting plate on which the samples rest during measurement. The largest displacements were obtained when the sample was evenly constrained around its periphery by the clay. Comparison of a uniformly constrained sample to one with constraints imposed only on two opposite sides is shown in Figure 3. The more constrained sample had higher displacements near the resonance peak and the peak was shifted to higher frequency. An upward shift of resonance frequencies was also detected with an HP 4194 impedance analyzer. Larger displacements were also observed when Rainbows were lifting weights.⁴ The enhanced displacement observed with better clamping was likely due to the stiffening of a Rainbow and increase in the contact area between the sample and the plate on which it is resting. The flattening of the sample is of less importance since the FEM predicts the lowering of the resonance frequencies. The boundary condition with a sample uniformly constrained at its periphery was used for all of the sample measurements reported thereafter in this paper.

For the linear piezoelectric response, the general expression for the converse piezoelectric effect at constant stress is

$$x = dE \quad (1)$$

where x is the field-induced strain, d is the piezoelectric constant, and E is electric field.

The field-induced displacement of Rainbow actuators is not uniform. The largest displacement is obtained at the center of a Rainbow. Since the displacement is not uniform and is dependent on both the geometry and the material properties, it is appropriate to use the effective piezoelectric constants. The effects of the AC driving field strength on the resonance properties of PLZT 6.0/56/44 Rainbow is shown in Figure 4. On the vertical axis is a new bender piezoelectric coefficient $b_{33}(\text{eff})$. Previously, the effective d_{33} coefficient was used to characterize the Moonie bender.¹⁰ Use of the effective d_{33} coefficient permits the direct comparison of samples with the same diameter. Since the effective d_{33} coefficient for Moonie benders¹⁰ and for circular unimorphs¹ is proportional to the diameter of the sample squared, to compare samples with different diameters it is useful to introduce a new piezoelectric constant, $b_{33}(\text{eff})$, which permits the direct comparison of benders with different geometries. To calculate the $b_{33}(\text{eff})$ coefficient for benders general piezoelectric Equation 1 was adopted for the Rainbow geometry

$$d_{33}(\text{eff}) = \frac{y}{t} * \frac{t_{\text{oxide}}}{V} \quad (2)$$

$$b_{33}(\text{eff}) = \frac{d_{33}(\text{eff})}{D^2} \quad (3)$$

where y is the displacement at the center of the bender under field, t is its total thickness, t_{oxide} is the thickness of the oxide layer, V is the applied voltage, and D is the diameter of a sample.

The use of the $b_{33}(\text{eff})$ coefficient permits a direct comparison of benders with different diameters. In the case of a bar-shaped bender, the $d_{33}(\text{eff})$ coefficient should be divided by the length of the bender squared.

The continuous reduction in the resonance frequency with the increasing driving voltage is in agreement with resonance behavior of conventional ceramic resonators. The lowering of the fundamental resonance frequency as the driving field strength is increased has been observed previously in homogeneous ferroelectric ceramic resonators.¹¹ Holland and EerNisse propose that the domain wall contribution is enhanced with increasing field magnitude. The enhanced domain switching should result in larger piezoelectric and dielectric constants. They further state that the nonlinear effects should be especially large near the resonance where the strain amplification is proportional to the mechanical Q (the reciprocal elastic loss tangent). The reduction of mechanical Q and enhanced piezoelectric coupling coefficients (associated with lowering of the resonance frequency) were observed in PZT ceramics with compositions near the morphotropic phase boundary at higher fields.⁸ Beige and Schmidt¹² made quantitative predictions for the shift of the resonance frequency as a function of nonlinear elastic or piezoelectric coefficients for a bar-shaped sample. The resonance frequency, $\Delta\omega_r$, is linearly dependent on the electric field, E_3 , for a resonator with nonlinear piezoelectricity:

$$\Delta\omega_r = - \frac{d_{311} \omega_r E_3}{s_{11}^E} \quad (4)$$

where d_{311} is the lowest order nonlinear piezoelectric coefficient, ω_r is the resonance frequency, and s_{11}^E is the elastic compliance. Depending on its magnitude, the piezoelectric nonlinear contribution to the shift of resonance frequency may be important for an applied DC bias, but should be negligible for the AC drive condition.

For elastic nonlinearities, the change in resonance frequency has a quadratic dependence on the electric field magnitude:

$$\Delta\omega_v = - \left[\frac{32 (s_{111}^E)^2}{9 \pi^2 s_{11}^E} + \frac{9 s_{1111}^E}{32} \right] \frac{\omega_r d_{31}^2 E_3^2 Q^2}{(s_{11}^E)^3} \quad (5)$$

where s_{111}^E and s_{1111}^E represent the lowest order nonlinear elastic compliance coefficients, s_{11}^E is the linear elastic compliance coefficient, and d_{31} is the piezoelectric coefficient.

The elastic and piezoelectric nonlinear contributions to the shift in resonant frequencies with the changing electric field also occur for Rainbow samples but with different functional dependencies than for the bar-shaped samples described by Beige and Schmidt. Furthermore, with Rainbows there is a geometric contribution to the field dependence of the resonant frequency. The FEM predicts that as a Rainbow develops curvature during the cool down step it will become mechanically stiffer, i.e., its resonant frequencies will increase for all modes.⁵ This effect is the strongest for the fundamental bending mode – the mode shown in Figure 4. The stiffening of the Rainbow during the cool down step implies that the potential energy for a Rainbow in equilibrium is asymmetrical. As the magnitude of the electric field increases, a Rainbow should become progressively flatter. Flattening of the Rainbow should result in the decrease of the resonant frequencies. The magnitude of this contribution is currently unknown, but is qualitatively consistent with the observed lowering of the resonant frequency with increasing AC fields.

The field-induced displacement at 700 Hz of the same PLZT 6.0/56/44 Rainbow sample over a wide range of applied fields is shown in Figure 5. The interferometer apparatus was used to measure the displacements with gradually increasing fields applied in the poling direction. The displacements were then measured while the field was reduced. There is reasonable agreement between the two displacement curves for high and low field regions. However, for the intermediate field region, the displacements for the increasing field are significantly higher than for the decreasing field. Since the sample was well aged prior to testing, it is possible that the difference in piezoelectric activity is due to the de-aging effects on the domain wall activity. The retention of the piezoelectric activity at low fields implies that the sample remains in the poled state. In the inset in Figure 5, $b_{33}(\text{eff})$ shows an upward trend from the lowest measured fields. This behavior is in marked contrast with properties of PLZT bulk resonators measured well below the fundamental piezoelectric resonance.^{7,8} In those samples there was a range of electric fields extending from zero to several hundred V/cm in which the piezoelectric properties were independent of the driving field strength. At higher fields, nonlinear piezoelectric contributions, similar to those shown in Figure 5, were observed. The likely reason for the

enhanced piezoelectric response of the Rainbow at 700 Hz is its proximity to the fundamental bending mode. As the driving voltage is increased, the resonant frequency is shifted toward the measuring frequency. At the highest field level tested, the resonant frequency is estimated to be 1725 Hz, as compared to approximately 3 KHz at 500 V/cm, thus greatly increasing its influence on the measured displacements at 700 Hz.

At frequencies (300 Hz and 30 KHz) well removed from the fundamental bending resonant frequency (3 KHz), the piezoelectric nonlinearities are not observed at moderate field levels as shown in Figure 6. Piezoelectric nonlinearities become important at approximately 300 V/cm field level at 300 Hz— in good agreement with bulk resonators.^{7,8} The response of the sample near its low field resonant frequency, 3 KHz, is fairly flat over the entire driving field range. The nonlinear domain wall contribution has the opposite field dependence on resonant frequency compared to the change of shape at 3 KHz. In addition, the mechanical Q is likely to be reduced for the very high displacements observed at 3 KHz, also contributing to the reduced displacement amplitude for high drive conditions. The displacement of the Rainbow at 30 KHz is well below not only the displacement at the resonant frequency but also that at 300 Hz. Clearly, low frequency bending modes are essential for obtaining large field-induced displacements.

The effect of the DC bias field on the fundamental resonant frequency is shown in Figure 7. Bias applied in the same direction as the poling field reduces the resonant frequency. For the forward bias, the oxide layer shrinks laterally (because the d_{31} coefficient is negative) causing flattening of the Rainbow sample, which in turn lowers its stiffness resulting in the decrease of the resonant frequency. When DC bias is applied in the opposite direction, the measured resonant frequency increases. Thus the observed shifts of resonant frequency with DC bias are consistent with the changes in the sample geometry. While the contributions of piezoelectric and dielectric nonlinearities can not be completely discounted, it should be noted that for the PZT bulk resonators the effects of DC bias on the location of the radial mode resonant frequency are negligible.¹³

Dielectric hysteresis loops and displacements were measured simultaneously at low-frequency, high-field conditions. The results are shown in Figure 8. There is good agreement between the reduction in switchable polarization and field-induced displacement. In fact, comparing the results for the lowest and highest frequencies in Figure 8, there is a 15% reduction in the polarization and a 17% reduction in the displacement. The correspondence between the two values indicates that at higher frequencies certain ferroelastic – and not 180° – domains cannot switch and their contribution is lost. Examining the shapes of hysteresis loops shown in Figure 9, it is clear that at higher frequencies complete switching of the Rainbow sample is not possible. The saturation of the hysteresis loop for one orientation but not for the other suggests that the potential well for the domain switching is not symmetrical. The preferred polarization in virgin Rainbow samples was previously observed¹⁴ and asymmetry of the loop is a common occurrence in these devices.

The coercive field for both polarities as well as the average coercive field are shown in Figure 10. The coercive field after the initial rise shows rapid reduction with increasing frequency. The asymmetry of the hysteresis loop is reflected in the different coercive field values for the two polarities. The average coercive field increases with frequency up to 1 Hz. At higher frequencies the coercive field reduction coincides with

the reduction of the switchable polarization and field-induced displacements. Bulk PLZT ceramics exhibit coercive fields proportional to the logarithm of frequency in the same frequency range as is used in this study.¹⁵ Additional experimental data at less than 1 Hz frequency is needed to determine if the coercive field rises faster than logarithmically with frequency which would suggest that an interfacial region may exist between the PLZT and the reduced layer. The resistive interfacial layer should maintain a greater fraction of the applied voltage at higher frequencies, resulting in a more rapid escalation of the coercive field than in the bulk sample.

For the Rainbow samples based on PLZT 1.0/53/47 ceramics, the effects of AC and DC bias were qualitatively similar to those observed for the PLZT 6.0/56/44 Rainbows and will not be further discussed in this report.. The frequency dependence of displacement for the Rainbow samples with drastically different oxide thickness ratios is shown in Figure 11. The same field level was maintained for each sample. The highest displacement was obtained for the Rainbow with the oxide and reduced layers of approximately equal thickness. A significant reduction in displacement in the frequency range well below that of the fundamental bending mode was observed in two of the three samples. Two samples with a thicker oxide layer contain the neutral (zero stress) axis in the oxide layer. The sample with the thinnest oxide layer has compressive stress throughout that layer. Since one of the two samples with the neutral axis in the oxide layer as well as the sample with the compressive stress throughout the oxide layer exhibit the low frequency displacement drop off, it is unlikely that the low frequency displacement relaxation is due to the presence of internal stress. Possibly there is an interfacial region, which acts electrically at low frequencies as a resistor in series with PLZT, thus causing a frequency-dependent voltage drop across the PLZT layer. The origin of the high impedance interfacial region may be: 1) a highly defective (containing microcracks) PLZT layer, 2) an intermediate layer formed between the PLZT and reduced layers during the reduction step, or 3) an insufficient amount of lead at the interface.

In PLZT 1.0/53/47 Rainbow samples, only partial hysteresis switching was possible even at the lowest frequencies. The coercive fields were significantly higher than when measured prior to high frequency testing. Partial debonding of the top electrode for one of the samples and degradation of polarization switching were observed and indicate the need for further study of these effects.

SUMMARY

The high frequency properties of PLZT Rainbow ceramics were investigated over a wide range of frequencies and electrical driving conditions. The results indicate that the Rainbow samples have low frequency bending resonant modes. These modes are highly sensitive to electrical and mechanical boundary conditions. Increasing the AC driving fields shifts the fundamental mode to a lower frequency. With a DC bias, either stiffening or softening of the sample is possible. All of the observed shifts in resonant frequencies with AC or DC driving fields are consistent with the field-induced changes in the shape of the Rainbow – flattening a Rainbow always leads to the reduction of the resonant frequency.

The low frequency reduction in field-induced displacement was observed at both high and low fields. At high field strengths, the polarization and the displacement have similar reductions with increasing frequency, indicating that the ferroelastic contribution to both is lost. The reduction of the displacement at low frequencies could not be correlated to the presence of the neutral axis in the oxide layer.

The observed nonlinear effects have the potential to be used in low frequency tunable devices. Alternatively, modifying the Rainbow geometry can reduce the effects of nonlinearities for devices which would benefit from linearity of response.

REFERENCES

1. M. R. Steel, F. Harrison and P. G. Harper, "The piezoelectric bimorph: An experimental and theoretical study of its quasistatic response," *J. Phys. D: Appl. Phys.*, **11**, 979 (1978).
2. A. G. Kuzin, N. S. Mirgorodskii, V. P. Pikarnikov and V. V. Soroka, "Piezoelectric light-beam deflectors. I. Theory of bimorph deflectors and experimental tests," *Sov. Phys. Tech. Phys.*, **21**, 1128 (1976).
3. G. H. Haertling "Rainbow Ceramics - A New Type of Ultra-High-Displacement Actuator," *Am. Cer. Soc. Bull.*, **73**, 93 (1994).
4. E. Furman, G. Li and G. H. Haertling, "Electromechanical Properties of Rainbow Devices," in ISAF 94: Proceedings of the Eighth IEEE International Symposium on Applications of Ferroelectrics, to be published.
5. E. Furman, G. Li and G. H. Haertling, "An Investigation of the Resonance Properties of Rainbow Devices," *Ferroelectrics*, **160**, 357 (1994).
6. R. S. Woollett and C. L. LeBlanc, "Ferroelectric Nonlinearities in Transducer Ceramics," *IEEE Trans. Sonics and Ultrasonics*, **SU-20**, 24 (1973).
7. Q. M. Zhang, W. Y. Pan, S. J. Jang and L. E. Cross, "Domain Wall Excitations and their Contributions to the Weak-signal Response of Doped Lead Zirconate Titanate Ceramics," *J. Appl. Phys.*, **64**, 6445 (1988).
8. S. Li., W. Cao, R. E. Newnham and L. E. Cross, "Electromechanical Nonlinearity of Ferroelectric Ceramics and Related Non-180° Domain Wall Motions," *Ferroelectrics*, **139**, 25 (1993).
9. B. Jaffe, W. R. Cook, Jr. and H. Jaffe, "Piezoelectric Ceramics" (Academic Press, London, 1971).
10. K. Onitsuka, A. Dogan, J. Tressler, Q. Xu, S. Yoshikawa and R. E. Newnham, "Metal-Ceramic Composite Transducer, the 'Moonie'," App. 25, V.2 in Material Research Laboratory, The Pennsylvania State University, 1994 O.N.R. Annual Report (1994).
11. R. Holland and E. P. EerNisse, "Accurate Measurement of Coefficients in a Ferroelectric Ceramic," *IEEE Trans. Sonics and Ultrasonics*, **SU-16**, 173 (1969).
12. H. Beige and G. Schmidt, "Electromechanical Resonances for Investigating Linear and Nonlinear Properties of Dielectrics," *Ferroelectrics*, **41**, 39 (1982).
13. K. Uchino, H. Negishi and T. Hirose, "Drive Voltage Dependence of Electromechanical Resonance in PLZT Piezoelectric Ceramics," pp. 47-49 in Proceedings of the 7th Meeting on Ferroelectric Materials and Their Applications, *Japanese Journal of Applied Physics*, **28**, supplement 28-2, 47 (1989).
14. G. H. Haertling, "Compositional Study of PLZT Rainbow Ceramics for Piezo Actuators," in ISAF 94: Proceedings of the Eighth IEEE International Symposium on Applications of Ferroelectrics, to be published.

15. K. Furuta and K. Uchino, "Electric-Field-Induced Strain in (Pb, La)(Zr, Ti)O₃ Ceramics," *Advanced Ceramic Materials*, 1, 61 (1986).

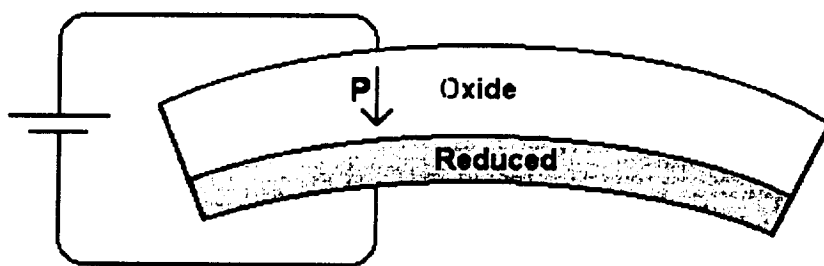


Figure 1. Rainbow geometry and poling direction.

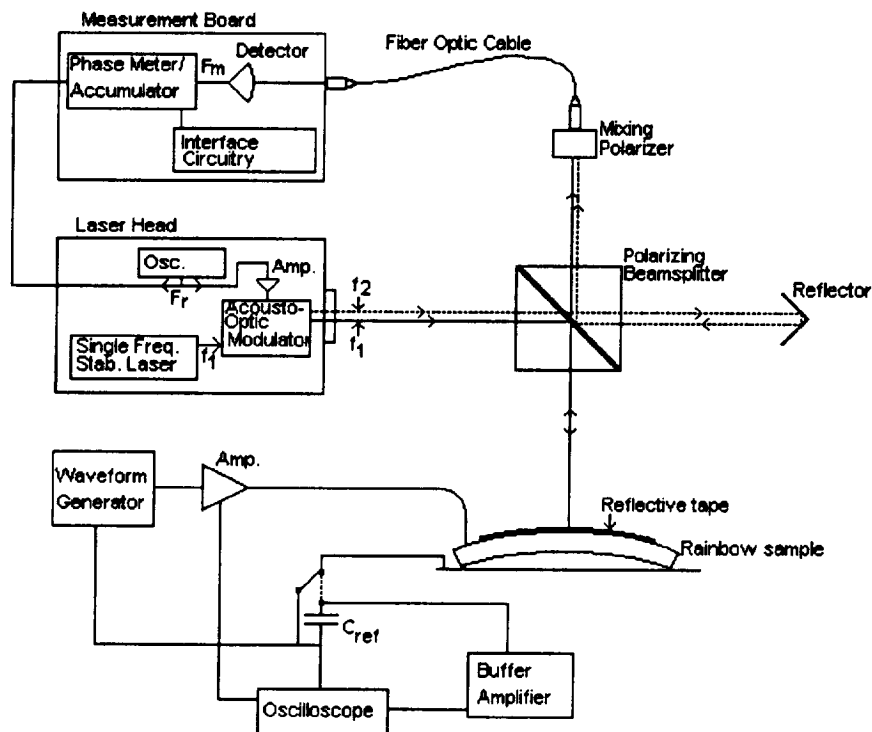


Figure 2. Experimental arrangement for measuring hysteresis loops and displacements for Rainbow samples.

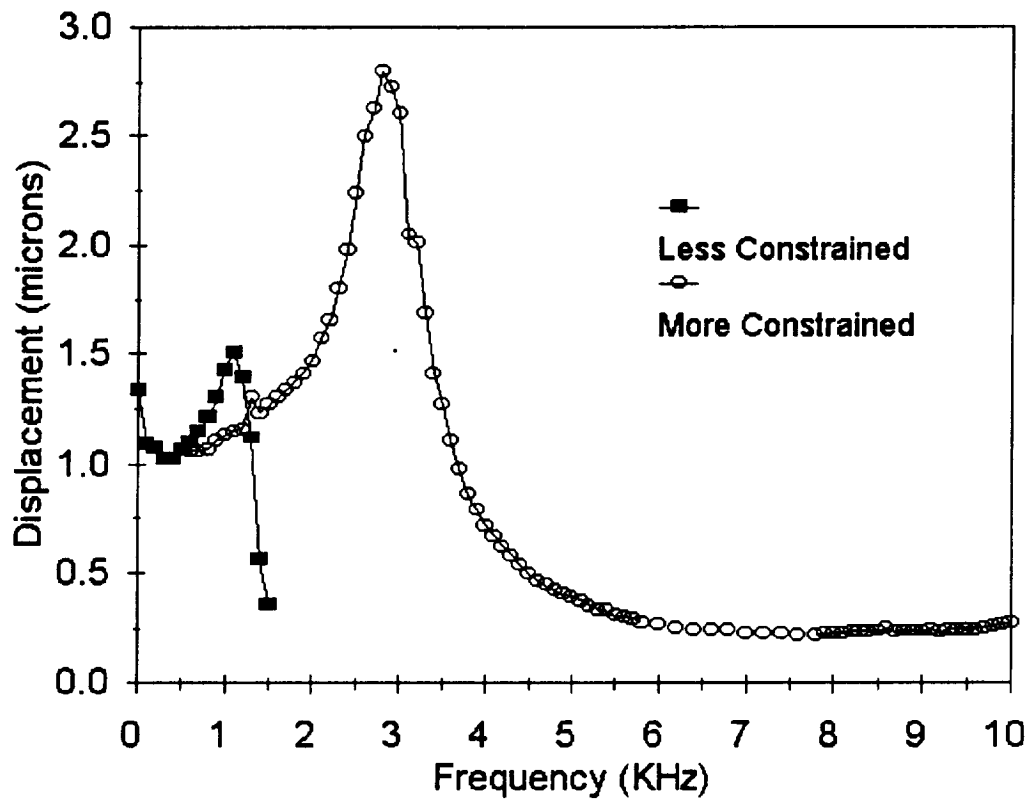


Figure 3. Effects of mechanical boundary conditions on fundamental bending mode resonance frequency of PLZT 1.0/53/47 Rainbow. Sample diameter = 3.18 cm, total thickness = 706 μm , AC Voltage = 20V.

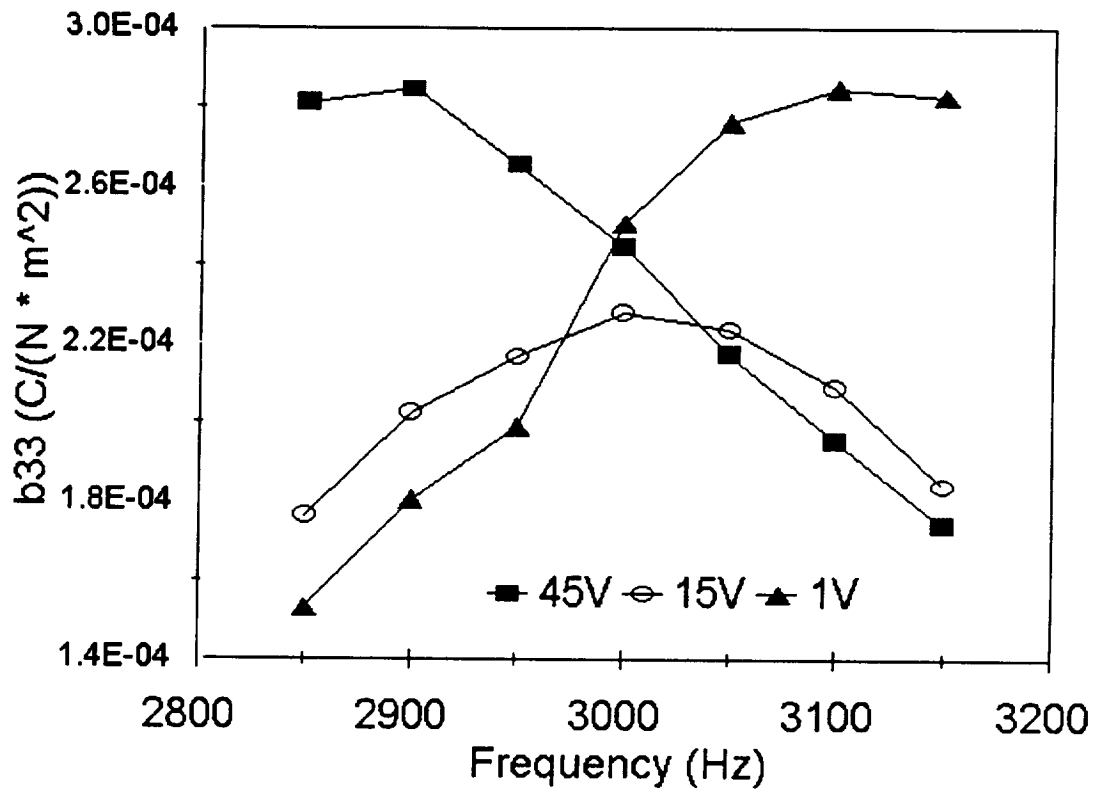


Figure 4. Effect of AC field strength on fundamental bending mode frequency for PLZT 6.0/56/44 Rainbow. Sample diameter = 3.18 cm, total thickness = 508 μm , reduced layer thickness = 107 μm .

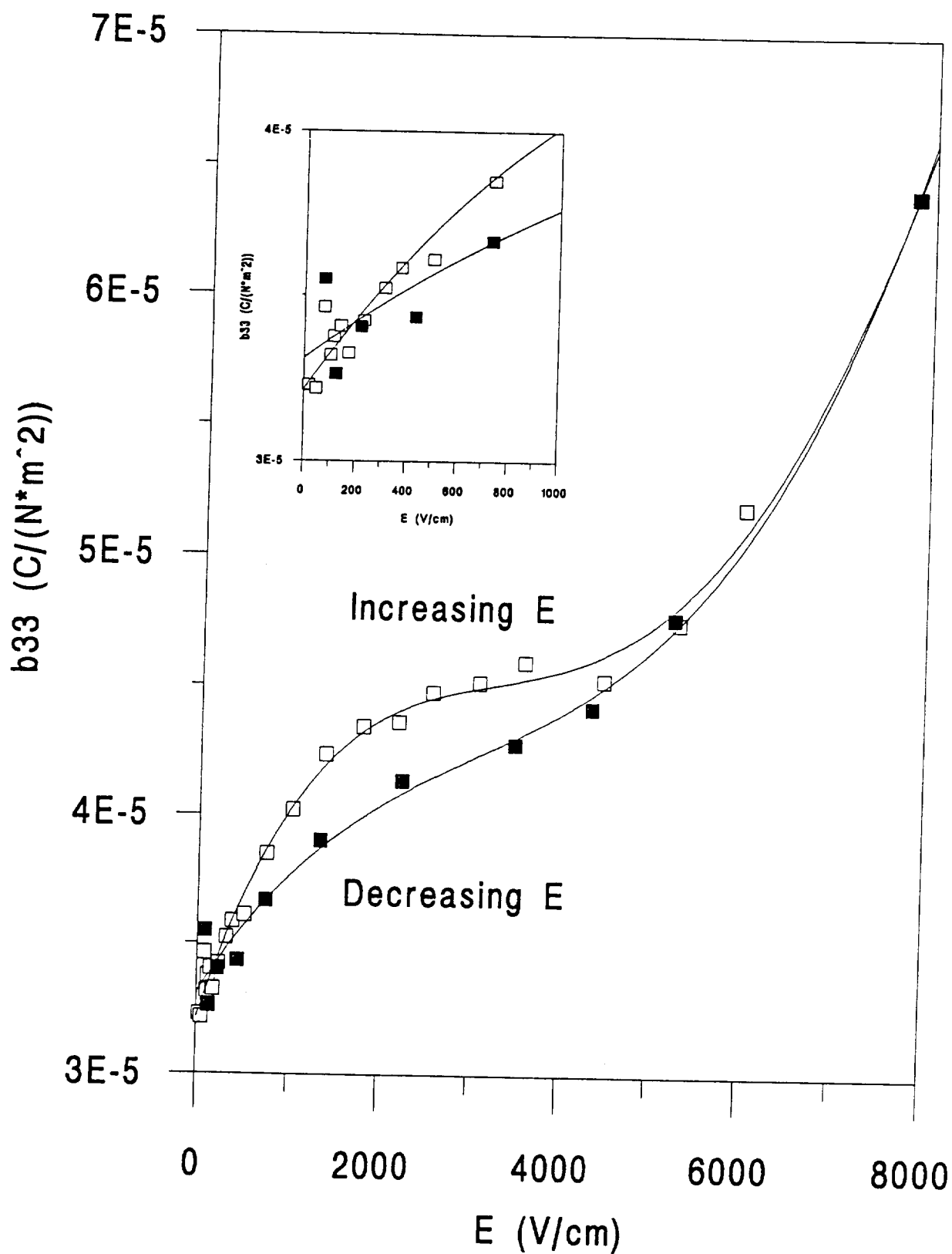


Figure 5. Field-induced displacements of PLZT 6.0/56/44 Rainbow at 700 Hz for increasing and decreasing AC field strength. Sample diameter = 3.18 cm, total thickness = 508 μm , reduced layer thickness = 107 μm .

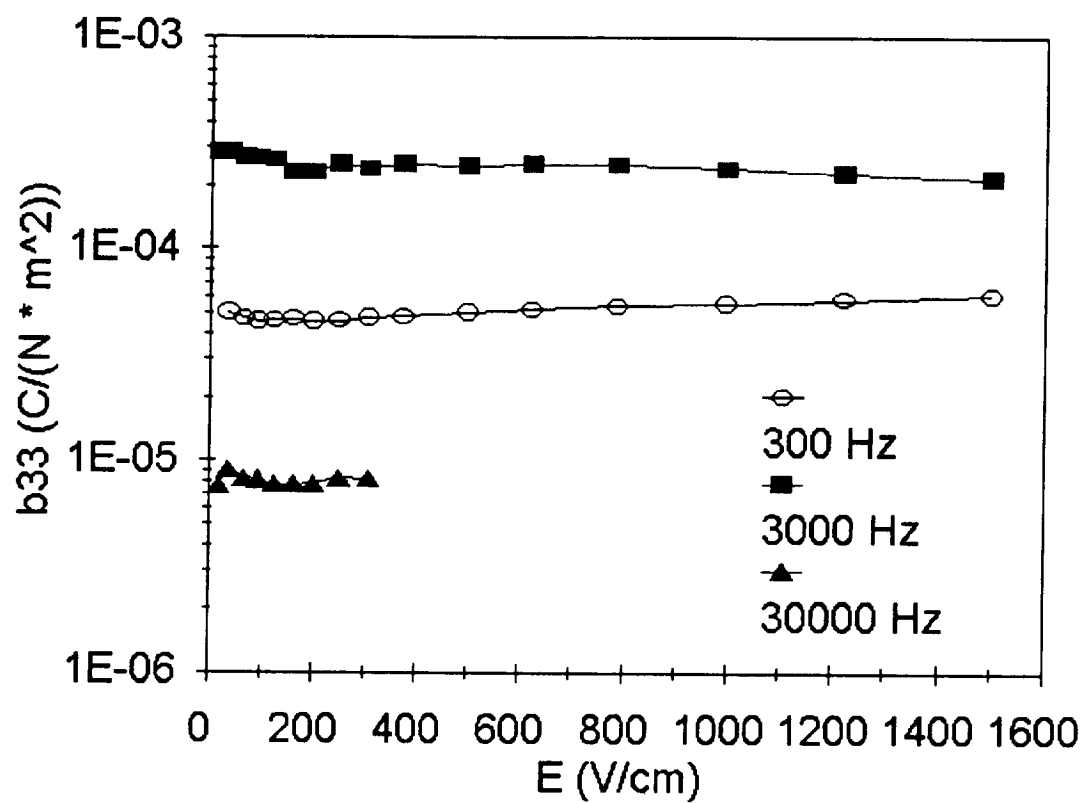


Figure 6. b_{33} coefficients for PLZT 6.0/56/44 Rainbow at 300 Hz, 3 KHz, and 30 KHz for increasing AC field strengths. Sample diameter = 3.18 cm, total thickness = 508 μm , reduced layer thickness = 107 μm .

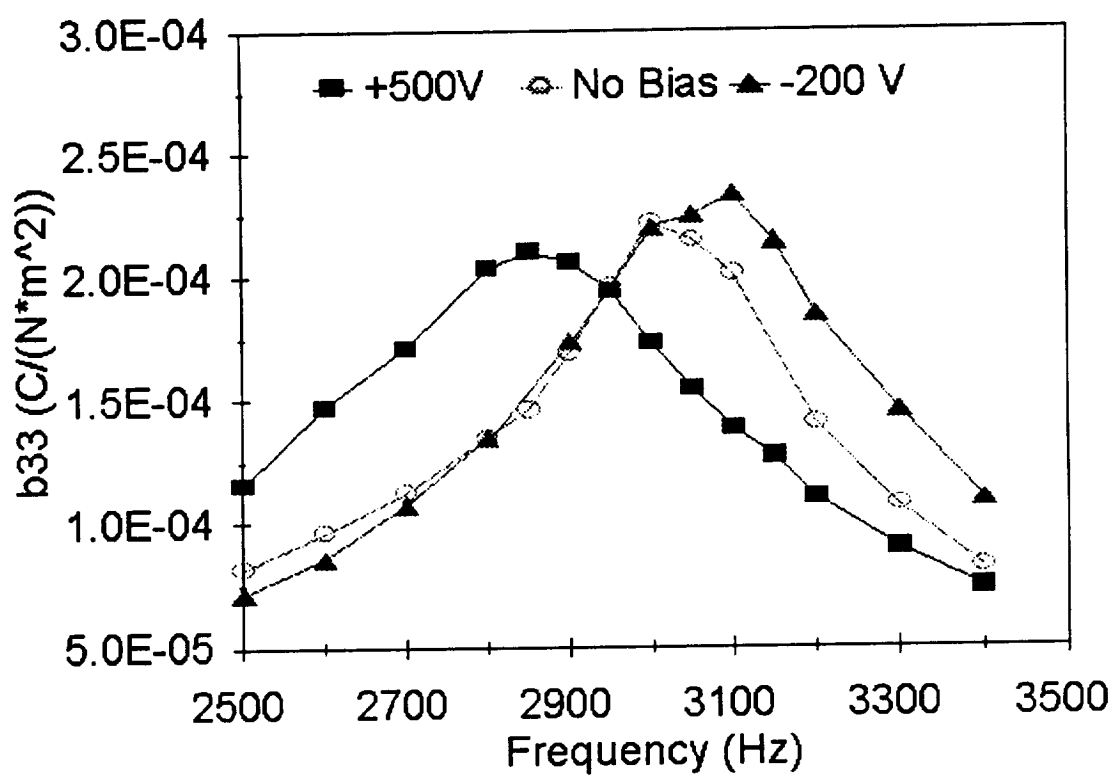


Figure 7. Effect of DC bias field on the fundamental bending mode resonance frequency for PLZT 6.0/56/44 Rainbow. Sample diameter = 3.18 cm, total thickness = 508 μm , reduced layer thickness = 107 μm .

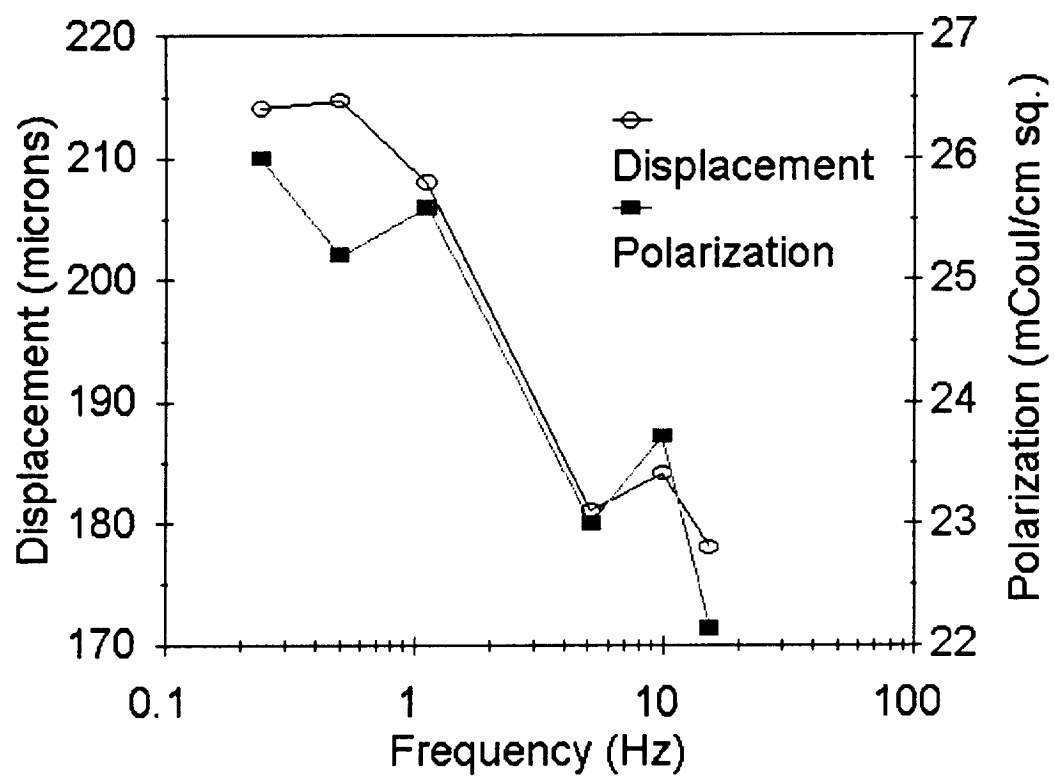


Figure 8. Frequency dependence of spontaneous polarization and displacement of PLZT 6.0/56/44 Rainbow in the low frequency range. Sample diameter = 3.18 cm, total thickness = 508 μm , reduced layer thickness = 107 μm .

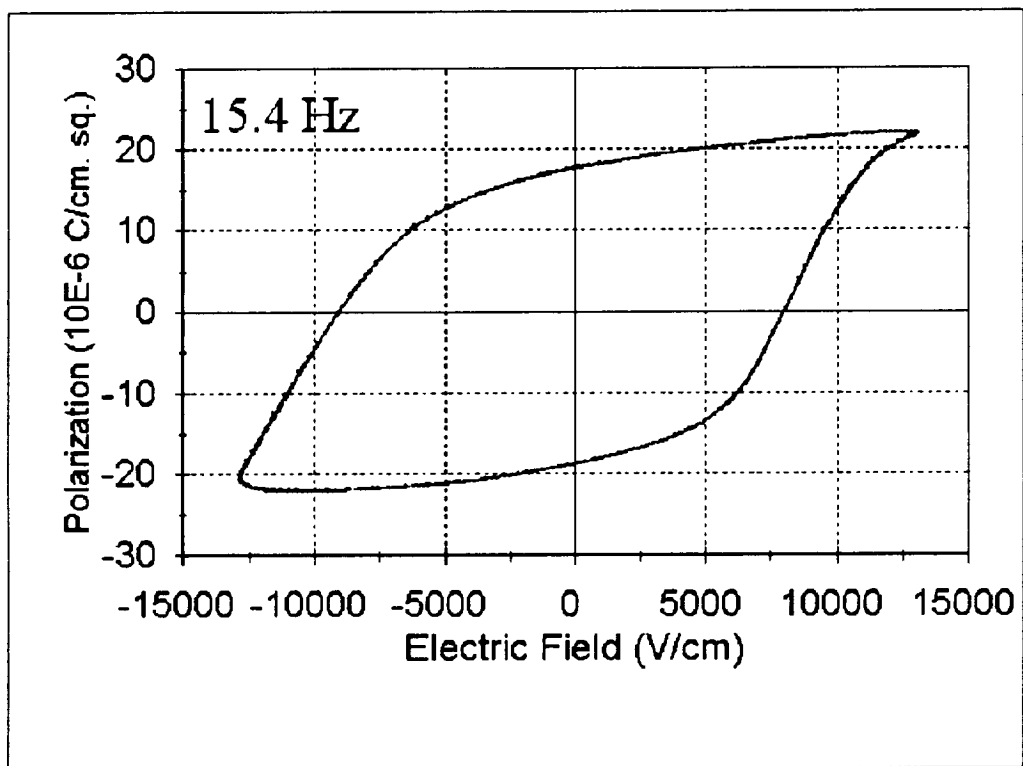
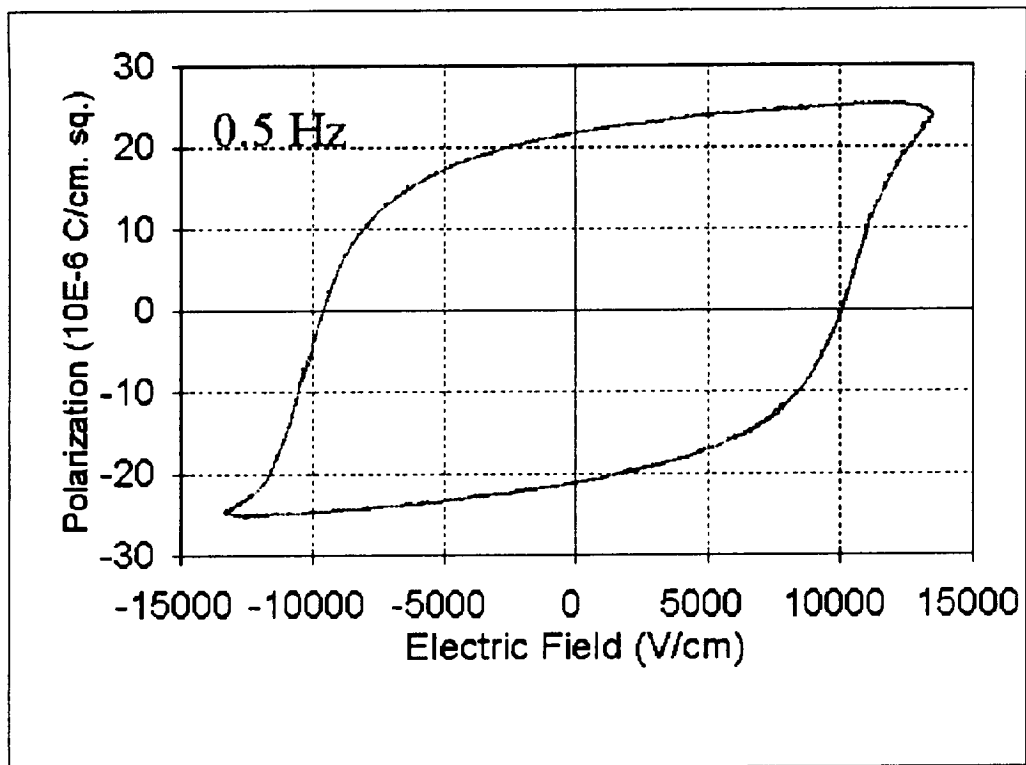


Figure 9. Hysteresis loops of PLZT 6.0/56/44 Rainbow at different frequencies. Sample diameter = 3.18 cm, total thickness = 508 μm , reduced layer thickness = 107 μm .

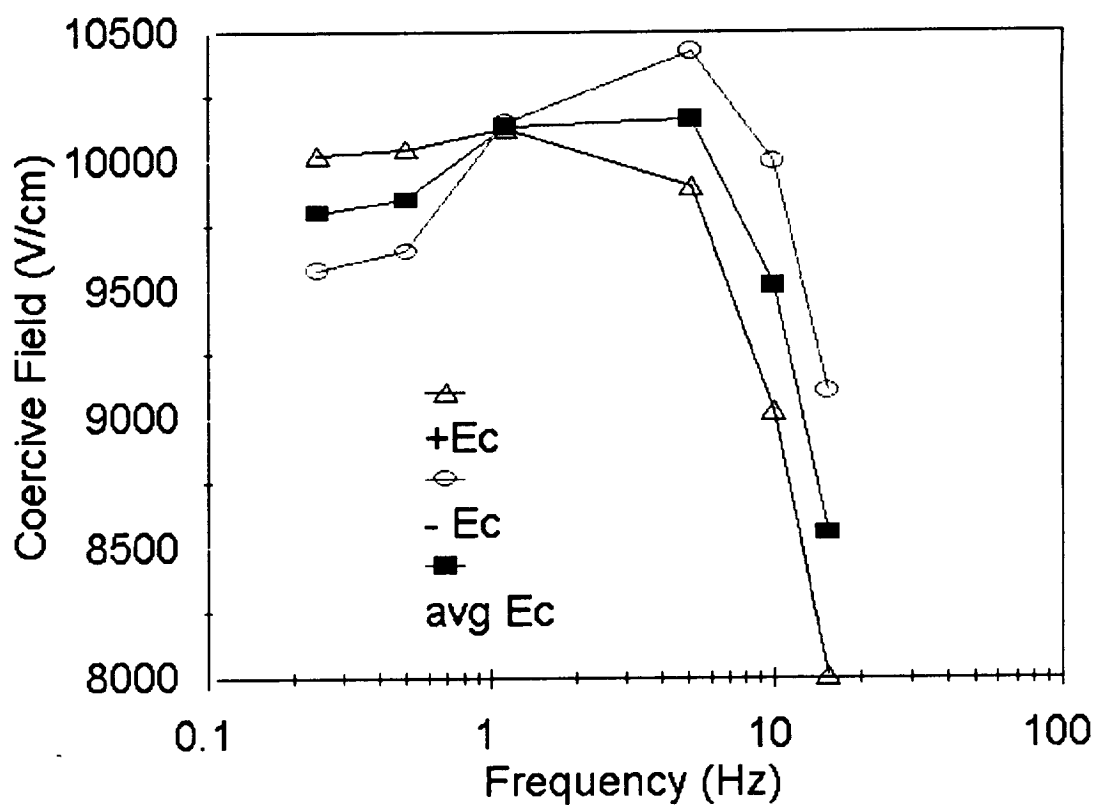


Figure 10. Frequency dependence of average, positive, and negative coercive fields for PLZT 6.0/56/44 Rainbow. Sample diameter = 3.18 cm, total thickness = 508 μm , reduced layer thickness = 107 μm .

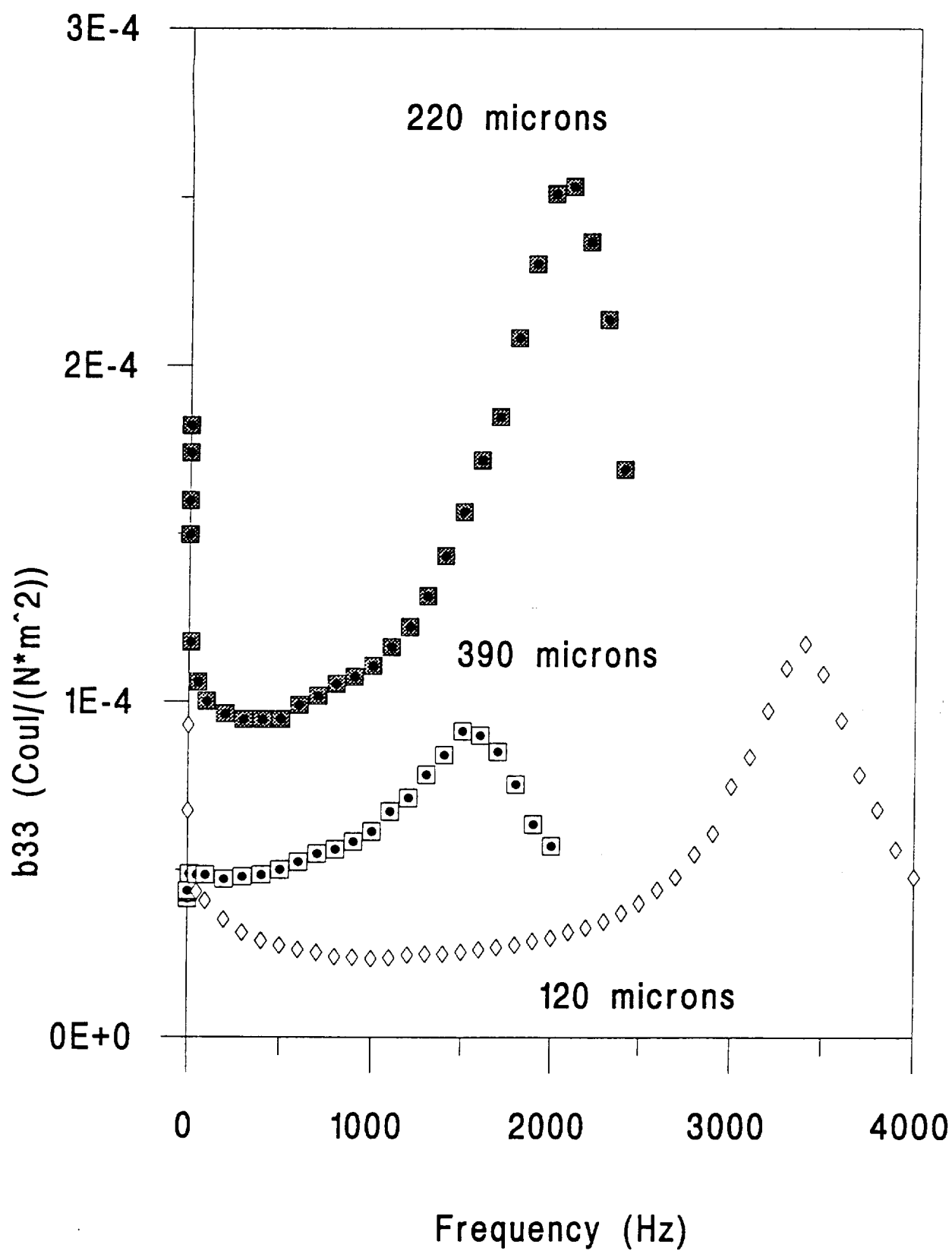


Figure 11. b_{33} coefficients for PLZT 1.0/53/47 Rainbows with different oxide layer thicknesses. Sample diameter = 2.22 cm, total thickness = 432 μm , E field = 2.5 KV/cm.

Part V.

General Studies of Rainbow Processing and Properties

General Studies of Rainbow Processing and Properties

Recent developments in the technology of piezoelectric and electrostrictive ceramic actuators have amply demonstrated that the materials required for future applications will need to be more sophisticated (multifunctional and smart), the techniques for strain amplification more innovative and cost effective, and the performance of the devices more reliable in harsh environments such as space. Such applications include positioners, active structures, acoustic canceling components, variable focus elements, pumps, switches, linear actuators and multifunction devices. Of these, some involve very high electromechanical displacements on the order of several millimeters. Unfortunately, the materials presently available for these devices generally achieve less than 0.1 mm total strain in any practical size element, and thus, are not directly suitable for such large displacements. Consequently, various techniques for amplifying the strain have been developed and reported.

The most recently developed strain amplifying method for piezoelectric and electrostrictive ceramic materials which shows promise for meeting some, if not many, of the high strain applications is known as the RAINBOW technology. This acronym denotes the basic active structure of the Rainbow device which is produced by a special high temperature chemical reduction process and stands for Reduced And Internally Biased Oxide Wafer. In their most basic sense, Rainbow ceramics can be thought of as pre-stressed, monolithic, axial-mode benders, similar in operation to the more conventional unimorph and bimorph type benders. But because of their unique dome or saddle-like configuration, Rainbow ceramics are able to produce much higher displacements ($> 1\text{mm}$) and sustain significantly greater loads (10 kg) than normal benders.

This section reports on some of the newer methods developed within the last year for producing the Rainbow ceramics, as well as evaluating some of their properties and characteristics. These include:

- a. Rainbow actuator compositional work in the PLZT system
- b. Hot forming of curved shapes of piezo ceramics
- c. Slipcasting of tubes and solid rods
- d. Tape casting of thin sheets and disks
- e. Rainbow reduction of curved shapes with granular carbon
- f. Rainbow reduction of tubes with granular carbon

Rainbow PLZT Compositional Work

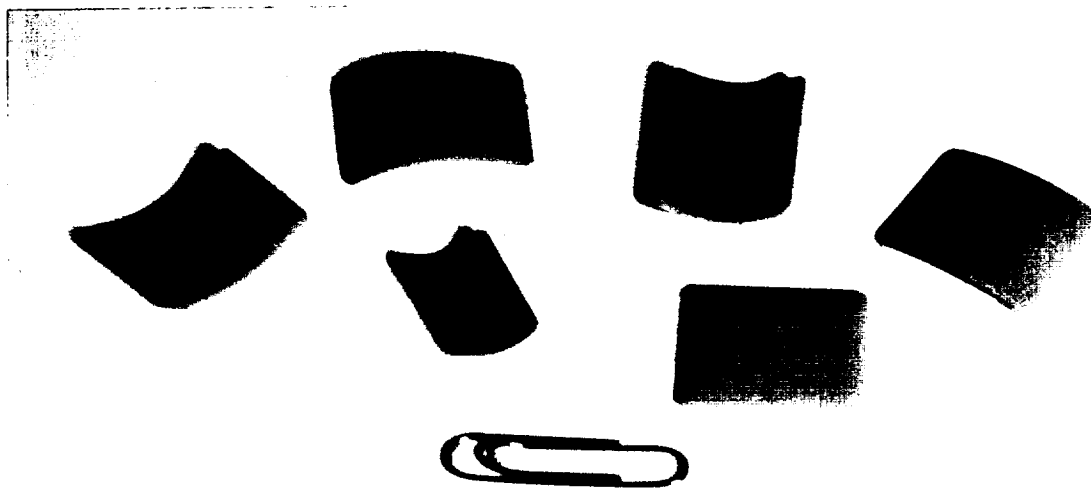
On-going studies have shown that the PLZT compositional system is one which yields materials possessing some of the highest coefficients for piezoelectric and electrostrictive actuators. It has also been found that PLZT ceramics are near ideal for achieving the ultra-high displacements recently reported for the Rainbow (Reduced and Internally Biased Oxide Wafer) actuators. In order to determine the optimum composition or compositions

for these Rainbow actuators, a study was conducted by preparing and processing selected formulations throughout the PLZT system. Results from this study indicate that, like the conventional direct extensional-mode materials, the maximum Rainbow bending displacements occur in materials located compositionally at the morphotropic ($FE_{\text{rhom}} - FE_{\text{tet}}$) and Curie point (FE - PE, PE - AFE) phase boundaries. Examples of specific compositions for each of these regions are 2/53/47, 9/65/35 and 8.5/70/30 (La/Zr/Ti), respectively. Microstructural (grain size), electrical (dielectric constant, dissipation factor) and electromechanical (axial displacement) data are presented for selected compositions in the system.

A full paper on this subject was presented at ISAF-94 at Penn State. Although not yet published, a copy of the paper is included in Part VI of this report.

Hot Forming of Curved Piezo Patches

Previous work (many years ago) on the high temperature creep properties of PZT and PLZT ceramics pointed out that it is entirely possible to hot mold a high lead-containing piezoelectric ceramic with a suitable mandrel and a modest amount of weight. Some preliminary experiments were recently conducted on PZT-2Bi, PLZT 5.5/65/3, PLZT 1/53/47, and PLZT 9/65/35 in order to re-evaluate this conclusion. Lapped, planar samples were mounted inside of an alumina cylindrical tube with approximately 175 grams of weight in order to induce the plate to conform to the shape of the tube while at an elevated temperature. A typical temperature and time was 1100°C for one hour although good results were also be obtained as low as 1000°C for several hours. Thicknesses of the plates were typically in the range of 0.025 - 0.035 inches. The photograph below shows some of the parts after molding. Radii of curvature for the molded parts ranged from very large (essentially flat) to approximately one inch. Although simple curvatures are shown here, it is believed that almost any shape could be molded with the proper mandrels.

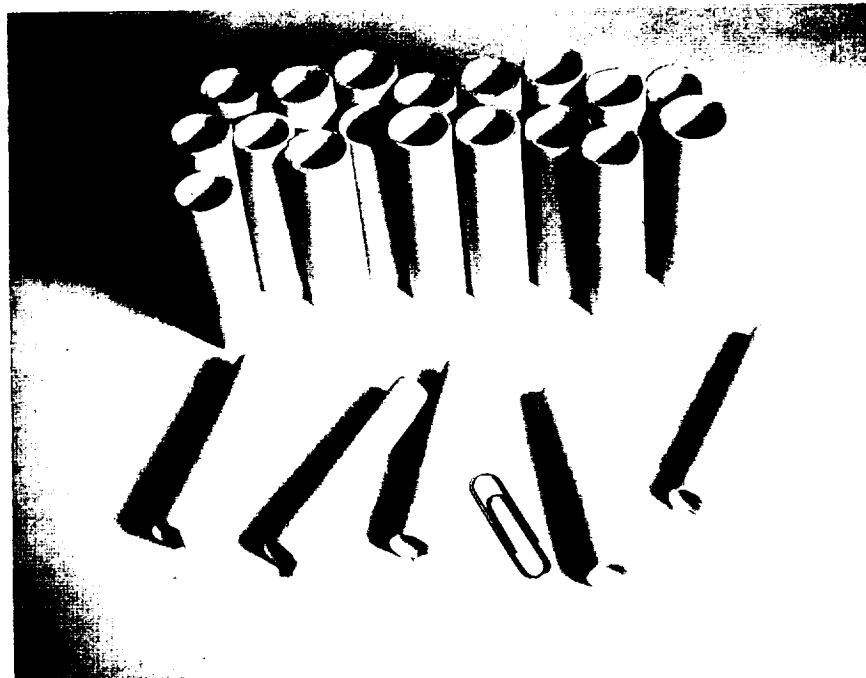


Hot Molded Parts of PZT and PLZT Piezoelectric Plates

Slipcasting of Piezo Ceramics

Another technology which is useful to employ in the fabrication of circular, oval or odd shaped tubes for Rainbows or conventional piezo devices is slipcasting. In this process, ceramic slip (ceramic powder suspended in water) is poured into a plaster mold for a given length of time and then the excess slip poured off leaving a hollow "shell" of semi-dry ceramic material in the shape of the mold. During further drying, the ceramic shape shrinks away from the outer plaster mold, thus leaving it free to be removed by means of a relatively simple process of turning the mold over (in the case of a tube) or taking the mold apart in the case of a complex shape. After complete drying, the "green" ceramic parts are sintered (fired) at an elevated temperature of approximately 1250°C for 4 hours. A selection of slipcast tubes of various compositions is shown below.

Solid rods or irregularly-shaped rods can also be fabricated via slipcasting. This is easily accomplished by continually keeping the mold filled with ceramic slip until it is apparent that the shape is completely cast solid. After drying, the part is removed from the mold and sintered to final density.

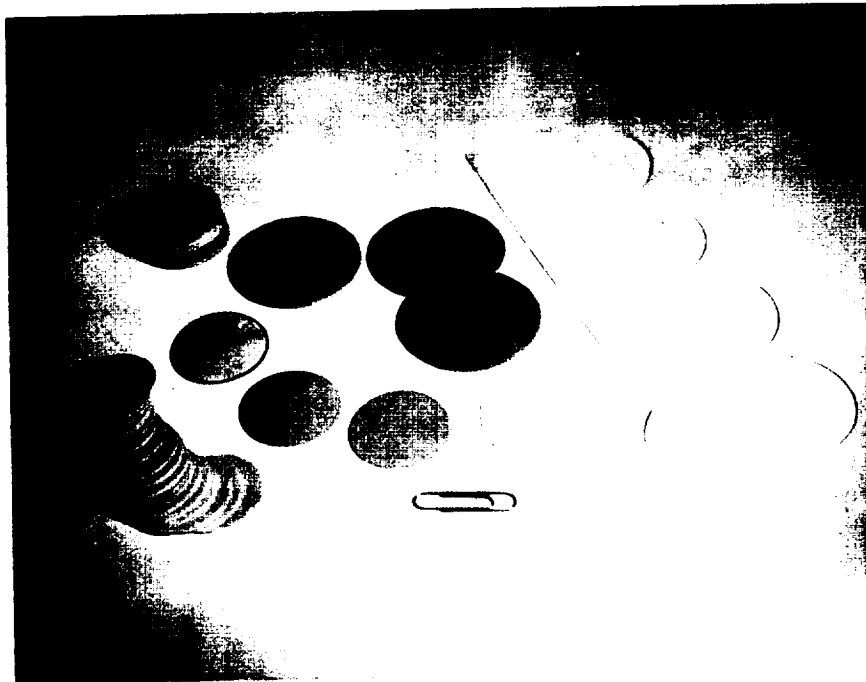


Slipcast Tubes of PLZT Compositions 1/53/47, 5.5/56/44 and 9/65/35

Tapecasting of Piezo Disks

An investigation was also conducted on the development of a suitable tapecasting process for thin and thick disks which could be used as Rainbow actuators or as conventional piezo elements. In this process, appropriate binders, plasticizers, deflocculants

and solvents are mixed with the ceramic powder and cast onto a flat surface with the aid of a doctor blade which dispenses the ceramic slip at a given, uniform thickness. After drying, the organic solvents are no longer present in the tape, thus leaving it in a solid, flexible condition such that it can be easily cut with a sharp knife, scissors, paper cutter or any type of typical "cookie cutter." The "green" parts are then slowly fired ($3^{\circ}\text{C}/\text{minute}$) to approximately 600°C in order to burn off the organic binder and then fired at a more usual faster rate ($5^{\circ}\text{C}/\text{minute}$) to achieve final density. The tapecast process has the advantage of economically producing thin or thick plates of ceramic with small-to-large area without the necessity of sawing and lapping. Fired piezo disks ranging in thickness from 0.010 to 0.035 inches and in diameter from 0.250 to 3.0 inches were fabricated and tested. Many of these disks were further processed into Rainbow elements. Typical examples are shown below.



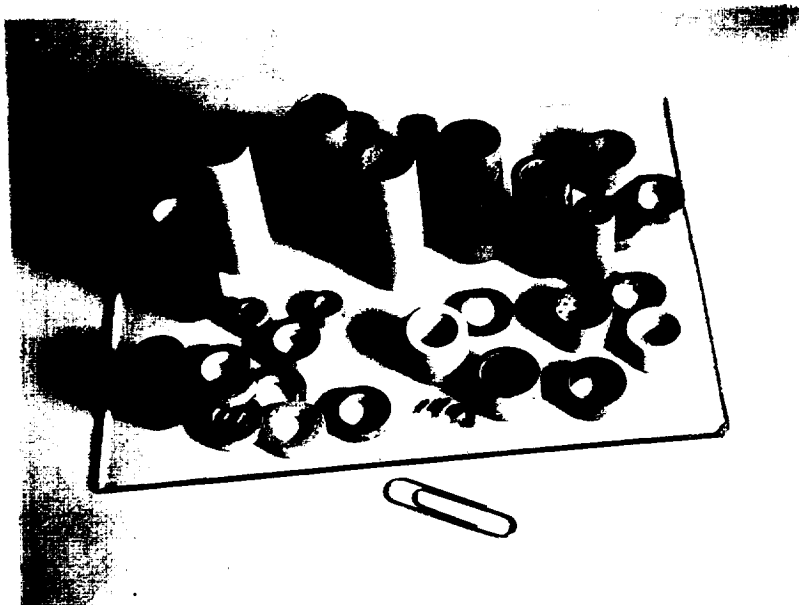
Tapecast Sheet, Punched Disks and Fired Parts of PLZT 1/53/47

Rainbow Reduction with Granular Carbon

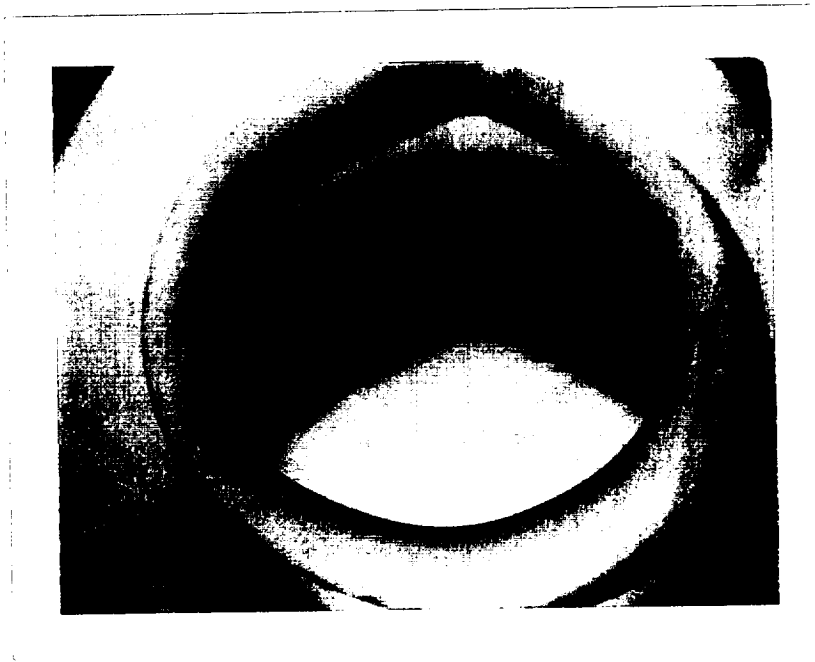
The chemical reduction of irregular shapes, such as have been described above, is quite difficult with a solid carbon block normally used in the Rainbow process. Therefore, granular carbon, in a size range from -20 to +84 mesh, was used to form a reduction surface of the same topography as that of the irregular piezo plate. The carbon particles in contact with the bottom surface of the piezo plate were found to be effective in chemically reducing that surface while the top surface remained unaffected since it was exposed to the normal oxidizing atmosphere of the furnace. It was determined that the kinetics of reduction for

the granular carbon was essentially the same as that for the solid carbon blocks; i.e., typical reduction temperatures and times ranged from 950 - 975°C for one to two hours.

Granular carbon was also used to reduce the interior and exterior surfaces of open or closed-end piezo tubes. Examples of these are shown in the photos below.



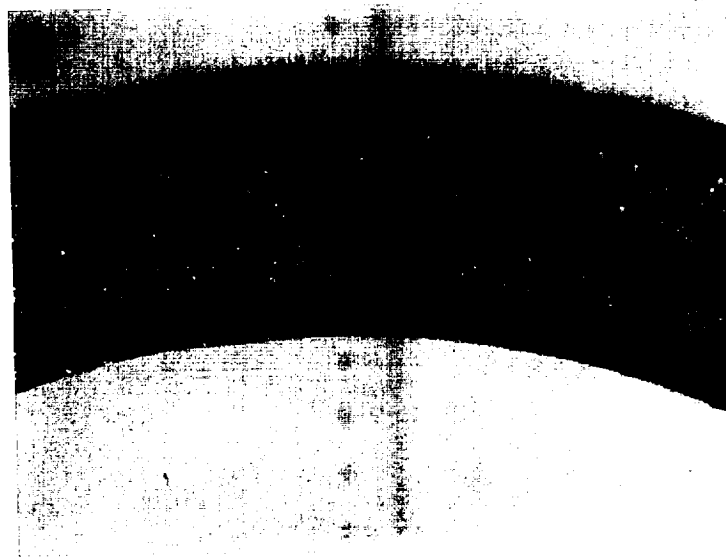
Examples of Rainbow Reduced PLZT Tubes



Rainbow Reduction of the Inside Surface of an Irregular Tube



A Closeup View of the Above Tube



A Closeup View of a PLZT Tube Reduced on Both Inside and Outside Walls

Part VI.

Publications

Rainbow Ceramics—A New Type of Ultra-High-Displacement Actuator

A new method for producing ultra-high-displacement, monolithic, transducer ceramics has recently been developed. The technique consists of selectively reducing one surface of a high-lead-containing piezoelectric or electrostrictive wafer with graphite in an oxidizing atmosphere at an elevated temperature. The resulting stress-biased wafer is referred to as a "rainbow" ceramic because of its unique, domed structure that leads to high electromechanical displacement and enhanced load-bearing capability.

GENE H. HAERTLING*

Clemson University, Clemson, South Carolina 29634-0907

In the last several years, the technology of using piezoelectric and electrostrictive ceramic materials as solid-state actuators for small ($<10\ \mu\text{m}$) and precise mechanical movement devices has undergone considerable investigation and development.¹⁻⁶ More recently, it has become quite evident that these same types of solid-state devices are desirable in newer applications—linear motors, cavity pumps, switches, loud speakers, noise-canceling devices, variable-focus mirrors, and laser deflectors—that require very large displacements ($>1000\ \mu\text{m}$). The direct extensional strain in most piezoelectric or electrostrictive ceramic materials is at best a few tenths of one percent. Therefore, the means of amplifying this strain is essential to their successful use in these applications.

Some well-known techniques for producing large displacements in these materials include flextensional composite structures, unimorph benders, and bimorph benders. However, each of these technologies has its limitations in regard to size, weight, maximum displacement, or load-bearing capability. A more recent

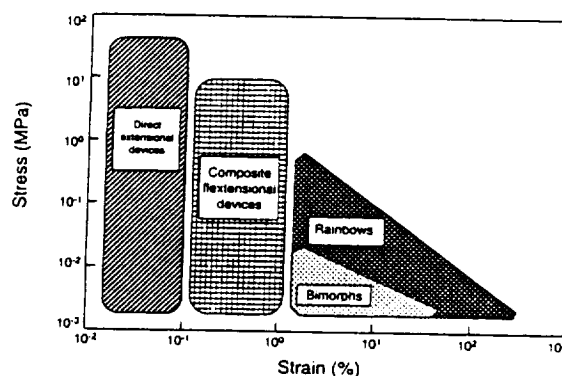


Fig. 1. Comparison of ceramic actuator technologies.

device, the "moonie," was reported by Sugawara *et al.*⁷ in 1992. This metal-ceramic composite actuator is a type of flextensional transducer which is able to convert and amplify (by approximately 10 times) the radial displacement of a piezoelectric disk into a linear axial motion. Displacements as high as $20\ \mu\text{m}$ have been achieved at a sustaining stress of 0.5 MPa.

When the stress/strain capabilities of all of these technologies are considered, it is evident that there is still a real need for additional techniques which will produce even higher strains or

Presented at the 95th Annual Meeting of the American Ceramic Society, Cincinnati, OH, April 19, 1993 (Symposium XVII, Paper No. SXVII-2-93).

Supported by NASA-Langley Research Center, Hampton, VA, under Grant No. NAG-1-1301.

*Member of the American Ceramic Society.

displacements. At the same time, the device must sustain reasonable stresses or loads. This paper describes such a technology. A new type of monolithic ceramic bender which is capable of achieving very high axial displacements ($>1000\text{ }\mu\text{m}$ (40 mils)) and sustaining moderate pressures ($\sim 0.6\text{ MPa}$ (85 psi)) has been developed. Known as a "rainbow" (reduced and internally biased oxide wafer) ceramic, this unique structure possesses a wider range of stress/strain characteristics than other bender types. Therefore, it promises to find application in a multitude of future devices. Key features of the rainbow are simplicity, quick processing, ease of fabrication, surface mountable configuration, and low cost. The particular ranges and regions for each of the technologies previously mentioned are shown on a stress/strain diagram in Fig. 1.

Rainbow Technology

In its most basic sense, rainbow technology consists of a new processing method for treating conventional, high-lead-containing piezoelectric or electrostrictive ceramic wafers, such as PZT (lead zirconate titanate), PLZT (lead lanthanum zirconate titanate), PBZT (lead barium zirconate titanate), PSZT (lead stannate zirconate titanate), and PMN (lead magnesium niobate). This technology involves the high-temperature chemical reduction of one surface of a wafer, thereby producing a stress-biased, domelike structure, as shown schematically in Fig. 2. The stress achieved in the ceramic by means of the single-sided reduction process is a critical feature of the structure. The stress produces a state of tension toward the bottom or reduced (concave) side of the wafer and compression toward the top or unreduced side. Therefore, the wafer assumes either a dome or a saddle shape, depending on the magnitude of the stress and the diameter-to-thickness ratio of the wafer. When both the stress and the diameter-to-thickness ratio are high, the rainbow wafer takes on the higher-profile, saddle shape. The change in shape of the wafer after reduction is believed to be due to the reduction in volume of the reduced layer (largely metallic lead) compared to the unreduced material. The change is also due to the differential thermal contraction between the reduced and unreduced layers on cooling to room temperature.

The reduced side of the piezoelectric serves as a mechanical support for the device, the source of the internal stress, and one of the device electrodes. It is necessary to deposit only one additional electrode on top of the unreduced piezoelectric for operational purposes. However, it is beneficial to also electrode the reduced layer to ensure good contact for the electrical leads. Use of the reduced piezoelectric as a stress-biasing support member as well as one of the electrodes effectively eliminates the bonding problems usually encountered in transducer fabrication and operation.

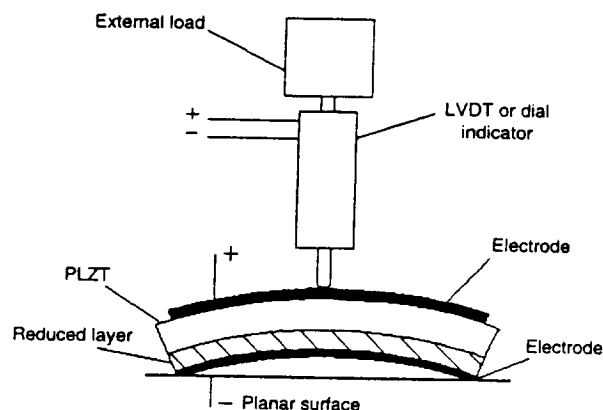


Fig. 2. Experimental setup for measuring displacement of rainbows (rainbow wafer shown in cross section not to scale).

After attaching leads to the two electrodes, the device is completed and ready for activation with an appropriate voltage. Similar to other piezoelectric devices, rainbows can be operated with direct-current, pulsed-direct-current, or alternating-current voltages. However, the largest displacements are usually achieved when driven with alternating current at frequencies less than 40 Hz. In operation, the dome height of the rainbow varies as a function of the magnitude and polarity of the voltage. The axial motion thus produced is largely a consequence of the lateral contraction produced in the material via the lateral piezoelectric coefficient. Therefore, the materials with the highest d_{31} coefficients generate the highest displacements. This is also true for electrostrictive materials. Those materials with the largest lateral coefficients produce the highest motion.

Rainbows can also be stacked to amplify a given linear motion. Each individual device approximates one-half of a clamshell structure. Two devices can be placed together to form a completed clamshell. These two rainbow elements can then be operated mechanically in series to produce twice the displacement of one element. Additional elements, in pairs, can be added to form a linear actuator of unusually high displacement in a relatively small volume. Electrically, the cascaded units can be operated in series or parallel. In series, the connections are simpler, but more voltage is required to maximize the displacement. In parallel, more displacement is achieved at a lower voltage, but at the expense of more-complicated lead arrangements.

The rainbow structure has been produced in both atmosphere-fired and hot-pressed ceramics, particularly the PLZT piezoelectric and electrostrictive compositions, such as 2/53/47 (La/Zr/Ti), 5.5/56/44, 8.6/65/35, and 8/70/30. Since these materials are also pyroelectric and ferroelectric in nature, rainbow

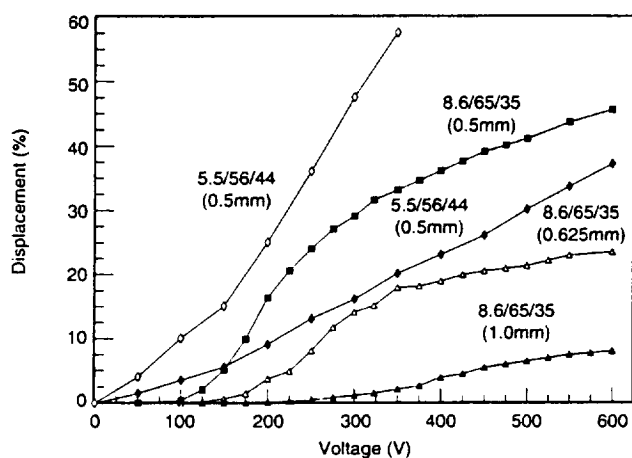


Fig. 3. Rainbow actuator characteristics of selected PLZT compositions (\diamond) alternating-current voltage and (Δ), (\blacksquare), (\blacklozenge), (\blacktriangle) direct-current voltage; wafer thickness in parentheses; wafer 31.75 mm in diameter).

devices produced from them can rightly be considered as multifunction, smart components. This multifunction characteristic is important since it substantially increases the number of potential applications. Typical devices include linear actuators, reciprocating and cavity pumps, switches, speakers, benders, vibrators, hydroprojectors and receivers, optical deflectors, variable focus mirrors and lenses, accelerometers, relays, acoustic-canceling devices, sensors, and smart systems. Of these, the first 10 have already been demonstrated in prototype devices.

Making a Rainbow

Piezoelectric and electrostrictive PLZT compositions were prepared from raw-material oxides via a conventional mixed-oxide process. Calcining was conducted at 975°C for 2 h in closed alumina crucibles. The milled and dried powders were first cold pressed as preform slugs and then hot pressed at

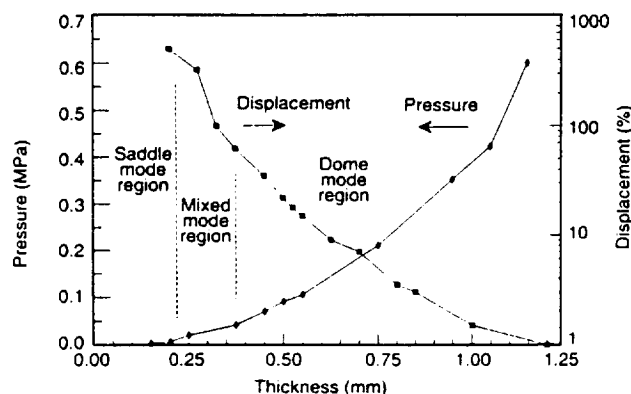


Fig. 4. Effect of wafer thickness on pressure and displacement behavior of PLZT 5.5/65/35 rainbows (wafer 31.75 mm in diameter).

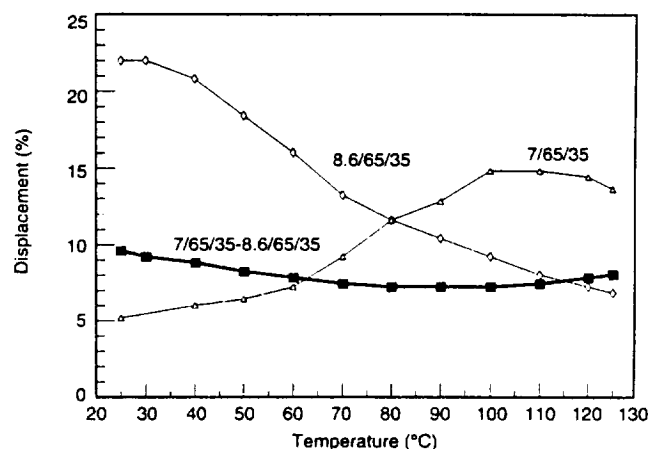


Fig. 5. Temperature-dependent displacement characteristics of (\diamond) 8.6/65/35 and (Δ) 7/65/35 compositions and for (\blacksquare) temperature-compensated rainbow clamshell (wafer 0.625 mm thick and 31.75 mm in diameter).

1200°C for 6 h at 14 MPa. This procedure yielded a fully dense material with a grain size of approximately 5 μ m. Subsequent steps in the fabrication of the wafers included grinding of the slug diameter, slicing the slug into wafers, and finish lapping of the wafers to the prescribed thickness.

A rainbow was produced from a lapped part by placing the wafer on a flat carbon (graphite) block which was resting on a zirconia carrier plate. A second zirconia plate was placed on top of the wafer to shield that side of the wafer from chemical reduction. The assembly was inserted into a small box furnace maintained at a temperature of 975°C. After approximately 1 h at temperature, the assembly was removed and allowed to cool to room temperature in the open air. When cool, the dome-shaped wafer was removed from the carbon block, brushed lightly to remove any metallic lead particles, and then electroded with silver epoxy paint (5504N, E. I. du Pont de Nemours and Company, Wilmington, DE) at 200°C for 30 min. A more complete description of a similar process was previously reported.⁸

Standard electrical measurements of capacitance, dissipation, direct-current hysteresis loop, planar coupling, and direct-current strain loop were conducted on each of the wafers. More extensive long-term testing was performed on selected materials by mounting the leadless wafers in a dial indicator assembly, as shown schematically in Fig. 2. This setup permitted external weights to be applied to the sample during testing. For the pressure measurements, a special air cell was constructed which allowed high pressure to be applied to the top of the wafer and atmospheric pressure on the bottom of the wafer during electrical operation.

Testing the Rainbow

Two types of actuator materials were tested in this study: piezoelectric, atmosphere-sintered PLZT 5.5/56/44 and electrostrictive, hot-pressed PLZT 8.6/65/35. Their displacement characteristics as a function of voltage are given in Fig. 3, with wafer thickness and voltage drive as additional parameters. Figure 3 shows that displacements as high as 57% were obtained for the particular wafers tested. As expected, the thinner wafers yielded the highest displacements. The displacement of the piezoelectric material was generally lower than that of the electrostrictive material when operated on direct current (one polarity only) but was substantially higher when driven by alternating current (open diamonds in Fig. 3). The alternating-current case for 8.6/65/35 is not shown since electrostrictors have the same displacement for voltages of either polarity. Note that 5.5/56/44 was significantly better than 8.6/65/35 at low voltages. This was also expected because of the linear versus quadratic behavior of the two types of materials.

Displacement and pressure data for PLZT 5.5/56/44 as a function of wafer thickness are presented in Fig. 4. The left ordinate scale represents the maximum allowable pressure differential across the wafer thickness before the wafer "bottoms out" to the planar surface and stops flexing (usually <0.5 mm thickness), or the wafer mechanically fractures (>0.5 mm thickness). The right ordinate logarithmic scale is the percent displacement (based on wafer thickness) of the device when operated at 450 V direct current under just the loading of the dial gauge spring (80 g). Also indicated in Fig. 4 are the wafer thickness regions where the saddle and dome modes of operation are dominant for a wafer 31.75 mm (1.25 in.) in diameter. The data shown in Fig. 4 indicate that rainbow displacements span an unusually large range from zero to at least 500%, with actual displacements up to 1 mm (0.040 in.) for a 0.2-mm- (0.008-in.-) thick wafer. Such large displacements are not possible when operating under significant pressure differentials, as shown in Fig. 4, or under moderate point-loading situations (not shown). The maximum point-loading capability measured to date is 10 kg on a 31.75-mm-diameter, 1.5-mm-thick disk.

The temperature characteristics of selected PLZT compositions 8.6/65/35 and 7/65/35 are given in Fig. 5. Since 8.6/65/35 has a Curie point around room temperature, it exhibited a reduction in displacement with increased temperature. On the other hand, 7/65/35, having a Curie point at about 140°C, experienced an increased displacement with increased temperature. When these two elements are placed back-to-back, as in a clamshell configuration, their net displacement as a function of temperature was very low. This resulted in a nearly temperature-independent rainbow unit. Temperature compensation can be refined even further by mixing-and-matching more elements in units of two.

When several units are stacked together, temperature compensation can be affected and total displacement can be maximized. The maximum displacement obtained to date with a group of four clamshell units (eight rainbow wafers) is 5.1 mm (0.2 in.).

Rainbows Show Promise

A new type of monolithic ceramic bender (designated as a rainbow) has recently been developed. The rainbow is capable of achieving ultra-high axial displacements (up to 500% or more, based on wafer thickness) and sustaining moderate loads of approximately 10 kg. Actual displacements as high as 1 mm have been obtained from single-element devices 0.2 mm thick. The rainbow structure was achieved in commercially available, atmosphere-sintered or hot-pressed piezoelectric and electrostrictive ceramics by means of a high-temperature chemical reduction process. Desirable features of the rainbows are simplicity, moderate load-bearing capability, temperature compensation characteristics, easy fabrication, and low cost. It is anticipated that this technology will have numerous applications in commercial and industrial markets.

References

- ¹H. Honmou, R. Ishikawa, and S. Takahashi, "Automatic Optical Fiber Polarization Control System Using Multilayer Piezoelectric Actuators," *Jpn. J. Appl. Phys.*, **24**, [Suppl. 24-3] 187-89 (1985).
- ²K. Uchino, "Electrostrictive Actuators: Materials and Applications," *Am. Ceram. Soc. Bull.*, **65** [4] 647-52 (1986).
- ³K. Uchino, M. Yoshizaki, K. Kasai, H. Yamamura, N. Sakai, and H. Asakura, "Monomorph Actuators Using Semiconductive Ferroelectrics," *Jpn. J. Appl. Phys.*, **26** [7] 1046-49 (1987).
- ⁴M. A. Ealey and P. A. Davis, "Standard SELECT Electrostrictive Lead Magnesium Niobate Actuators for Active and Adaptive Optical Components," *Opt. Eng.*, **29** [11] 1373-82 (1990).
- ⁵W. P. Robbins, D. L. Polla, and D. E. Glumac, "High-Displacement Piezoelectric Actuator Utilizing a Meander-Line Geometry-Part I: Experimental Characterization," *IEEE Trans. Ultrason., Ferroelectr., Freq. Control*, **38** [5] 454-67 (1991).
- ⁶Q. C. Xu, S. Yoshikawa, J. R. Belsick, and R. E. Newnham, "Piezoelectric Composites with High Sensitivity and High Capacitance for Use at High Pressures," *IEEE Trans. Ultrason., Ferroelectr., Freq. Control*, **38** [6] 634-39 (1991).
- ⁷Y. Sugawara, K. Onitsuka, S. Yoshikawa, Q. C. Xu, R. E. Newnham, and K. Uchino, "Metal-Ceramic Composite Actuators," *J. Am. Ceram. Soc.*, **75** [4] 996-98 (1992).
- ⁸G. H. Haertling, "Reduction/Oxidation Effects in PLZT Ceramics," pp. 699-711 in *Proceedings of the 4th International SAMPE Electronics Conference* (Albuquerque, NM, June 12-14, 1990). Edited by R.E. Allred, R.J. Martinez, and K.B. Wischmann. Society for the Advancement of Materials and Process Engineering, Covina, CA, 1990.

Ferroelectrics, 1994, Vol. 154, pp. 101-106
Reprints available directly from the publisher
Photocopying permitted by license only

© 1994 Gordon and Breach Science Publishers S.A.
Printed in the United States of America

CHEMICALLY REDUCED PLZT CERAMICS FOR ULTRA-HIGH DISPLACEMENT ACTUATORS

GENE H. HAERTLING

Clemson University, Clemson, South Carolina, USA

(Received August 9, 1993)

Abstract A new and unique processing method for fabricating stress-biased, monolithic ceramic elements for ultra-high displacement actuators is reported. The technique consists of chemically reducing one surface of a high lead containing piezoelectric or electrostrictive wafer such as PLZT with solid graphite in an oxidizing atmosphere at an elevated temperature. This process produces a dome-like wafer structure which is the key to its high displacement characteristics and its enhanced load bearing capabilities. This new type of ceramic bender is capable of (1) achieving displacements as high as 3 mm from a single element, (2) sustaining point loads of about 10 kg and (3) distributed pressures of approximately 0.6 MPa. Designated as Rainbow ceramics, they have been successfully produced from both sintered and hot pressed material.

INTRODUCTION

Recent developments in the technology of piezoelectric and electrostrictive ceramic actuators have amply demonstrated that the materials required for future applications will need to be more sophisticated (multifunctional and smart), the techniques for strain amplification more innovative and cost effective, and the performance of the devices more reliable in harsh environments.¹⁻³ Such applications include positioners, active structures, acoustic canceling components, variable focus elements, pumps, switches, linear actuators and multifunction devices. Of these, some involve very high electromechanical displacements on the order of several millimeters. Unfortunately, the materials presently available for these devices generally achieve less than 0.1 mm total strain in any practical size element, and thus, are not directly suitable for such large displacements. Consequently, various techniques for amplifying the strain have been developed and reported.⁴⁻⁵

The most recently developed strain amplifying method for piezoelectric and electrostrictive ceramic materials which shows promise for meeting some, if not many, of the high strain applications is known as the RAINBOW technology.⁶ This acronym denotes the basic active structure of the Rainbow device which is produced by a special high temperature chemical reduction process and stands for Reduced And Internally Biased Oxide Wafer. In their most basic sense, Rainbow ceramics can be thought of as pre-stressed, monolithic, axial-mode benders, similar in operation to the more conventional unimorph and bimorph type benders. But because of their unique dome or saddle-like configuration, Rainbow ceramics are able to produce much higher displacements (> 1mm) and sustain significantly

greater loads (10 kg) than normal benders.

This paper reports on the details of the process for producing the Rainbow ceramics, as well as evaluating some of their properties and characteristics.

DESCRIPTION OF THE RAINBOW CERAMICS

The Rainbow technology fundamentally consists of a new processing method that is applied to standard, high lead-containing piezoelectric and electrostrictive ceramic wafers which are individually transformed by the process into a monolithic, composite structure consisting of a pre-stressed dielectric (the piezoelectric) and a chemically-reduced, electrically conductive layer which acts as the pre-stressing element and as one of the electrodes for the final device. Since the materials (e.g., PLZT, PZT, PMN, PBZT) are ferroelectric, they are multifunctional, by nature, and are capable of performing both actuator and sensor functions, simultaneously.

The high temperature chemical reduction process involves the local reduction of one surface of the ceramic, thereby achieving an anisotropic, stress-biased, dome or saddle-shaped wafer with significant internal tensile and compressive stresses which act to increase the overall strength of the material. According to previously reported work⁷, the chemical reduction process proceeds via simple reactions consisting of oxidation of the solid carbon (graphite) block to carbon monoxide and further oxidation of the carbon monoxide gas to carbon dioxide with the associated local reduction (loss of oxygen) of the PLZT oxide in contact or in near contact with the carbon block.

In regard to operation, the Rainbow is similar to a device known in the industry as a unimorph bender. A unimorph is composed of a single piezoelectric element externally bonded to a flexible metal foil which is stimulated into action by the piezoelectric element when activated with an ac or dc voltage and results in an axial buckling or displacement as it opposes the movement of the piezoelectric element. However, unlike the unimorph, the Rainbow device is a monolithic structure with a piezoelectrically inactive, integral electrode which is fabricated such that it put an internal compressive stress bias on the piezoelectric element; thus producing the dome structure, rendering it more rugged and able to sustain heavier loads than normal. The integral electrode (usually the bottom electrode) consists of metallic lead intimately dispersed throughout the semiconductive oxide layer. A typical cross-section of a Rainbow wafer is shown in Figure 1. The change in shape of the wafer after reduction is believed to be due to the reduction in volume of the bottom reduced layer (largely metallic lead) compared to the unreduced material, as well as the differential thermal contraction between the reduced and unreduced layers on cooling to room temperature.

After depositing an appropriate electrode on the piezoelectric (top) surface, the Rainbow is completed and ready for operation. Like other piezoelectric devices, Rainbows may be operated with a dc, pulse dc, or ac voltage; however, when driven with ac, the largest displacements are usually achieved at 40 Hz or less. In operation, the dome height of the Rainbow varies as a function of the magnitude and polarity of the voltage. The axial motion of the dome is largely a consequence of the lateral contraction produced in the material via the lateral d_{31} coefficient.

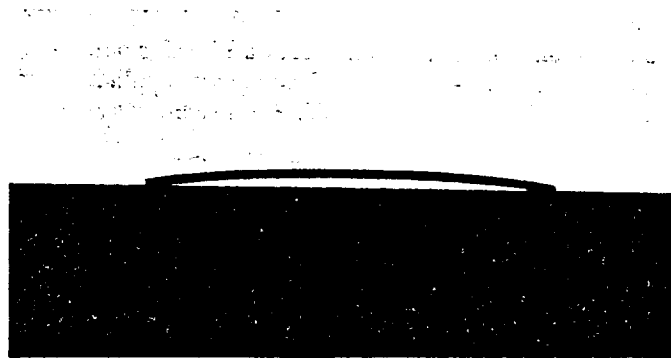


FIGURE 1. A typical cross-section of a PLZT Rainbow wafer illustrating its domed structure.

When a given polarity of voltage is applied, the dome will decrease in height depending on the magnitude of the voltage; and alternatively, when the polarity is reversed, the dome will increase in height. Since d_{31} is a major factor, the materials with the highest d_{31} coefficients generate the highest displacements. This is also true for the electrostrictors; i.e., those with the largest lateral s_{12} coefficients produce the highest motion. Although the longitudinal d_{33} also plays a part in the total displacement, its contribution is insignificant compared to d_{31} .

EXPERIMENTAL

The processing steps for producing Rainbows are simple and few in number. Five hundred gram batches of PLZT piezoelectric (5.5/56/44, 1/53/47) or electrostrictive (8.6/65/35, 9/65/35) compositions were prepared via the mixed oxide process. Calcining was carried out at 925°C for two hours in closed alumina crucibles; milling was performed in a high alumina ball mill with distilled water; and final densification was achieved either by sintering at 1250°C for 6 hours in oxygen or hot pressing at 1200°C for 6 hours at 14 MPa. This procedure yielded high density (>97%) material with an average grain size of approximately four microns. A Rainbow was produced from a lapped wafer by placing the wafer on a flat graphite block and introducing the assembly into a furnace held at temperature in normal air atmosphere. The part was treated at a temperature of 975°C for approximately one hour, removed from the furnace while hot and naturally cooled to room temperature in about 45 minutes. When cool, the dome-shaped wafer was lifted from the carbon block, sanded lightly on the reduced (concave) side to remove any metallic lead and to expose the reduced layer, and then electroded for test and evaluation. Both silver-loaded epoxy (DuPont 5504N) and fired-on silver (DuPont 7095) electrodes were utilized in the evaluation process.

Microstructure, X-ray, mechanical, electromechanical, dielectric and hysteresis loop measurements were made on selected Rainbow wafers of varying diameter and

thickness. Testing for voltage-dependent mechanical displacement involved the use of a standard dial indicator micrometer and/or a LVDT mounted on a rigid stand. During point load measurements, external weight was applied to the wafer via the top side of the dial indicator or LVDT. The test setup is shown in Figure 2.

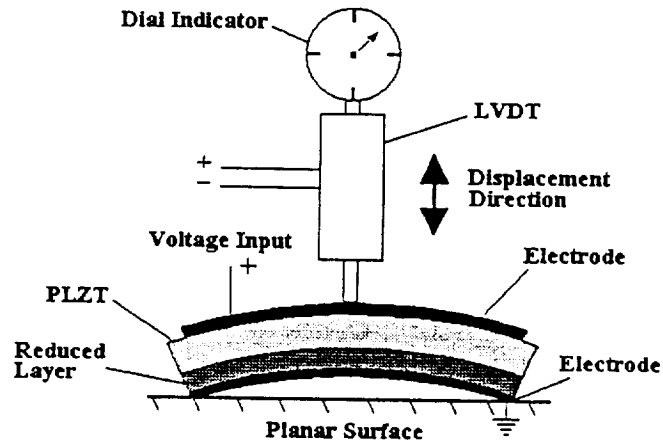


FIGURE 2. Experimental setup for measuring Rainbow displacements (not to scale).

RESULTS AND DISCUSSION

A polished cross-section of a PLZT 8.6/65/35 wafer (975°C for 1 hour) is given in Figure 3. This micrograph reveals a very abrupt boundary between the reduced and unreduced areas of the wafer. This result is quite surprising since the reduction process is undoubtedly a diffusion-controlled process with an ever

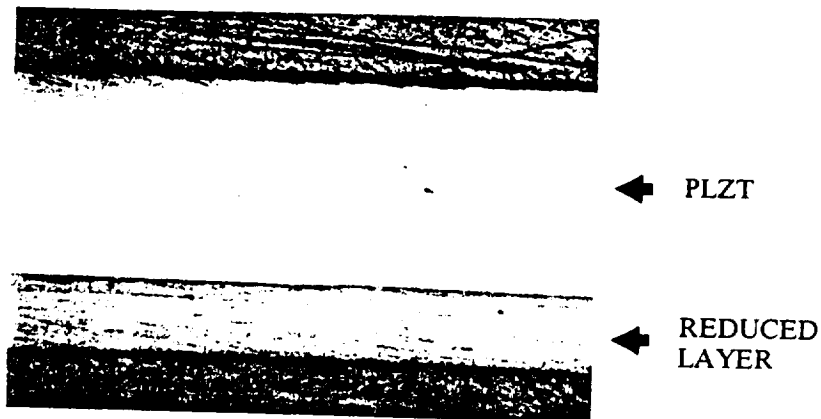


FIGURE 3. A polished cross-section of a PLZT Rainbow wafer.

increasing path length for diffusion of oxygen to the surface. In addition, the experimental data of Figure 4 show that the thickness of the reduced layer grows at a near linear rate.

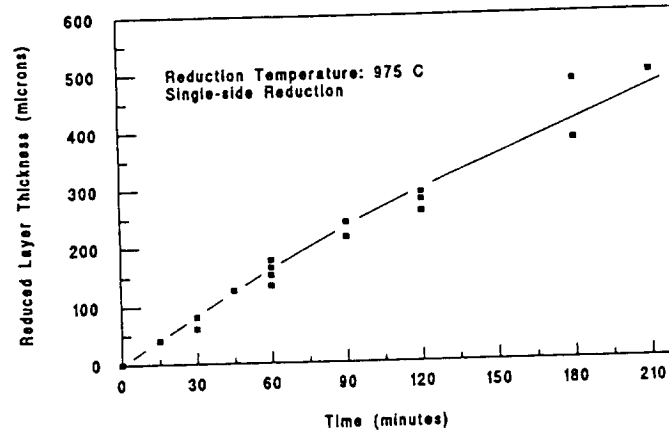


FIGURE 4. Effect of reduction time on the reduced layer thickness.

As mentioned previously, the reduced layer is composed of the solid products of the reduction reaction; i.e., conductive metallic lead and the oxides of Pb, La, Zr and Ti which form along with the unreduced material. This was confirmed by X-ray analysis of the reduced layer which revealed the presence of metallic lead and minor amounts of other oxides. Four-point probe measurements on the reduced layer also revealed it as a good conductor with ohmic behavior and a specific resistivity of 3.8×10^{-4} ohm-cm.

Displacement data for selected Rainbow materials are given in Figure 5. As

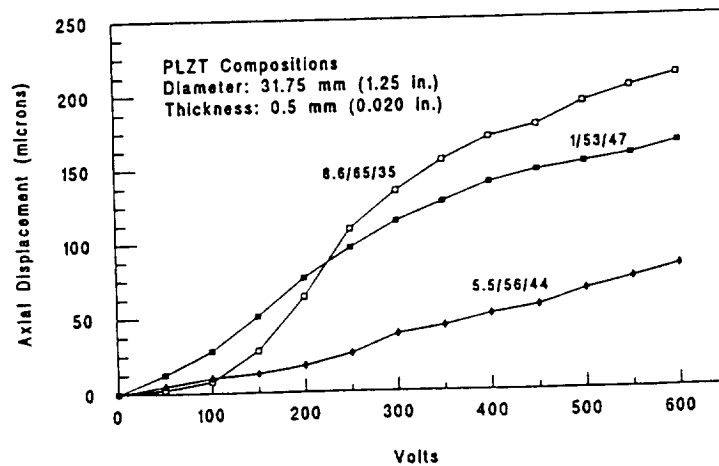


FIGURE 5. Voltage dependent displacement characteristics of PLZT Rainbows

seen from the figure, both piezoelectric, linear (5.5/56/44, 1/53/47) and electrostrictive, non-linear (8.6/65/35) behavior are exhibited by these compositions. The most striking feature in Figure 5 is the very high displacements achieved by these Rainbow ceramics at moderate electric fields; e.g., 400 volts is equivalent to a field of 10 kV/cm. A maximum displacement of 200 microns was obtained from PLZT 8.6/65/35, which is equivalent to 40% effective strain based on wafer thickness. Although not shown here, larger diameter wafers (100 mm) have yielded displacements as large as 3000 microns (3 mm).

An summary view of a variety of Rainbow elements is given in Figure 6. The largest wafers illustrated here are 50 mm in diameter and the smallest are 1.5 mm square. Thicknesses range from 0.15 mm to 1.25 mm. Some parts are polished (before reduction) while others are lapped and/or electroded.

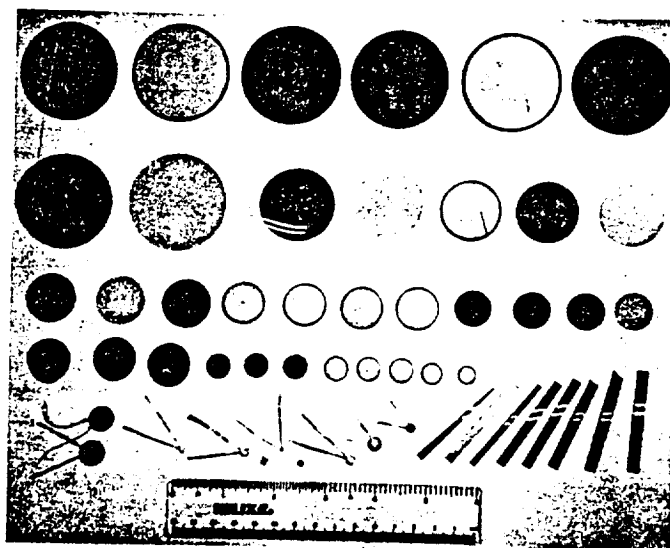


FIGURE 6. A summary of Rainbow ceramics showing various sizes and shapes.

This work was supported by NASA-Langley Research Center, Hampton, VA, under Grant No. NAG-1-1301.

REFERENCES

1. R. Newnham, Q. Xu, S. Kumar and L.E. Cross, *Ferroelectrics*, **102**, 259 (1990).
2. S. Trolier-McKinstry and R. Newnham, *MRS Bulletin*, **XVIII**, No.4, 27 (1993).
3. K. Uchino, *Bull. Am. Ceram. Soc.*, **65**, No. 4, 647 (1986).
4. K. Uchino, M. Yoshizaki, K. Kasai, H. Yamamura, N. Sakai and H. Asakura, *Japan. J. Appl. Phys.*, **26**, No. 7, 1046 (1987).
5. Y. Sugawara, K. Onitsuka, S. Yoshikawa, Q. Xu, R. Newnham and K. Uchino, *J. Am. Ceram. Soc.*, **75**, No. 4, 996 (1992).
6. G. Haertling, *J. Am. Ceram. Soc.*, accepted for publication (1993).
7. G. Haertling, *Proceedings of 4th Intl. SAMPE Conf.*, **4**, 699 (1990).

Composition and Microstructure of Chemically Reduced PLZT Ceramics

G. Li, E. Furman, and G. Haertling
Department of Ceramic Engineering
Clemson University
Clemson, South Carolina 29634-0907

Abstract -- Hot-pressed PLZT ceramic wafers were chemically reduced by a special processing technique on one of the major surfaces to form oxide-reduced layer composite structures. Devices based on such structures have promising characteristics. The composition and microstructure of the reduced layer as well as the oxide-reduced layer interface from several different PLZT ceramics were examined and analyzed by means of X-ray diffraction and SEM. A variety of the oxide phases, such as PbO , ZrO_2 , ZrTiO_4 and LaTiO_3 , were revealed in the reduced PLZT samples by X-ray diffraction in addition to the anticipated metallic lead phase. SEM micrographs showed that the reduced PLZT ceramics were composed of various fine-grained particles, and the Pb grains formed a continuous phase. It was found that the oxide-reduced layer interface region consisted of a mixture of unreduced and reduced phases. The thickness of the mixed phase region was associated with the grain size of the original PLZT ceramics.

INTRODUCTION

A new type of ultra-high-displacement, multi-function actuator, named RAINBOW (Reduced And Internally Biased Oxide Wafer), has recently been developed using a special processing technique. This technique involves chemical reduction of one of the major surfaces of a high lead-containing ferroelectric ceramic wafer by placing the wafer on a flat carbon block at an elevated temperature, thus producing a dome-shaped, oxide-reduced layer composite structure. When an electric field is applied across such a composite wafer, large axial displacement is generated. A detailed description of Rainbow technology can be found in Ref. [1]. Since the electromechanical properties of a Rainbow actuator are dependent upon the physical properties such as thermal expansion, elasticity, and electrical conductivity of its reduced layer, a thorough investigation of the composition and microstructure of reduced PLZT ceramics is desirable for the characterization and application of Rainbow actuators. The PLZT ceramics were chosen for this study because they are easily reduced and have excellent electromechanical characteristics.

The composition and microstructure of the reduced layer as well as the configuration of the oxide-reduced layer interface for several PLZT Rainbow samples have been investigated by X-ray diffraction (XRD) and scanning electron microscopy (SEM).

SAMPLE PREPARATION AND EXPERIMENTAL PROCEDURES

The Rainbow samples used were prepared from hot-pressed PLZT ceramics 1.0/53/47, 5.5/57/43 and 9.5/65/35, where the numbers denote the atom ratios $\text{La}/\text{Zr}/\text{Ti}$ of the PLZT compositions. All of the Rainbows were produced under the conditions of 975 °C / 60 min (reduction temperature / time).

Fractured, polished, and etched surfaces of the Rainbow samples were used in both X-ray diffraction and SEM analyses. For X-ray diffraction, the as-reduced surfaces of the Rainbows were lapped off approximately 50 μm and slightly polished to expose the internal structures. This procedure was employed because a thin reoxidized layer is often formed on reduced surfaces during fabrication. X-ray diffraction was first performed on the polished surfaces. Thereafter, the same surfaces were etched with an HCl/HF solution for further study. X-ray diffraction patterns of fractured surfaces were obtained from the powders prepared by crushing the completely reduced wafers.

Cross-sectional surfaces of the Rainbow samples were usually used for the SEM analyses of this study. The fractured surfaces were obtained by breaking the Rainbows along their diameters. The surfaces were also polished by using progressively finer diamond pastes with a finish of 0.25 μm . The polished surfaces were then etched, cleaned, and coated with a carbon or gold film before examination. In some cases, the polished surfaces were directly examined under SEM.

All of the X-ray diffraction experiments were performed on an X-ray diffractometer (Scintag XDS 2000~) with Ni-filtered $\text{Cu K}\alpha$ radiation at a scan rate of 2 degree per minute. A JOEL scanning electron microscope operating at an accelerating voltage of 15 keV was used for the SEM analyses.

EXPERIMENTAL RESULTS

X-ray Diffraction Analysis

Figures 1(a)-1(c) show the X-ray diffraction patterns from the polished surface of the reduced layer of Rainbows 1.0/53/47, 5.5/57/43 and 9.5/65/35, respectively. It was found in all cases that the strongest peaks in the patterns were produced by the metallic lead phase. The remaining weaker peaks were caused by a number of oxide phases formed during the reduction process. As is indicated in the figures, the oxide phases identified include PbO (litharge), ZrO_2 , ZrTiO_4 , TiO_2 , LaTiO_3 and $\text{La}_{0.66}\text{TiO}_{1.993}$ (JCPDS 26-827).

The X-ray diffraction pattern of the etched reduced surface of Rainbow 5.5/57/43 is demonstrated in Figure 2. It can readily be seen by comparing Figure 2 with Figure 1(b) that, upon etching, almost all of the Pb peaks were greatly depressed while those of the oxide phases underwent little change. This result indicates that it is primarily the Pb phase that was etched away from the surface.

It should be noted that the intense diffraction peaks of the Pb phase shown in Figures 1(a)-1(c) may partly result from the grinding and polishing treatments on the sample surfaces prior to analysis. Since the metal Pb is a very soft material relative to the oxide phases, when a reduced sample is ground or polished, the Pb phase is deformed and smeared over the surface. Consequently, the relative amount of Pb phase on the surface is increased, thereby enhancing the intensity of the Pb diffraction peaks.

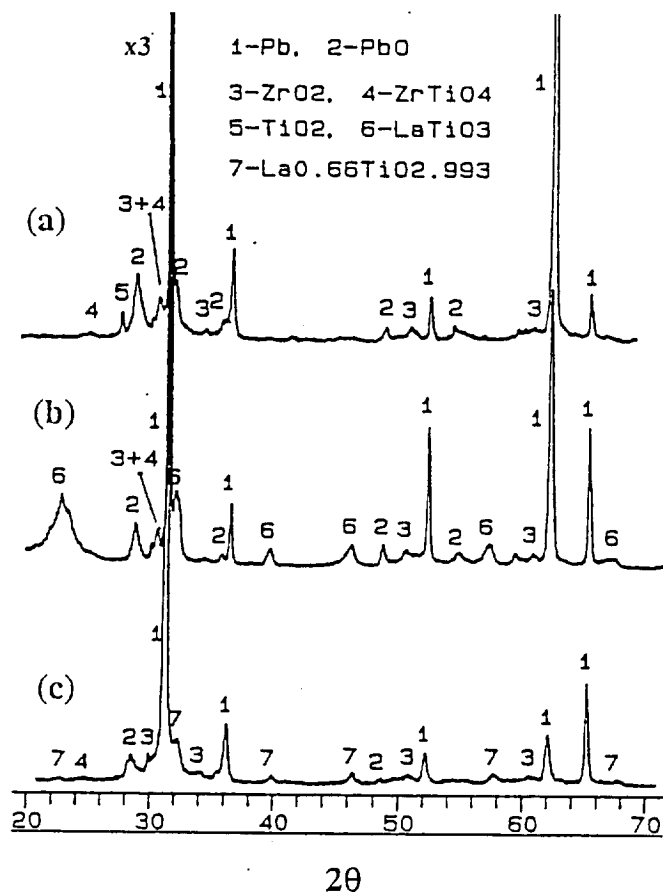


Figure 1. X-ray diffraction patterns from the polished surface of the reduced layer of Rainbows (a) 1.0/53/47, (b) 5.5/57/43 and (c) 9.5/65/35.

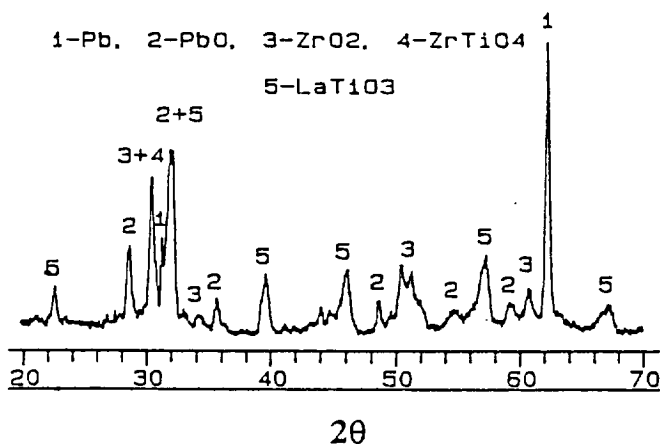


Figure 2. X-ray diffraction pattern from etched reduced surface of Rainbow 5.5/57/43.

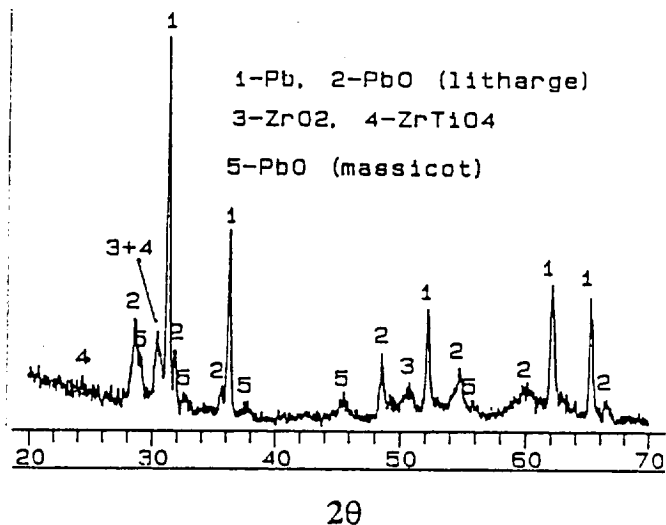


Figure 3. X-ray diffraction pattern of the powder obtained from reduced PLZT 1.0/53/47 sample.

For this reason, the X-ray diffraction of fractured surfaces better reflects the actual states of the various phases in the sample. Since it is practically difficult to obtain a large fracture surface of the reduced layer, the powders from completely reduced wafers which contain various small fracture surfaces were used instead. The diffraction pattern of such powder for Rainbow 1.0/53/47 is shown in Figure 3. As can be seen, the intensity ratios of the major metallic lead peaks to the oxide phase peaks are considerably reduced compared to those of the polished surface shown in Figure 1(a), indicating the presence of smearing in the polished samples. It is, however, worth noting that the Pb diffraction peaks from the powder remain the strongest, and this is also true for the other PLZT Rainbow samples studied. Figure 3 also shows the existence of PbO (massicot) phase which was not observed in Figures 1(a)-1(c).

SEM Analysis

Figure 4 shows the SEM micrograph of the fractured cross-sectional surface of Rainbow 1.0/53/47. The upper portion of the micrograph shows the PLZT layer and the lower portion is the reduced layer. These layers are separated by a PLZT-reduced layer interface where the unreduced and reduced phases were found to coexist. A micrograph of higher magnification on the reduced regions, which is given in Figure 5(a), indicates that the region was composed of various fine-grained particles. A similar microstructure was also observed in Rainbows 5.5/57/43 and 9.5/65/35, as is shown in Figures 5(b) and 5(c) respectively. The small uniformly distributed particles, about 0.2 μm in diameter, as can be seen in the figures, were identified to be the Pb grains by means of X-ray diffraction coupled with an extraction technique. The microstructure of the reduced layer seems relatively insensitive to the microstructure of the original PLZT composition.



Figure 4. SEM micrograph of fractured cross-sectional surface of Rainbow 1.0/53/47 near the PLZT/reduced layer interface.

The secondary electron image of a polished surface of the reduced layers is usually featureless. It was, however, found that some characteristics of the polished surfaces can be revealed via a backscattered electron imaging technique. Figure 6 is a backscattered electron image of Rainbow 1.0/53/47 near the PLZT-reduced layer interface. Again the lower portion is the reduced layer. The darkest areas seen in Figure 6 are most likely the thoroughly reduced regions. This is because that the reduction process leads to a relatively loose structure by decomposing the original dense PLZT phase with an accompanying oxygen loss, thereby contributing less to the backscattered electron signals. From the morphology of the oxide-reduced layer interface it can be deduced that the reduction reaction was initiated along the PLZT grain boundaries and then proceeded toward the center of the grains.

The SEM image of the etched reduced surface of Rainbow 5.5/57/43, whose X-ray diffraction pattern has been given in Figure 2, is displayed in Figure 7. The grains exposed by etching, which can be seen in Figure 7, are considered to be the oxide phases identified in the corresponding X-ray diffraction pattern. The fact that the oxide grains appear isolated indicates that the Pb grains, which were mostly etched away from the surfaces, form a continuous phase. The continuity of the lead phase is further supported by high conductivity of the reduced layers.

DISCUSSIONS

The results of the above X-ray diffraction analyses indicate that a number of different phases are produced as a result of the chemical reduction of a PLZT ceramic in forming the Rainbow structure. The phases found include the metallic lead phase, and seven oxide phases: PbO (litharge), PbO (massicot), ZrO_2 , $ZrTiO_4$, TiO_2 , $LaTiO_3$, and $La_{0.66}TiO_{2.993}$. The original PLZT phase was not observed in the reduced samples. It is noted that while the exact number and composition of the phases in a particular reduced PLZT sample strongly depend on the original PLZT composition, the phases of Pb, PbO (litharge), ZrO_2 , and $ZrTiO_4$ are common among the samples studied; and of them, the Pb phase gives rise to the strongest X-ray diffraction.

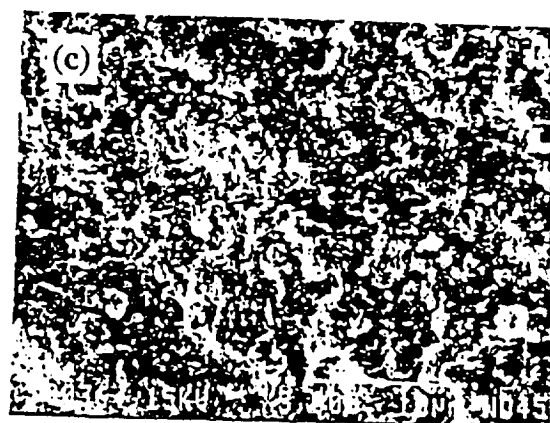
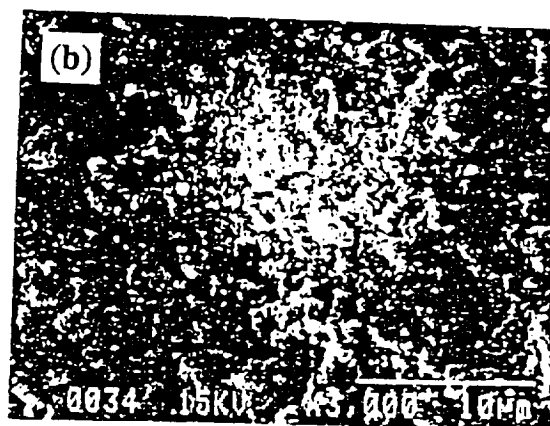
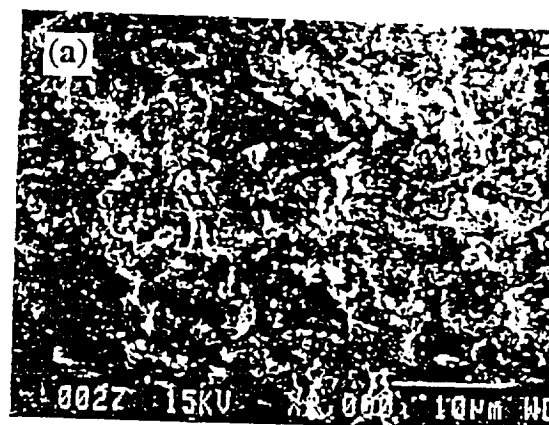


Figure 5. SEM micrograph of the reduced layer of Rainbows (a) 1.0/53/47, (b) 5.5/57/43 and (c) 9.5/65/35.

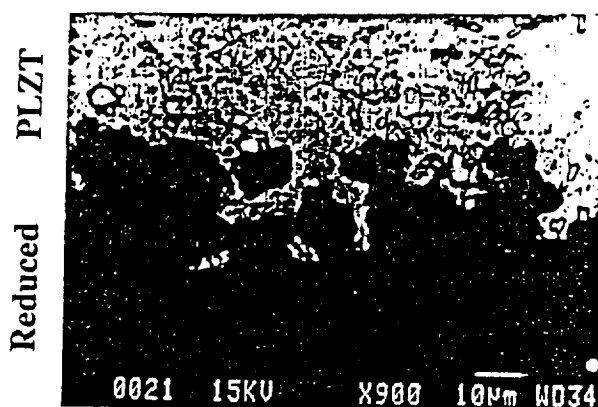


Figure 6. Backscattered electron image of Rainbow 1.0/53/47 near the PLZT/reduced layer interface.



Figure 7. SEM micrograph of etched reduced layer of Rainbow 5.5/57/43.

Chemical reduction of PZT and PLZT ceramics has been reported in the literature [2-3]. In his investigation of PLZT ceramics reduced by carbon blocks [3], Haertling showed that the reduction reaction is accomplished via the interaction between carbon monoxide and loosely held oxygen atoms in the PLZT perovskite lattice. It is therefore considered that, except for the oxygen and slight Pb losses during reduction, the reduced layer should contain the same amount of chemical elements as the unreduced PLZT ceramic. In other words, the chemical reduction simply decomposes the PLZT crystal structure by attacking the lattice oxygen ions and, at the same time, produces new phases by rearranging the constituent elements.

Based on this consideration, the volume fraction of the lead phase in a reduced PLZT sample may not be as large as it seems in the X-ray diffraction as, for example, shown in Figure 3. This is reasonable since along with the volume fraction of each phase many other factors may contribute to the relative peak intensities of the X-ray diffraction pattern in a multiphase material. In fact, for the conceivable uses of Rainbow actuators, it is not critical whether the Pb phase is dominant or not. The main concern is that the Pb phase must be a continuous phase so that the reduced layer has good conductivity. The fact that the metallic lead in the reduced layer occurs with very fine particles, as was shown in the

SEM micrographs, suggests that even a small volume fraction of lead phase can render the reduced layer electrically conductive. This may explain why the reduced PLZT ceramic exhibits excellent conductivity.

There is a region along the PLZT-reduced layer interface where the PLZT and reduced phases coexist. The dimension (normal to the interface) of the region is defined as the thickness of the interface in a Rainbow. It was found that the interface thickness was related to the grain size of the phase before reduction. This is easily understood considering that the reduction process is initialized along grain boundaries as illustrated in Figure 6. For Rainbow 1.0/53/47, whose PLZT layer displays a larger grain size, the thickness was found to be approximately 20 μm . Rainbows 5.5/57/43 and 9.5/65/35 have an interface thickness of about 2 μm and 5 μm , respectively. The configuration of the PLZT-reduced layer interface is very likely important for some specific properties of Rainbow actuators such as fatigue and loading capability and will be investigated further.

SUMMARY

The composition and microstructure of chemically reduced PLZT ceramics (the reduced layer of the Rainbow) have been studied by XRD and SEM. Key results are summarized as follows.

(1) A number of different crystalline phases have been found in the PLZT ceramics reduced via the RAINBOW process. The phases found include metallic lead and seven oxide phases: PbO (litharge), PbO (massicot), ZrO_2 , ZrTiO_4 , TiO_2 , LaTiO_3 , and $\text{La}_{0.66}\text{TiO}_{1.993}$. The original PLZT phase was not observed. The exact number and composition of the phases for a particular reduced sample are dependent on the PLZT composition, but among the samples studied, the phases of Pb, PbO (litharge), ZrO_2 , and ZrTiO_4 are commonly observed, with the Pb phase producing the strongest X-ray diffraction.

(2) The reduced PLZT ceramics are composed of various fine-grained particles, and the smallest grains, about 0.2 μm , correspond to the lead phase. This microstructural characteristic is relatively insensitive to the PLZT composition. It is shown that the metallic Pb grains constitute a continuous phase in the reduced PLZT ceramics, which is consistent with the good electrical conductivity of these materials.

(3) Near the interface between the PLZT and reduced phases of a Rainbow, the two phases coexist. The thickness of the interface was found to be associated with the grain size of the PLZT phase. The values of the interface thickness for Rainbows 1.0/57/43, 9.5/65/35 and 5.5/57/43 are about 20, 4, and 2 μm , respectively.

ACKNOWLEDGMENT

This work was supported by NASA under contract No. MAG-1-1301.

REFERENCES

- [1] G. H. Haertling, "Rainbow ceramics - a new type of ultra-high-displacement actuator," *Bull. Am. Ceram. Soc.*, vol. 73, pp. 1-4, 1994.
- [2] N. R. Rajopadhye, S. V. Bhoraskar, S. Badrinarayan and A. P. B. Sinha, "Photoacoustic and X-ray photoelectron spectroscopic studies in reduced lead zirconate titanate ceramics," *J. Mat. Sci.*, vol. 23, pp. 2631-2636, 1988.
- [3] G. H. Haertling, "Reduction/oxidation effect in PLZT ceramics," in *Proceedings of 4th International SAMPE Electronics Conference*, vol. 4, pp. 699-711, 1990.

Gene H. Haertling
Gilbert C. Robinson Department of Ceramic Engineering
Clemson University, Clemson, SC 29634-0907

Abstract -- On-going studies have shown that the PLZT compositional system is one which yields materials possessing some of the highest coefficients for piezoelectric and electrostrictive actuators. It has also been found that PLZT ceramics are near ideal for achieving the ultra-high displacements recently reported for the Rainbow (Reduced and Internally Biased Oxide Wafer) actuators. In order to determine the optimum composition or compositions for these Rainbow actuators, a study was conducted by preparing and processing selected formulations throughout the PLZT system. Results from this study indicate that, like the conventional direct extensional-mode materials, the maximum Rainbow bending displacements occur in materials located compositionally at the morphotropic ($FE_{rhomb} - FE_{tet}$) and Curie point ($FE - PE$, $PE - AFE$) phase boundaries. Examples of specific compositions for each of these regions are 2/53/47, 9/65/35 and 8.5/70/30 (La/Zr/Ti), respectively. Microstructural (grain size), electrical (dielectric constant, dissipation factor) and electromechanical (axial displacement) data are presented for selected compositions in the system.

INTRODUCTION

It has long been known that the PLZT compositional system is a very versatile one which yields materials possessing maximum dielectric properties and some of the highest known electromechanical coefficients for piezoelectric devices such as speakers, hydrophones, ignitors, accelerometers, motors, sensors and actuators [1-2]. In general, these optimum properties are found in materials located compositionally along the morphotropic (MPB) phase boundary ($FE_{rh} - FE_{tet}$) separating the rhombohedral and tetragonal ferroelectric phases, as shown in Figure 1 by the double cross-hatched region. Other properties of interest (e.g., pyroelectric and electrooptic) are optimized in compositions located along the boundaries separating the FE polar phases from the antiferroelectric (AFE) and paraelectric (PE) non-polar phases. Compositions which typify these materials are more popularly known as electrostrictive relaxors and are indicated in Figure 1 by the single cross-hatched region identified as the SFE (slim FE hysteresis loop) region [3].

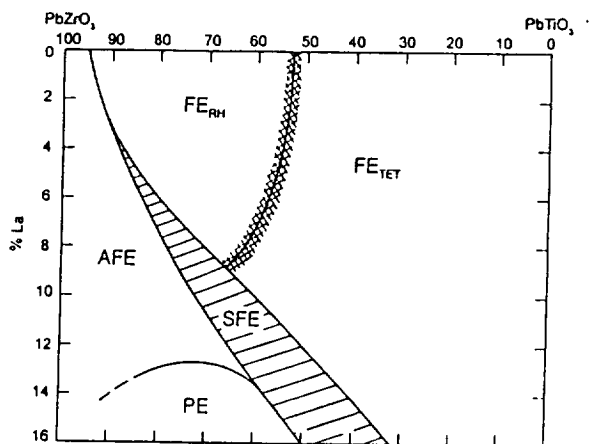


Figure 1. Room temperature phase diagram of the PLZT system showing phase stability regions and phase boundaries of interest.

Although the PLZT relaxor materials were developed over two decades ago for electrooptic applications such as shutters, displays and modulators, they have now been found to be quite suitable for electrostrictive actuator devices where non-memory, lower hysteresis properties are required.

Also, it has recently been reported that PLZT ceramics are excellent materials for achieving ultra-high displacements when they are processed into Rainbow actuator benders which are similar in operation to the unimorph benders with the exception that the Rainbows are a monolithic structure [4-5]. As single-element Rainbows, the PLZT materials are able to achieve very high displacements (up to 3mm) at moderate loading or lesser displacements at loads of up to 10 kg. A variety of applications are foreseen for these devices, however, before they can be developed it is necessary that the phenomena producing the high displacement in these materials be understood more thoroughly and that the composition of the material selected for a given application be the optimum one.

Therefore, it is the purpose of this investigation to (1) study the characteristics of a broad range of compositions in the PLZT solid solution system as Rainbow benders, (2) identify specific compositions with maximum displacement properties and (3) gain more insight into the strain amplification mechanisms involved in the Rainbow ceramics.

EXPERIMENTAL PROCEDURE

Several series of compositions in the PLZT system were prepared from the raw material oxides via a conventional mixed oxide process as outlined in the flowsheet of Figure 2. These

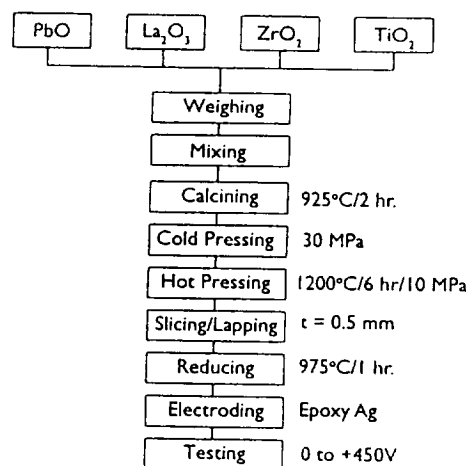


Figure 2. Flowsheet for Rainbow process.

compositions, compounded according to a B-site formula[3], ranged in Zr/Ti ratio from 90/10 to 30/70 and La content from 1 to 15 atom percent. A total of sixty individual compositions were formulated, weighed, wet mixed with distilled water, dried and calcined at 925°C for 2 hours in closed alumina crucibles. The milled and dried powders were first cold pressed as pre-form slugs and then hot pressed at 1200°C for 6 hours at 10 MPa. This procedure yielded a fully dense material with grain sizes

varying from 1.5 to 6 microns. Subsequent steps in the fabrication of the wafers included slicing and lapping them to a thickness of 0.5 mm.

A Rainbow was produced from a lapped part by placing the wafer on a flat graphite block which was supported on a zirconia carrier plate. A second zirconia plate of the same size as the wafer was placed on top of the wafer in order to shield the top side of the wafer from chemical reduction and to minimize thermal shock to the part during processing. The assembly was placed into a furnace preheated to 975°C and held there for one hour, removed from the furnace while hot and cooled naturally to room temperature in about 45 minutes. When cool, the dome shaped wafer was lifted from the graphite block, sanded lightly on the reduced (concave) side to remove any metallic lead particles and to expose the reduced layer, and then electroded with DuPont 5504N epoxy silver paint cured at 200°C for 30 minutes. Although a silver electrode was applied to the reduced side of the wafer, it was used primarily to insure good electrical contact to the conductive reduced PLZT which actually was the bottom electrode. Since the reduced PLZT layer was measured to be 0.15mm thick for the selected reducing conditions, the net thickness of the PLZT piezoelectric was 0.35mm.

Standard electrical measurements of capacitance (1 kHz), dissipation factor and dc hysteresis loops were run on all of the samples after electroding. Displacement measurements were usually made using a positive pulse voltage source and a mechanical dial indicator [8], however, selected tests were also run using a LVDT in order to compare results and to obtain the full displacement loop with + and - voltages.

Grain size measurements were determined from optical micrographs of polished and etched parts at a magnification of x1250 using the linear intercept method.

RESULTS AND DISCUSSION

Grain Size

Grain sizes of the hot pressed PLZT parts ranged from 1.5 microns (um) average diameter to 6.0 um. In general, the larger grain size materials were found to be located along each of the phase boundaries mentioned previously; i.e., between the AFE, PE and FE phases, while compositions in the interior of the phase stability regions possessed minimal grain sizes with the 4% La series having the smallest. Examples of this behavior are illustrated in Figures 3 and 4 as functions of Zr/Ti ratio and La content, respectively. The reason for this behavior is not

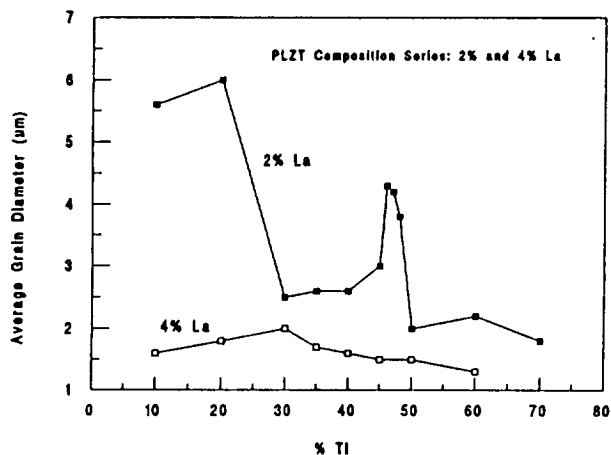


Figure 3. Grain size as a function of composition for materials in the PLZT system at 2 and 4 atom % La.

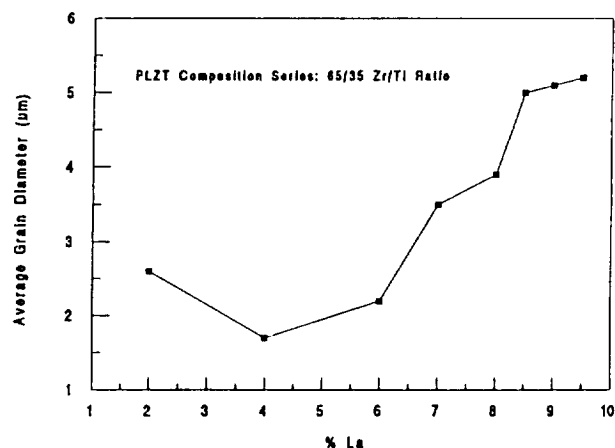


Figure 4. Grain size as a function of composition for materials in the PLZT system at a Zr/Ti ratio of 65/35.

understood at this time; however, previous experience with PLZT materials for electrooptics confirms the existence of large grain sizes (up to 15 um) for 9/65/35. Obviously, this present set of grain sizes exists for the materials hot pressed at the selected conditions, and this would change as the as the temperature or time was varied; but when comparing all compositions at the same conditions, one can only speculate at this stage that chemical and structural factors such as excess lead oxide in the B-site formula, vacancies in the lattice or mixed phases in the phase boundary compositions are instrumental in producing these results.

Grain size is an important factor in the displacement characteristics of Rainbows just as it is already known to be a significant factor in other properties of piezoelectrics such as dielectric constant, coupling and d constant. Figure 5 shows the effect of grain size on axial displacement for composition 1/53/47.

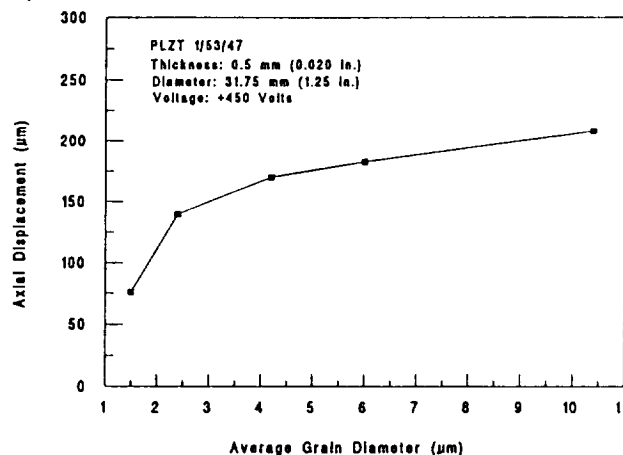


Figure 5. Grain size dependence of axial displacement for PLZT 1/53/47 Rainbow.

The grain sizes for this composition were obtained by hot pressing at temperatures from 1000 to 1200°C. As can be seen, grain sizes less than approximately 2 um lessen the displacement characteristics and those greater than about 8 microns are of little additional benefit. An optimum grain size range is estimated to be from 6 to 7 microns.

Electrical Properties

Dielectric Properties - Small-signal dielectric properties of

several compositions of varying Zr/Ti ratio at 2% and 6% La concentration are given in Figures 6 and 7, respectively. Values

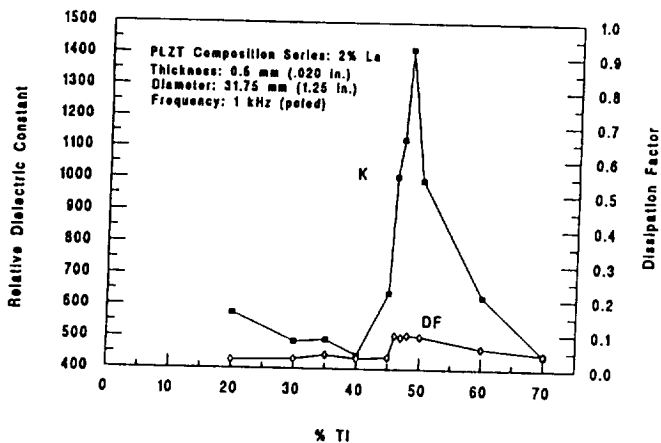


Figure 6. Small signal dielectric properties of composition series at 2% La.

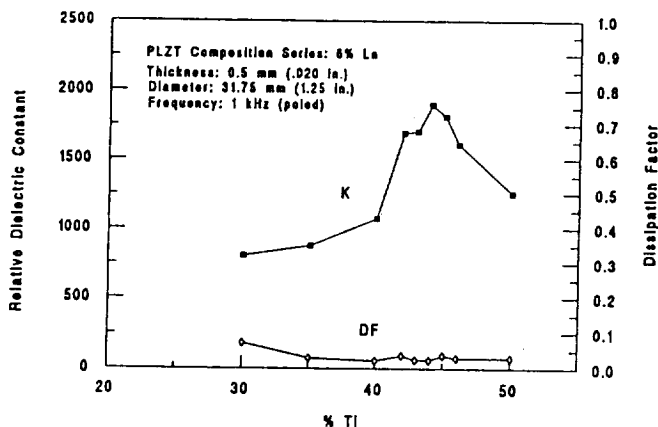


Figure 7. Small signal dielectric properties of composition series at 6% La.

ranged from a low of 444 for 2/60/40 to a high of 1896 for 6/56/44. As expected, dielectric constant peaked at the MPB for both series of compositions, however, the anomaly was especially pronounced for the 2% La series. The maximum value of 1416 was possessed by composition 2/52/48. Dissipation factors ranged from 2.4% to 9.7% with the higher values occurring in the MPB compositions.

A second series of compositions with varying La contents at Zr/Ti ratios of 65/35 and 70/30 are shown in Figures 8 and 9, respectively. In this series, dielectric constants were observed to increase in a regular manner from low values at 2% La to maximum values at 8.5 - 9% La. Actual values ranged from 486 to 3264 for the 70/30 group, and the 65/35 values also fell within this range. Dissipation factors as high as 9.8% and as low as 2.8% were measured, again with the higher values occurring at the FE - AFE and FE - PE phase boundaries. These values are typical of those obtained in previous work on PLZT materials.

Hysteresis Loops - Typical examples of dc hysteresis loops for compositions 1/53/47 and 9/65/35 are given in Figure 10. The loop in Figure 10 (A) was taken on the ferroelectric Rainbow element (1/53/47) in its virgin condition before any other measurements were made. It should be noted that on the initial application of positive voltage to +450V there was approximately 60% of the total remanent polarization switched rather than the usual 50% one ordinarily observes in a virgin,

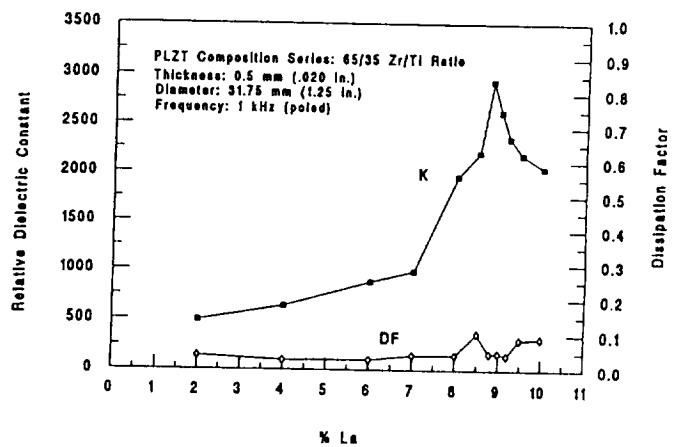


Figure 8. Small signal dielectric properties of composition series at 65/35 Zr/Ti ratio.

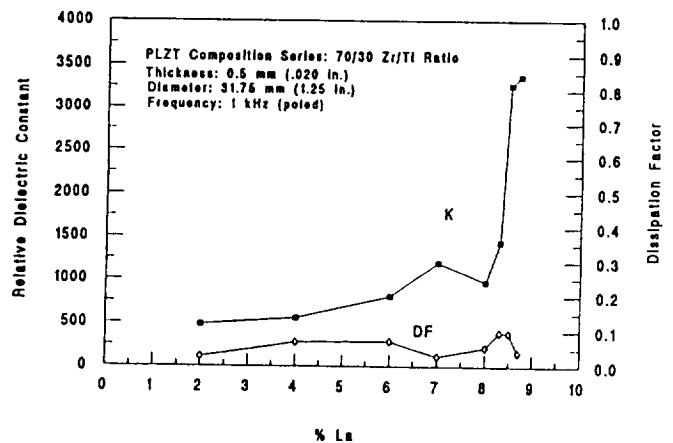


Figure 9. Small signal dielectric properties of composition series at 70/30 Zr/Ti ratio.

randomly oriented ceramic. This behavior is highly unusual and indicates that the Rainbow ceramic was partially poled before testing. Additional audio and piezoelectric tests of other virgin parts also indicated that the elements were partially poled to varying degrees; i.e., some very little and others as high as 75%.

One explanation for this condition occurring in the electrically virgin state is that the mechanical compressive and tensile stresses produced in the Rainbow wafer during processing are acting together to switch some of the domains in this soft ferroelectric/ferroelastic material. Since uniform stress is a

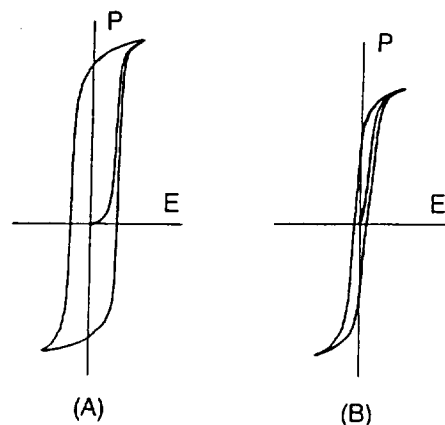


Figure 10. Typical hysteresis loops for Rainbow PLZT compositions (A) 1/53/47 and (B) 9/65/35.

symmetrical quantity, it is recognized that it alone is insufficient to produce a net polarization in a given direction even though it may be of sufficient magnitude to switch domains; however, a stress gradient such as produced by the Rainbow bending process is a vector quantity and can, indeed, produce the observed effect. This non-uniform stress is believed to be responsible for the partial poling of the Rainbow wafers.

Measured properties on the above wafer were: $P_R = 44.8 \text{ uC/cm}^2$, $E_C = 7.5 \text{ kV/cm}$, dielectric constant = 1210 and dissipation factor = 0.047.

The virgin loop of Figure 10(B) is a typical one for the electrostrictive (9/65/35) type of Rainbow materials and is very similar to that obtained on bulk electrooptic material. Measured properties on this wafer were: $P_{10\text{KV/CM}} = 28.3 \text{ uC/cm}^2$, dielectric constant = 3142 and dissipation factor = 0.085. As a matter of course, no unsymmetrical hysteresis loops were observed in the electrostrictive materials, and none was expected, since there are no stable domains in these materials at zero electric field. Conceivably, a high enough stress could precipitate stable domains in a very near-ferroelectric material, however, a study of this effect is beyond the scope of this investigation.

Displacement Loops - Displacement vs. electric field (butterfly) loops for the Rainbow wafers described above are shown in Figure 11. As before, Figure 11(A) illustrates the Rainbow axial motion as the sample is electrically switched from zero to +450V, to -450V and back to zero, however, in this case this loop was not taken on the virgin wafer. It may be noted that this loop is remarkably similar to that observed when measuring the direct extensional (longitudinal, lateral) displacements via the piezoelectric d_{33} or d_{31} coefficients. The value of displacement in the + voltage direction was measured at 190.5 μm , and the total amount of displacement (+/-) was 432 μm .

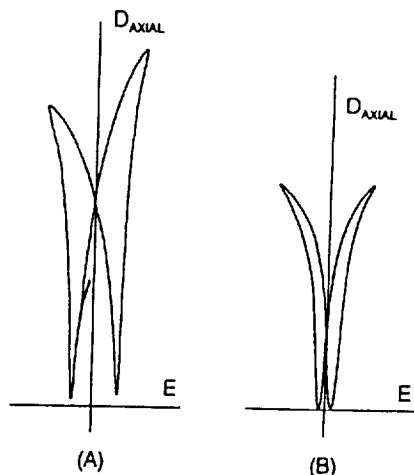


Figure 11. Axial displacement loops of samples in Figure 10.

Figure 11(B) shows the displacement loop of the electrostrictive Rainbow material (9/65/35) mentioned above. Since 9/65/35 is a relaxor material there should be little or no memory, and the same value and sign of displacement should be obtained whether a + or a - voltage is applied. One can see by switching this sample through a full voltage loop that a small amount of remanent displacement (strain) is present which is probably due to the close proximity of this composition to a FE phase. A further indication of this incipient FE phase is the higher than normal value of P_{10} ($P_{10} = 28.4$ vs. 18.0 uC/cm^2) as given above. Measured value of total displacement for this wafer was 178 μm .

Displacement vs. Composition - Displacement data as a function of composition in the PLZT phase diagram is shown in Figure 12. In this figure, the stars indicate the location of most

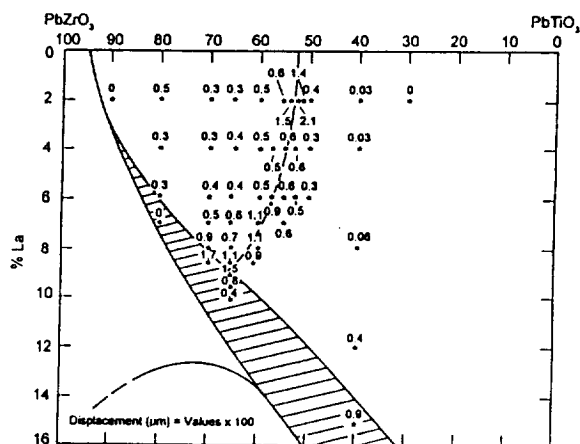


Figure 12. Rainbow displacement data for the PLZT system overlaid with the phase diagram of Figure 1 (values in microns are to be multiplied by 100).

of the compositions prepared, and the values given are those obtained from the dial micrometer measurements at zero to +450 volts. As such, they represent approximately one-half of the total switching displacement available from the FE materials but all of the displacement available from the SFE relaxor materials. It may be noted in this diagram that the maximum displacements were found to occur along the same phase boundaries mentioned previously; i.e., the $FE_R - FE_T$, $FE - PE$ and $FE - AFE$ boundaries, where other properties also are maximized. It should also be mentioned that the phase boundaries shown in Figure 12 are the same as those of Figure 1 because Figure 1 was simply overlaid on the displacement data and drawn in. The location of these boundaries were determined to be nearly identical to those which could be located by the displacement data. A comparison of these boundary locations at various levels of La are given in Table 1.

Table 1. Morphotropic phase boundary compositions determined from displacement data compared with ref. 3.

% La	PLZT (Ref. 3)	PLZT Rainbow (This Work)
2	2/53/47	2/53/47
4	4/55/45	4/55/45
6	6/58/42	6/57/43
7	7/60/40	7/61/39
8	8/62/38	8/60/40
Boundary	8.6/65/35	8.5/70/30

The values of displacement varied from essentially zero (equivalent to the direct extensional modes) to a high of 210 μm for composition 2/52/48, which would indicate that maximum displacement occurs just on the tetragonal side of the MPB boundary. Other maxima occur at 9/65/35 (152 μm) and 8.5/70/30 (168 μm) for the electrostrictive materials at their respective boundaries. It is interesting to note that no significant anomaly or trend occurred near the AFE - FE boundary where one would expect a large electric field induced volume change in

going from a small AFE unit cell to a larger FE unit cell. For compositions 2/90/10 and 4/90/10 which are near this boundary, it was observed that the Rainbow curvature was reversed from convex up (reduced side concave) to near flat or convex down (reduced side convex). In some cases, an electroded part of this type exhibited an axial displacement which could be tested simply by turning the wafer upside down and then operating as normal. Obviously, this region of the phase diagram should be studied further, but such depth was beyond the scope of this investigation.

Some of the possible reasons for maximum Rainbow displacements to occur at phase boundaries are (1) maximum piezoelectric constants (d_{33} and d_{31}) occur at the boundary, (2) mixed or metastable phases exist, (3) maximum domain reorientation is possible, (4) higher mechanical compliance of the structure exists, (5) electric field enforced phases are possible and even probable in some cases and (6) larger grain sizes may occur in the mixed phase region at the boundary. To some degree, all of these effects are probably operative in the Rainbow devices, however, a more in-depth study is required to identify the dominant mechanisms.

Figures 13 through 17 deal with a closer look at the compositional variation of displacement as a function of Zr/Ti

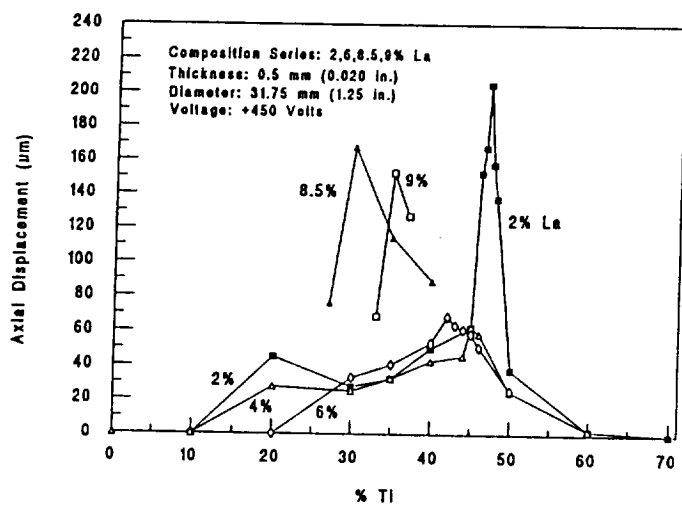


Figure 13. Displacement characteristics of PLZT Rainbow ceramics as a function of Zr/Ti ratio at selected levels of %La.

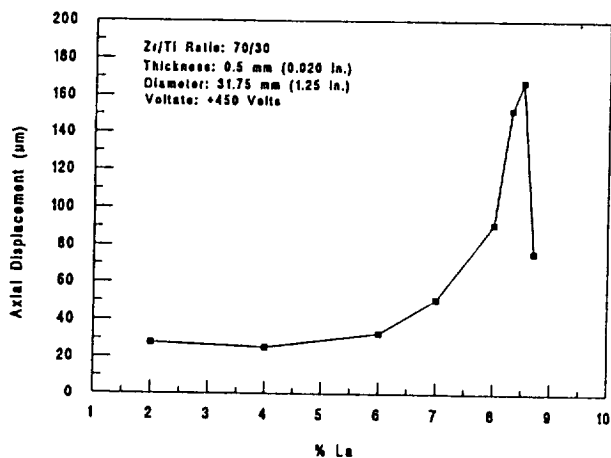


Figure 14. Displacement characteristics of PLZT Rainbow ceramics as a function of La content at a 70/30 Zr/Ti ratio.

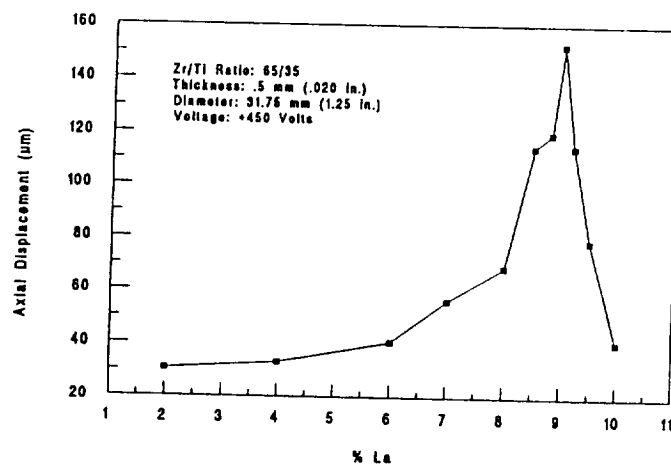


Figure 15. Displacement characteristics of PLZT Rainbow ceramics as a function of La content at a 65/35 Zr/Ti ratio.

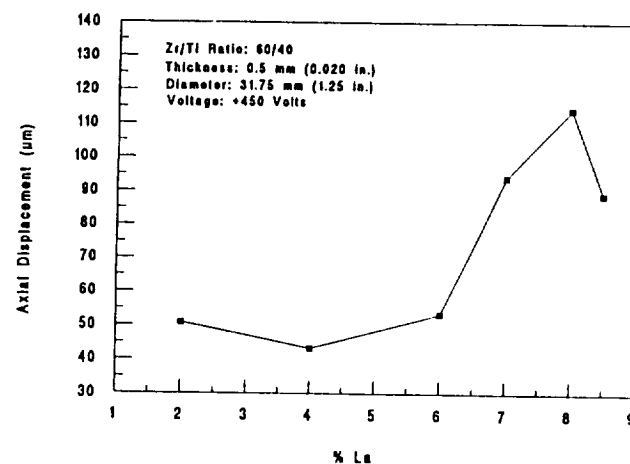


Figure 16. Displacement characteristics of PLZT Rainbow ceramics as a function of La content at a 60/40 Zr/Ti ratio.

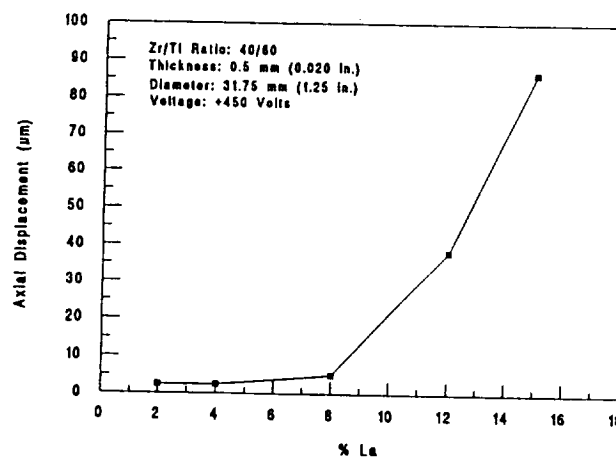


Figure 17. Displacement characteristics of PLZT Rainbow ceramics as a function of La content at a 40/60 Zr/Ti ratio.

ratio (% Ti) at several levels of La concentration or of % La at several different Zr/Ti ratios. Each of these figures again emphasizes the significantly larger displacements existing in the phase boundary compositions.

CONCLUSIONS

This investigation indicates that the PLZT compositional system is a very fruitful area for producing and studying the unique characteristics of the Rainbow ceramics. No difficulty was experienced in fabricating any of the compositions into Rainbow wafers with the exception of four compositions near the AFE - FE phase boundary. The results of this investigation clearly show that (1) maximum axial displacement is obtained in compositions in or near the morphotropic phase boundary or the phase boundary separating the FE phases from the non-polar (AFE, PE) phases, (2) grain size is a factor in achieving high displacement, i.e., larger grain size is desirable, (3) the compressive and tensile stresses produced in the Rainbow process are instrumental in partially pre-poling the Rainbow ceramic and (4) other mechanisms, in addition to the piezoelectric d_{31} coefficient, are very likely responsible for the unusually large displacements observed. A maximum displacement of 210 microns for a single, dome-mode Rainbow ceramic was found to occur in PLZT 2/52/48 when activated from zero to +450 volts. Since all of the displacements in this investigation were obtained on Rainbow ceramics with a diameter-to-thickness ratio (31.75 mm x 0.5 mm or 63.5 to 1) conducive to producing a dome-type displacement rather than a saddle type, significantly higher displacement values are to be expected for larger diameter and thinner parts with a higher ratio [4].

ACKNOWLEDGEMENT

This work was supported by NASA under grant No. NAG-1-1301 and ONR under grant No. N0014-94-1-0563.

REFERENCES

1. D. Berlincourt, "Current Developments in Piezoelectric Applications of Ferroelectrics," *Ferroelectrics*, 10, 111-119, 1976.
2. G.H. Haertling, "Piezoelectric and Electrooptic Ceramics," in *Ceramic Materials for Electronics*, Relva Buchanan, ed., 139-225, Marcel Dekker, Inc., New York, 1986.
3. G.H. Haertling and C.E. Land, "Hot Pressed (Pb,La)(Zr,Ti)O₃ Ferroelectric Ceramics for Electrooptic Applications," *J. Am. Ceram. Soc.*, 54, 1-11, 1971.
4. Gene H. Haertling, "Rainbow Ceramics - A New Type of Ultra-High-Displacement Actuator," *Bull. Am. Ceram. Soc.*, 73, 93-96, 1994.
5. Gene H. Haertling, "Chemically Reduced PLZT Ceramics for Ultra-High Displacement Actuators," *Ferroelectrics*, 154, 101-106, 1994.

The Dielectric, Piezoelectric and Hydrostatic Properties of PLZT Based Rainbow Ceramics

15AF-94
(Perm State)
0

S. Sherrit, H.D. Wiederick and B.K. Mukherjee
Royal Military College of Canada, Kingston, Ontario K7K 5L0, Canada

and

G.H. Haertling
Clemson University, Clemson, South Carolina 29634-0907, USA.

ABSTRACT

It has recently been shown that the selective reduction of one surface of a high-lead-containing piezoelectric or electrostrictive ceramic wafer results in a stress-biased wafer with a unique domed structure that leads to high electromechanical displacement and enhanced load-bearing capability. These ceramics have been called rainbow ceramics and their very high displacements make them very promising materials for transducers and actuators. The dielectric, piezoelectric and hydrostatic properties of a variety of PLZT based rainbow ceramics have been measured and analysed. The samples exhibited a strong piezoelectric effect in the poling direction (effective d_{33} of the order of 10^{-8} C/N) under low planar and hydrostatic pressures but as the pressure was increased there was a marked decrease in the strength of the piezoelectric response which passed through a minimum and then increased to the level of typical values for PZT ceramic. Some samples were plated and these had a low pressure hydrostatic voltage coefficient that was considerably greater than that of PZT along with a reasonable level of thickness mode electro-mechanical coupling. However, as the hydrostatic pressure was increased, the hydrostatic voltage coefficient decreased towards typical values for PZT. The rainbow ceramics show considerable promise as material for actuators and, possibly, for shallow water sonar transducers.

and hydrostatic properties of a range of PLZT based rainbow ceramic specimens which are described in Table 1. The specimens had a lanthanum content of 1.0 % and a lead zirconate content of 53 %. The samples were 0.5 mm thick discs which were electroded with Dupont 5504N silver epoxy and they all had a dome like appearance. Samples 4 and 5 had their rims glued to 1 mm thick brass plates whose diameters are given in Table 1. A specimen without electrodes was used to determine the density which was found to be $7575 \pm 100 \text{ kgm}^{-3}$.

Table 1: The Specimens

Sample Number	Diameter/ Plate Diameter (cm)	Plate
1	1.31	none
2	3.15	none
3	3.14	none
4	3.16 plate - 3.4	brass
5	1.31 plate - 1.32	brass

INTRODUCTION

A new type of ceramic bender has recently been produced by the high temperature chemical reduction of one surface of a high-lead-containing piezoelectric or electrostrictive ceramic wafer which results in a stress-biased dome like structure that is capable of achieving very high axial displacements [1]. The reduced (concave) side of the wafer can serve as one of the electrodes. This type of ceramic has been called a "rainbow" (reduced and internally biased oxide wafer) ceramic. When a voltage is applied to a rainbow ceramic, the dome height varies as a function of the magnitude and polarity of the voltage and this motion is largely a consequence of the lateral contraction produced in the material due to the lateral piezoelectric coefficient d_{31} . Rainbow ceramics have been produced using ceramics such as lead zirconate titanate (PZT), lead lanthanum zirconate titanate (PLZT) and lead magnesium niobate (PMN). Single elements of rainbow ceramics, 0.2 mm thick, have produced displacements of 1 mm which represents a very high strain of 500%. Since rainbow ceramics are also easy and cheap to produce, they show considerable promise as materials for actuators and sonar activators. This paper reports on the measurement and analysis of the dielectric, piezoelectric

RESONANCE MEASUREMENTS

A Hewlett Packard Model 4192 Impedance Analyser was used to measure the impedance of the samples as a function of frequency. In addition to radial and thickness mode resonances, the samples showed bending mode resonances; in the case of sample 1 the bending mode resonance occurred at about 30 kHz. The impedance spectra of the samples have been analysed using Smits' method [2] and our own techniques [3] although it should be stressed that the geometry of these dome shaped samples does not correspond strictly to the geometry assumed in deriving the resonance equations. An analysis of the thickness and radial mode resonances of samples 1, 2 and 3 gave the material constants shown in Tables 2 and 3 in which the symbols used have the usual definitions as given in the IEEE Standard on Piezoelectricity [4]. These tables show that there are large differences in the material constants measured for the various samples and this is likely to be due to small differences in the curvatures and aspect ratios of the dome shaped samples. The curvature is a result of the reduction process and small variations in composition and processing conditions would produce differences in

Table 2: Thickness mode material constants measured at 4 MHz and 20°C

	Sample 1	Sample 2	Sample 3
k_t	0.359(1 - 0.12i)	0.355(1 - 0.31i)	0.327(1 + 0.12i)
c_{33}^D (10^{11} N/m ²)	1.35(1 + 0.020i)	1.06(1 + 0.069i)	1.19(1 + 0.068i)
ϵ_{33}^S (10^{-9} F/m)	8.39(1 - 0.33i)	6.87(1 - 1.1i)	11.3(1 - 0.35i)
h_{33} (10^9 V/m)	1.62(1 + 0.049i)	1.23(1 + 0.15i)	0.99(1 + 0.33i)

Table 3: Radial mode material constants measured at 20°C

	Sample 1	Sample 2	Sample 3
s_{11}^E (10^{-11} m ² /N)	1.55(1 - 0.023i)	1.81(1 - 0.023i)	2.15(1 - 0.038i)
s_{12}^E (10^{-11} m ² /N)	-0.517(1 - 0.023i)	-0.742(1 - 0.023i)	-1.22(1 - 0.038i)
d_{31} (10^{-12} C/N)	-140(1 - 0.088i)	-123(1 - 0.085i)	-83(1 - 0.22i)
ϵ_{33}^T (10^{-9} F/m)	13.3(1 - 0.0915i)	11.6(1 - 0.077i)	7.8(1 - 0.21i)
σ^p	0.334	0.410	0.566
k_p	0.52(1 - 0.043i)	0.48(1 - 0.047i)	0.43(1 - 0.11i)

the curvatures of the samples which would significantly affect the material constants.

In Figure 1, which shows the thickness resonance of sample 1, the experimental points are compared to the fit obtained by using the material constants found for this sample. It can be seen that the fit is acceptable around the fundamental mode but there is significant dispersion at higher frequencies. Besides, the first thickness resonance occurs close to 4 MHz and it follows that a non-dispersive material would have a second resonance at around 12 MHz whereas this occurs at about

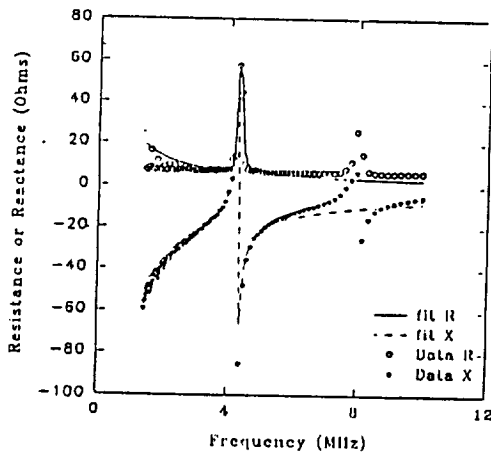


Figure 1. The resistance and reactance versus frequency for sample 1. The experimental points are compared with the lines which represent fits obtained by using the derived material constants.

7.5 MHz in the figure. Finally the figure shows that the base-lines for the data and the fit differ substantially at frequencies higher than the first resonance frequency. All of this evidence points to a significant dispersion in the dielectric, elastic and piezoelectric constants of the material.

Another interesting feature is that the second thickness mode resonances of the larger samples are inductive and yield negative values of permittivity; this is due to the high conductivities of these samples at high frequencies.

Samples that were bonded to plate electrodes had thickness resonances that saturated the measuring circuit while their radial modes were smaller than those for the unbonded samples. This suggests that the electrode plate acts to clamp d_{31} more than d_{33} with a resulting enhancement in k_t .

DIELECTRIC MEASUREMENTS

The capacitances of the specimens were measured at a frequency of 1000 Hz at room temperature. The average values for the permittivity, the dielectric constant and the loss tangent for samples 1, 2 and 3 are given in Table 4.

Table 4: Dielectric Constants (averaged over samples 1, 2 and 3)

Property	Units	Value
Permittivity ϵ_{33}^T	10^{-9} F/m	14 ± 1
Dielectric Constant K_{33}^T		1540 ± 110
Loss Tangent $\tan \delta$		0.086 ± 0.012

THE PIEZOELECTRIC CHARGE CONSTANT

The value of the piezoelectric charge constant, d_{33} , for the material was obtained by using a point force head on a Berlincourt type d_{33} meter which was operated at a frequency of 200 Hz. The value of d_{33} was found to vary over the surface of the samples; to find if this was due to coupling to the bending mode of the sample, measurements were made at 12 points spaced 1 mm apart along a diameter of the slightly domed samples. Our results for sample 1 are shown in Figure 2 where the three curves represent the values obtained (a) when the measurements were made with the curvature of the dome shaped sample facing downwards so that the sample formed a cavity with the base plate of the meter with the positive terminal at the point head (indicated as "+ up" data in the figure), (b) when the measurements were made with the sample curvature facing upwards ("+" down" data in the figure) and (c) the average of the two measurements made in (a) and (b). Figure 4 shows that the apparent d_{33} values are quite large and can reach up to 12,000 pC/N at the centre of the specimen. It is likely that this large value is due to the addition of the normal uniaxial compression of the ceramic material and the bending modes of the dome shaped sample. In order to elucidate this better the d_{33} was measured as a function of uniaxial compression

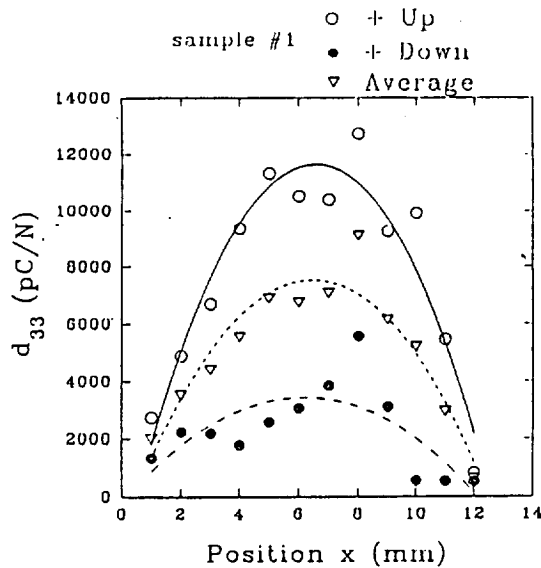


Figure 2. The effective d_{33} value as a function of distance along a diameter of sample 1. The significance of the three curves has been explained in the text.

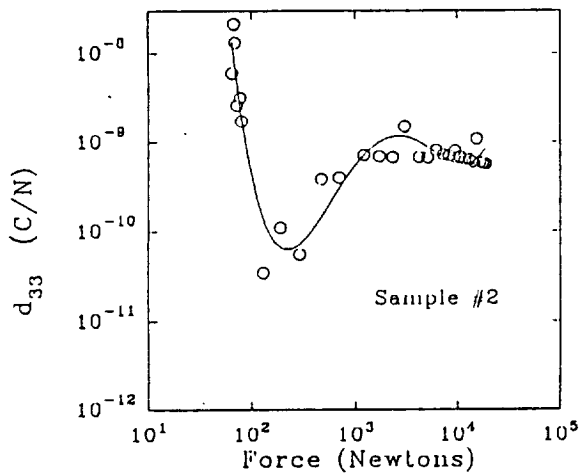


Figure 3. The effective d_{33} as a function of the compressional force applied to sample 2.

sion using a method which has been reported earlier [5]. Our results for sample 2 are shown in Figure 3 and it can be seen that d_{33} has a value of about 10,000 pC/N at low applied force but it then decreases rapidly as the dome shaped sample is flattened out as a result of increasing force and it passes through a minimum at a force of about 200N from which point it rises up to typical ceramic values as the ceramic undergoes compression. It can therefore be concluded that the large d_{33} values are indeed caused by the bending of the dome shaped sample when a stress is applied; after the rainbow material has become flat, it begins to act like a plain bulk ceramic disc.

It should be noted that the voltage - force curves of the specimens show hysteresis and this behaviour is very similar to that shown by bulk PZT discs [5]. The hysteresis is due to the time-dependence of the piezoelectric response of the rainbow ceramic.

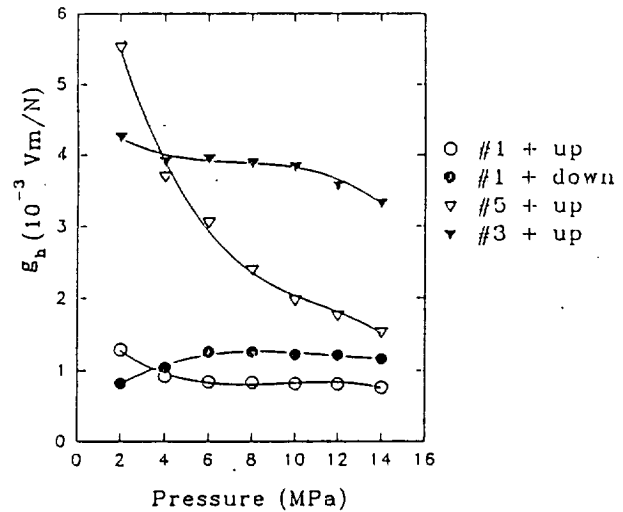


Figure 4. The hydrostatic voltage coefficient, g_h , as a function of the hydrostatic pressure for different samples and orientations.

HYDROSTATIC PROPERTIES

The hydrostatic voltage constants, g_h , of the rainbow specimens have been measured at a frequency of 400 Hz and as a function of pressure using a SENSOR g_h apparatus. Our results for samples 1, 3 and 5 are shown in Figure 4. Two series of measurements were carried out on sample 1: the results indicated by "+ up" correspond to the dome shaped sample being placed with its curvature facing down and forming a small cavity with the base plate of the apparatus while the results indicated by "+ down" correspond to the rainbow ceramic sitting on the base plate with its curvature facing up. The hydrostatic voltage response is the sum of the contributions arising from the bending of the dome shaped rainbow and the compression of the ceramic itself. In the case of sample 1, the bending effects are small since the edge of the rainbow ceramic can move laterally on the base plate and so the g_h value is close to that of standard bulk PZT ceramic. The small difference between the two series of measurements on sample 1 is probably due to the different contributions from the bending of the specimens. Samples 1 and 3 are similar in that both were not bonded to a base plate so that the hydrostatic pressures are identical on both faces and the dome does not undergo any flattening due to the hydrostatic pressures. Sample 3, which has the bigger radius, has a larger value of g_h and this is perhaps due to the larger bending deflections which are possible in this case. Sample 5 is a rainbow ceramic of the same radius as sample 1 but it is bonded to a brass plate about 1 mm thick so that the hydrostatic pressure is not now transmitted to the inner surface of the rainbow and the dome gradually flattens as the external static pressure is increased. At low pressures the flattening is negligible, but since the rim of the rainbow is bonded, the bending response to the signal is considerably greater than in the case where the rainbow is not bonded (as in sample 1) and hence the much larger value of g_h . As the pressure increases, the rainbow gradually flattens, the bending contributions decrease and the g_h value approaches that of a normal bulk PZT ceramic.

CONCLUSIONS

The set of PLZT based rainbow specimens analysed by us have shown a strong piezoelectric response under low planar and hydrostatic pressures but there is a marked decrease in the strength of the response as the pressure is increased. The larger response at low pressures is thought to be due to the bending of the samples and the consequent release of charge.

The resonance curves of the specimens were somewhat distorted by the presence of the bending modes. The material constants were determined for the radial and thickness modes of operation and these were found to exhibit geometric effects and dispersion.

The rainbow samples that were not bonded to a base plate had hydrostatic properties in the same range as ordinary bulk PLZT with some variation depending on the orientation of the sample in the measurement apparatus. However the rainbow samples that were bonded to electrode plates showed substantially better hydrostatic properties but, as the static pressure increased, these decreased to values similar to those of bulk PLZT.

The dielectric properties of the rainbow samples were similar to those of PLZT.

In conclusion, the rainbow ceramic material shows considerable promise as an actuator material where large displacements are required (solid state speakers, pumps, switches, positioners etc..) and, possibly, for shallow water sonar projectors. The large pressure dependences exhibited by the material reduce its applicability in deep water applications, although, with proper design, it may be possible to maintain a pressure-independent sensitivity that will be somewhat greater than that of PZT, the current standard in sonar transducer materials.

REFERENCES

- [1] G.H. Haertling, "Rainbow Ceramics - A new Type of Ultra-High-Displacement Actuator", *American Ceramic Society Bulletin*, vol.73, pp.93-96, January 1994.
- [2] J.G. Smits, "Iterative Method for Accurate Determination of the Real and Imaginary Parts of the Material Coefficients of Piezoelectric Ceramics", *IEEE Trans. Sonics and Ultrasonics*, vol.SU-23, pp.393-402, June 1976.
- [3] S. Sherrit, N. Gauthier, H.D. Wiederick and B.K. Mukherjee, "Accurate Evaluation of the Real and Imaginary Material Constants for a Piezoelectric Resonator in the Radial Mode", *Ferroelectrics*, vol.119, pp.17-32, 1991.
- [4] *IEEE Standards on Piezoelectricity*, ANSI/IEEE Std.176-1987.
- [5] S. Sherrit, D.B. Van Nice, J.T. Graham, B.K. Mukherjee and H.D. Wiederick, "Domain Wall Motion in Piezoelectric Materials under High Stress", *Proceedings of the Eighth IEEE International Symposium on Applications of Ferroelectrics - ISAF '92*, 1992, pp.167-170.

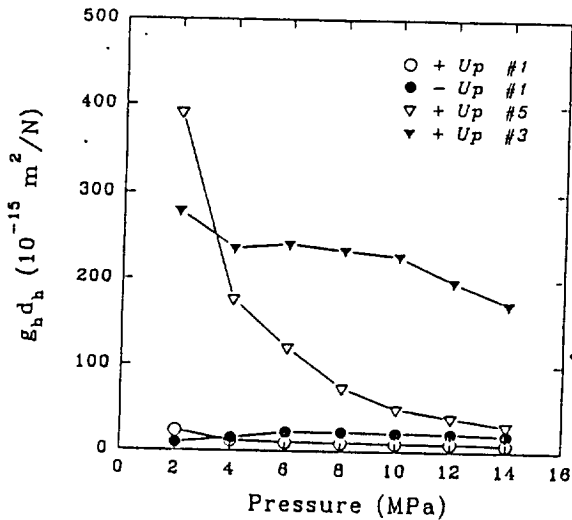


Figure 5. The hydrostatic figure of merit for samples 1, 3 and 5.

Figure 5 shows the hydrostatic figure of merit, $g_h d_h$, of samples 1, 3 and 5. The small rainbow (sample 1) has a figure of merit that is substantially lower than that of PZT while the larger rainbow ceramic (sample 3) has a figure of merit which is comparable to that of PZT.

The $g_h d_h$ values for sample 4 are shown as a function of pressure in Figure 6. This sample is a large rainbow ceramic, 3.16 cm in diameter, bonded to a 1 mm thick brass plate and its behaviour is qualitatively similar to that of sample 5 which is smaller. At high pressures the values are slightly lower than the nominal values for normal bulk PZT but they rise dramatically at low pressures. At low pressure this sample has a very high g_h value of about 0.8 Vm/N

Finally it may be noted that both Figures 3 and 6 show minima. This is explained by the fact that there are two contributions to charge generation: bending of the dome shaped samples and compression of the ceramic. These two contributions are not independent but are coupled with the strain being relieved by the bending action of the monomorph.

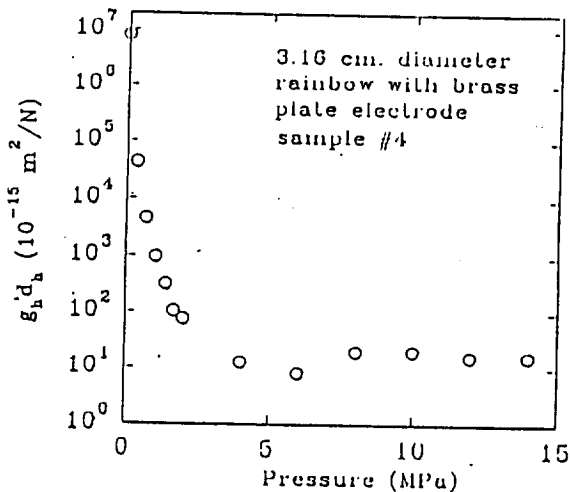


Figure 6. The hydrostatic figure of merit as a function of pressure for sample 4.

Electromechanical Properties of Rainbow Devices

E. Furman, G. Li and G. H. Haertling
The Gilbert C. Robinson Department of Ceramic Engineering
Clemson University, Clemson, South Carolina 29634-0907

Abstract — A stress-biased, domed, electromechanical bender called a Rainbow was recently developed. Displacement characteristics for Rainbow devices based on piezoelectric PLZT compositions were studied in the frequency range far below the fundamental resonant mode frequency. Experimentally obtained field-induced displacements were compared with those predicted by a finite element model. The model underestimated the observed displacements. Low frequency relaxation of the displacements was observed experimentally.

INTRODUCTION

There are a number of applications including pumps, speakers, laser deflectors, optical scanners, and relays for which displacements well above those obtained using linear actuators are desirable. For these applications, piezoelectric benders have traditionally been used [1-4]. Benders are based on a bimorph or unimorph structure. Bimorphs contain two electromechanically active layers, and unimorphs have an active and a constraining layer. In both cases, layers must have good bonding since bending occurs as a result of field-induced lateral strain being nonuniform in different parts of a structure. To accommodate this strain, the sample bends, producing vertical displacement. The key parameter for these devices is the piezoelectric d_{31} or electrostrictive Q_{12} coefficient, which should be maximized.

Recently, a new type of bender called a RAINBOW (Reduced And Internally Biased Oxide Wafer) was developed with promising characteristics [5]. Rainbow devices with maximum displacements of 3 mm and sustaining point loads up to 10 kg were demonstrated [6]. The trade-off between the displacement and load-bearing capabilities was established.

In this paper the electromechanical properties of Rainbow devices well below the fundamental resonance mode frequency will be described and compared to those predicted by a finite element model (FEM).

RAINBOW ACTUATORS

Rainbow actuators consist of an electromechanically active layer and a constraining layer, similar to conventional unimorphs. Unlike the unimorph, however, the Rainbow is a monolithic structure. The constraining layer is formed by exposing one side of a lead-containing ceramic to a reducing atmosphere at high temperature produced by placing a ceramic in contact with a carbon block. The reduction of lead lanthanum zirconate titanate (PLZT) ceramics occurs as a result of oxidation of the solid carbon block, first to carbon monoxide and then to carbon dioxide gases [7]. The reduced layer is no longer piezoelectric, and is, in fact, a good electrical conductor due to a presence of a large amount of lead. The reduced layer functions as the electrode and the constraining part of the bender.

Rainbows also differ from unimorph benders by the presence of large internal stresses developed during the process of reduction and cooling to room temperature. Because of the volume decrease during the reduction step and the higher thermal expansion of the reduced layer compared to the oxide layer, the stress-free equilibrium dimensions of the reduced layer are smaller than for the oxide layer. To retain continuity at the interface between the oxide and the reduced layers and to minimize stored elastic energy, the sample develops curvature. For the Rainbows with a large reduced/oxide layer thickness ratio, the oxide layer is in compression throughout its volume. For a sufficiently small reduced/oxide layer thickness ratio, the neutral axis is in the oxide layer with the oxide material close to the interface being in compression and further away in tension.

EXPERIMENTAL PROCEDURE

Batches with various PLZT compositions were prepared using the mixed oxide method. The powders were calcined at 925 °C for two hours in closed alumina crucibles. The samples were either sintered at 1250 °C for 6 hours in oxygen or hot pressed at 1200 °C for 6 hours at 14 MPa. For the reduction process, a lapped sample was placed on a graphite block and introduced into a preheated furnace held at 975 °C for approximately one hour, and then removed from the hot furnace. Silver electrodes were used throughout the testing [6].

Field-induced displacement was determined using LVDT-based apparatus. Displacements were determined for the forward-biased case and for the complete loop cycling. For the forward-biased case a Rainbow was poled at room temperature with approximately 900 volts applied until the displacement stabilized, and then the displacement was measured in the poling direction quasi-statically from zero volts to the poling voltage. The procedures for determinations of the thermal expansion coefficients and elastic constants will be published elsewhere [8].

MODELING

Finite-element modeling of complicated piezoelectric structures has been used successfully [9]. For this study the ABAQUS commercial FEM package (Hibitt, Karlsson & Sorenson, Inc., version 5.2) was used to simulate thermo-mechanical and electromechanical properties for the Rainbow devices. The model uses linear piezoelectric, dielectric, and elastic properties of the oxide and reduced layers.

The constituent equations for the piezoelectric media used in the modeling are:

$$S_i = s_{ij}^E T_j + d_{ij}^E E_j \quad (1)$$

$$D_i = d_{ij} T_j + \epsilon_{ij}^E E_j \quad (2)$$

where S_i is the strain, D_i is the polarization, T_j is the stress,

E_j is the electric field, s_{ij}^E is the elastic compliance, ϵ_{ij}^T is the dielectric permittivity, and d_{ij} is the piezoelectric compliance.

Modeling of Rainbow devices includes three major parts: 1) the definition of material properties and sample geometry, 2) the modeling of the cool down from the reducing temperature to room temperature, and 3) the determination of the response to the specified set of boundary conditions.

For the modeling of the cool down step nonlinear analyses were used to account for the considerable stiffening of the Rainbow structure during this step. The model permits linear analyses of the piezoelectric properties. Currently, nonlinear piezoelectric effects and electrostrictive properties cannot be modeled. For the calculation of the field-induced displacements a structure based on 60 elements gave satisfactory results for the modeling of the quasi-static field-induced displacements.

RESULTS AND DISCUSSION

In the case of piezoelectric ceramics there are three piezoelectric, two dielectric, and five elastic coefficients which are permitted by symmetry to be nonzero. The complete set of these values are known for only a few ceramics. Fortunately, for PZT 5 all of the above properties have been characterized [10]. PZT 5 is a soft PZT, and it should have values similar to those of PLZT ceramics with low lanthanum content. Piezoelectric, dielectric, and elastic constants of PZT 5 were used in the model. In addition, Young's modulus, Poisson's ratio, densities, and thermal expansion coefficients for the reduced layer formed from PLZT 5.5/57/43 (La/Zr/Ti) ceramics have been experimentally determined [8]. The data used in the modeling work are shown in Table 1. A rate of formation of the reduced layer of 127 $\mu\text{m}/\text{hour}$ was used in the model.

To verify the model, a comparison was made between the predicted displacement from the FEM model and the analytical model of the cantilevered bimorph [3]. For one bimorph, the FEM predicted a field-induced displacement of 61 microns compared to the 50 microns predicted by the analytical model. The FEM correctly predicted the field-induced displacement to be proportional to the length of the cantilever squared, again in good agreement with the analytical model.

There was reasonable agreement between the experimentally determined spontaneous displacements measured at the center of a Rainbow after cool down and the modeling predictions as is shown in Table 2. Rainbow devices were found to be partially poled during the cool down which lowers their spontaneous displacement (Rainbow devices become flatter when poled).

Table 1. (a) PZT 5 data used for the oxide layer modeling, and (b) experimental data for the reduced layer prepared from PLZT 5.5/57/43.

Material	Property	Magnitude
(a) PZT 5	c_{11}^E	$12.1 \cdot 10^{10} \text{ N/m}^2$
	c_{12}^E	$7.54 \cdot 10^{10} \text{ N/m}^2$
	c_{13}^E	$7.52 \cdot 10^{10} \text{ N/m}^2$
	c_{33}^E	$11.1 \cdot 10^{10} \text{ N/m}^2$
	c_{44}^E	$2.11 \cdot 10^{10} \text{ N/m}^2$
	d_{33}	$374 \cdot 10^{-12} \text{ C/N}$
	d_{31}	$-171 \cdot 10^{-12} \text{ C/N}$
	d_{15}	$584 \cdot 10^{-12} \text{ C/N}$
	$\epsilon_{11}^T / \epsilon^0$	1730
	$\epsilon_{33}^T / \epsilon^0$	1700
(b) Reduced Layer	Density	8.00 gm/cm^3
	Young's modulus	$6.86 \cdot 10^{10} \text{ N/m}^2$
	Poisson's ratio	0.381
	Thermal Expansion	$\sim 10 \cdot 10^{-6} \text{ }^\circ\text{C}^{-1}$

The experimentally obtained displacements are significantly higher than those predicted by the model (Table 2). There are appreciable variations from sample to sample in the ratio of total displacement to the forward biased displacement. The larger experimental displacement compared to the model may be accounted for by considering additional nonlinear contributions from the non-180° domain walls and phase boundaries [11] and higher linear piezoelectric coefficients.

The model was used to compare the effects of the reduced/oxide layer thickness ratio on a Rainbow's field-induced and cool down displacements. The magnitude of the displacement on cool down is determined by the difference in the effective thermal expansion coefficients between the oxide and reduced layers, the geometry of a sample, and the elastic constants. Figure 1 shows that the maximum predicted spontaneous displacement should occur for the reduced/oxide layer thickness ratio of approximately one. This result is in qualitative agreement with Timoshenko's model of the bi-metal thermostat [12], which also predicts maximum displacement near the layer thickness ratio of one for the two layers having properties of the oxide and reduced layers. As is also shown in Figure 1, the maximum field-induced and cool down displacements occur at the same Rainbow geometry. This result is applicable if the magnitude of the electric field is kept constant in the oxide layer as the geometry changes, which was done in the case described in Figure 1. For the case of constant voltage across the oxide

Table 2. Experimental results and FEM predictions of electromechanical properties.

Oxide Layer Composition	Reduction Temperature/Time ($^\circ\text{C}$ / minutes)	Total Rainbow Thickness (μm)	Full Cycle Voltage (Volts)	Experimental Full Cycle Displacement (μm)	Experimental Forward Bias Displacement (μm)	Calculated Forward Bias Displacement (μm)	Experimental Cool Down Displacement (μm)	Calculated Cool Down Displacement (μm)
1.0 / 53 / 47	975 / 105	762	± 1026	301	116	40	547	789
6.0 / 59.5 / 40.5	975 / 90	635	± 912	177	78	42	759	844
6.0 / 59.5 / 40.5	975 / 105	864	± 912	150	35	27	742	705
6.0 / 57 / 43	975 / 60	508	± 1026	357	129	51	1067	828
6.0 / 56 / 44	975 / 75	508	± 912	307	140	53	668	884

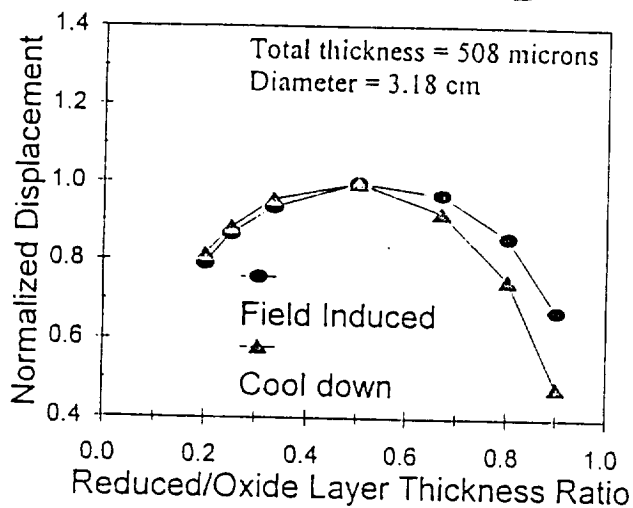


Figure 1. Normalized displacements induced by cool down and application of voltage.

layer the displacement continues to increase with the reduction of the oxide layer thickness. This is consistent with the electrical energy stored in the oxide layer being inversely proportional to its thickness, permitting greater field-induced lateral strain which increases the degree of bending of a Rainbow.

The shapes of the Rainbow samples having different diameters before and after the electric field application are shown in Figure 2. The flatter samples have no applied voltage; the more curved Rainbows bend up as a result of voltage applied in the opposite direction to the poling direction (the magnitude of movement is exaggerated). For the thicker Rainbows, there is less flattening in the middle portions. The model predicts this shape as a result of the nonlinear cool down step. Because FEM predicts that the

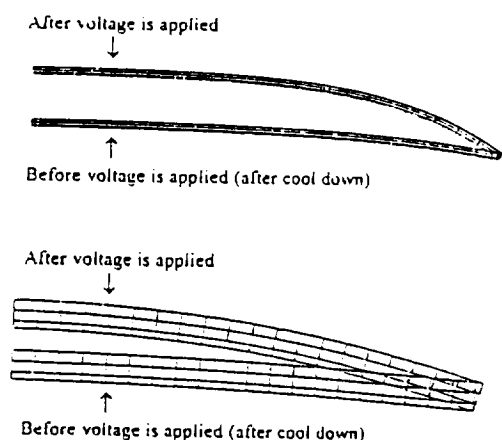


Figure 2. Shapes of Rainbows with diameter 6.35 cm (top) and 1.59 cm (bottom) before and after voltage is applied. Reduced/oxide layer thickness ratio: 1:3, thickness: 508 μ m, applied voltage: 500 V for both samples.

curvature of a Rainbow is nonuniform, it is not compatible with the predictions of linear models, mentioned above, which ignore nonlinear effects. In particular, the model predicted smaller displacement than the diameter squared dependence of the field-induced displacement.

Rainbow samples are capable of significant load-bearing capability. As is shown in Figure 3, there is excellent reproducibility in field-induced strain for a sample with up to 500 grams point load applied to the center of the sample.

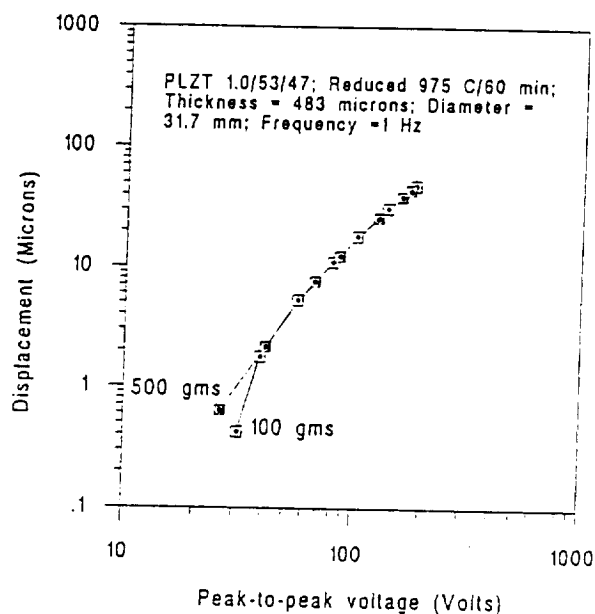


Figure 3. Field-induced displacements as a function of voltage for different loading conditions.

Rainbow samples have pronounced low frequency relaxation of the field-induced strain. It usually is manifested strongly for only one polarity. The response is relatively fast for the other polarity. An example of the low frequency contribution to the Rainbow displacement is shown in Figure 4. This sample was poled at 800 volts, and the field-induced displacements were measured at ± 53 volts. It can be observed that the field-induced displacement fits a straight line on semilog paper, indicating that the displacement becomes especially large at low frequencies.

The intriguing possibility to consider is whether the strong frequency-dependence of displacements and displacements exceeding the FEM's predictions are enhanced in Rainbow devices compared to conventional benders. Because Rainbows have large internal stresses it is reasonable to expect greater density of ferroelastic domain walls compared to ferroelectric devices without the macro-scale internal stresses, which could lead to enhanced displacements. Another possible contributing factor to the large displacements observed in Rainbow devices is unique to its structure.

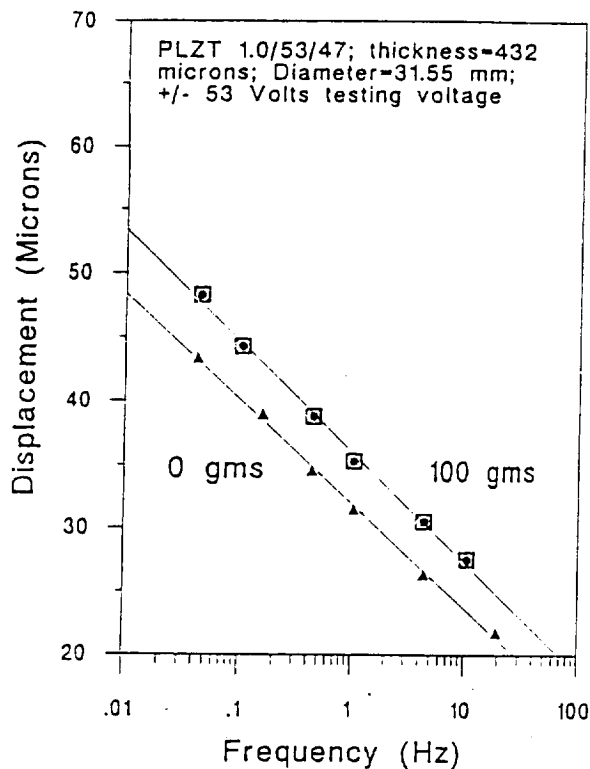


Figure 4. Field-induced displacements as a function of frequency for different loading conditions.

Because of the gradual change in the stress level in the oxide layer, different domain orientations are favored in different parts of the sample. Free charges may be trapped to compensate for polarization discontinuity at high temperature where conductivity is relatively high. As the sample is cooled down rapidly to room temperature it remains partially poled, and there may be net trapped charge in the bulk of the sample. Slow migration of charges during the domain switching may account for low frequency enhanced displacements. Finally, since a greater volume fraction of the oxide layer is in compression, higher switchable polarization should be available compared to the unstressed bender, as was shown for thin films in compression [13].

CONCLUSIONS

Electromechanical properties of Rainbow devices were studied at low frequencies and the results were compared to the FEM. The distinguishing characteristic of Rainbow devices is large and nonuniform stress on a macroscopic scale. Possible reasons for larger than expected displacements and frequency-dependent properties were discussed, and are believed to be related to a unique Rainbow structure.

ACKNOWLEDGMENT

This work is supported by NASA under grant No. NAG-1-1301 and by ONR under grant No. N0014-94-1-0563.

REFERENCES

- [1] J. van Randeraat and R. E. Settingington (Ed.), *Piezoelectric Ceramics*. N. V. Philips' Gloeilampenfabrieken, Eindhoven, The Netherlands, 1974.
- [2] A. G. Kuzin, N. Mirgorodskii, V. Pikarnikov and V. Soroka, "Piezoelectric Light Beam Deflectors. I. Theory of Bimorph Deflectors and Experimental Tests," *Sov. Phys. Tech. Phys.*, vol. 21, pp. 1128-1130, 1976.
- [3] M. R. Steel, F. Harrison and P. G. Harper, "The Piezoelectric Bimorph: An Experimental and Theoretical Study of its Quasistatic Response," *J. Phys. D.: Appl. Phys.*, vol. 11, pp. 979-989, 1978.
- [4] J. K. Lee and M. M. Marcus, "The Deflection-Bandwidth Product of Poly(vinylidene Fluoride) Benders and Related Structures," *Ferroelectrics*, vol. 32, pp. 93-101, 1981.
- [5] G. H. Haertling, "Rainbow Ceramics - A New Type of Ultra-High-Displacement Actuator," *Am. Cer. Soc. Bull.*, vol. 73, pp. 93-96, 1994.
- [6] G. H. Haertling, "Chemically Reduced PLZT Ceramics for Ultra-High Displacement Actuators," *Ferroelectrics*, vol. 154, pp. 101-106, 1994.
- [7] G. H. Haertling, "Reduction/Oxidation Effects in PLZT Ceramics," pp. 699-711 in *Proceedings of the 4th International SAMPE Electronics Conference*, pp. 699-711, 1990.
- [8] E. Furman, G. Li and G. H. Haertling, "An Investigation of the Resonance Properties of Rainbow Devices," accepted for publication in *Ferroelectrics*.
- [9] R. Leach, "Simulation of Piezoelectric Devices by Two- and Three-Dimensional Finite Elements," *IEEE Trans. Ultrasonics, Ferroel., and Frequency Control*, vol. 37, pp. 233-247, 1990.
- [10] D. A. Berlincourt, D. R. Curran and H. Jaffe, "Piezoelectric and Piezomagnetic Materials and Their Function in Transducers," in *Physical Acoustics*, vol. 1 Part A, New York: Academic Press, 1964, Ch. 3.
- [11] S. Li, W. Cao, R. E. Newnham and L. E. Cross, "Electromechanical Nonlinearity of Ferroelectric Ceramics and Related non-180° Domain Wall Motions," *Ferroelectrics*, vol. 139, pp. 25-49, 1993.
- [12] S. Timoshenko, "Analyses of Bi-Metal Thermostats," *J.O.S.A. & R.S.I.*, vol. 11, pp. 233-251, Sept. 1925.
- [13] B. Tuttle, et. al., "Chemically Prepared Pb(Zr,Ti)O₃ Thin Films: the Effects of Orientation and Stress," in *Proc. of IEEE 8th Int. Symp. on Appl. of Ferroelectrics*, 1992, pp. 344-348.

AN INVESTIGATION OF THE RESONANCE PROPERTIES OF RAINBOW DEVICES

E. FURMAN, G. LI and G. H. HAERTLING

*Gilbert C. Robinson Department of Ceramic Engineering, Clemson University,
Clemson, South Carolina 29634-0907 USA*

(Received December 1, 1993; in final form December 1, 1993)

In the last fifteen years considerable progress has been made in developing novel materials and devices for electromechanical actuator applications based on a variety of ferroelectric materials. Recently a novel type of high displacement actuator was developed. It is a monolithic, domed, stress-biased wafer consisting of oxide and reduced layers. These actuators are envisioned to be used in a variety of applications for which the knowledge of the resonance modes is essential. In this paper measurements of the resonant modes are compared to the predictions of the finite-element model. A number of low frequency modes were observed and identified as the bending modes. A higher frequency radial mode was determined to be less dependent on the sample dimensions than the bending modes. Effects of the boundary conditions on the resonant modes were modeled and investigated experimentally. For the modeling aspect of the study it was necessary to measure elastic constants, thermal expansion coefficients, and bulk densities of the oxide and reduced portions of the actuator. Experiments to measure these properties were performed and are described.

Keywords: unimorph, bender, actuator, piezoelectric, Rainbow, resonance, bending modes, radial mode, finite element analyses

I. INTRODUCTION

In the last fifteen years there has been considerable progress in developing novel materials and devices for electromechanical actuator applications based on a variety of ferroelectric materials.¹ Much of the work was directed toward developing materials with enhanced electric field-induced strain. Currently linear strain actuators are based on piezoelectric, electrostrictive and antiferroelectric materials. For actuation, these devices rely on either piezoelectric d_{33} , d_{31} , electrostrictive Q_{11} , Q_{12} , or an antiferroelectric-ferroelectric phase transition volume change. Unfortunately, the maximum realizable strain in these devices is less than one percent.² For a multilayer actuator with a one centimeter thickness, the maximum obtainable total displacement is less than 10 microns.

There are a number of applications including pumps, speakers, laser deflectors, optical scanners and relays for which displacements well above 10 microns are desirable. For these applications piezoelectric benders have traditionally been used.³⁻⁶ Benders are based on a bimorph or unimorph structures. Bimorphs contain two active layers bonded together, and unimorphs have an active and a passive layer. In both cases, bending occurs as a result of field-induced lateral strain. To accommodate this strain, the sample bends, producing vertical displacement. Key parameters for these devices are piezoelectric d_{31} or electrostrictive Q_{12} coefficients. A further advantage of benders is their lower mechanical impedance, which allows more effective energy coupling into gases and liquids. One consequence of the

higher compliance of benders is a reduction of the resonant frequencies compared to stiffer linear actuators.⁶

Benders are used in three types of applications: quasi-static, non-resonant dynamic, and resonant.³ For the non-resonant dynamic and resonant applications, knowledge of resonant modes of a bender device is of crucial importance.

Recently a new type of bender called a RAINBOW (Reduced And Internally Biased Oxide Wafer) was developed which has promising characteristics.⁷ Rainbow devices with 1 mm displacement and a 10 kg load-bearing capability were built.

The purpose of this paper is to describe the resonant properties of Rainbow devices. The basic structure and the principle of operation of Rainbow devices is described in section II. In section III the experimental procedures for preparation and characterization of Rainbow devices are given. Section IV describes the finite-element modeling procedure. In section V experimental results are compared with the finite-element model. Likely mechanisms for the various vibration modes are identified.

II. RAINBOW ACTUATORS

A unimorph consists of a piezoelectric or electrostrictive active layer bonded to a metal foil. Electric field induced lateral dimensional change in an active layer is opposed by a flexible metal plate. Rainbow actuators, similar to conventional unimorphs, consist of an electromechanically active layer and inactive layer. Unlike the unimorph, the Rainbow is a monolithic structure. The inert layer is formed by exposing one side of a lead-containing ceramic to a reducing atmosphere at high temperature produced by placing a ceramic in contact with a carbon block. The reduction of lead lanthanum zirconate titanate (PLZT) ceramics occurs as a result of oxidation of the solid carbon block, first to carbon monoxide and then the carbon dioxide gases.⁸ The reduced layer is a good electrical conductor, and it acts both as the electrode and inert part of the bender.

Rainbows also differ from unimorph benders by the presence of large internal stresses developed in the process of reduction and cooling down to room temperature. Various steps involved in internal stress and shape development of a Rainbow are shown in Figure 1. Because of the volume reduction occurring during the reduction step and larger thermal expansion of the reduced layer compared to the oxide layer, stress-free equilibrium dimensions of the reduced layer are smaller than for the oxide layer. External stresses shown in Figure 1(b) must be present in order to prevent the composite from bending. The removal of external forces results in a net bending moment, which accounts for the Rainbow shape.

III. EXPERIMENTAL PROCEDURE

PLZT ceramics were prepared using a conventional mixed-oxide process. Following calcination at 925°C for 2 hours in a closed alumina crucible, the milled and dried powders were cold pressed as preform slugs and then hot pressed at 1200°C for 6 hours at 14 MPa. Hot pressed PLZT samples were placed on a graphite block, and

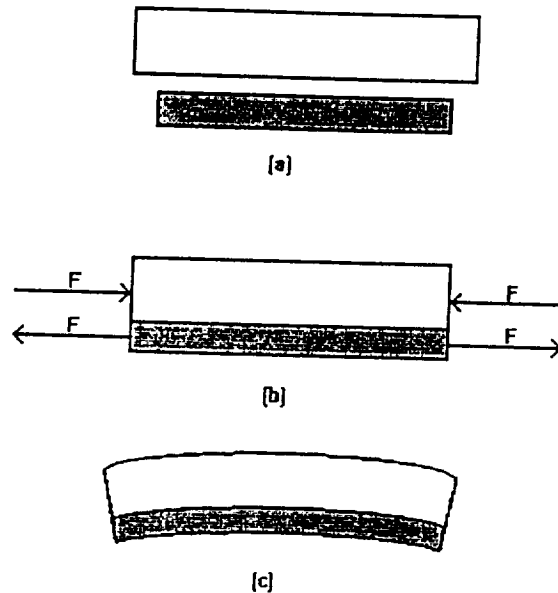


FIGURE 1 Formation of a Rainbow device, showing the oxide layer (light) and the reduced layer (dark): (a) at zero stress level; (b) with compressive force applied to the oxide layer and tensile force to the reduced layer to match the layers at the boundary; (c) after the removal of external forces.

the assembly entered into the furnace preheated to 975°C. Exposure of the samples to the reducing atmosphere ranged from 45 minutes for a typical Rainbow sample to many hours for the completely reduced samples used in the measurements of the coefficient of thermal expansion, and elastic constants of the reduced layer. For electrical studies, samples were electroded with silver epoxy paint (5504N, E. I. du Pont de Nemours & Co.) at 200°C for thirty minutes. Further details of Rainbow preparation can be found in reference 7.

The majority of the characterization work described in this paper was performed on PLZT ceramics with the nominal composition 5.5/57/43 (La/Zr/Ti). This composition was chosen because of the large lateral strain observed in PLZT samples with this composition, and its proximity to the morphotropic phase boundary insured high electromechanical coefficients.⁹

Densities of the oxide and reduced samples were measured using a water immersion method. Ultrasonic pulse-echo measurements were performed on the oxide and completely reduced samples. Panametrics model 5052PR Ultrasonic Pulser/Receiver was used with 10 MHz longitudinal and 5 MHz shear transducers acoustically coupled to samples polished with five micron powder. The samples had less than two percent variation in thickness and a diameter-to-thickness ratio sufficiently large to avoid diffraction effects.

A HP 54504A digital storage oscilloscope was interfaced with the pulser, and both excitation and echo responses were recorded. Measurements of shear velocity (v_s) and longitudinal velocity (v_l), combined with the measurements of densities, permitted calculation of Young's modulus (Y) and Poisson's ratio.

An Orton dilatometer model 1600D with an environmental chamber was used to perform thermal expansion measurements from room temperature up to 1000°C.

Completely reduced samples were measured in flowing nitrogen, and unreduced PLZT samples in air.

Resonant modes of the Rainbow devices were characterized with an HP 4194 impedance analyzer. Samples were supported at the center of the top and bottom surfaces with point contacts for the majority of the experiments.

In the model, both resonant and antiresonant modes were characterized. The resonant modes were obtained by specifying the short circuit electrical boundary conditions. The open circuit electrical boundary conditions were used for the determination of antiresonant modes.

IV. MODELING

The finite-element modeling, FEM, of complicated piezoelectric structures had successfully been used in the past.¹⁰ For this study the ABAQUS commercial FEM package (Hibitt, Karlsson & Sorenson, Inc., version 5.2) was used to simulate thermomechanical and electromechanical properties of the Rainbow devices. The model uses linear piezoelectric, dielectric, and elastic properties of the oxide and reduced layers.

The constituent equations for the piezoelectric media used in the modeling are:

$$S_i = s_{ij}^E T_j + d_{ij}^t E_j \quad (1)$$

$$D_i = d_{ij} T_j + \epsilon_{ij}^T E_j \quad (2)$$

where S_i is the strain, D_i is the polarization, T_j is the stress, E_j is the electric field, s_{ij}^E is the elastic compliance, ϵ_{ij}^T is the dielectric permittivity, and d_{ij} is the piezoelectric compliance.

Rainbow modeling includes three major parts; (1) definition of material properties and sample geometry, (2) modeling of the cool down from the reducing temperature to room temperature and (3) determination of response to the specified set of the boundary conditions.

In the case of piezoelectric ceramics there are 3 piezoelectric, 2 dielectric and 5 elastic nonzero coefficients, and their values are known only for a few ceramics. Fortunately, for PZT 5 all of the above properties have been characterized.¹¹ PZT 5 is a soft PZT, and it should have values similar to those of PLZT ceramics used in this study. Piezoelectric, dielectric, and elastic constants of PZT 5 were used in the model. Actual values used are listed in the Appendix. In addition, Young's modulus, Poisson's ratio, densities, and thermal expansion coefficients for the oxide and reduced layers were determined in this study and were used in the modeling.

The parameters and sample geometry were entered into two separate models. The simpler model is a two dimensional axisymmetrical model. A full three dimensional model was also developed for a more complete characterization of the resonant modes.

For the modeling of the cool down step nonlinear analyses were used because of the considerable stiffening of the Rainbow structure during this step.

For the calculation of the resonant and antiresonant modes using the axisymmetric model, a structure based on 60 elements gave satisfactory results (about 2% stiffer than the model with 120 elements). A relatively small number of elements

was sufficient because of the primary interest in the frequency range below 100 KHz.

V. RESULTS AND DISCUSSION

Measurements of densities and elastic constants for the oxide and reduced layers based on PLZT 5.5/57/43 nominal composition are summarized in Table I. A slightly larger density and Poisson's ratio for the reduced layer compared to the oxide layer is due to a large quantity of lead metal present in the reduced layer as determined by X-ray diffraction.⁸ The specific gravity of lead is 11.35 and it has a large Poisson's ratio of 0.43.¹² The pulse-echo measurements used gave elastic constants at a constant displacement. A large measured value of Poisson's ratio for the oxide layer is consistent with the literature values for the PZT materials for the constant displacement condition.¹³

Lead metal with its high coefficient of thermal expansion of $16 \times 10^{-6} \text{ }^{\circ}\text{C}^{-1}$ contributes to a higher value of thermal expansion of the reduced layer compared to the oxide layer.¹² It was not possible to determine the precise values of coefficient of thermal expansion up to 975°C for the oxide and reduced layers due to creep observed in both materials at high temperature. Creep in the oxide layer occurred for temperatures above 750°C , and for the reduced layer above 850°C . Creep of the oxide layer is more pronounced compared to the reduced layer, and amounted to 1.2 percent change of the measured sample length for a room temperature to 1000°C thermal cycling. CTE values in Table I represent actual values used in the modeling, and resulted in a fairly good agreement between the predicted and measured curvatures of a Rainbow on cool down. The amount of the volume change during the reduction of PLZT at 975°C was not estimated directly, but was considered as a contributor to the effective thermal expansion constant of the reduced layers. In the temperature range where creep is not significant, the following measured CTE values were obtained: for the oxide sample $6.7 \times 10^{-6} \text{ }^{\circ}\text{C}^{-1}$ in the range of 27 to 700°C , and for the reduced sample $8.2 \times 10^{-6} \text{ }^{\circ}\text{C}^{-1}$ in the range of 80 to 850°C . A significant creep in the oxide layer at higher temperatures is the reason for the lower oxide CTE used for the whole temperature range. Similarly, volume reduction during the reduction at 975°C is the justification for the higher value of its CTE used.

A comparison between the experimental determination of the resonant frequencies for the different boundary conditions and axisymmetric FEM is made in Table II. Experiments were performed on the Rainbow with the oxide composition of 5.5/57/43. Two boundary conditions were used: (1) a sample supported at top

TABLE I
Experimental data obtained for the PLZT 5.5/57/43 oxide and reduced layers

Property	Oxide layer	Reduced layer
Density (gm/cm^3)	7.93	8.00
Young's modulus (N/m^2)	7.79×10^{10}	6.86×10^{10}
Poisson's ratio	0.377	0.381
Thermal Expansion ($^{\circ}\text{C}^{-1}$)	$\sim 5 \times 10^{-6}$	$\sim 10 \times 10^{-6}$

TABLE II
Effect of the boundary conditions on antiresonant frequencies of PLZT 5.5/57/43
Rainbow determined experimentally and from the axisymmetric modeling

Boundary Condition	Experimental Frequency (Hz)	Modeling Frequency (Hz)
No Sideways Constraint	1534	1611
	1642	
	6547	
	7100	7218
	7368	
	7608	
	16816	
	18116	18544
	32290	35347
	not observed	57086
	76740	74854
Sideways Constraint	3844	2353
	4189	
	5900	
	10900	9767
	12533	
	14370	
	27000	23224
	not observed	42117
	not observed	66277
	76969	74008

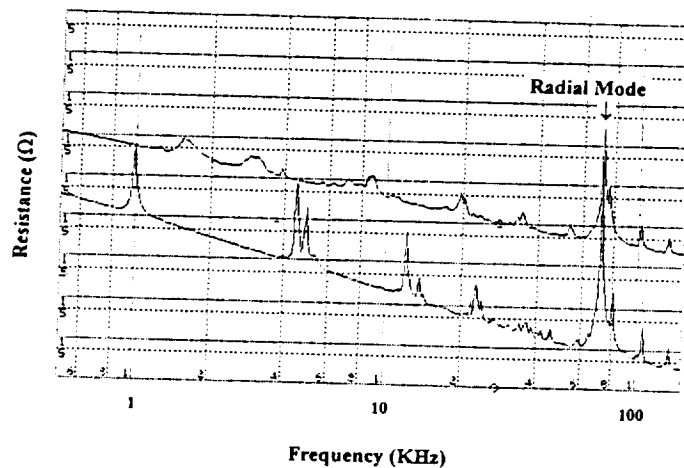


FIGURE 2 Resonance spectra for PLZT 1/53/47 Rainbow for two boundary conditions: (a) plane/point support; (b) point/point support. The two spectra are separated vertically for clarity.

and bottom surfaces with point contacts and (2) a sample resting on a rigid plate with point contact at the top center. Good agreement between the model and experiment was observed for the point contact arrangement. The model predicted frequencies that are typically slightly higher than the experiment. Increasing the number of elements used in the modeling reduced the stiffness of a Rainbow and

TABLE III

Resonant modes of PLZT 5.5/56/44 Rainbow determined experimentally and predicted by the axisymmetric and three dimensional models.

Experimental Frequency (Hz)	Axisymmetric Model (Hz)	Three Dimensional Model (Hz)
1501	1566	1525
		1537
		3612
6200		6394
		6915
7100	7102	7179
		9929
		11344
		14366
15000		14883
		16687
		19027
	18265	19379
		19746
		23056

(Dimensions: 3.20 cm diameter; thickness 0.053 cm; reduced layer thickness 0.015 cm)

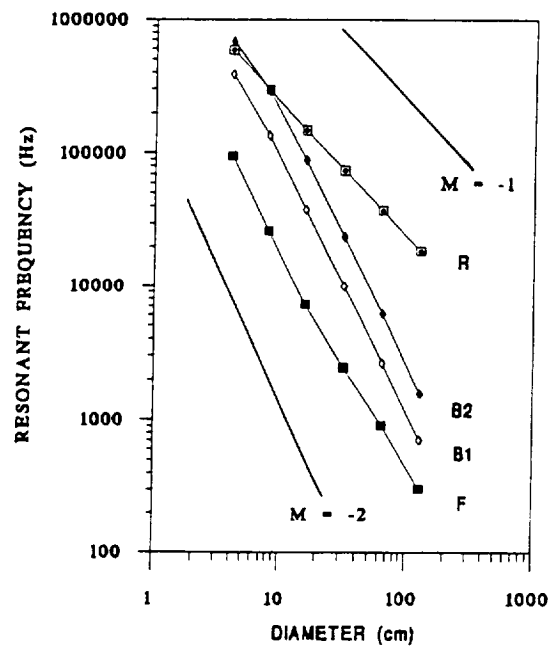


FIGURE 3 Axisymmetric modeling of the effect of the Rainbow sample diameter on the resonant frequency. Modeling parameters: number of elements: 60, reduced layer thickness: 0.015 cm, total thickness: 0.053 cm. M: ideal slopes for comparison. F: fundamental mode, B1, B2: pure bending modes, R: radial mode.

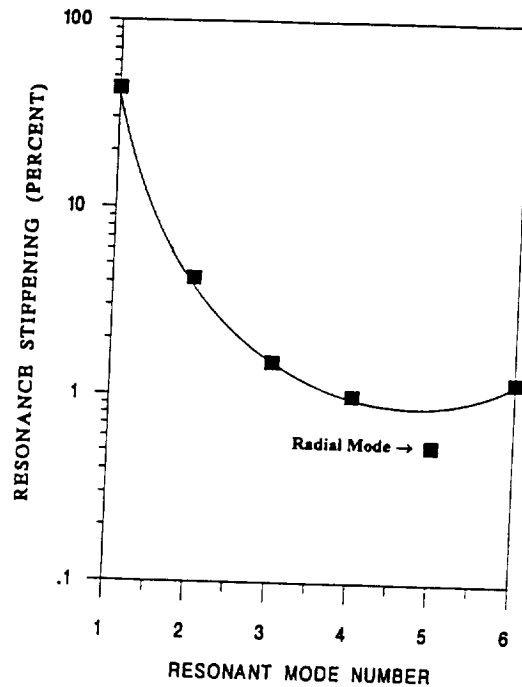


FIGURE 4 Axisymmetric modeling of the resonance stiffening during the cool down step. Stiffening is the change in frequency on cool down divided by the frequency prior to cool down, expressed in percent.

resulted in further improvement in its ability to predict actual resonant spectrum. A number of observed modes are not predicted by the axisymmetric model because they do not contain infinite fold rotational axes of symmetry. For the plane-to-point boundary condition, observed modes occur at significantly higher frequencies than those predicted by the model. The model does not account for the frictional forces present as a result of a lateral displacement of a Rainbow.

The experimentally obtained resonance spectra for PLZT 1/53/47 Rainbow for two different boundary conditions are shown in Figure 2. In addition to stiffening of the modes for plane/point support, broadening and damping of the modes occurred. As compared to the radial mode occurring at 72 KHz, the low frequency modes are weaker; in fact, some of the modes predicted by the model were not observed experimentally. The radial mode is also less sensitive to the boundary conditions as compared to low frequency modes.

The principle advantage of the three dimensional FEM model is that the full spectrum of possible resonant modes becomes available for the analyses. This is achieved at the price of significantly higher computational time. For a few samples on which three dimensional modeling was performed, good agreement with the axisymmetric model was obtained. An example of this is shown in Table III, in which the experimental data is also included.

The shape of the mode has to be consistent with the boundary conditions provided. For the case where sideways motion of the Rainbow is restricted to a planar motion, the resonant mode shapes and the order in which they occur follow the predicted modes for a circular membrane.¹⁴

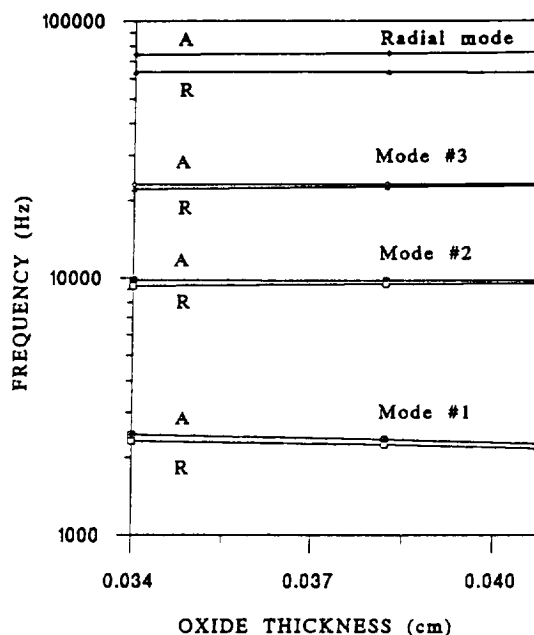


FIGURE 5 Axisymmetric modeling of the resonance and antiresonance mode frequencies as a function of the oxide layer thickness. Modeling parameters: number of elements: 60, total thickness: 0.051 cm, diameter: 3.175 cm. R: resonance mode, A: antiresonance mode.

For the oxide PLZT circular disc, the lowest frequency mode is the resonant or planar mode. In the case of a Rainbow device, the radial mode is no longer the lowest mode of resonance. There are two types of modes which may occur in a Rainbow at lower frequencies: the thin sphere breathing mode which has no harmonics, and a flexure or bending mode existing in a composite structure.^{11,15} Resonance modes for the Rainbow samples with different diameters were modeled to determine the mode of vibration. The radial and the sphere breathing mode frequencies are proportional to the inverse of the diameter, for the bending mode the resonant frequency is proportional to the inverse of the diameter squared. The results of the axisymmetric modeling are shown in Figure 3. Over a wide range of frequencies, the radial mode follows a slope of -1 . Except for the smallest diameter case, the second and third lowest modes follow closely a slope of -2 indicating a pure bending mode. For the lowest mode, Rainbows with small diameters have a bending mode resonance as deduced from the slope, but for larger diameters the slope does not fit either the thin sphere breathing mode or bending mode.

It already has been shown (Figure 2) that the low frequency modes are more sensitive to the boundary conditions as compared to the radial mode. It can be observed from Figure 4 that the low frequency modes are also more sensitive to the cool down step. The resonance modes for the Rainbow cooled down from 975°C were compared to a similar sample which was not cooled down. All of the modes for the cooled down sample were at a higher frequency implying that the stiffening of the structure occurs during the cool down step. However, the relative change of the resonant frequency, plotted on the vertical axes, is again the highest

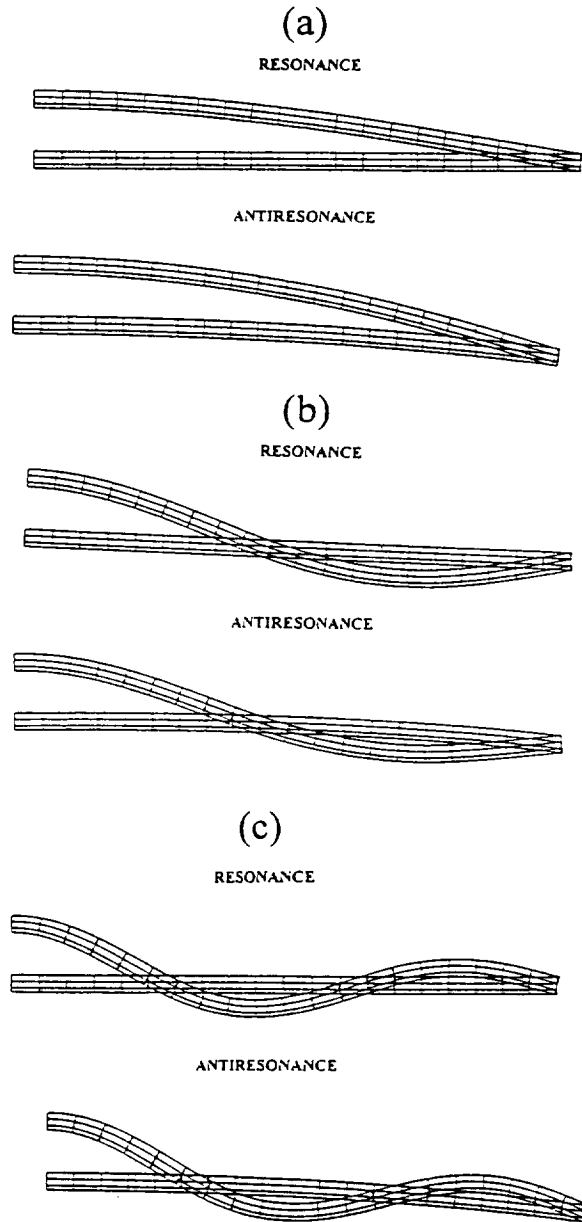


FIGURE 6 Axisymmetric modeling of the shapes of the resonant and antiresonant modes for the five lowest frequencies. (a) first mode; (b) second mode; (c) third mode; (d) fourth mode; (e) fifth mode. Modeling parameters: number of elements: 60, reduced layer thickness: 0.013 cm, total thickness: 0.051 cm, diameter: 3.175 cm.

for the low lying modes. The fifth mode is a radial mode and the least sensitive to the effect of the cool down.

In addition, the effect of the oxide to reduced thickness ratio for Rainbows with constant total thickness was modeled. The strength of the resonance is proportional

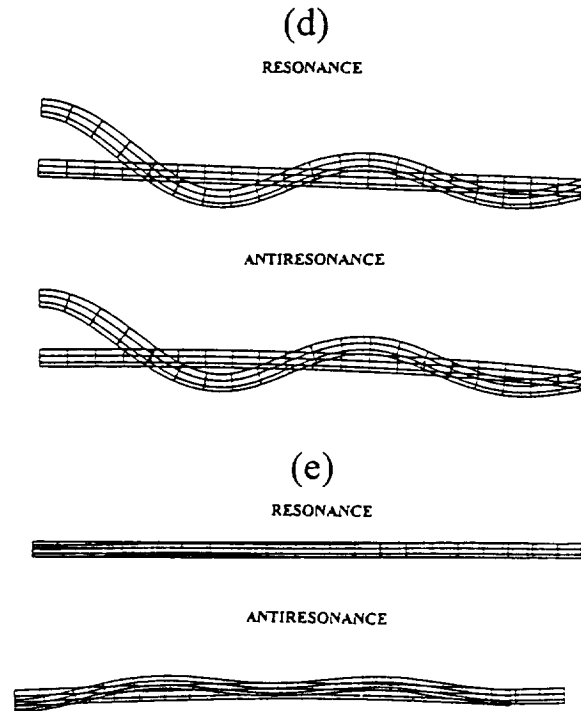


FIGURE 6 (Continued)

to the frequency separation between resonant and antiresonant modes divided by the resonant frequency. Figure 5 illustrates that the strengths of modes 1 through 3 are inversely proportional to the oxide layer thickness. The radial mode is the strongest mode observed since it has the largest separation between resonant and antiresonant modes.

Shapes of the modes provide useful information for possible applications, and also provide information about possible coupling between the modes. The five lowest frequency modes for the typical Rainbow device are shown in the Figure 6. For each mode, the structure which is more flat represents the Rainbow after cool down. From the previous discussion, the first mode may not be a simple bending mode. Its shape is characterized by the entire surface moving in phase. The second, third, and fourth modes each have one additional nodal circle represented by a nodal point in the cross sections shown. Inner and outer surfaces of a Rainbow are now moving out of phase. Stavsky and Loewy¹⁵ have indicated that for a composite circular plate there is a coupling between the radial and bending modes. They have considered a purely elastic system. Apparently their conclusion is also applicable for the case of a piezoelectric composite system. As can be seen from the fifth mode in addition to lateral motion associated with the radial mode, there is also bending present. Bending is more pronounced for the antiresonant mode. The radial mode is usually stronger than the bending modes, as determined by a separation in frequency between the resonant and antiresonant conditions.

For this sample geometry, the resonant and antiresonant frequencies for the sixth mode (a bending mode) occur between the resonant and antiresonant modes of the much stronger radial mode.

The knowledge of the location and shape of the resonant modes can be beneficial in the design of Rainbow-based devices. For speaker applications it is advantageous to work well below second mode. Because of its shape, different parts of the Rainbow are being displaced out of phase near this resonance, which would diminish speaker efficiency. For pumps, it may be useful to operate at the first resonant mode, where the volume displacement should be large. Figure 3 can be used as a guideline for the determination of the appropriate geometry to operate at resonance.

VI. CONCLUSIONS

Experimental characterization and finite-element modeling of the resonant modes of Rainbow devices were presented. A good agreement between the experimentally determined resonances and finite element modeling was obtained. The identity of various modes was deduced from the frequency dependence of the resonant mode on its diameter. A large number of low frequency bending modes exist in the Rainbow devices. The coupling between the bending and radial modes was established.

The effects of the boundary conditions on the resonance behavior of Rainbow devices were investigated. The more constraining boundary conditions resulted in higher resonant frequencies. The bending modes were more affected by the boundary conditions as compared to the radial mode.

The thermal expansion coefficients, elastic constants, and densities were measured for the oxide and completely reduced samples. Higher values of the thermal expansion coefficient, Poisson's ratio, and density observed in the reduced layer are all consistent with a large amount of metallic lead present in the reduced samples.

APPENDIX

Material Parameters for PZT 5¹¹

c_{11}^E	$12.1 \cdot 10^{10} \text{ N/m}^2$
c_{12}^E	$7.54 \cdot 10^{10} \text{ N/m}^2$
c_{13}^E	$7.52 \cdot 10^{10} \text{ N/m}^2$
c_{33}^E	$11.1 \cdot 10^{10} \text{ N/m}^2$
c_{44}^E	$2.11 \cdot 10^{10} \text{ N/m}^2$
d_{33}	$374 \cdot 10^{-12} \text{ C/N}$
d_{33}	$-171 \cdot 10^{-12} \text{ C/N}$
d_{15}	$584 \cdot 10^{-12} \text{ C/N}$
$\epsilon_{11}^T/\epsilon^0$	1730
$\epsilon_{33}^T/\epsilon^0$	1700

ACKNOWLEDGEMENTS

The authors would like to express their appreciation to Dr. Feiling Wang and Professor Erik Skaar for valuable discussions. This work is supported by NASA-Langley Research Center (Contract No. NAG-1-1301).

REFERENCES

1. K. Uchino, *Ceramic Bulletin*, **65**, 647 (1986).
2. L. E. Cross, *J. of Intell. Mater. Syst. and Struct.*, **2**, 241 (1991).
3. J. van Randerdaat and R. E. Settingington (Ed.), "Piezoelectric Ceramics" (N. V. Philips' Gloeilampenfabrieken, Eindhoven, The Netherlands, 1974).
4. A. G. Kuzin, *et al.*, *Sov. Phys. Tech. Phys.*, **21**, 1128 (1976).
5. M. R. Steel, F. Harrison and P. G. Harper, *J. Phys. D.: Appl. Phys.*, **11**, 979 (1978).
6. J. K. Lee and M. M. Marcus, *Ferroelectrics*, **32**, 93 (1981).
7. G. H. Haertling, *Am. Cer. Soc. Bull.*, **73**, 93 (1994).
8. G. H. Haertling, pp. 699-711 in Proceedings of the 4th International SAMPE Electronics Conference, Ed. R. E. Alfred, R. J. Martinez and K. B. Wischmann, (Society for the Advancement of Materials and Process Engineering, Covina, GA, 1990).
9. B. Jaffe, W. R. Cook, Jr. and H. Jaffe, "Piezoelectric Ceramics" (Academic Press, London, 1971).
10. R. Learch, *IEEE Trans. Ultrasonics, Ferroel., and Frequency Control*, **37**, 233 (1990).
11. D. A. Berlincourt, D. R. Curran and H. Jaffe, Ch. 3 in "Physical Acoustics," vol. 1 Part A, Ed. W. P. Mason (Academic Press, New York, 1964).
12. "CRC Handbook of Tables for Applied Engineering Sciences, Second Edition, Ed. R. Boltz and G. Tuve (CRC Press, 1973).
13. "Landolt-Bornstein Numerical Data and Functional Relationships in Science and Technology," Ed. K.-H. Hellwege and A. M. Hellwege (Springer-Verlag, Berlin, 1981) vol. 16, p. 123.
14. P. M. Morse and K. U. Ingard, "Theoretical Acoustics" (McGraw-Hill, New York, 1968).
15. Y. Stavsky and R. Loewy, *J. Acoust. Soc. Am.*, **49**, 1542 (1971).

RAINBOWS AND FERROFILMS - SMART MATERIALS FOR HYBRID MICROELECTRONICS

Gene H. Haertling

Gilbert C. Robinson Department of Ceramic Engineering
Clemson University, Clemson, SC 29634-0907

ABSTRACT

This review paper describes the materials, processing, properties and applications of the newly developed ultra-high displacement Rainbows and thick/thin ferroelectric Ferrofilms. Their applicability to hybrid and fully integrated microelectronics is discussed in regard to each of these areas of concern.

INTRODUCTION

Current trends have shown that industrial and commercial hybrid microelectronic components designed for the automobile, home, office and factory are becoming an increasingly more important segment of present-day automation. The materials for such applications are required to be more sophisticated in that they must be able to perform more than one function (e.g., actuation and sensing) during operation or provide a unique combination of highly specialized properties. These materials are now commonly known as smart or intelligent materials and are exemplified by such general groups as ferroelectrics, piezoelectrics, pyroelectrics, electrooptics, electrostrictive materials and composites.

Key factors in the application of these materials to hybrid circuits and microelectronics are (1) their ability to be scaled down in size (i.e., miniaturized or fully integrated) without loss of bulk properties, (2) their capability of achieving the proper form factor for the substrate and (3) their processing compatibility with other components on the substrate. Recent research and development work has shown that significant progress has been made in the last several years in each of these areas.¹⁻⁵ A new processing technique has recently led to the development of ultra-high displacement

ceramic actuators which have been coined as RAINBOWS (Reduced And Internally Biased Oxide Wafers), an acronym for the chemical reduction process used to transform ordinary planar piezoelectric and electrostrictive wafers into domed, high displacement, two-dimensional bending actuators of moderate load-bearing capability.^{6,7} Rainbow devices such as speakers, pumps, switches, deflectors and linear actuators have been made in sizes as large as 10 cm. in diameter and as small as 2 mm. in diameter or length.

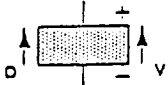
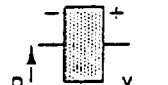
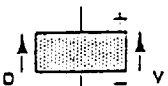
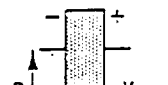
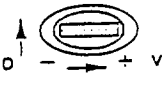
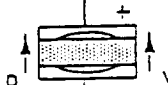
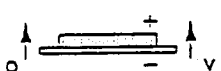
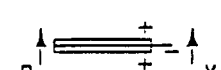

An assessment of the present-day ceramic actuator technologies for bulk materials is given in Table 1. As seen from the table, a variety of direct extensional configurations, composite flextensional structures and bending mode devices are used to achieve an electromechanical output. Trade-offs between stress generating/loading capability and displacement are commonly made when designing for particular applications. Maximum displacement can be seen to be achieved with composite or bender structures; however, this is usually accomplished at the expense of less load bearing capability, greater complexity and higher cost. The recent introduction of the Rainbow bender to this family of actuators has served to either extend the stress capability of the bender technologies without sacrificing displacement or extending the displacements achievable with equal load-bearing capacity. Additionally, because of their unique dome or saddle-type structure, small discrete Rainbow elements for hybrid circuits can be fabricated from larger, bulk processed wafers.

For the fabrication and integration of actuator/sensors and other devices at the microelectronic (micron) level, one must consider different technologies than those previously mentioned. Among these techniques are vacuum deposition, spinning, dipping, chemical vapor deposition and laser ablation; however, those which have been reported to successfully produce both thin (0.02 - 5 μm in this paper) and thick (5 - 30 μm in this paper) films of the above mentioned materials are considerably fewer in number, and the most promising of these, in the near term, is dipping. Using an automated dipping apparatus, Li, et.al.,⁸ were successful in fabricating thin and thick films of PLZT ferroelectric and electrooptic compositions on Ag, Si, sapphire and glass substrates. Films as thick as 15 microns have yielded properties quite similar to those of the bulk material and show excellent promise for future devices.

It is the object of this review paper to describe the materials, processing and properties of two types of recently developed smart materials; i.e., Rainbows for discrete and hybrid structures and thick/thin ferroelectric films (Ferrofilms)

for hybrid and integrated structures. Examples of typical applications are discussed.

Table 1. Present-Day Ceramic Actuator Technologies

Type	Configuration	Max. Stress* (MPa)	Actuator Movement (w/Voltage)	Actuator Type (P or E)	Actuator Displacement (%) ⁺
Monolithic (d_{33} mode)		40	Expansion	P	0.40
Monolithic (d_{31} mode)		40	Contraction	P	-0.15
Monolithic (s_{11} mode)		40	Expansion	E	0.24
Monolithic (s_{12} mode)		40	Contraction	E	-0.08
Composite Structure (d_{33} mode) (flexten.)		10	Contraction	P	-1.0
Composite Structure (d_{33}/d_{31}) (Moonie)		0.028	Expansion	P/E	1.3
Unimorph (bender)		0.002	Expansion/ Contraction	P/E	10
Bimorph (bender)		0.002	Expansion/ Contraction	P/E	20
Rainbow Monomorph (bender)		0.020	Expansion/ Contraction	P/E	35-500

Notes: V = Voltage; D = Actuator Displacement; P = Piezoelectric; E = Electrostrictor
^{*} = Max. generated stress; ⁺ = Displacement at ± 10 kV/cm based on thickness

MATERIALS

Although a number of different compositions have been successfully prepared as Rainbows and Ferrofilms, those most compatible to the specific processes used and most amenable to achieving the desired properties are in the PLZT solid solution family. Typical high displacement ferroelectric compositions are 1/53/47 (La/Zr/Ti) and 5.5/56/44 for low and high dielectric constant applications, respectively; whereas, the usual compositions for the electrooptic, electrostrictive-type applications are 9/65/35 or 8.6/65/35.⁹ These specific compositions are pointed out in the PLZT phase diagram given in Figure 1. As may be noted, the ferroelectric materials are morphotropic phase boundary compositions and the non-memory, electrostrictive materials are compositionally located along the ferroelectric-to-paraelectric phase boundary.

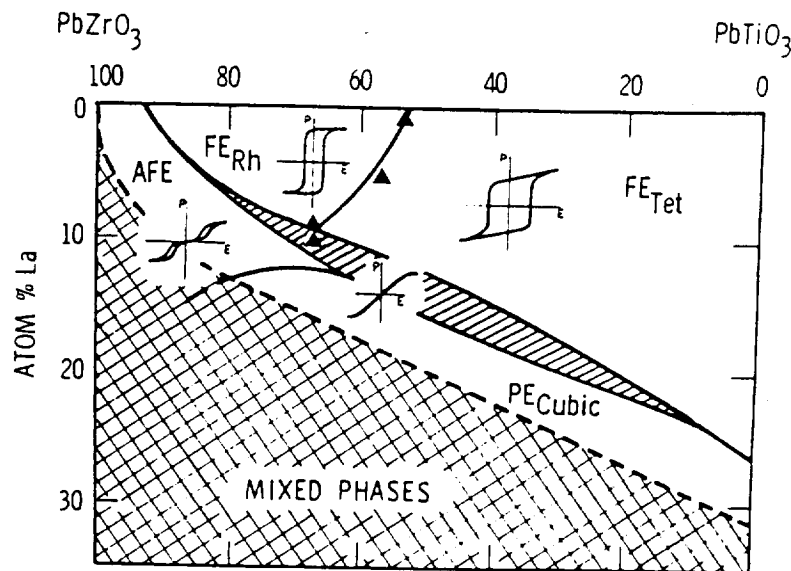


Figure 1. Room Temperature Phase Diagram of the PLZT System
Compositions are indicated by triangular markers

PROCESSES

In this section, the specific processes which have been reported for both the Rainbows and the Ferrofilms are described. Since Rainbows are produced via a bulk-type process and the Ferrofilms are fabricated with a thick/thin film technique, they are distinctly different, by nature, and thus, are discussed in

separate sections.

Rainbow Process

The Rainbow technology fundamentally consists of a new processing method that is applied to standard, high lead-containing ferroelectric, piezoelectric and electrostrictive ceramic wafers which are transformed by the process into a monolithic, composite structure consisting of a stressed dielectric and a chemically reduced, electrically conductive layer which acts as the stressing element as one of the electrodes for the final device. Since all of the materials are ferroelectric or electrically-enforced ferroelectric materials, they are multifunctional and smart, by nature, and are thus capable of performing both actuator and sensor functions, simultaneously.

The high temperature chemical reduction process involves the local reduction of one surface of a planar ceramic plate, thereby achieving an anisotropic, stress-biased, dome or saddle-shaped wafer with significant internal tensile and compressive stresses which act to increase the overall strength of the material and provide its unusually high displacement characteristics. According to previously reported work, the chemical reduction process proceeds via simple reactions consisting of the oxidation of the solid carbon (graphite) block to carbon monoxide and further oxidation of the carbon monoxide gas to carbon dioxide with the associated loss of oxygen from the PLZT oxide in contact or in near contact with the graphite block.

Rainbow ceramics are produced from conventionally sintered or hot pressed ceramic wafers by means of a few simple steps requiring approximately two hours of additional time as shown in the process flowsheet of Figure 2. A Rainbow is produced from an as-received wafer by placing it on a flat graphite block, placing a protective zirconia plate of the same size on top of the wafer and introducing the assembly into a furnace held at temperature in a normal air atmosphere. The part is treated at a temperature of 975°C for one hour, removed from the furnace while hot and cooled naturally to room temperature in about 45 minutes. A reduced layer approximately 150 μm thick is produced in the wafer under these treatment conditions. When cool, the dome shaped wafer is lifted from the graphite block, brushed lightly on the reduced (concave) side to remove any metallic lead particles and to expose the reduced layer, and then electroded for test and evaluation. A variety of electrodes can be used such as epoxy silver, fired-on silver and vacuum deposited metals. After depositing appropriate electrodes, the Rainbow is completed and ready for operation.

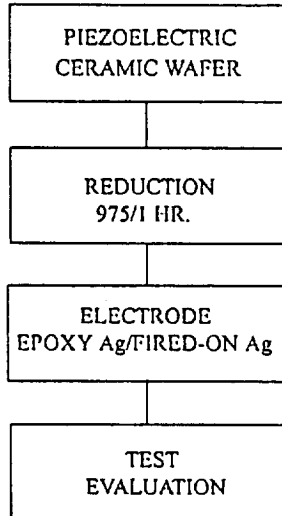


Figure 2. Process Flowsheet for PLZT Rainbow Ceramics

In regard to operation, a Rainbow is similar to a device known in the industry as a unimorph bender. A unimorph is composed of a single piezoelectric element externally bonded to a flexible metal foil which is stimulated into action by the piezoelectric element when activated with a ac or dc voltage and results in an axial buckling or displacement as it opposes the movement of the piezoelectric element. However, unlike the unimorph, the Rainbow is a monolithic structure with internal compressive stress bias on the piezoelectric element; thus producing the dome structure, rendering it more rugged and able to sustain heavier loads than normal. The integral electrode (usually the bottom electrode) consists of metallic lead intimately dispersed throughout the semiconductive oxide layer. The change in shape of the wafer after reduction is believed to be due to the reduction in volume of the bottom reduced layer (largely metallic lead) compared to the unreduced material, as well as the differential thermal contraction between the reduced and unreduced layers on cooling to room temperature.

Like other piezoelectric devices, Rainbows may be operated with a dc, pulse dc, or ac voltage; however, when driven with ac, the largest displacements are usually achieved at 100 Hz or less. In operation, the dome height of the Rainbow varies as a function of the magnitude and polarity of the voltage. When a given polarity of voltage is applied, the dome decreases in height depending on the magnitude of the voltage; and alternatively, when the polarity is reversed, the dome increases. The large axial motion of the dome

is largely due to contributions from a lateral contraction produced in the material via the d_{31} coefficient and a stress-directed domain switching process.

It should be noted that although Rainbows are processed in bulk wafer form, after heat treatment they may be diced or scribed into smaller elements for a pick-and-place operation onto a hybrid substrate. This technique is possible since each individually diced element possesses a smaller but similar dome structure with a radius of curvature identical to the larger wafer. Even though the displacements of the smaller individual elements are proportionately less than the parent wafer, they nevertheless, are large enough (5 - 50 microns) to be useful in some devices. Some typical examples of sizes and shapes of Rainbows are shown in Figure 3.

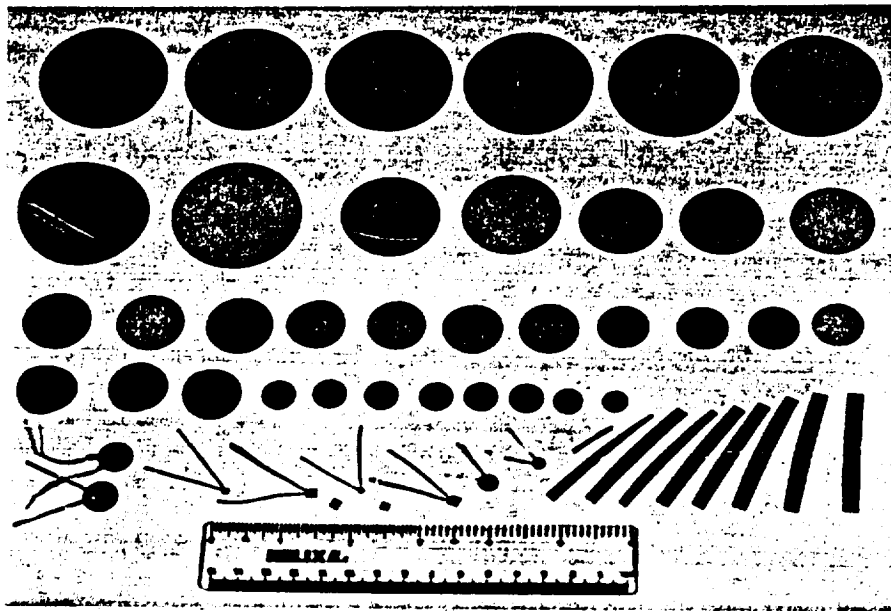


Figure 3. Typical Examples of Sizes and Shapes of Rainbows

Ferrofilm Process

Thick and thin films of ferroelectrics, piezoelectrics and electrostrictive materials are presently being fabricated from a water-soluble, acetate-precursor, liquid chemical system (Metal Organic Decomposition type) using an automated dipping process. An operational flowsheet for this process is given in Figure 4; however, the details of the process and the apparatus have

previously been reported as part of a overall effort involving the intelligent processing of ferroelectric films.¹⁰

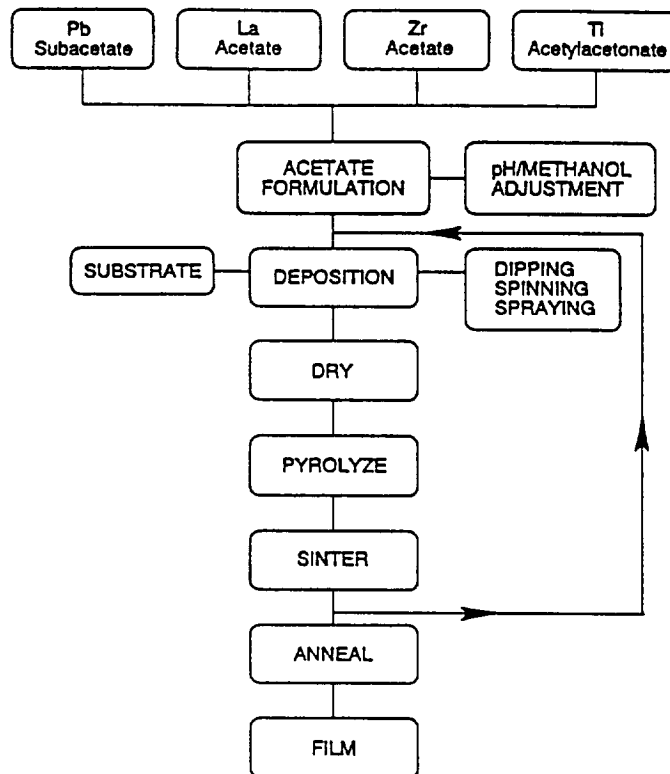


Figure 4. Process Flowsheet for PLZT Acetate MOD Process

Briefly, the process consists of formulating the stock solution from as-received precursors of Pb (lead subacetate), La (lanthanum acetate), Zr (zirconium acetate) and Ti (titanium acetylacetonate) by mixing them together in the requisite amounts along with the appropriate amount of methyl alcohol for viscosity control. This simple, five minute operation yields a clear, light yellow solution which is water soluble and stable for long periods of time. The solution is then deposited on the selected substrate via automatically controlled dipping and withdrawal operations. Drying occurs in a matter of a few seconds, and the coated substrate is subsequently sintered very quickly by introducing it directly into a furnace pre-heated to the sintering temperature. Multiple dipping, drying, sintering and cooling cycles are required in order to build up the necessary film thickness for the specific device. Depending on the dilution ratio of the solution, individually dipped layer thicknesses may vary from approximately 0.05 to 0.3 μm , yielding films

as thick as 12 μm for a 40 layer device. For a cycle time of three minutes, the total time required to dip a 40-layer device is about two hours.

The final sintered film deposited on a suitable substrate such as a 0.125 mm thick Ag foil is usually transparent and crack-free with a smooth, shiny surface. After applying suitable electrodes such as air dried Ag, epoxy Ag or vacuum deposited metals, the film is ready for operation; however, it should be remembered that poling may be required if it is a ferroelectric thick film. Some examples of electroded and unelectroded thick films on Ag substrates are shown in Figure 5.

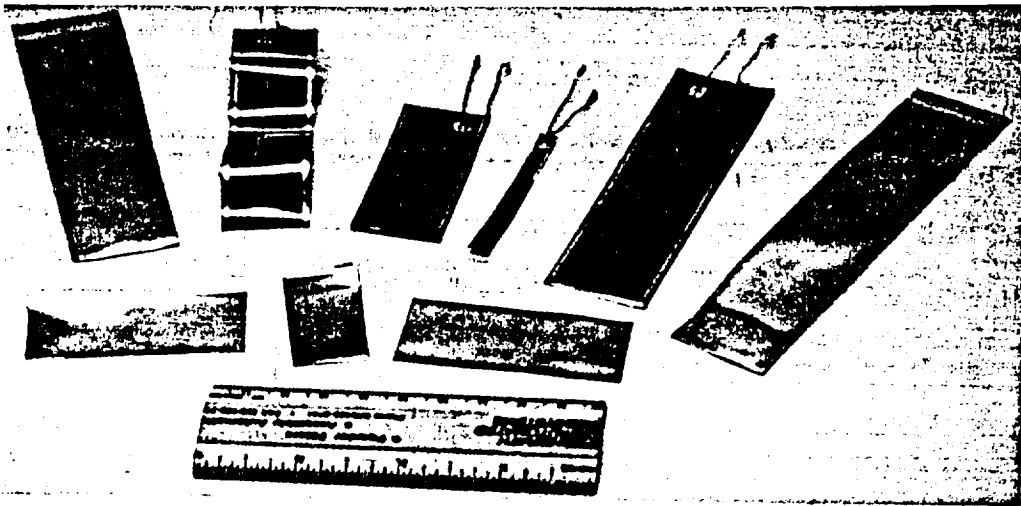


Figure 5. Typical Examples of Unelectroded and Electroded Ferrofilms

Although Ferrofilms lend themselves well to a number of different fabrication processes at the totally integrated level, for discrete components at the hybrid microelectronics level the dipping technique has been found to be reliable and predictable and can easily be implemented in a totally hands-off environment. In addition, industrial equipment is readily available to dip very large as well as small, discrete parts at minimal cost. The acetate process, being water insensitive, is especially suitable for the dipping process since the open solution is usually exposed to the atmosphere for long periods of time and during this period must withstand chemical interactions as well as minimal evaporation of solution.

PROPERTIES

In the last two years since the Rainbow ceramics were first developed at

Clemson University, there has been a considerable on-going effort to (1) understand the details of the reduction process in the PLZT materials, (2) measure their properties and characterize their unusually high displacement and load bearing capabilities as benders, (3) model their electromechanical behavior and frequency dependent properties and (4) construct working models illustrating various proof-of-principle applications. Some of this data for the Rainbow ceramics will be presented in this section, along with the limited amount of data available, to date, for the Ferrofilms. In most instances, a standard Rainbow size of 31.75 mm diameter and 0.5 mm thick was used to obtain the data. Additional technical data on the Rainbow ceramics has been reported in a document prepared by Sheritt, et.al., of the Royal Military College of Canada.¹¹

Rainbows Characteristics

Dielectric Properties - The temperature dependent dielectric behavior for two PLZT compositions; i.e., 1/53/47 and 8.6/65/35, are shown in Figures 6 and 7, respectively. It can be seen from Figure 6 that a gradual rise occurs in the relative dielectric constant (1 kHz) of 1/53/47 from a room temperature value of approximately 1100 to about 2700 at 200°C. No peak is observed in this range for this composition because its Curie point is 330°C. On the other hand, composition 8.6/65/35 in Figure 7 shows a change in K from 3200 to 5700 over this same temperature range with a peak occurring at 105°C, which is its usual Curie point as determined from small signal measurements. Since this composition is an electrostrictive, relaxor-type material, this Curie point does not coincide with its loss in polarization which occurs at about 20°C; thus, making it one of the most sensitive, high displacement, electrostrictive Rainbow materials. It may be noted that the dielectric constants and dissipation factors for both compositions are comparable to previously reported values, and this indicates that the Rainbow reduction process does not change the dielectric properties of the unreduced part of the structure.

Hysteresis Loops - Typical examples of dc hysteresis loops for compositions 1/53/47 and 9/65/35 are given in Figure 8. The loop in Figure 8(A) was taken on the ferroelectric Rainbow element (1/53/47) in its virgin condition before any other measurements were made. It should be noted that on the initial application of positive voltage to +450V there was approximately 60% of the total remanent polarization switched rather than the usual 50% one ordinarily observes in a virgin, randomly oriented ceramic. This behavior is highly unusual and indicates that the Rainbow ceramic was partially poled before testing. Additional audio and piezoelectric tests of other virgin parts also

indicated that the elements were partially poled to varying degrees; i.e., some very little and others as high as 75%.

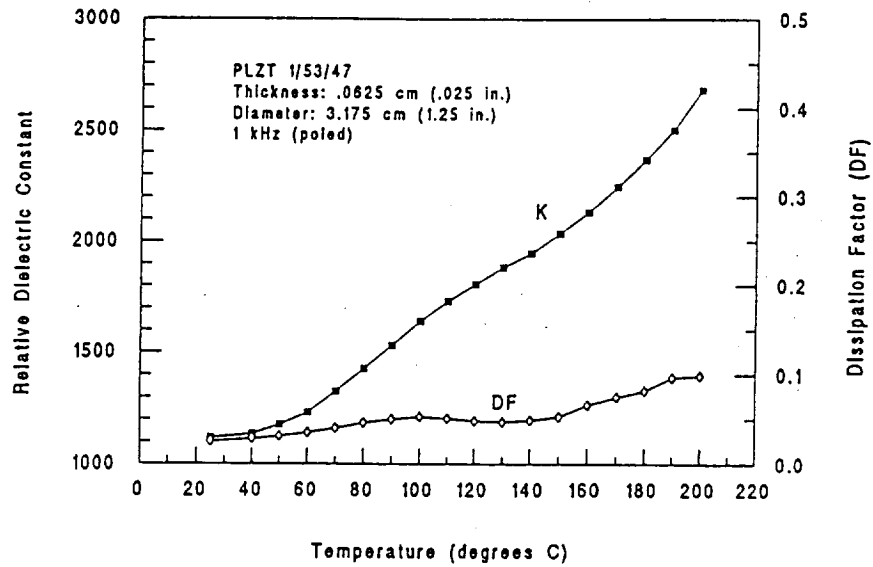


Figure 6. Temperature Dependent Dielectric Properties of PLZT Rainbow 1/53/47

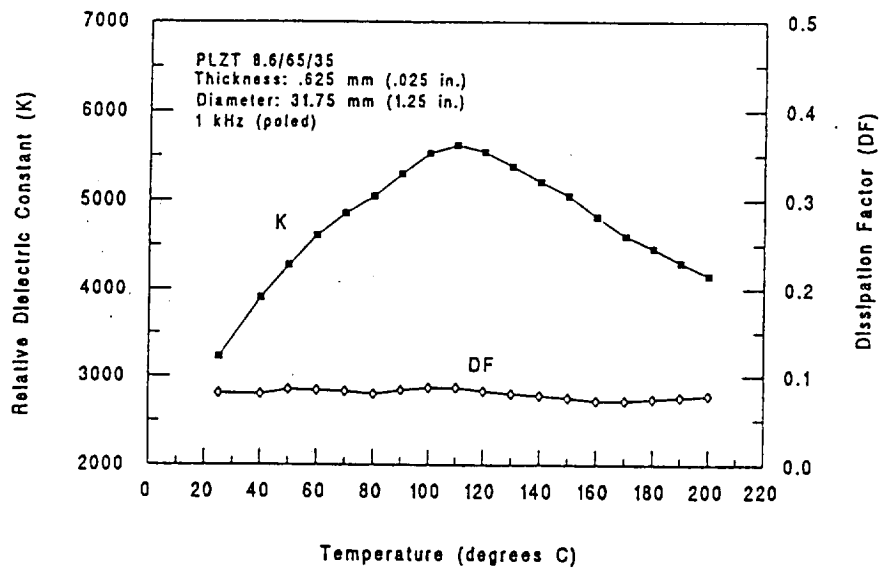


Figure 7. Temperature Dependent Dielectric Properties of PLZT Rainbow 8.6/65/35

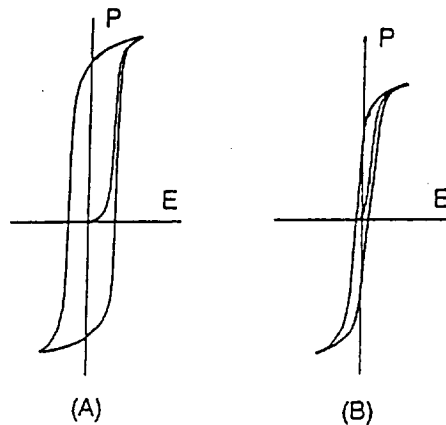


Figure 8. Virgin Hysteresis Loops for Rainbow PLZT Compositions (A) 1/53/47 and (B) 9/65/35

One explanation for this condition occurring in the electrically virgin state is that the mechanical compressive and tensile stresses produced in the Rainbow wafer during processing are acting together to switch some of the domains in this soft ferroelectric/ferroelastic material. Since uniform stress is a symmetrical quantity, it is recognized that it alone is insufficient to produce a net polarization in a given direction even though it may be of sufficient magnitude to switch domains; however, a stress gradient such as produced by the Rainbow bending process is a vector quantity and can, indeed, produce the observed effect. This non-uniform stress is believed to be responsible for the partial poling of the Rainbow wafers. Measured properties on the above wafer were: $P_R = 44.8 \text{ uC/cm}^2$, $E_C = 7.5 \text{ kV/cm}$, dielectric constant = 1210 and dissipation factor = 0.047.

The virgin loop of Figure 8(B) is a typical one for the electrostrictive (9/65/35) type of Rainbow materials and is very similar to that obtained on bulk electrooptic material. Measured properties on this wafer were: $P_{10\text{kV/cm}} = 28.3 \text{ uC/cm}^2$, dielectric constant = 3142 and dissipation factor = 0.085. As a matter of course, no unsymmetrical hysteresis loops were observed in the electrostrictive materials, and none was expected, since there are no stable domains in these materials at zero electric field. Conceivably, a high enough stress could precipitate stable domains in a very near-ferroelectric material, however, this was not experimentally confirmed.

Displacement Loops - Displacement vs. electric field (butterfly) loops for the Rainbow wafers described above are shown in Figure 9. As before, Figure

9(A) illustrates the Rainbow axial motion as the sample is electrically switched from zero to +450V, to -450V and back to zero, however, in this case this loop was not taken on the virgin wafer. It may be noted that this loop is remarkably similar to that observed when measuring the direct extensional (longitudinal, lateral) displacements via the piezoelectric d_{33} or d_{31} coefficients. The value of displacement in the + voltage direction was measured at 190.5 μm , and the total amount of displacement (+/-) was 432 μm .

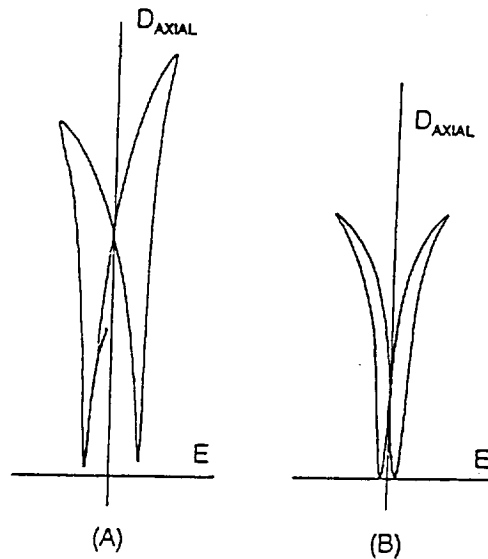


Figure 9. Axial Displacement Loops for Rainbow PLZT Compositions (A) 1/53/47 and (B) 9/65/35

Figure 9(B) shows the displacement loop of the electrostrictive Rainbow material (9/65/35) mentioned above. Since 9/65/35 is a relaxor material there should be little or no memory, and the same value and sign of displacement should be obtained whether a + or a - voltage is applied. One can see by switching this sample through a full voltage loop that a small amount of remanent displacement (strain) is present which is probably due to the close proximity of this composition to a FE phase. A further indication of this incipient FE phase is the higher than normal value of P_{10} ($P_{10} = 28.4$ vs. 18.0 uC/cm^2) as given above. Measured value of total displacement for this wafer was 178 μm .

Displacement Characteristics - The displacement characteristics as a function of applied voltage are given in Figure 10 for some selected compositions. One of the most striking features of this figure is the very high displacements

achieved by these Rainbow ceramics at moderate electric fields; e.g., 400 volts is equivalent to an electric field of 10 kV/cm. Composition 8.6/65/35 is noted to possess the highest displacement of 210 μm at a maximum voltage of 600 volts, however, its displacement is characteristically non-linear because of its electrostrictive nature. Compositions 1/53/47 and 5.5/56/44 are ferroelectric materials, and thus, are more linear in behavior. As a general rule, the displacements of the ferroelectric materials are lower than those of the electrostrictive compositions, particularly when operated at higher voltages and one polarity; however under bipolar operation, the displacement values of the ferroelectric materials will commonly be double the values shown in Figure 10.

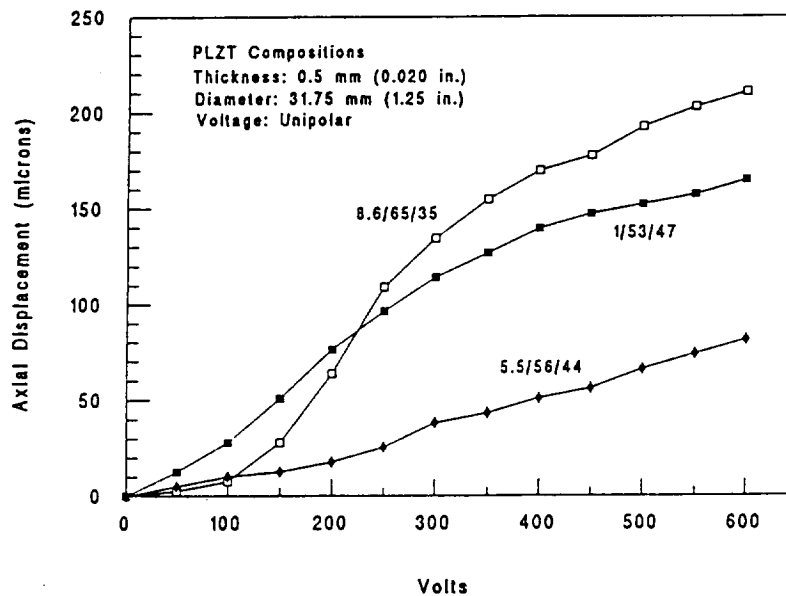


Figure 10. Axial Displacement Characteristics of Rainbow PLZT Compositions as a Function of Voltage

A measure of the difference in displacement between the planar (lateral extensional mode) direction and the orthogonal axial (Rainbow bender mode) direction is given in Figure 11 for PLZT 8.6/65/35, which also shows the temperature dependence of these two modes. This figure clearly demonstrates the very large displacement amplification of the bending phenomenon when one considers the data showing a change in displacement from approximately 0.07% to 22% at 25°C; i.e., an amplification of 315%. Although not shown on the figure, both displacements are negative (i.e., a contraction) when voltage is applied.

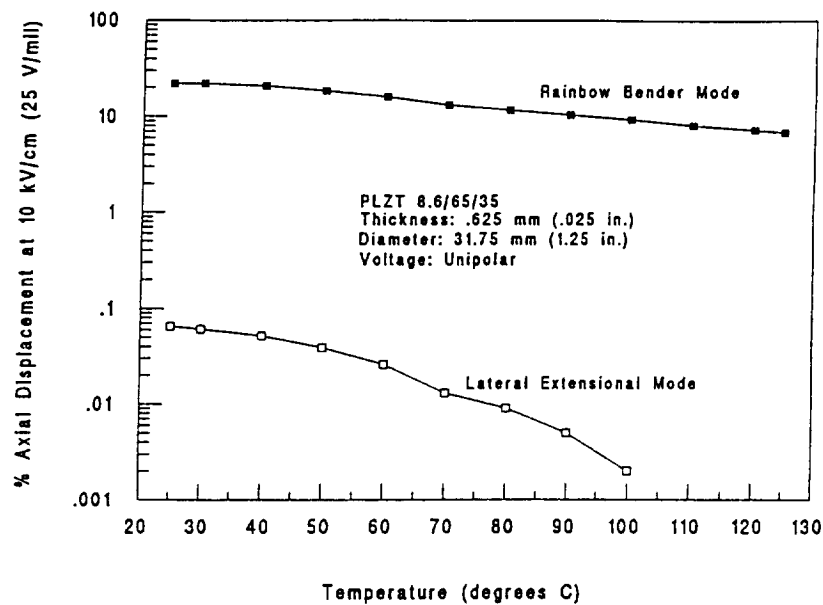


Figure 11. Temperature Dependence of Electrostrictive Lateral and Rainbow Bending Displacements in PLZT 8.6/65/35 Ceramics

Figure 12 illustrates the profile of the vertical bending displacement across the diameter of a Rainbow wafer during activation at 10 kV/cm. As might be anticipated, the highest displacement is in the center of the wafer, dropping off to zero at the circumference. This zero displacement at the edge of the wafer is beneficial because a Rainbow can be conveniently placed on a planar surface and operated as a linear actuator device or its circumference can be sealed off, and it can be operated as a cavity-mode pump.

The variation of a Rainbow's axial displacement as a function of wafer diameter is given in Figure 13. For a 0.5 mm thick wafer of composition 1/53/47, the values of displacement can be seen to vary from 170 μm for a diameter of 31.75 mm (1.25 inch) to approximately 3 μm at 6.5 mm diameter. Thus, a discrete 15 mm diameter Rainbow component on a hybrid substrate could be expected to have a displacement of about 40 μm when operated with a single polarity and about 80 μm when operated bipolar.

Wafer thickness has been found to have a significant effect upon axial displacement primarily because of the change in motional mode; i.e., from dome to saddle-type, as the wafer thickness is reduced to approximately one one-hundredth of the diameter. For example, a 31.75 mm (1.25 inch) diameter wafer usually develops a saddle-mode configuration when its

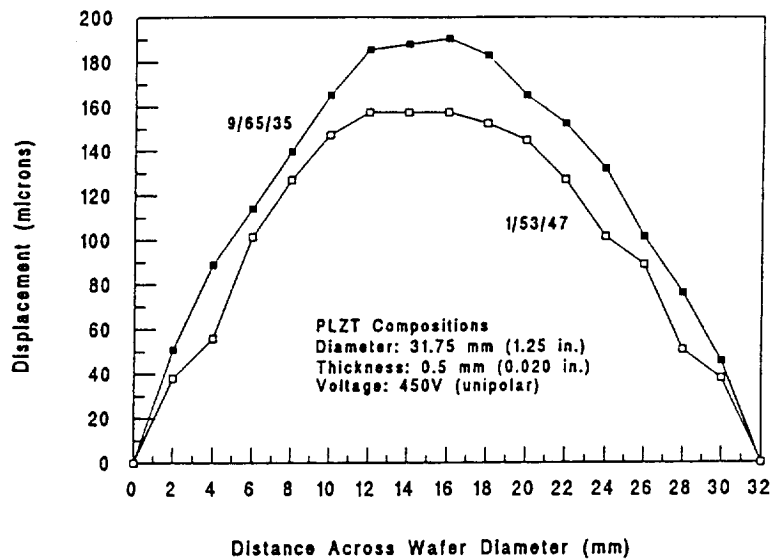


Figure 12. Profile of Displacements Measured Across Rainbow Wafer Diameter for PLZT 1/53/47 and 9/65/35

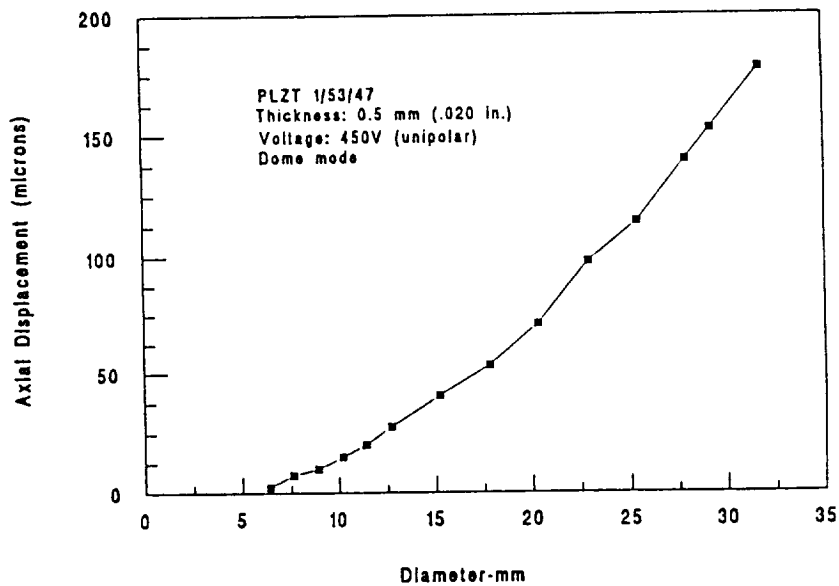


Figure 13. Variation of Axial Displacement as a Function of Rainbow Wafer Diameter for PLZT 1/53/47

thickness is less than 0.32 mm (0.013 inch). Saddle-mode operation provides maximum displacement with minimum load bearing capability; and therefore,

should only be considered for special applications. Figure 14 illustrates the unusually large range of displacements obtained for Rainbows as a function of thickness. Please note that the displacement axis is a log scale.

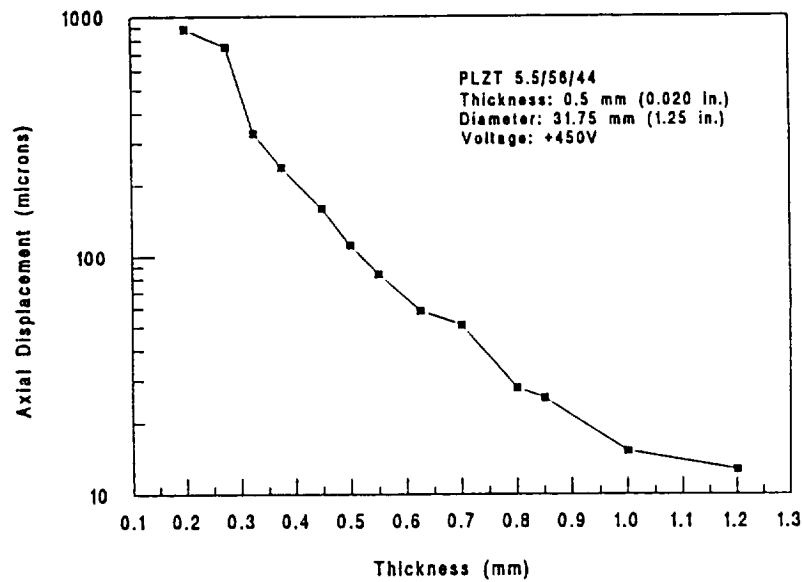


Figure 14. Effect of Thickness on Axial Displacement for PLZT 5.5/56/44

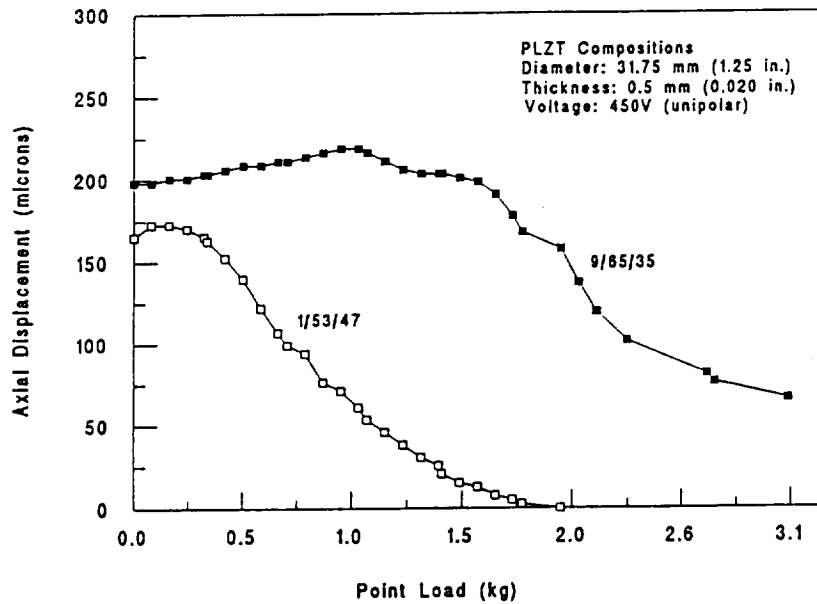


Figure 15. Point Load-Bearing Properties of Rainbow PLZT Compositions

The effect of an unconstrained point load on the displacement of an activated Rainbow is given in Figure 15 for compositions 1/53/47 and 9/65/35. PLZT 1/53/47 can be seen to be relatively ineffective when loaded with a dead weight of 1.5 kg (3.3 lbs), whereas, composition 9/65/35 is still effective at a load of over 3 kg. This result is not too surprising since the elastic modulus of 9/65/35 (10.9×10^4 MPa) is noticeably higher than that of 1/53/47 (5.7×10^4 MPa). Another point to note from the figure is the increase in displacement with the introduction of a finite amount of load on the device. This effect was previously reported by Furman, et. al.¹² The tradeoff between thickness and maximum sustainable point loading is given in Figure 16 for 1/53/47.

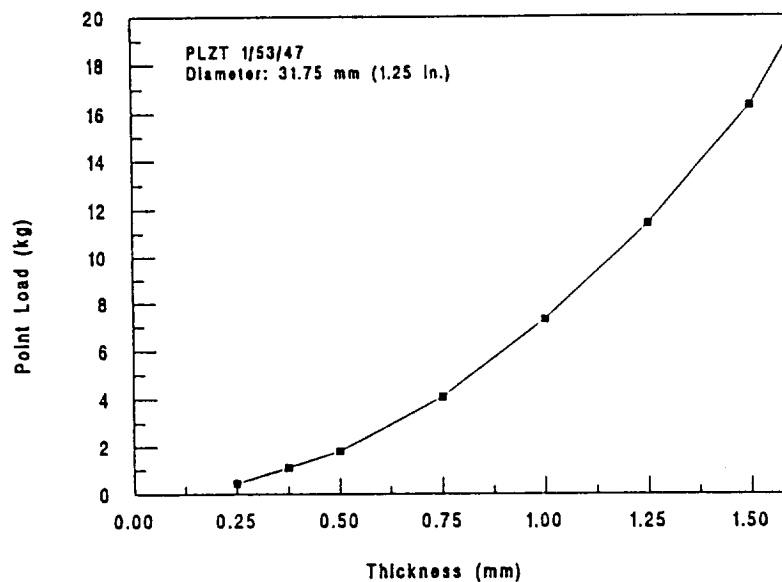


Figure 16. Maximum Sustainable Point Load for Rainbow PLZT 1/53/47 as a Function of Thickness

Another concern of actuator designers is the amount of force that can be generated by an actuator when voltage is applied. This is shown in Figure 17 for a 1/53/47 Rainbow of standard size. As can be seen, the force generated is a linear function of voltage until the onset of saturation for this particular configuration. A maximum force of 1.3 kgf was achieved at 450 volts.

Finally, displacement and sustainable overpressure data for PLZT 5.5/56/44 as a function of wafer thickness are presented in Figure 18. The left ordinate scale represents the maximum allowable pressure differential across the wafer thickness before the wafer contacts the planar surface and stops flexing

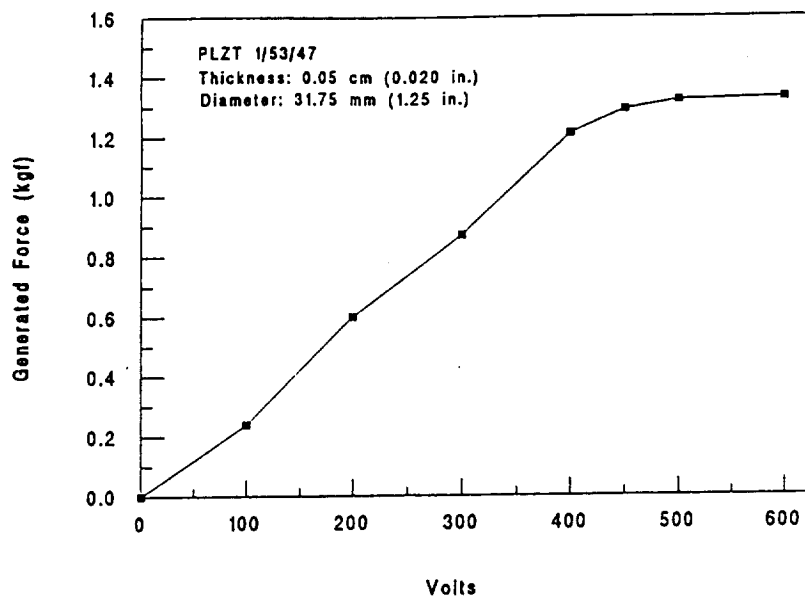


Figure 17. Effect of Applied Voltage on the Force Generated by a PLZT 1/53/47 Rainbow Wafer

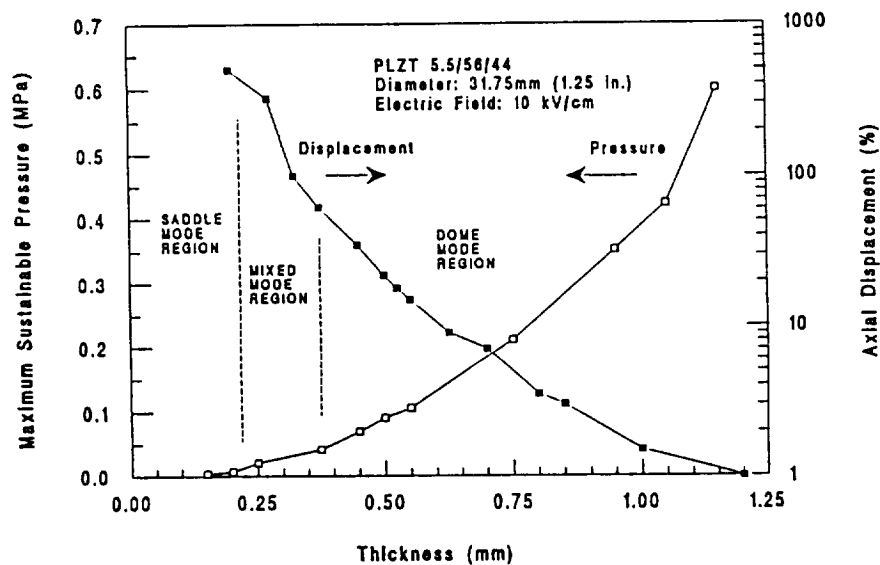


Figure 18. Sustainable Pressure and Displacement Characteristics for Rainbow PLZT 5.5/56/44 as a Function of Thickness

usually <0.5 mm thickness) or the wafer mechanically fractures (>0.5 mm thickness). The right ordinate log scale is the percent displacement (based on wafer thickness) of the device when operated at 450 volts dc while only under

the loading of the dial gage (80 grams). Also indicated on the figure are the wafer thickness regions where the saddle and dome modes of operation are dominant for a wafer 31.75 mm (1.25 in.) in diameter. The data shown in the figure indicate that Rainbow displacements span an unusually large range from near zero to at least 500% with actual displacements of up to 1 mm (0.040 in.) for a 0.2 mm (0.008 in.) thick wafer. Of course, such large displacements are not possible when operating under significant pressure differentials or under moderate point loading situations near its capacity.

Resonance Characteristics - The resonant, frequency dependent properties of a standard Rainbow wafer is given in Figure 19 which displays both impedance and phase angle as a function of frequency. Some outstanding features of this figure are the large radial resonance anomaly at 70 kHz and the several bending resonances between 1 to 20 kHz. Other resonances not shown in this figure are (1) overtone resonances of the fundamental radial resonance in the range from 100 kHz to 1 MHz, (2) thickness resonances in the low megahertz range around 4 and 8 MHz for the fundamental and first overtone and (3) very low frequency structurally-dependent resonances in the range of 25 to 500 Hz which can be noted when a Rainbow is operated as part of a working device.

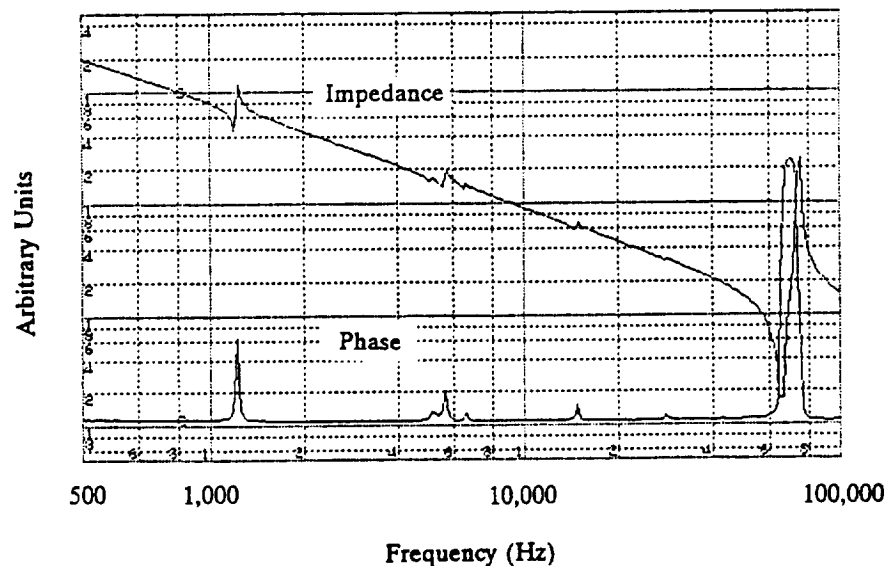


Figure 19. Resonance Characteristics of a Rainbow PLZT 1/53/47 Wafer

Table of Properties - A summary of selected properties which have been determined, to date, for the Rainbow ceramics are given in Table 2. In

addition to these, a number of advantages and features of the Rainbows are: (1) simplicity, (2) solid-state type, (3) monolithic, (4) pre-stressed for greater strength and durability, (5) can sustain/generate moderate loads, (6) mechanical overload protection, (7) medium fast response, (8) very high axial displacement, (9) surface mountable, (10) above-the-plane displacement, (11) no bonding layers, (12) temperature compensation possible, (13) can be stacked to multiply strain, (14) easy to fabricate and (15) cost effective.

Table 2. Some Selected Properties of Rainbow Ceramics

Thermal Expansion	-	10.0 x10 ⁻⁶ /°C (reduced layer) 5.4 x 10 ⁻⁶ /°C (oxide layer)
Modulus of Rupture	-	1.58 x10 ² MPa (22,500 psi)
Modulus of Elasticity	-	5.7 x10 ⁴ MPa (8.1 x10 ⁶ psi)(bending)(1/53/47) 10.9 x10 ⁴ MPa (15.5 x10 ⁶ psi)(bending)(8.6/65/35) 6.9 x10 ⁴ MPa (reduced layer)(acoustic)(5.5/56/44) 7.8 x10 ⁴ MPa (oxide layer) (")(")
Acoustic Velocity	-	4015 m/sec (reduced layer) 4248 m/sec (oxide layer)
Poisson's Ratio	-	0.38 (reduced layer) 0.38 (oxide layer)
Resistivity	-	3.8 x 10 ⁻⁴ ohm-cm
Effective d ₃₃ (saddle)	-	2.5 x 10 ⁻⁶ m/V (bending mode)
d ₃₃ (dome)	-	2.8 x10 ⁻⁷ m/V (bending mode)
Hysteresis	-	5 - 35%
Displacement (31.8 mm)	-	178 microns (0.007 inch)(0 - 450V)(dome mode) 381 microns (0.015 inch)(+/- 450V)(dome mode) 1143 microns (0.045 inch)(0 - 450V)(saddle mode) (102 mm dia.) - 3175 microns (0.125 inch)(0 - 450V)(saddle mode) 1016 microns (0.040 inch)(0 - 450V)(dome mode)
Capacitance (1.25" dia.)	-	15 nF (PLZT composition 1/53/47) K = 1200 30 nF (PLZT composition 5.5/56/44) K = 2400 60 nF (PLZT composition 9/65/35) K = 3800

Ferrofilms

The properties of Ferrofilms were determined from PLZT composition 2/53/47 prepared via the acetate process and automatically dip coated for 40 layers onto Ag substrates ranging in thickness from 0.025 to 0.25 mm, yielding an overall film thickness of approximately 12 μm . Standard, 1-mm diameter, vacuum evaporated Cu electrodes were deposited on the surface of the films for testing.

Dielectric Properties - The small-signal dielectric measurements of the PLZT thick films revealed that they possess properties very similar to bulk material of the same composition. For the particular composition evaluated, relative dielectric constants (1 kHz) ranged from 1400 to 1800 and dissipation factors from 3.5% to 4.6%.

Hysteresis Loops - Hysteresis loops (1 KHz) were obtained with an ac looper constructed in-house because thick films require higher voltages ($>100\text{ V}$) than normally available from standard thin film testers. An example of a typical loop is shown in Figure 20. As can be seen, the loop (polarization vs. electric field) is very square with sharp, saturated loop tips at maximum field, indicating a high degree of domain switching and good, insulating characteristics well into saturation at 100 kV/cm. The loop of Figure 20 displays typical properties for these films; i.e., that of: $P_R = 42\text{ }\mu\text{C}/\text{cm}^2$ and $E_c = 15.7\text{ kV}/\text{cm}$ (40 V/mil). It should be recognized that this low value for E_c is more typical for bulk material than for thin films which characteristically possess E_c s of 75 kV/cm or higher.

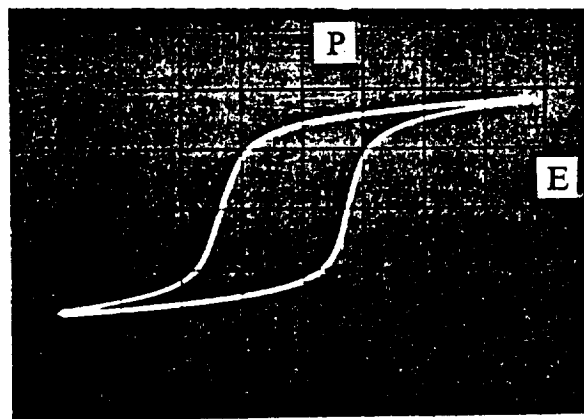


Figure 20. Typical Hysteresis Loop of Ferrofilm PLZT 1/53/47 on Ag

APPLICATIONS

A number of examples of applications are given in this section in order to demonstrate the versatility of the Rainbow and Ferrofilm technologies. These working models are essentially discrete, proof-of-principle devices which require further engineering design, miniaturization and modification in order for them to be suitable for hybrid microelectronics or integrated structures. In any case, it is believed that the Rainbow technology best serves the application range from macroelectronics to millielectronics, whereas the thick/thin Ferrofilms are best suited for the range from millielectronics to microelectronics.

The Rainbow devices shown in Figures 21 and 22 are typical examples of a number of applications envisioned for this technology. As can be seen, they range from actuators to sensors, and speakers to pumps. A more extensive list of applications include (1) linear actuators, (2) cavity/piston pumps, (3) loud speakers, (4) reciprocating motors, (5) relays/switches/thermostats, (6)

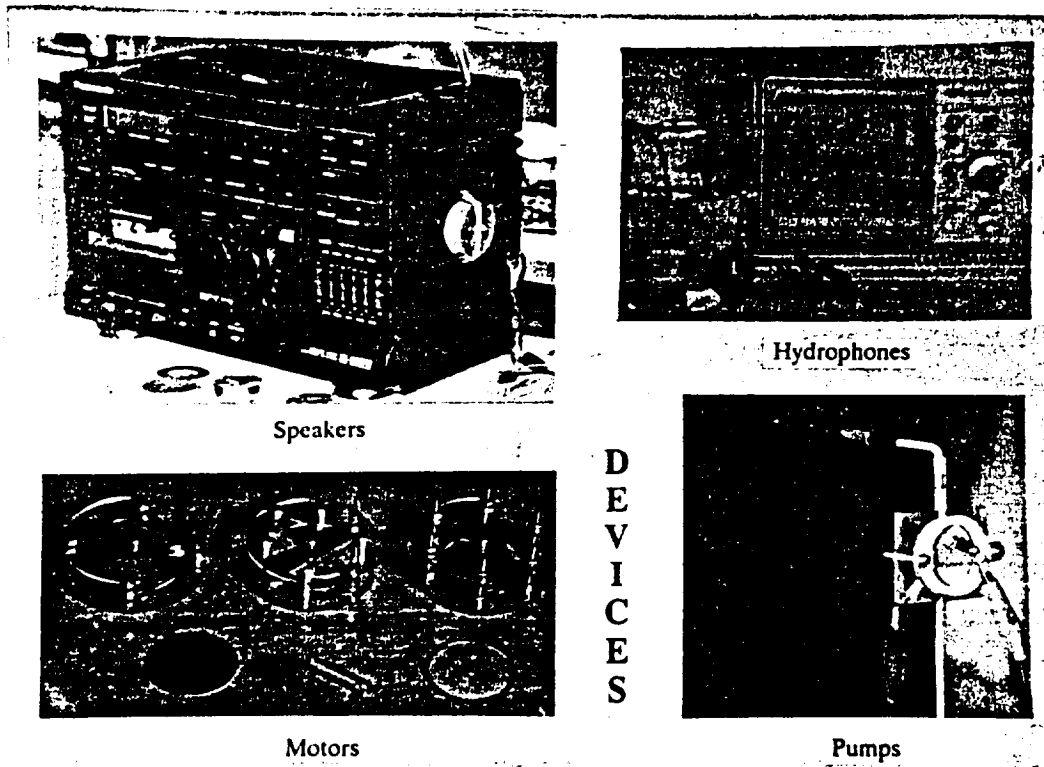


Figure 21. Examples of Working Model Devices Using Rainbow Ceramics as Actuators

sensors, (7) hydrophones/hydroprojectors, (8) variable-focus mirrors/lenses, (9) optical deflectors/scanners, (10) vibrating delivery systems, (11) liquid delivery systems, (12) antivibration/noise cancelling devices, (13) displays, (14) sonic and ultrasonic devices and (15) auto-leveling platforms.

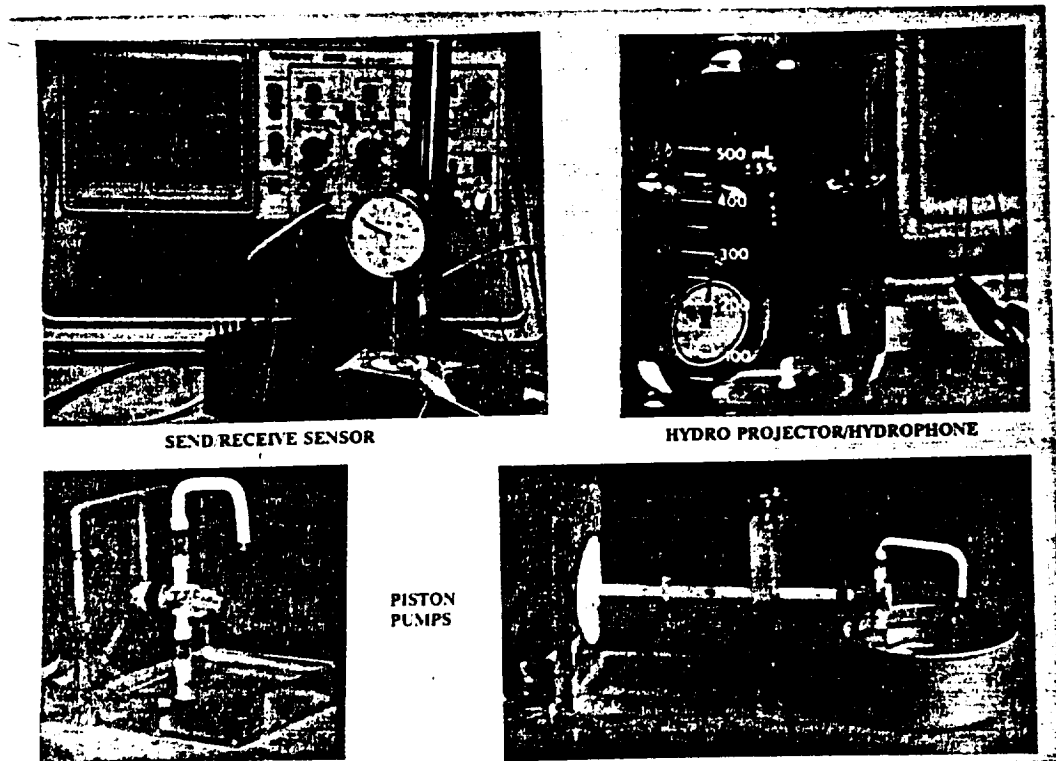


Figure 23. Additional Examples of Working Models Using Rainbow Ceramics as Actuators and Sensors

A single Ferrofilm device is shown in Figure 23. It simply consists of a 25 x 50 mm x 12 μ m thick film which was dip coated onto a 0.125 mm thick Ag substrate and electroded on the top major surface with vacuum-deposited Cu. After poling the film at 70 volts, the film/substrate is mounted to a resonating enclosure (in this case the enclosure is a cardboard box) and connected to the output of a radio. As with most ferroelectric/piezoelectric audio devices, the quality of the audio is only moderate, at best, when operated over the full audio range of the radio.

CONCLUSIONS

The prospects for utilizing Rainbows and Ferrofilms in discrete hybrid and

totally integrated microelectronics are promising for future applications involving smart ceramics such as ferroelectrics, piezoelectrics, pyroelectrics, electrooptics and electrostrictive materials. Rainbows have opened up a new dimension in ultra-high displacement actuators while Ferrofilms have now bridged the gap from bulk materials to thin films. The key to adapting these materials to specific devices and applications is the manner in which answers are found to questions concerning their reproducibility, reliability, longevity and cost effectiveness. Further development and design work are obviously needed in order to answer these questions.

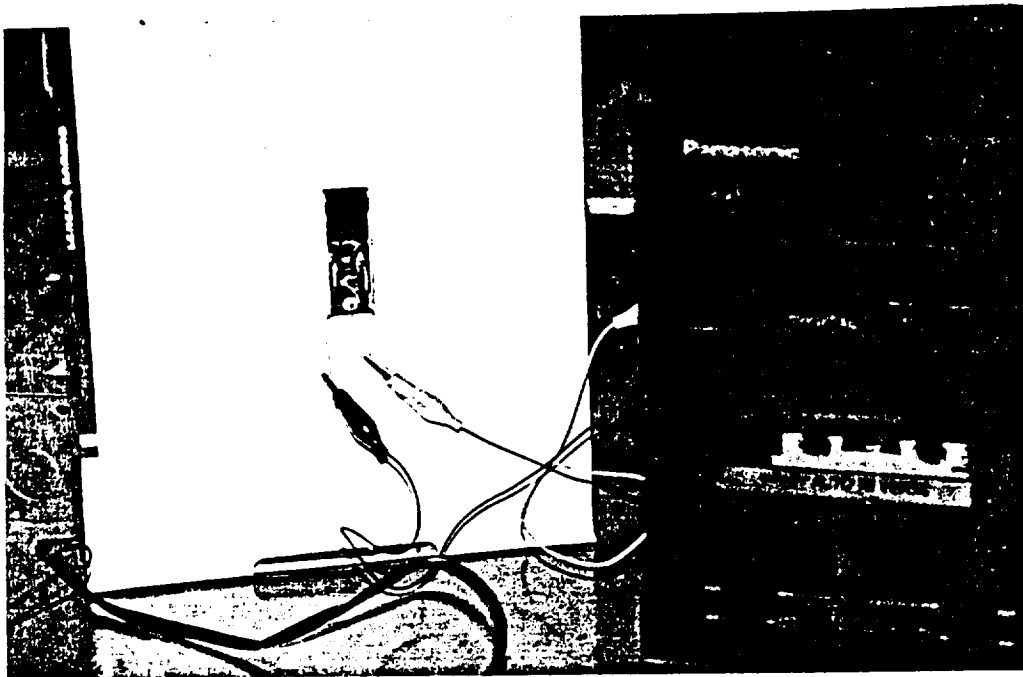


Figure 23. A Ferrofilm Speaker for a Stereo System

REFERENCES

1. L.H. Sheppard, "Advances in Processing of Ferroelectric Thin Films, Bull. Am. Ceram. Soc., 71, No. 1, 85-95 (1992)
2. P.C. Fazan, "Trends in the Development of ULSI DRAM Capacitors," Integrated Ferroelectrics, 4, 247-256 (1994)

3. R. Watton, "Ferroelectric Materials and IR Bolometer Arrays: From Hybrid Arrays Towards Integration," *Integrated Ferroelectrics*, 4, 175-186 (1994)
4. E.M. Lenoe, W.N. Radicic and M.S. Knapp, "Implications of Smart Materials in Advanced Prosthetics," *Proceedings SPIE on Smart Structures and Materials*, 2189, 84-104 (1994)
5. C.C. Hsueh, T. Tamagawa, C. Ye, A. Helgeson and D.L. Polla, "Sol-Gel Derived Ferroelectric Thin Films in Silicon Micromachining," *Integrated Ferroelectrics*, 3, 21-32 (1993)
6. G.H. Haertling, "Rainbow Ceramics - A New Type of Ultra-High Displacement Actuator," *Bull. Am. Ceram. Soc.*, 73, No. 1, 93-96 (1994)
7. G.H. Haertling, "Chemically Reduced PLZT Ceramics for Ultra-High Displacement Actuators," *Ferroelectrics*, 154, 101-106 (1994)
8. K.K. Li, G.H. Haertling and W-Y Howng, "An Automatic Dip Coating Process for Dielectric Thin and Thick Films," *Integrated Ferroelectrics*, 3, 81-91(1993)
9. G.H. Haertling, "Dielectric and Electrooptic Properties of Acetate Derived PLZT X/65/35 Thin Films," *Integrated Ferroelectrics*, 3, 207-215 (1993)
10. G.H. Haertling, "Intelligent Processing of Ferroelectric Films," *Bull. Am. Ceram. Soc.*, 73, No. 8, 68-73 (1994)
11. S. Sherit, H.D. Wiederick and B.K. Mukherjee, "Evaluation of PLZT Based RAINBOW Ceramic Samples Developed by Dr. Gene Haertling at Clemson University," Report No. DREA CR/94/436, Royal Military College of Canada, Kingston, Ontario, Canada, June (1994)
12. E. Furman, G. Li and G.H. Haertling, "Electromechanical Properties of Rainbow Devices," *Proceedings of the 9th ISAF Meeting*, State College, June (1994)